

**Stability of Iron Corrosion
Phases expected in a
Repository in Lower
Cretaceous Clay**



Gesellschaft für Anlagen-
und Reaktorsicherheit
(GRS) gGmbH

Stability of Iron Corrosion Phases expected in a Repository in Lower Cretaceous Clay

Sven Hagemann
Heike Mönig

September 2021

Remark:

This report refers to the research project 02E11314 which has been funded by the German Federal Ministry of Economic Affairs and Energy (BMWi).

The study was conducted by the Gesellschaft für Anlagen- und Reaktorsicherheit (GRS) gGmbH.

The authors are responsible for the content of the report.

GRS - 587
ISBN 978-3-947685-73-8

Keywords:

Containment, Corrosion, Modelling, Radionuclides, Repository

Table of contents

	Zusammenfassung	1
1	Introduction.....	7
2	Factors influencing the corrosion process in a repository in clay	11
2.1	Reference concept for the storage of HLW in clay formation in northern Germany.....	11
2.2	Types of iron-based materials used or employed in a repository.....	13
2.2.1	Lower Cretaceous deposits in Lower Saxony	14
2.2.2	Mineralogy	19
2.2.3	Change of predominant clay minerals.....	23
2.2.4	Alteration of minerals during excavation, storage and reuse as backfill	26
2.2.5	General considerations on the genesis of the pore water chemistry of the Lower Cretaceous clays in Northern Germany.....	26
2.2.6	Assumptions regarding the initial state of porewaters in a repository in Lower Cretaceous clay formations	36
2.2.7	Analytical data on deep groundwater samples in Northern Germany	36
2.2.8	Geology, mineralogy, and geochemistry of the host rock at the model site NORD	43
2.2.9	Model pore water composition of a Lower Cretaceous clay	47
2.3	Time-dependent variables	51
2.3.1	Temperature	51
2.3.2	Saturation state of clay	54
3	Previous investigations of iron and steel corrosion in clay systems or in contact with brines	57
3.1	Overview	57
3.2	Germany.....	58
3.3	USA: Waste Isolation Pilot Plant (WIPP).....	60
3.4	Switzerland.....	64
3.4.1	Disposal concept	64

3.4.2	Experimental results	66
3.5	France	72
3.5.1	Repository concept.....	72
3.5.2	Experimental and modelling results	73
3.6	Sweden	86
3.7	Japan.....	87
3.8	Czech Republic	88
3.9	Miscellaneous studies on geochemical processes.....	88
3.9.1	Corrosion in the presence of H ₂ S.....	88
3.9.2	Reduction of Fe(III) oxides by H ₂ S.....	89
3.9.3	Reduction of pyrite by H ₂ S.....	90
3.9.4	Microbial conversion of hydrogen to methane.....	90
3.9.5	Reduction of iron(III) in oxides and clay minerals by H ₂	90
3.9.6	Anaerobic reduction of sulphate by elemental hydrogen	90
3.9.7	Green rust formation.....	91
3.9.8	Corrosion in a humid, anaerobic atmosphere.....	91
3.9.9	Corrosion in contact with sand	91
3.9.10	Corrosion in unsaturated systems.....	91
3.10	Natural analogues.....	92
3.10.1	Corrosion of archaeological artefacts.....	92
3.10.2	Meteorites.....	96
3.11	Synthesis: Geochemical evolution of the near field and corrosion.....	97
3.12	Synthesis: corrosion products.....	103
3.12.1	Iron (III) oxides and oxyhydroxides	103
3.12.2	Iron(II) carbonates, chlorides, and hydroxides	103
3.12.3	Magnetite.....	104
3.12.4	Green rusts.....	105
3.12.5	Iron sulphides	106
3.12.6	Iron-containing clay minerals	107
4	Synthesis and characterization of iron corrosion phases.....	111

4.1	Selection of solid phases for thermodynamic investigation	111
4.2	Fe-Hibbingite, $\text{Fe}_2(\text{OH})_3\text{Cl}$	111
4.2.1	Experimental procedures	111
4.2.2	Experiment at 40 °C.....	115
4.3	Hibbingite - $(\text{Fe,Mg})(\text{OH})_3\text{Cl}$	116
4.4	Amakinite – $(\text{Fe,Mg})(\text{OH})_2$	117
4.5	Chukanovite.....	121
4.6	Solid solution $(\text{Fe,Mg})_2(\text{OH})_2\text{CO}_3$	123
4.7	Akaganeite.....	124
4.8	Other Fe(II) containing solids	126
4.8.1	Fe(II) analogue to kambaldaite, $\text{NaNi}_4(\text{CO}_3)_3(\text{OH})_3 \cdot 3\text{H}_2\text{O}$	127
4.8.2	Other Fe(II) hydroxo chlorides and Fe(II) analogue of nepskoite.....	128
4.8.3	Fe(II) analogue to Northupite, $\text{Na}_3\text{Mg}(\text{CO})_2\text{Cl}$	128
5	Prediction of long-term redox conditions in the nearfield	129
5.1	Preliminary remarks	129
5.2	Calculation of the redox level in the near field assuming different chemical boundary conditions.....	130
5.2.1	Purpose and border conditions of the calculations	130
5.2.2	Dimensions of the borehole, the liner and the container /reaction masses	131
5.2.3	Geochemical modelling of the corrosion process inside the liner	132
5.2.4	Corrosion reaction a – Reduction of sulphate suppressed, carbonate not buffered	134
5.2.5	Corrosion reaction b – reduction of sulphate suppressed, carbonate not buffered, hydrogen pressure fixed at 100 bar	136
5.2.6	Corrosion reaction c: Reduction of sulphate suppressed, carbonate buffered by fixed CO_2 partial pressure.....	137
5.2.7	Corrosion reaction d: Reduction of sulphate suppressed, CO_2 partial pressure fixed at 0.02574 bar, H_2 pressure fixed at 100 bar.....	138
5.2.8	Corrosion reaction e: Reduction of sulphate allowed, CO_2 partial pressure fixed at 0.02574 bar, H_2 partial pressure fixed at 100 bar	138

5.2.9	Corrosion reaction f: reduction of sulphate suppressed, carbonate not buffered, hydrogen pressure fixed at 100 bar, quartz limited to 10 %, siderite (aged) suppressed	139
5.2.10	Corrosion reaction g : reduction of sulphate suppressed, carbonate not buffered, hydrogen pressure fixed at 10 bar, quartz limited to 10 %, siderite (aged) suppressed	141
5.2.11	Corrosion reaction h : reduction of sulphate allowed, carbonate not buffered, quartz limited to 10 %, siderite (aged) suppressed, unlimited supply of pyrite	142
5.2.12	Summary	145
5.3	Predominant speciation and solubility of selected radionuclides	147
5.3.1	Selenium	147
5.3.2	Uranium.....	149
5.3.3	Plutonium	150
5.3.4	Technetium.....	151
5.3.5	Solubility of Se, U, Pu and Tc in model pore water at p _{cH} 6.4 to 9.6 and p _{H₂} 0.008 to 100 bar	152
6	Summary and conclusions	155
7	References	161
	List of tables	193
	List of figures.....	197

Zusammenfassung

Für Endlagerkonzepte im Tongestein ist bei allen im Rahmen eines Langzeitsicherheitsnachweises zu betrachtenden Entwicklungen des Endlagersystems mit einem Zutritt von Porenwässern zu den eingelagerten Abfallbehältern zu rechnen. Im Fall norddeutscher Tonformationen, die für die Errichtung eines Endlagers für wärmeentwickelnde radioaktive Abfälle in Frage kommen, ist zudem von salinaren Porenwässern auszugehen. Die zutretenden Lösungen führen zu einer fortschreitenden Korrosion der Behälter, die nach einem gewissen Zeitraum, insbesondere bei ausreichenden Lösungsmengen, zum Ausfall der Abfallbehälter und zur Mobilisierung von Radionukliden in das Nahfeldsystem führen können. Die aus der Abfallmatrix freigesetzten Radionuklide treffen dort auf ein geochemisches Milieu, das stark von der Korrosion der metallischen Komponenten im Nahfeld (Behälter, Liner, Einbauten) bestimmt wird. Es fußt zwar auf den geochemischen Gegebenheiten in der Wirtsgesteinsformation, wird aber lokal entscheidend durch die festen, gelösten und gasförmigen Korrosionsprodukte geprägt. Die Mobilität der Radionuklide in der direkten Umgebung der Abfälle wird dann durch folgende Prozesse beeinflusst:

- Reduktions-/ Oxidationsprozesse, sowie Bildung von Komplexen und Festphasen unter den Randbedingungen des geochemischen Milieus (Redoxniveau, Wasserstoffionenkonzentration, Lösungszusammensetzung), und
- die Sorption von Radionukliden an den gebildeten Korrosionsphasen

Für eine Bewertung und Quantifizierung dieser Prozesse ist es notwendig, einerseits die Korrosion selbst, d.h. ihre Kinetik und die Art der Produkte, beschreiben zu können, andererseits ein ausreichendes Verständnis zu den Eigenschaften der Korrosionsprodukte hinsichtlich ihrer thermodynamischen Stabilität und ihrer Sorptionseigenschaften gegenüber Radionukliden zu entwickeln.

Während im parallel laufenden Vorhaben KORSO¹ die elektrochemische Untersuchung der unter anaeroben Bedingungen ablaufenden Korrosionsprozesse und die Korrosionskinetik im Mittelpunkt stand, widmete sich das Vorhaben KORPHA den

¹ „Korrosions- und Sorptionsprozesse an Stahloberflächen bei hohen Temperaturen und Drücken im anaeroben salinaren Milieu“ BMWI-Fkz 02 E 11496A

thermodynamischen Aspekten der Korrosion. Auf dieser Grundlage wurden Abschätzungen für das geochemische Milieu und die Löslichkeit von Radionukliden vorgenommen.

Das Projekt „Redoxprognose“² hat gezeigt, dass für die bei der Korrosion von Eisen entstehenden Eisen (II/III)- und Eisen(III)-Verbindungen in der Literatur weit auseinanderliegende Löslichkeiten vorliegen /HAG 14/. Diese hängen offenbar sowohl von den Bildungsbedingungen der Festphasen als auch von der Analysemethode zur Bestimmung der Löslichkeiten ab. Sofern die Randbedingungen der Korrosion nicht eindeutig voraus sagbar sind, lassen sich auch Löslichkeiten möglicher Korrosionsphasen nicht sicher prognostizieren. Aussagen über das geochemische Nahfeldmilieu müssen daher immer von einer Bandbreite möglicher thermodynamischer Charakteristika ausgehen. Zu berücksichtigen sind zudem weitere für die Entwicklung des Redoxniveaus relevante Prozesse, wie die Entstehung und der Verbleib von Korrosionswasserstoff und das Auftreten kinetisch gehemmter Prozesse. Hierzu gehören die anorganisch ablaufende oder mikrobiell katalysierte Reduktion von Sulfat und die Bildung von Magnetit bei nur mäßig erhöhten Temperaturen.

Zusammensetzung von Porenwässern norddeutscher Unterkreidetone

Aufgrund fehlender analytischer Daten kann derzeit über den Chemismus von Porenwässern in norddeutschen Unterkreidetonformationen nur spekuliert werden. Daten aus anderen Lagerstätten wie auch Untersuchungen zum Kompaktionsverhalten von salzhaltigen Tonen lassen aber auf zwei grundsätzlich mögliche Ton- und Lösungstypen schließen:

- Porenwässer in Tonformationen, in denen Kaolinit und Illit vorherrschen, können einen stark salzhaltigen Charakter haben. Dieses wäre in Norddeutschland in der Formation Apt oder älter der Fall. Historische Messungen ergaben Konzentrationen von bis zu 5,6 mol/l Chlorid für Tonproben in Tiefen von 1000 bis 1100 m. Dies entspricht einer Halitsättigung. Die untere Grenze wäre eine Lösungskomposition in der Nähe des Salzgehalts des Meerwassers (0,5 mol/l). Falls die Formation Kontakt mit meteorischen Wässern gehabt hat, könnte auch eine Verdünnung des Salzgehalts eingetreten sein.

² FKZ (BMBF) 02 C 0983.

- Bei den Smektit-dominierten Tonen kann eher mit schwach mineralisierten Wässern gerechnet werden, da durch die Kompaktion Ionen bevorzugt ausgepresst werden. Somit würden in einem möglichen Endlager in den Formationen Alb oder jünger schwach salzhaltiges Tonporenwasser mit einer Mineralisierung um 10 g/l vorhanden sein.

Das Auftreten salinärer Lösungen in begleitenden Sandsteinlagen (z.B. im Hils-Sandstein) ist allein noch kein Nachweis für das Vorhandensein salinärer Tonporenwässer.

Auf der Basis dieser Überlegungen und der Salinitätsgradienten, die durch die Bohrungen in der Umgebung des Schachts Konrad ermittelt wurden, wurde eine Porenwasserzusammensetzung für den Modellstandort NORD (Projekt AnSichtT) abgeleitet. Es handelt sich dabei um ein NaCl/CaCl₂ dominiertes Wasser, das an den Mineralen der Formation gesättigt ist (u.a. Goethit, Pyrit, Calcit, Dolomit, Gips und Siderit). Seine Chloridkonzentration beträgt etwa 3 mol/l.

Vorherrschende Festphasen bei der Korrosion von Eisen

Die Korrosion eisenhaltiger Behältermaterialien und Liner führt zu stark reduzierenden Verhältnissen. Nach Ende der aeroben Phasen im Endlager (einige 10 bis 100 Jahre) treten als Korrosionsphasen im Kontakt mit dem Behälter praktisch ausschließlich Eisen(II)-Phasen auf. Hierzu gehören, je nach geochemischen Milieu Hibbingit (ein basisches Chlorid), Chukanovit (ein basisches Carbonat), Siderit/ Artinit (Carbonate, teils mit Mg gemischt), evtl. auch Amakinit (ein Hydroxid, gemischt mit Mg), je nach Verfügbarkeit von Sulfid auch Pyrit sowie andere Sulfide. Anfänglich in kleinen Mengen vorhandene reine Eisen(III)-Phasen werden im Verlaufe der anaeroben Korrosion zu Eisen(II/III)-Phasen reduziert. Magnetit wird bei anaeroben Korrosionsexperimenten in Kontakt mit Ton nur in untergeordnetem Maße gefunden. Seine Bildung ist also offensichtlich kinetisch gehemmt oder die lokalen chemischen Verhältnisse lassen seine Bildung nicht zu. Gelegentlich sind geringe Mengen an Maghemit ($\gamma\text{-Fe}_2\text{O}_3$) und chloridhaltigem Akaganait ($\beta\text{-Fe}^{3+}\text{O}(\text{OH}, \text{Cl})$) zu finden, letzterer aber nur vorübergehend.

Bedeutsam ist die Neubildung von eisenhaltigen Silikaten sowohl in den inneren als auch der äußeren Korrosionsschichten. Hierzu gehören 1:1 Phyllosilikate aus der Kaolinit/Serpentin-Gruppe (Greenalit, Berthierin, Odinit, Cronstedtit) und 2:1 Tonminerale aus der Smektit-Gruppe (Nontronit, Saponit, Beidellit, Fe-Montmorillonit). Sie entstehen

durch Diffusion von Silikat aus dem umliegenden Tonmaterial in Richtung Korrosionsfront oder durch Diffusion von Eisen in den umliegenden Ton.

Zu beachten ist allerdings, dass Korrosionsuntersuchungen in Kontakt mit salzhaltigen Tonen bislang nicht stattgefunden haben. Die bisherigen Erfahrungen zeigen, dass die Eisenkorrosion in freier Lösung sowohl eine andere Kinetik als auch andere Korrosionsprodukte zeigt, so dass bisherige Forschungen zur Korrosion in Salzlösungen nicht auf reale Einbaubedingungen im Ton übertragbar sind.

Stabilität von Korrosionsphasen

Im Zuge des Vorhabens wurden wichtige Korrosionsphasen synthetisiert und thermodynamisch charakterisiert. Hierzu gehören reiner Fe-Hibbingit und Chukanovit. Im Fokus standen außerdem Mischphasen, wie sie bei Anwesenheit von Magnesium zu erwarten sind. Hierzu gehören Hibbingit, $(\text{Fe,Mg})_2(\text{OH})_3\text{Cl}$, Fe/Mg-Chukanovit, $(\text{Fe,Mg})_2(\text{OH})_2\text{CO}_3$ und Amakinit $(\text{Fe,Mg})(\text{OH})_2$. Für Amakinit konnte gezeigt werden, dass es sich um eine ideale feste Lösung mit variablem Mg/Fe-Verhältnis handelt. Dies erlaubt eine verbesserte Prognose des geochemischen Milieus im Nahfeld. Die Untersuchungen waren aber auf Temperaturen bei oder nahe 25°C ausgelegt. Daten zur Stabilität der Phasen bei höheren Temperaturen (bis 80°C), wie sie in den ersten Jahrhunderten nach Verschluss relevant sind, müssen noch gewonnen werden. Zur Stabilität Fe(II)-haltiger Tonminerale liegen weiterhin nur wenige experimentelle Daten vor.

Redoxniveau im Nahfeld eines Endlagers im Verlaufe der Behälterkorrosion

Auf Basis der neuen Erkenntnisse zur Stabilität von Eisenkorrosionsphasen und der Zusammensetzung von Tonporenwässern wurde der Reaktionsverlauf bei der Korrosion eines Behälters aus Gusseisen berechnet. Als Grundlage dienten dabei aktuelle untersuchte Endlagerkonzepte für Standorte im Tongestein. Hier ist die Einlagerung von Endlagerbehältern in einer Quarzsand-Schüttung vorgesehen, die von einem Stahl liner eingefasst sind. Dabei wurden verschiedene Variablen berücksichtigt, um die Bandbreite möglicher Systementwicklungen abschätzen zu können:

- Zulassen oder Unterdrücken der Sulfatreduktion durch Wasserstoff
- Pufferung des CO_2 -Partialdrucks beim Ausgangswert oder Verzicht auf Pufferung

- Freie Entwicklung des H_2 -Partialdrucks oder Festlegung eines konstanten Maximaldrucks
- Masse des am Korrosionsgeschehen beteiligten Quarzsandes
- Verfügbarkeit von Pyrit als Senke für Korrosionswasserstoff und Quelle von Schwefelwasserstoff

Die Rechnungen erlaubten einen Einblick in die mögliche Ausprägung von Korrosionsprozessen unter salinaren Bedingungen und in Kontakt mit silikatischen Materialien. Je nach Randbedingung ändert sich die Sequenz der auftretenden Korrosionsphasen und somit auch die resultierenden Wasserstoffionenkonzentrationen (pH-Werte) und Wasserstoff-Partialdrücke. Dabei wurde klar, dass die Pufferung durch Silikat eine Beschränkung der Bandbreite der pH-Werte auf einen Bereich von 6.4 bis 9.6 verursacht. Die Bandbreite der Wasserstoffpartialdrücke lässt sich schwerer fassen, da in den statischen Rechnungen Diffusionsprozesse und Gastransport über Zweiphasenfluss nicht berücksichtigt werden konnten. Sollte es zu einem eher schnellen Verbrauch von Wasserstoff durch Reaktion mit Pyrit im Wirtsgestein kommen, so wären geringe Partialdrücke in der Größenordnung von 10^{-3} bar zu erwarten. Ist die Diffusion von Wasserstoff in das umgebende Wirtsgestein langsamer als die Gasproduktion an der Korrosionsfront, so können weitaus höhere Drücke erreicht werden. Als vorläufige Obergrenze wird 100 bar angenommen. Dies stimmt mit Benchmark-Berechnungen zum Druckaufbau in einem Endlager im Tongestein überein, die zu Maximaldrücken von 50 bar nach etwa 20000 bis 40000 Jahren kamen.

Auswirkungen auf die Radionuklidmobilität

Für die Bandbreite der so erhaltenen H_2 -Drücke und pH-Werte wurden für ausgewählte Radionuklide (Se, Tc, U, Pu) vorherrschende wässrige Spezies und Feststoffe berechnet. Hierzu wurde, die THEREDA-Datenbasis mit einigen Ergänzungen benutzt.

Dadurch wurde deutlich, dass generell mit niedrigen Oxidationsstufen zu rechnen ist (Se^0 oder Se^{-II} , Tc^{IV} , U^{IV} , Pu^{III} oder Pu^{IV}). Diese sind meist, aber nicht immer mit niedrigen Löslichkeiten verknüpft. Für Uran und Technetium war die Löslichkeit im gesamten betrachteten pH/ pH_2 -Feld gleich. Allerdings wurde eine Reduktion zu elementarem Technetium nicht berücksichtigt, die nach einer anderen Datenbasis (JAEA) zu erwarten wäre. Für Selen ergab sich eine Bandbreite von zwei Größenordnungen, die vor allem durch die nicht klar zu beantwortende Frage nach der Art der tatsächlich zu erwartenden Se-Oxidationsstufe (0 oder -II) verursacht wird. Für Plutonium ergab sich einer

Bandbreite von drei Größenordnungen. Hier wechseln sowohl Oxidationsstufe als auch stabile Festphasen, so dass sich große Unterschiede zwischen den einzelnen Rechnungen ergaben.

Für einige Elemente sollte in Zukunft verstärkt geprüft werden, welche Oxidationsstufen sich im Kontakt mit korrodierenden Stahlmaterialien tatsächlich einstellen, da sich thermodynamisch stabile Phasen aufgrund kinetischer Hemmungen oftmals nur verzögert bilden. Zukünftige Forschungsanstrengungen sollten sich auf die reduzierten Phasen/Spezies konzentrieren. Für diese liegen oftmals nur wenige verwendbare Daten vor. Dies trifft besonders für saline Verhältnisse zu.

Das Projekt zeigte, dass zur anaeroben Eisenkorrosion in Ton, insbesondere unter salzhaltigen Bedingungen, immer noch wesentliche Fragen offen sind. Voraussagen über zukünftige geochemische Entwicklungen im Nahfeld eines Endlagers müssen als spekulativ angesehen werden, solange grundlegende Daten über die geochemischen Eigenschaften von Tonen der Unterkreide nicht verfügbar sind und wichtige Korrosionsprozesse und Sekundärreaktionen von Reaktionsprodukten nicht unter realistischen Bedingungen untersucht wurden. Folgende Wissenslücken stellen sich dar:

- Analytische Daten zu Tonporenwässern in norddeutschen Formationen der Unterkreide
- Quellverhalten von Bentonit aus offenen Gruben (als potentielle Buffer) in Kontakt mit salzhaltigem Porenwasser aus kaolinitischen Tonen
- Korrosion von Stahl in salzhaltigen Tonen der Unterkreide (bisher konzentrierten sich die Korrosionsstudien auf Tonzusammensetzungen mit schwach mineralisierten Porenwässern)
- Reaktion von Korrosionswasserstoff mit in Ton oder primären Korrosionsprodukten vorhandenen Mineralien, Diffusion von H_2 in gesättigtem Ton der Unterkreide
- Einfluss von oxidiertem Bentonit aus dem Tagebau auf die Fe-Korrosion
- Relevanz der mikrobiellen Sulfatreduktion und der Methanproduktion unter salzhaltigen Bedingungen

Solche Fragen sollten durch zukünftige Forschungsaktivitäten näher betrachtet werden, um ein grundlegendes Verständnis der geochemischen Entwicklung des Nahfeldes und in der Folge des Migrationsverhaltens von Radionukliden zu ermöglichen.

1 Introduction

Iron-containing materials from the containers represent the most important source of redox-sensitive chemical elements in the near field. It is therefore assumed that the redox potential is primarily driven by the iron phases, notably iron corrosion phases that are present /JOB 97/, /WER 03/.

For repository concepts in argillaceous rock, an influx of pore waters to the emplaced waste containers is to be expected for all system developments to be considered within the framework of a long-term safety assessment. In the case of clay formations in northern Germany which are considered for the construction of a repository for heat-generating radioactive waste, saline pore waters are also to be assumed.

The inflowing solutions lead to progressive corrosion of the containers, which eventually can lead to a loss of its barrier function and the mobilisation of radionuclides into the near-field system. There, the radionuclides released from the waste matrix encounter a geochemical environment that is strongly determined by the corrosion of the metallic components in the nearfield (e. g. containers, liners). Although it is based on the geochemical conditions in the host rock formation, it is decisively influenced locally by the solid, dissolved, and gaseous corrosion products. The mobility of the radionuclides in the direct vicinity of the waste is then influenced by the following processes:

- reduction/oxidation processes at the surface of corrosion products
- formation of complexes and solids under the boundary conditions of the geochemical environment (redox level, hydrogen ion concentration, solution composition)
- the sorption of radionuclides on the corrosion phases formed

For evaluation and quantification of these processes, it is necessary to understand the corrosion itself, i. e. its kinetics and the type of products. On the other hand, the thermodynamic stability of the corrosion products and their sorption properties for radionuclides need to be known. These aspects were investigated in detail in two parallel planned projects to deepen the process understanding necessary for a suitable representation of the processes in long-term safety:

- The parallel running KORSO project focussed on the electrochemical investigation of corrosion processes taking place under anaerobic conditions, the type of corrosion

products and the corrosion kinetics. The corrosion products were characterised by spectroscopic and optical methods and served as a basis for determining the sorption behaviour of actinides.

- The project KORPHA, on the other hand, was dedicated to the thermodynamic aspects of corrosion and its significance for radionuclide solubility. For this purpose, the thermodynamic properties, especially of the metastable corrosion products, were to be investigated in detail. On this basis, estimates for the geochemical environment and the solubility of radionuclides could be made

In a previous project³, it has been shown that data on the solubilities of iron (II/III) and iron (III) compounds may vary considerably depending on the formation conditions of the solid phases and on the analytical methods used to determine the solubilities /HAG 14/. If the boundary conditions of corrosion cannot be predicted unambiguously, solubilities of possible corrosion phases cannot be predicted with certainty either. Predictions about the geochemical near-field environment must therefore always be based on a range of possible thermodynamic characteristics. The uncertainties regarding stability and chemistry of the corrosion phases are of great importance for the reliability of predictions of the geochemical environment in the near-field of a repository, which occurs when a solution phase is formed in the vicinity of ferrous materials.

The redox potential is essentially controlled by the presence of metallic iron, iron(II) and iron(III)-containing corrosion phases resulting from the large amounts of metallic container material /WER 03/. For the solubility of Fe(II) phases such as $\text{Fe}(\text{OH})_2$ as well as Fe(III) phases and mixed Fe(II/III) phases, no discrete values are observed, but ranges which can be of two orders of magnitude for Fe(II) phases and up to five orders of magnitude for Fe(III) phases. This causes an equally large variability of the iron(II) and iron(III) concentrations in solution. In cases where the active redox potential is determined by the thermodynamic activity ratio Fe(II)/Fe(III), a variability of only the Fe(III) concentration in five orders of magnitude would change the redox potential by up to 300 mV. This is of the same order of magnitude as the possible bandwidth for the redox potential calculated for the Swiss repository concept in Opalinus clay (200 mV, /WER 03/).

³ Project „Redoxprognose“ FKZ (BMBF) 02 C 0983

Depending on this, the corrosion itself is also influenced. The lower the solubility of a Fe(III) or Fe(II/III) phase, the stronger the electrochemical potential difference between the metal and the corrosion phase, the stronger the driving force of the corrosion and the higher the hydrogen pressures can build up without corrosion coming to a standstill. On the other hand, if the solubilities of the Fe(III)-containing phases are higher, the corrosion is more likely to lead to Fe(II) phases and possibly remain there. In the same way, the pH value is affected, which initially increases due to the primary reaction step in the corrosion of iron:



until saturation of Fe(OH)₂ occurs at pH 9.5. Due to the further reaction of Fe²⁺ to Fe³⁺ according to



the pH value drops again. If particularly stable (hardly soluble) Fe(III)-containing corrosion products develop, acidic solutions are to be expected, as they remove hydroxide from the solution. If, on the other hand, the reaction stops with Fe(II) products, neutral to basic solutions are to be assumed. This has a considerable influence on the speciation and mobility of radionuclides.

To be able to determine the geochemical environment in the near-field of a repository in clay rock and thus the oxidation state and mobility of radionuclides more reliably, it is, therefore, necessary to investigate both the identity and the thermodynamic stability of corrosion phases.

Project approach

The work in the project was organised in several steps. First, a description of the geological and chemical boundary conditions that are to be expected in a repository in the Lower Cretaceous Clay of Northern Germany is carried out. This includes, in particular, considerations on the probable composition of the expected pore waters. This is followed by a detailed summary and evaluation of the previous work on steel corrosion in clay rock. On this basis, corrosion phases were identified for which further thermodynamic data are required. For these phases, synthesis methods were researched or, if not available, newly developed. During solubility experiments, the physical and chemical

conditions for the formation of the phases were investigated. On this basis, model calculations were performed to predict possible developments of the geochemical environment in the nearfield of corroding repository casks and to estimate the effects on speciation and solubility of relevant radionuclides.

2 Factors influencing the corrosion process in a repository in clay

2.1 Reference concept for the storage of HLW in clay formation in northern Germany

Within the project AnSichT, a reference concept has been developed that describes the general repository layout, the placement of containers as well as other specifications of the repository operation /LOM 15/. A key feature of the concept is the placement of retrievable containers containing spent fuel in vertical boreholes (Fig. 2.1). These boreholes are planned to have a depth of approximately 19 m and a diameter of about 1.85 m. Liners made of cast steel are driven into the borehole to stabilize the cavity against the rock pressure. When the plastic clay rock had enclosed the liner tightly, discs made of clay are lowered into the borehole. They serve as a buffer and have a circular hole in the middle. The clay for these disks is taken from the formation. It may be mixed with clay material from other sites to improve the swelling properties of the discs. The outer liner is perforated so that the bentonite buffer may slowly become saturated. After the outer liner has been filled, another, the inner liner is placed in the middle of the discs. The containers are now emplaced in the remaining cavity together with sand so that the containers are surrounded by sand from all directions. Finally, the inner liner is tightly closed, and the remaining space between the outer and inner liners is filled with a 1 m bentonite plate. After that, the borehole is closed with a 5 m bentonite barrier made of the same material as the buffer. Above this barrier, an abutment of about 3 m made of concrete is placed.

Several boreholes are made accessible through drifts that are stabilized either by shotcrete walls (30 cm) or by an anchor-steel net system /AME 07//LOM 15/. When all boreholes are equipped and closed, the drifts will be backfilled with crushed claystone from the formation (same material as used for the buffer). It is expected that the saturation of the backfill may need up to 1000 years. The drifts are sealed by a combination of barriers (bentonite barriers and concrete abutments).

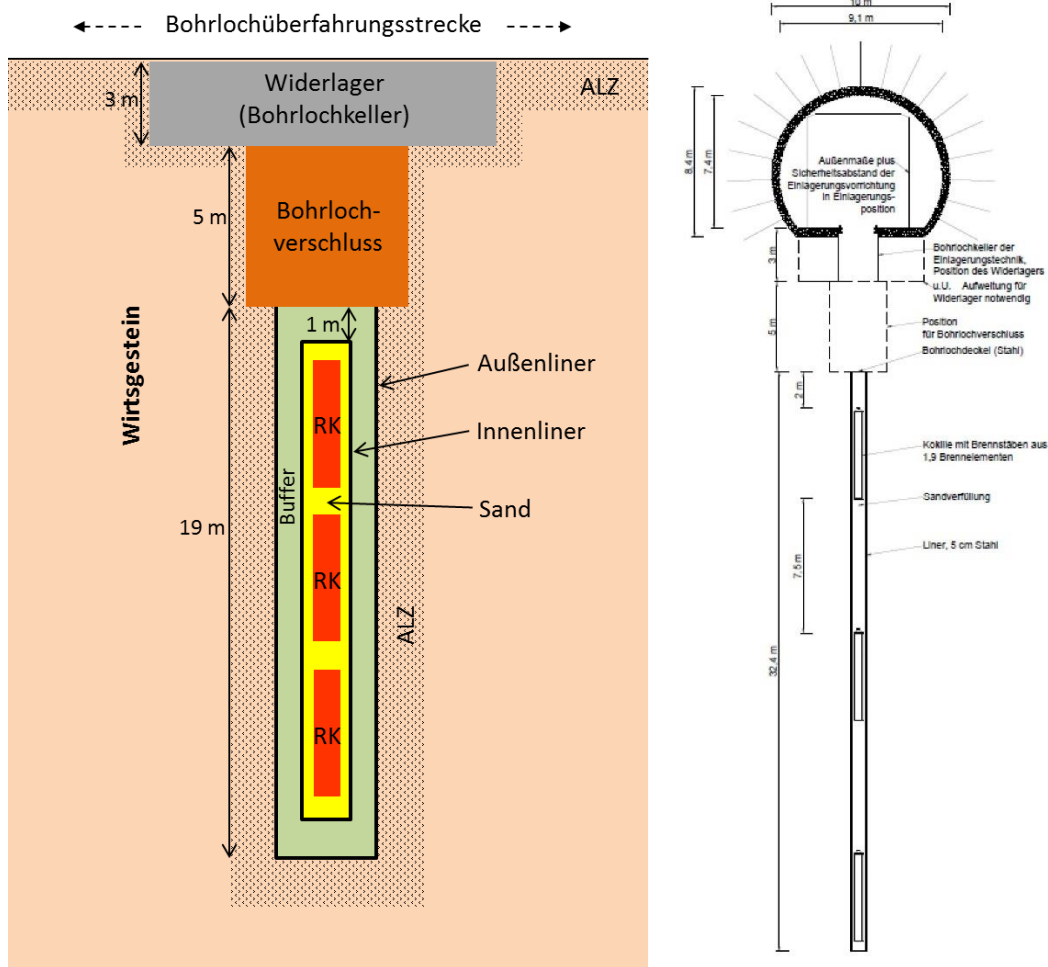


Fig. 2.1 Schematic description of a borehole for the emplacement of waste containers in clay rock. Left: concept in the project AnSichT (/LOM 15/), right: concept in the project RESUS /ALF 20a/

In the project RESUS, a slightly different concept was proposed for massive clay formations /ALF 20a/. It omits the outer liner and the buffer. The BSK containers are directly placed in the inner liner (5 cm steel) in a bed of sand. The liner is closed by a steel lid. The other elements are similar. For a clay formation with a lower thickness, storage in boreholes may not be applicable. In that case, waste containers may be stored in drifts. The concept was described in Jobmann et al. /JOB 15/ and Alferra et al. /ALF 20/. Waste containers are placed on a support made of compacted clay. They are located in horizontal drifts the walls of which are stabilized, e. g. by shotcrete. A buffer made from granule clay from the host formation is used to fill the void between containers and walls (Fig. 2.2). The concept was originally developed for the Molasse clay formations in southern Germany. Northern German Lower Cretaceous clay formations often show a considerable thickness and would allow storage in vertical boreholes.

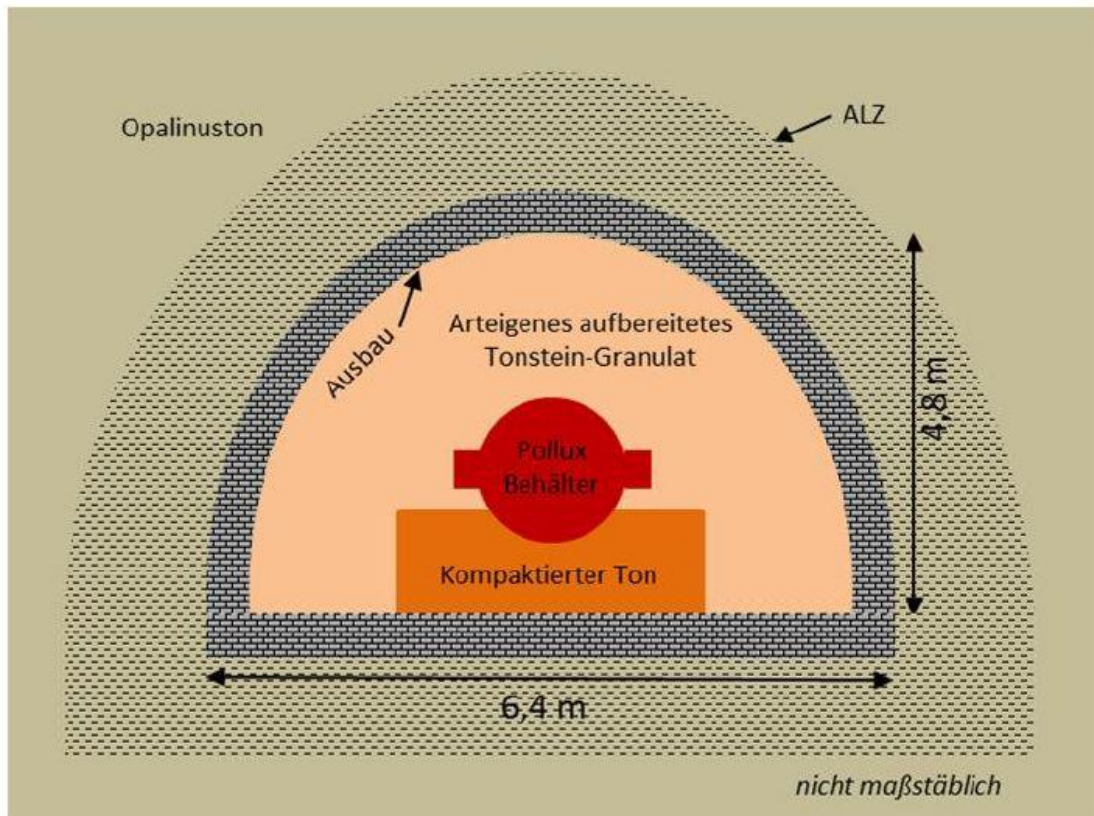


Fig. 2.2 Storage of waste containers in a drift /JOB 15a/

2.2 Types of iron-based materials used or employed in a repository

Within the vicinity of the radioactive waste emplaced in a borehole, iron-based materials are used for two purposes: as part of the materials used for the construction of containers and the liner or liners surrounding the waste containers in the borehole. Carbon steel is also used in the supporting structures that are needed to mechanically stabilize the drift, such as anchors and meshes and possibly reinforcing steel covered by shotcrete /LOM 15/.

The liners are planned to be produced from spheroidal grey cast iron GGG40 (EN-GJS-400-15). In currently discussed concepts, the outer hull of the waste containers (BSK) is made of fine-grained carbon steel (type 1.6210, 15MnNi6.3). According to Pfeiffer et al. /PFE 11/, the composition is as follows (Tab. 2.1).

Tab. 2.1 Composition of spheroidal grey cast iron GGG40 (EN-GJS-400-15) and fine-grained steel (type 1.6210, 15MnNi6.3) /PFE 11/

Element	GGG40 (EN-GJS-400-15) Content [Wt.-%]	Fine-grained carbon steel (type 1.6210, 15MnNi6.3) Content [Wt.-%]
C	3.45-3.80	0,12 - 0,18
Si		0,15 - 0,35
Mn	0.25 – 0.5	1,20 - 1,65
P	>0.04	≤ 0,015
S	0.005 – 0.01	≤ 0,005
Ni		0,5 - 0,85
Al		0,020 - 0,055
As		≤ 0,015
Cr		≤ 0,15
Cu		≤ 0,06
Mo		≤ 0,05
N		≤ 0,015
Nb		≤ 0,004
Sn		≤ 0,010
Ti		≤ 0,02
V		≤ 0,02
Fe	Difference to 100	Difference to 100

The densities of GGG40 and steel 1.6210 are approximately 7.1 g/cm³/MEU 21/, and 7.845 g/cm³ /RIC no year/, respectively.

2.2.1 Lower Cretaceous deposits in Lower Saxony

At the beginning of the Lower Cretaceous, the sea level rose worldwide. At that time there was a large epicontinental area in northern Central Europe, stretching from England across what is now the North Sea, the Netherlands, northern Germany, Poland, and parts of Russia. This area showed itself to be highly differentiated in detail. Highlands or mainland areas such as the Central European, the English-Armorican and the Fennoscandian-Sarmatian land masses lined this area, which is subdivided into several partial depressions alongside the mainland. These are the Danish, Polish, Dutch, and North German depressions.

An important tectonic part of the Central European depression is the Northern German Basin with its two geological main structures, the Lower Saxony Basin, and the Pompeckj Block /WAL 07/, /MCC 08/. The Lower Saxony Basin formed through a depression between the Central European mainland ("Rhenish Massif") in the south and the Pompeckj Plain in the north. That process occurred in the period of the late Jurassic and Lower Cretaceous but was completed before the beginning of the Albian /JOB 07/.

The Basin is about 200-250 km long and 70 km wide and is orientated from west-north-west to east-south-east (Fig. 2.3). It is divided into three parts due to different sediment thickness and lithological changes: Into a western part in the area of the Emsland, a central part in the area of Osnabrück-Bielefeld-Minden-Vechta-Sulingen and an eastern part, which extends over the area of Hannover-Braunschweig.

During the depression, the Basin has been covered by massive clayish sediments. In its north-western part sediments of the Lower Cretaceous series (100 – 145 Ma) prevail where they constitute extended and thick layers (up to several hundred meters, Fig. 2.5). Six intervals can be identified /GRA 12/:

- Albian (100.5 – 113.0 Ma)
- Aptian (113.0 – 126.3 Ma)
- Barremian (126.3 – 130.8 Ma)
- Hauterivian (130.8 – 133.9 Ma)
- Valanginian (133.9 – 139.4 Ma)
- Berriasian (139.4 – 145.0 Ma)

these areas show a change of sedimentation conditions and an oceanic influence. In the Albian, the sea space in north-western Germany continued to expand /AME 07/. Fig. 2.4 offers an overview of the Lower Saxony Lower Cretaceous Basin.

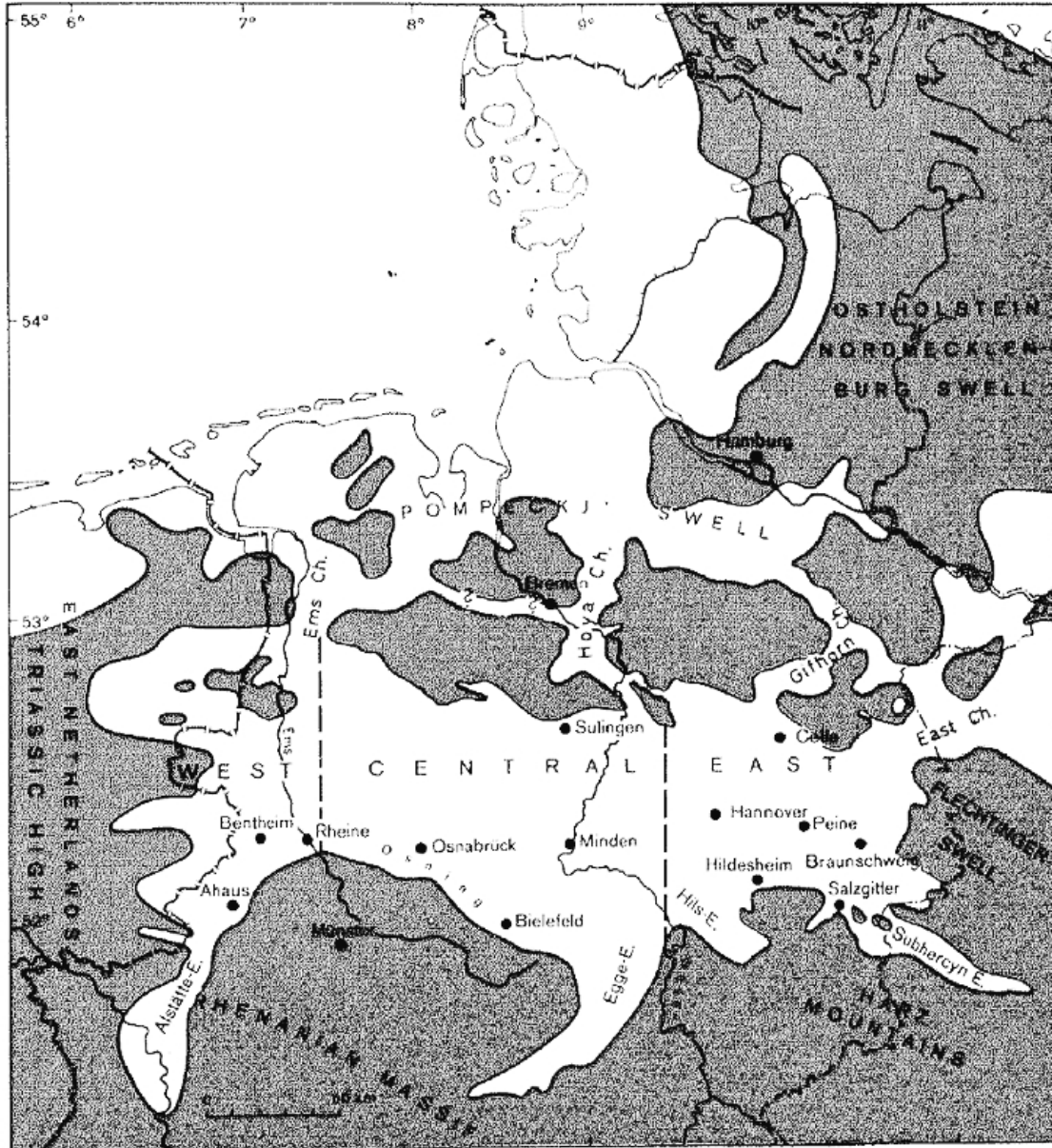


Fig. 2.4 Western, central and eastern part of the Lower Saxony Lower Cretaceous Basin (/KEM 73/)

Only in a part of Northern Germany are the clay deposits suitable for a repository. Preliminary criteria were developed by /HOT 07/. These include thickness and depth. Regions worthy of investigation cover a strip in southern Lower Saxony and some smaller

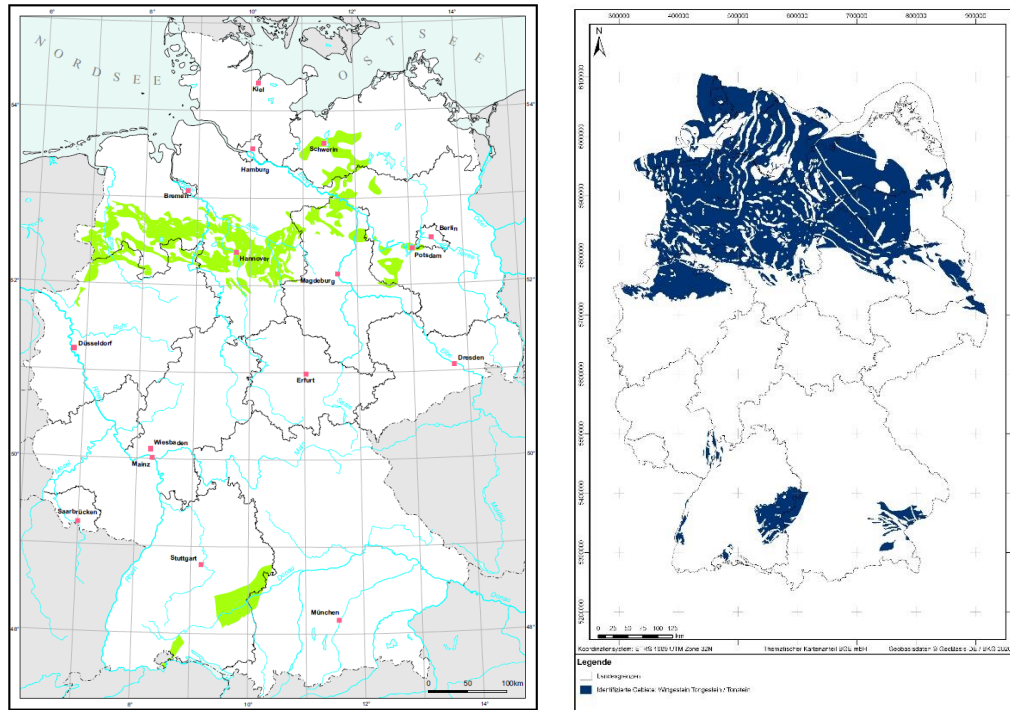


Fig. 2.6 Regions worthy of further investigation during the site selection process. Left: /HOT 07/ right: /BUN 20/

2.2.2 Mineralogy

The mineralogical composition of the clay rocks from the Lower Cretaceous is known from several localities in the eastern part of the Lower Saxony Lower Cretaceous Basin. Detailed descriptions may be found in /AME 07/ and /JAH 13/. The drillings Wichendorf 1/86, Hoheneggelsen KB9 and Ahlum 1 /MÜL 95/, the clay pit Hoheneggelsen (/LIP 55/) and Sarstedt /KEM 78/ as well as the drillings in and around shaft Konrad were used among others for this purpose.

The main minerals of Lower Cretaceous clay are quartz, feldspar, calcite, pyrite, gypsum, montmorillonite, illite, mica, kaolinite, chlorite as well as mixed layered clay minerals. Dolomite/ ankerite and siderite are found only locally. Dominant phases in the eastern part of the Lower Cretaceous Basin of Lower Saxony (Hauterivian and Barremian) are layered silicates (35 % to 52 %), quartz (13 % to 30 %) and carbonates (calcite, dolomite and siderite, 7 % to 55 %) (see /JAH 13/: Tab. 28 to 30). The transition zone Barremian/ Aptian shows increased smectite and alternating storage mineral contents. These again increase from the sub-Albian /JAH 13/.

The compositions of the clay rocks in the Hauterivian and Barremian can be found in Tab. 2.2 and Tab. 2.3 /JAH 13/.

The water content was determined on rocks of the sub-Barremian. It turned out that it was almost exclusively pore water. The content of water in the intermediate layers of smectite and illite is between 0.7 wt.% and 6.7 wt.% with an average value of 5.6 +/- 1.1 wt.% water /JAH 13/. Gerardi /GER 86/ stated that considerable pyrite contents can be detected in the Hauterivian and Barremian, occurring in locally detectable pyrite nodules and veins. The organic carbon content is most pronounced in the laminated shales of the sub-Barremian. Here values of up to 3.83 % can be detected (/MAT 91/, /JAH 13/).

Bensch and Hild dealt with the drill core of the Hoheneggelsen KB40 /BEN 98/, /HIL 00/. It showed a sequence of clayey-marly, partly laminated sediments of the early Lower Aptian, a clayey-dendritic mixture with different amounts of carbonate. Illite with an average content of 55 % in the fraction < 20 µm was the main component of the clay minerals. This was followed by kaolinite (28 %) and chlorite + vermiculite/illite alternating bearing minerals (17 %). Furthermore, /HIL 00/ described the drilling Kirchrode II/94, which consisted of clayey, slightly silty, partly brightly coloured sediments of the lower and middle Alb and grey, lithologically very uniform clays and clay marls of the upper Alb. Altogether the sediments were a mixture of clayey-dendritic material and bio-genetic carbonate. The dendritic material showed a high clay mineral content of up to 90 % /BEN 98/. The carbonate content is 15 – 34 %.

A characteristic property of Lower Cretaceous clay in Northern Germany is its content of organic carbon. Its concentration reaches a level of up to 30 %, especially in the Berriasian (Weald) interval. High organic carbon is typically correlated with high pyrite content (up to 11 %). In other intervals, the organic carbon content may be as low as 0.25 % and accompanied only with traces of pyrite /AME 07/.

Tab. 2.2

Ranges of the composition of clay rock in Hauterivian and Barremian in the sediments encountered in the Konrad 1 well /JAH 13/

Mineral	Hauterivian				Barremian					
	Lower Hauterivian		Upper Hauterivian		Lower Barremian		Medium Barremian		Upper Barremian	
	Range	Mean	Range	Mean	Range	Mean	Range	Mean	Range	Mean
Quartz	4 - 29	13	17 - 29	23	6 - 49	25	23 - 37	30	20 - 31	26
Feldspar	2 - 4	3	1 - 3	2	2 - 7	3	1 - 2	2	1 - 10	3
Muscovite/Illite	2 - 27	15	20 - 36	23	15 - 37	23	10 - 23	16	15 - 25	19
Kaolinite	2 - 15	8	12 - 20	15	4 - 23	13	14 - 24	19	15 - 27	20
Chlorite	2 - 8	4	6 - 8	6	2 - 8	5	5 - 6	5	5 - 10	8
Smectite	2 - 6	4	2 - 2	2	-	-	3 - 3	3	-	-
Mixed Layer	3 - 5	4	-	-	5 - 8	6	5 - 10	8	5 - 5	5
Σ clay minerals		35		46		47		51		52
Gypsum	2 - 2	2	-	-	2 - 12	7	2 - 2	2	2 - 5	4
Pyrite	1 - 8	5	2 - 9	5	3 - 33	8	3 - 8	5	2 - 9	5
Calcite	14 - 79	36	5 - 31	17	1 - 24	8	1 - 6	4	1 - 3	2
Dolomite	6 - 8	7	2 - 6	5	3 - 10	5	7 - 7	7	4 - 5	5
Siderite	12 - 12	12	-	-	3 - 14	6	-	-	-	-
Σ Carbonates		55		22		19		11		7
Goethite	20 - 20	20	-	-	3 - 3	3	-	-	-	-
Apatite	-	-	-	-	2 - 3	3	3 - 3	3	-	-
X ray amorphous Components	5 - 22	13	3 - 19	8	1 - 15	9	4 - 36	19	1 - 31	16
Organic Material	-	0,4	-	0,7	-	1,85	-	3	-	1,5

Tab. 2.3 Ranges of the composition of clay rock in from the Upper Barremian from the Wichendorf 1/86, Hoheneggelsen KB9 and Ahlum wells /JAH 13/

Mineral	Wichendorf 1/86		Hoheneggelsen KB9		Ahlum 1		Ahlum 1		Ahlum 1	
	Upper-Barremian		Upper Barremian		Upper Barremian		Middle Barremian		Upper Barremian	
	Range	Mean	Range	Mean	Range	Mean	Range	Mean	Range	Mean
Quartz	6 - 9	11,7	5 - 16	12,0	11 - 13	12,3	-	15	-	10
Feldspar	-	-	-	-	-	-	-	1	-	1
Muscovite/Illite	3 - 58	34,3	22 - 25	23,7	6 - 34	24,0	-	20	-	20
Kaolinite	12 - 28	19,1	9 - 24	18,7	17 - 25	21,7	-	20	-	20
Chlorite	0 - 3	0,4	0 - 0	0	0 - 0	0	-	10	-	10
Mixed Layer	-	-	-	-	-	-	-	-	-	-
Σ clay minerals		80,7		71,4		77,0		51		50
Gypsum	-	-	-	-	-	-	-	-	-	-
Pyrite	2 - 10	4,0	2 - 6	3,7	1 - 5	3,0	-	1	-	5
Calcite	0 - 10	3,6	0 - 39	13	0 - 23	7,7	-	10	-	(20)
Dolomite	-	-	-	-	-	-	-	5	-	1
Siderite	-	-	-	-	-	-	-	-	-	-
Σ Carbonates		3,6		13		7,7		7,72		3,85
X-ray amorphous components	-	-	-	-	-	-	-	15	-	10
Organic material	-	-	-	-	-	-	0,81 - 3,06	1,9	-	3,21

The montmorillonite/ smectite content of northern German Cretaceous clay sediments is much lower than in the Jurassic clay sediments considered as a host rock for an HLW repository at Bure (Callovo-Oxfordian, France) and Benken (Opalinus, Switzerland). At these two sites smectite constitute a significant part of the overall mineral composition /WEN 08/, /LER 11/.

2.2.3 Change of predominant clay minerals

Regarding the predominant clay minerals in Lower Cretaceous clay formation, analysis from a range of near-surface locations revealed that clay from the intervals Hauterivian to Barremian mostly consists of kaolinite (35–42 %), illite (50–58 %) and calcite (4–6 %) and rarely some chlorite. Montmorillonite is present only in minor amounts (2–3 %). It dominates in Aptian and younger sediments (up to 70 wt.-%) at the expense of the kaolinite fraction, especially in the fine fraction (<0.63 µm) (Fig. 2.7).

These findings were confirmed by an analysis of clay sediments from drillings around the Konrad mine /BRE 82/, /ECK 91/, /GAI 81/. It clearly showed that there is a sharp change in the mineralogical composition at the border between Aptian and Albian sediments. While clay stones up to Aptian consist almost exclusively of illite and kaolinite, smectites are the dominating clay minerals in younger formations (Fig. 2.8). Data differ a little bit. According to Brewitz, Aptian sediments show a very low smectite content /BRE 82/. Eckhardt found that the rather thin Aptian layer contains both smectite-rich and smectite-poor samples /ECK 91/.

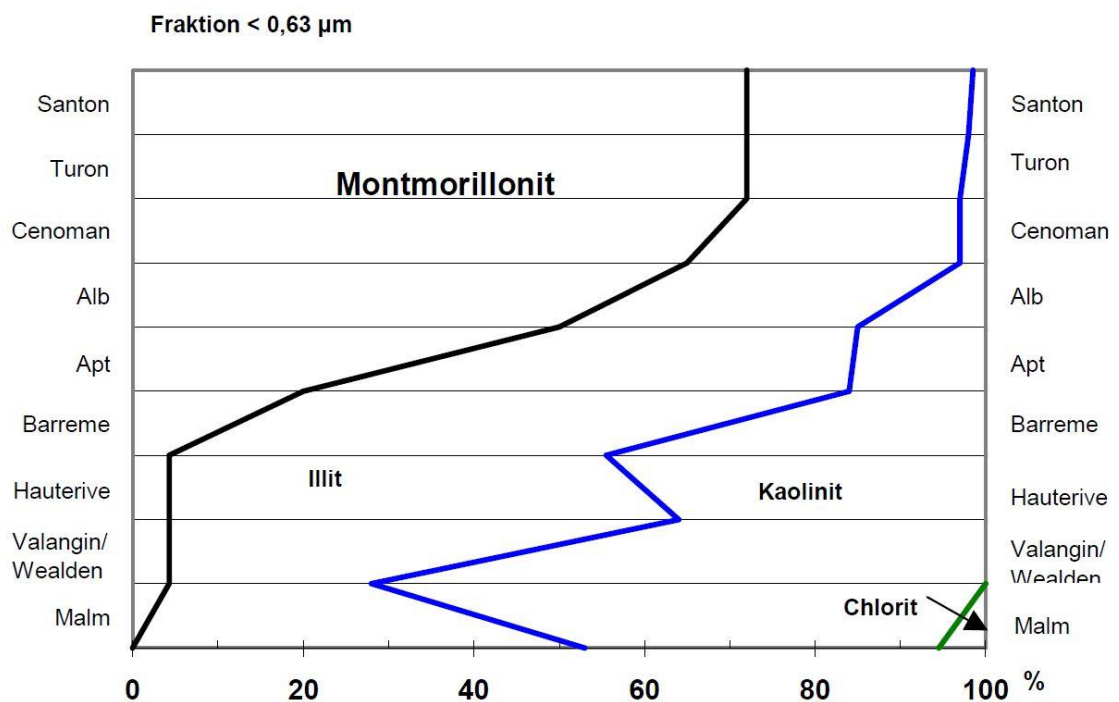
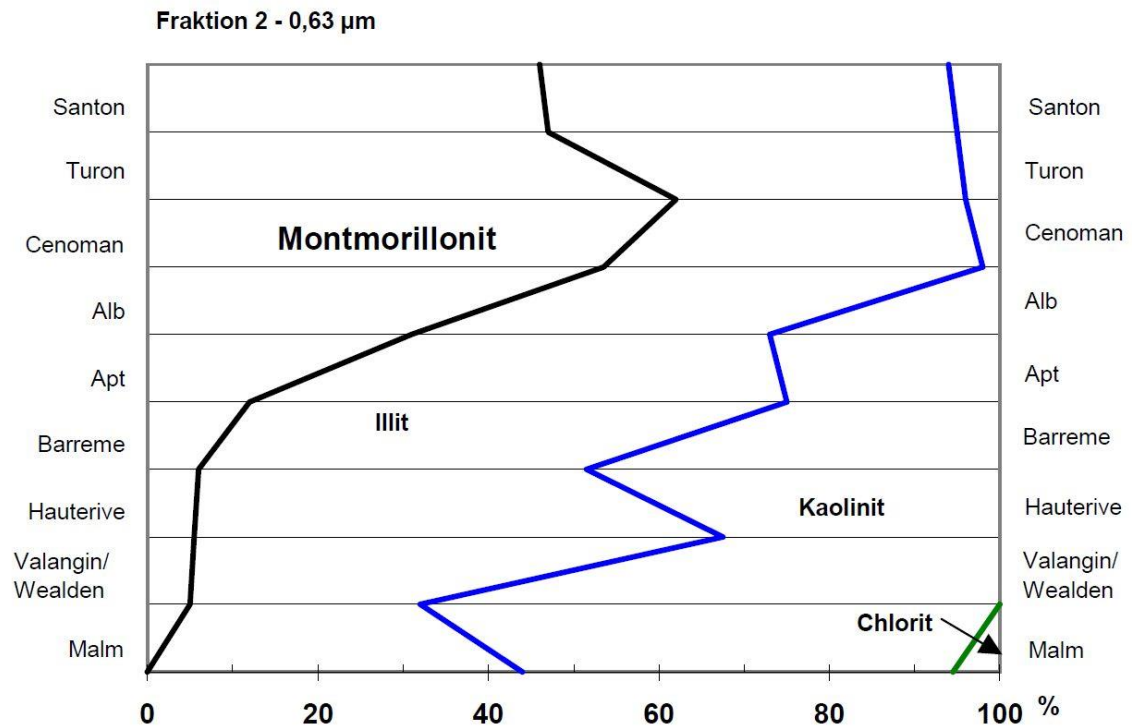


Fig. 2.7 Composition of clay minerals of Malm (Upper Jura) to Santon (Upper Cretaceous) in near-surface Lower Cretaceous clay samples (/AME 04/ based on /BRO 76/)

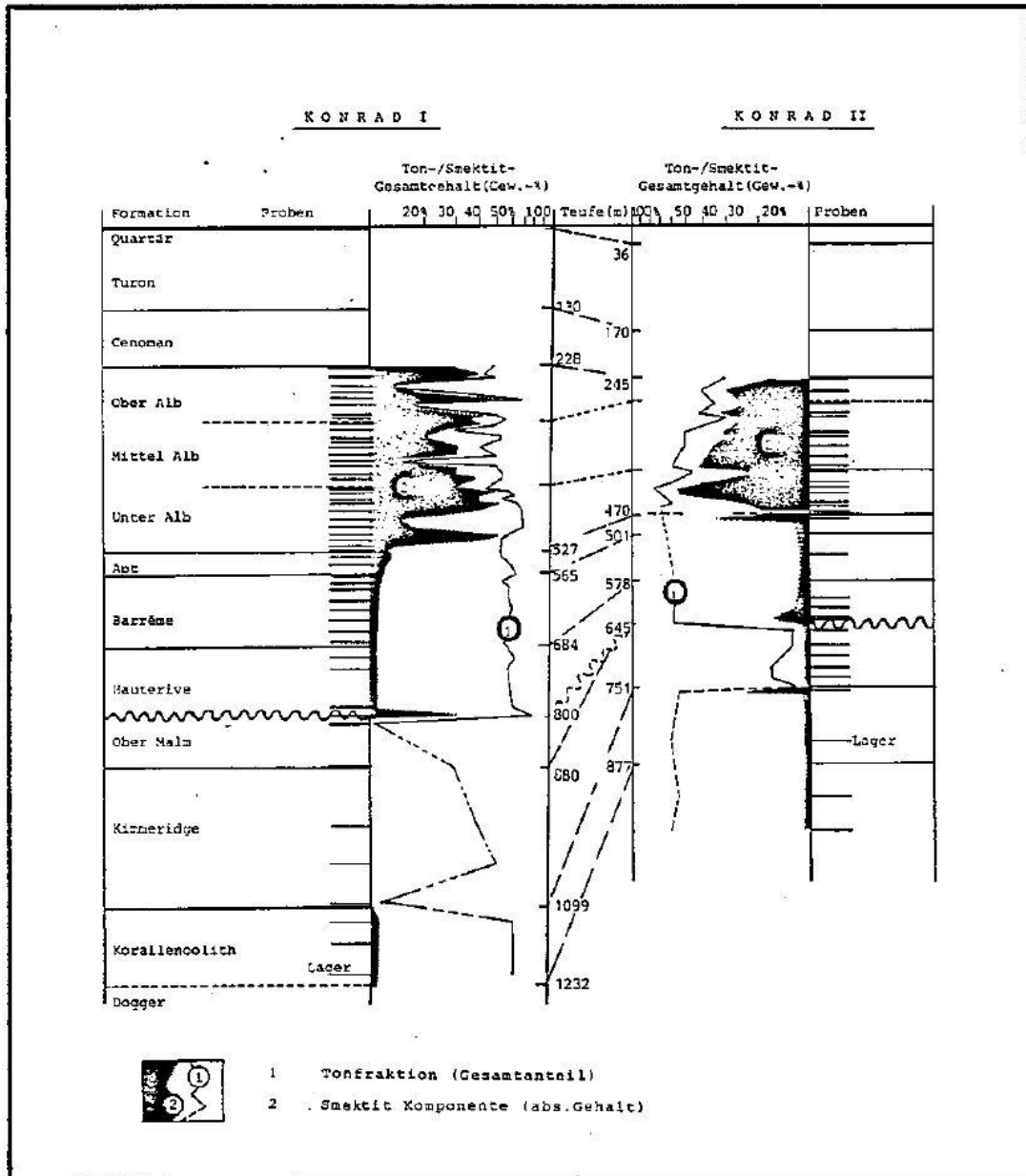


Fig. 2.8 Content of smectites (thick black line) and clay minerals (thin black line) in Hauterivian to Albian sediments at shafts 1 and 2 of the Konrad mine /BRE 82/

2.2.4 Alteration of minerals during excavation, storage and reuse as back-fill

In the concept developed in the AnSichT project, it was planned to use clay previously excavated as a buffer in the boreholes and the as backfill in the drifts. It may need to be mixed with bentonite from other sources to achieve the desired technical properties (especially concerning swelling). So far, it has not been investigated how the original anoxic clay would alter when stored for several years or even decades at the surface. If exposed to air and weather part of the clay would most probably be subject to mineralogical alterations. Fe(II) containing minerals such as pyrite, siderite, or Fe(II) containing clay minerals may be partially or fully oxidised leading to a change of pH and Eh. The organic content of the clays in combination with the increased specific surface and the access of oxygen will activate or attract bacteria. If the clay is stored openly without covering, rain-water would intrude into the clay and wash out the salt content. Moreover, the clay heap could become a biotope for plants and animals.

Moving clay from the underground mine to the surface will have an effect both on its chemical as well as its physical and mechanical properties. These effects, as well as the interactions of altered clay with the other components of the repository near-field, cannot be quantified now and mandate further investigations in the future.

2.2.5 General considerations on the genesis of the pore water chemistry of the Lower Cretaceous clays in Northern Germany

Origin of salinity of pore waters in deep clay formations

The clay formations in the North German basin are marine sediments that were in direct contact with brackish or seawater at the time of their formation. This is also indicated by the chemistry of the pore waters in comparison to seawater, where the same chemical elements occur. The composition was changed by diagenetic or, at higher temperatures, also metamorphic processes. Furthermore, the supply and mixing with fluids from other stratigraphic horizons must be considered /WOL 11/.

Compared to the composition of seawater, however, sulphate and magnesium are depleted. Sulphur can be reduced from sulphate to sulphide in an early phase by sulphate-reducing bacteria and is therefore bound in iron sulphides. The extent of the sulphate

reduction depends on the available quantity of oxidizable organic substance. Waters in the vicinity of oil deposits are often found to be completely free of sulphate /ENG 73/.

The decomposition of organic matter led to increased carbonate concentrations, which bound magnesium via intermediate stages in dolomite. The concentration of calcium was increased (released from sulphates or replaced by Mg in carbonates). Drastic increases of the secondary elements can be observed (e. g. Li, Zn, /ENG 73/), which were probably caused by the addition of sediments rather than by the contents in seawater. The increase of iodine could be attributed to the decomposition of iodine-rich organic matter. Calculations by Engelhardt (l.c.) suggest a reduction of up to 90 % of the initially existing pore volume.

Another important phenomenon is the chemical change of the pore solutions during the sinking of the clay formations and the resulting increasing lithographic pressure. As the depth of the clay layers increases, the pressure increases and compaction takes place, reducing the pore space at the same time.

The salinity of the clay pore waters is essentially a product of the latter process. Sodium and chloride are not chemically bound into or dissolved from clay or any of its mineral components. The content of these two ions is therefore exclusively due to the original seawater and the subsequent physical processes.

Different salt concentrations in clay pore waters and in waters in accompanying porous sediments

When estimating the salinity of clay pore waters in the Lower Cretaceous, it was often assumed that there was a correspondence between the concentrations in the accompanying porous sandstones (e. g. Hils sandstone) and the clay layers /NOW 13/. Moreover, the depth-dependent salinity gradient found in water-bearing, permeable formations was often applied to the surrounding claystone as well. An evaluation of the literature now showed that this simple picture does not apply.

Analyses of clay pore waters, especially those from great depths, are still an exception. Despite intensive drilling activities for oil and gas exploration that has taken place since the 19th century, information on pore water chemistry is rather scarce because the primary object of chemical analysis were those waters that accessed the borehole through porous media such as sandstone or limestone.

It took a relatively long time before it became clear that there can be a significant difference between the solution composition of water-bearing layers and clay pore waters. One of the few investigations extending over many hundreds of metres was carried out by Schmidt /SCH 73/ in two oil fields in the Louisiana Basin. On the basis of these data, Chilingarian /CHI 94/ showed that at a depth of 1000 m a total salt content of 10 to 20 g/l is found, while the accompanying sandstones had salinities of 120 to 160 g/l. Similar results were obtained from deposits in other geological regions of the world. At depths between 2000 and 14000 ft (600 to 4300 m), the ratio of chloride concentration in sandstone to claystone was between 10 and 20 /CHI 76/.

Like the Louisiana clay sediments, clay deposits in the Northern German Basin are of marine origin. We could find only one published source that gives information on their pore water chemistry. Von Engelhardt /ENG 63/ reported high saline clay pore waters in drill cores from Jurassic sediments (Malm to Liassic). They have similarly high salt concentration like the solution samples from nearby sandstone formations (Tab. 2.4).

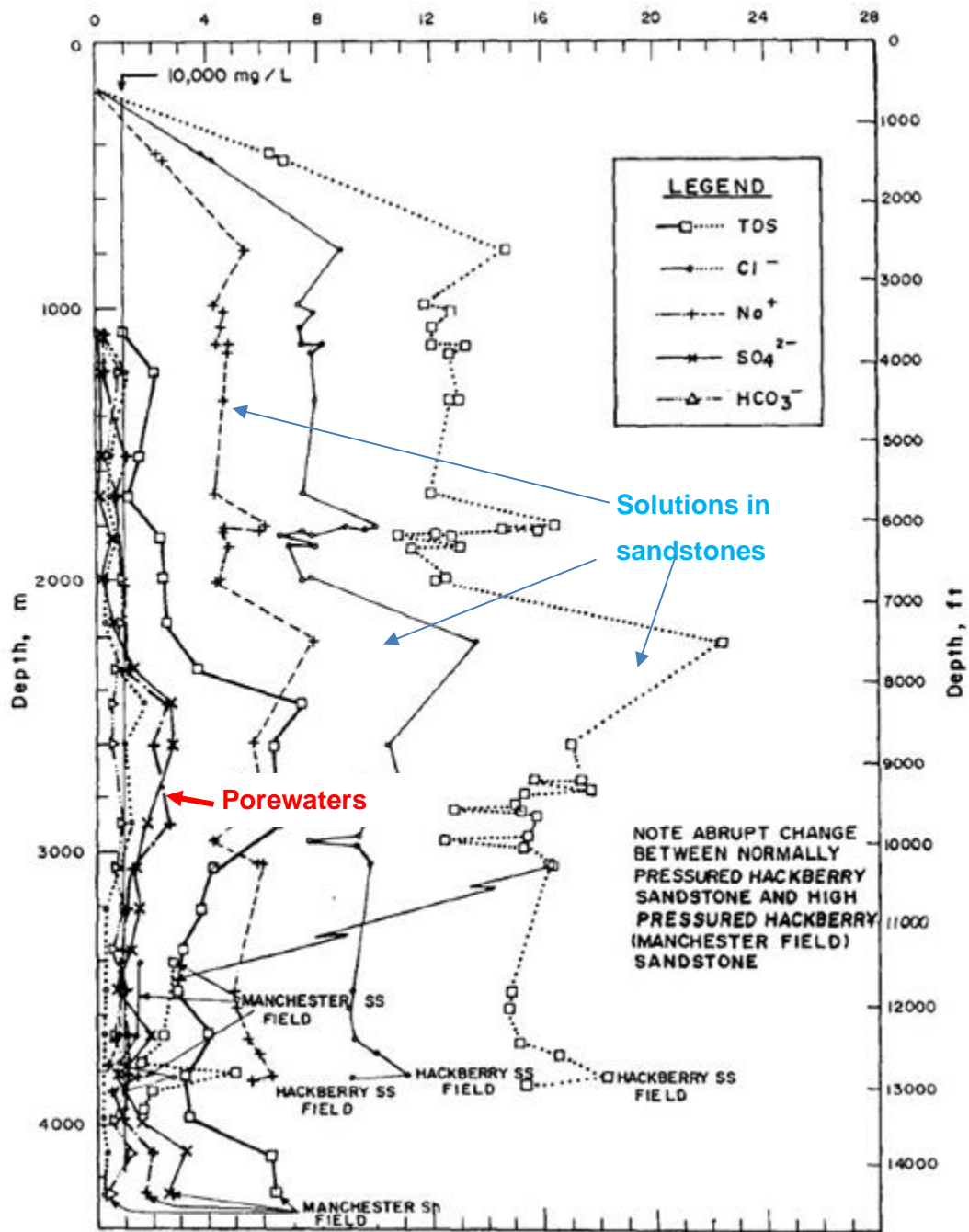


Fig. 2.9 Composition of clay pore waters and solutions in the accompanying sandstones in the Louisiana Basin (in /CHI 94/)

Tab. 2.4 Analyses of clay pore waters and accompanying waters from the North German area /ENG 63/

<u>Malm</u>			<u>Permeable marls</u>		
	<u>Shales</u>			<u>Permeable marls</u>	
	Depth m	Aeq.Cl/l		Depth m	Aeq.Cl/l
Aldorf	1111-16	3,1	Barenboedel	830	5,3
"	1076-80	3,5	Lingen	975	5,4
"	1080-86	4,3	Barenburg	1035	3,5
"	1071-76	5,6	Scheerhorn	1412	4,7
<u>Dogger</u>			<u>Sandstones</u>		
	<u>Shales</u>			<u>Sandstones</u>	
	Depth m	Aeq.Cl/l		Depth m	Aeq.Cl/l
Vorhop 29	1450-56	1,8	Kronenberg	625	3,0
Vorhop 34	1375-80	2,3	Rühme	600-750	2,3
"	1381-85	4,6	Wesendorf	500-1000	3,4
"	1404-06	2,5	Lüben	1275	3,3
			Elsfleth	1560	2,8
<u>Liassic</u>			<u>Sandstones</u>		
	<u>Shales</u>			<u>Sandstones</u>	
	Depth m	Aeq.Cl/l		Depth m	Aeq.Cl/l
Vorhop-Kn.	1820-31	3,1	Eldingen	1500-1600	2,9
			Wesendorf	1900	3,6

(Sea water: 0,53 Aeq.Cl/l)

Development of pore water chemistry during compaction of marine clay sediments

Why are the salinities in Northern German Jurassic sediments so much higher than in the Louisiana Basin? The diagenesis of the sediments may give an answer to that. It includes early settling and subsequent compaction due to the increasing amount of younger sediments that cover the older. The process of compaction of marine clay deposits has been investigated in detail in laboratory experiments with montmorillonite slurries in salt solutions /KRY 63/, /ENG 63/, /CHI 73/, /ROS 76/. For this purpose, clays were first washed with distilled water and then mixed with a salt solution of known concentration. The solution was then gradually pressed out by applying pressure.

It was found that the initially pressed solutions had the same or a higher salt concentration than the original starting solution. Thus, some of the water is initially retained. At higher pressures (up to 800 bar) the salt load of the effluent more and more decreased. For example, von Engelhardt /ENG 63/ obtained only a 0.2 molar NaCl solution at 800 bar, whereas the starting solution had 1 mol/l. At pressures above 800 bar, the effect was reversed, and the concentration of the solutions pressed out rose again. However,

according to /CHI 94/, this could not be confirmed by any other investigators. Remarkably, the final porosities achieved in the squeezing tests do not depend on the initial salt concentration.

According to /ENG 63/ the observations can be explained by the fact that the water in clay slurries is distributed between the free pore solution (slightly increased concentration) and the double layer around the clay particles (low salt concentration). Initially, the somewhat saltier solution is squeezed out of the free pores between the particles, but with increasing pressure, more low-salt solution is released from the double layers. The authors further assumed that at the same time the flow paths close and become impermeable to ions. Internal filtration then takes place so that the salt concentration increases in the remaining pores. The concentration could lead to local precipitation of halite.

The effect of salinity decrease is much less pronounced in kaolinitic clays than in smectitic clays, as shown in Fig. 2.10. Squeezing tests with seawater-saturated clay samples lead only to a slight reduction of the salinity of the squeezed solutions, even at very high pressures and low residual water contents /KRY 63/. Chilingarian /CHI 94/ stated that even at high pressures the distance between individual kaolinite particles at 80 Å is still significantly greater than that of the double layer. In this case, the particle boundaries remain passable for hydrated ions. It can be concluded that the clay pore waters in kaolinitic clays are in exchange with the waters in sandstones. In this case, salt concentrations above the seawater concentration are also possible.

This approach could also explain the high salt content of clay cores (shale/ claystone and marl) from the Northern German Basin (Jurassic sediments from Malm, Dogger, and Lias) at depths between 500 and 1900 m. Malm and Dogger sediments are also reported to be low in smectites /ECK 91/. They contain pore waters with total equivalent concentrations of up to 1.8 to 5.6 mol/l /ENG 63/. It must be stressed that the authors' method to calculate the pore water salinities includes several uncertainties and must be considered with care. For example, the calculated pore volume is based on measurements of the evaporation loss at 105 °C. At this temperature, part of the interlayer water, absorbed water, but also hydrate water is evaporated. This water cannot be assigned to any pore space with a free solution. If pore water is present at all, the amount is probably quite small. On the other hand, the eluted ions can have different origins: deposited in the intermediate layers, sorbed on surfaces, bound in soluble salts or from free pore space. The elution experiment thus provides information about a mobilizable ion-water ratio but

does not necessarily fully corresponds with the real pore water concentration. Nevertheless, the calculated concentrations are very high and may be close to saturation of halite.

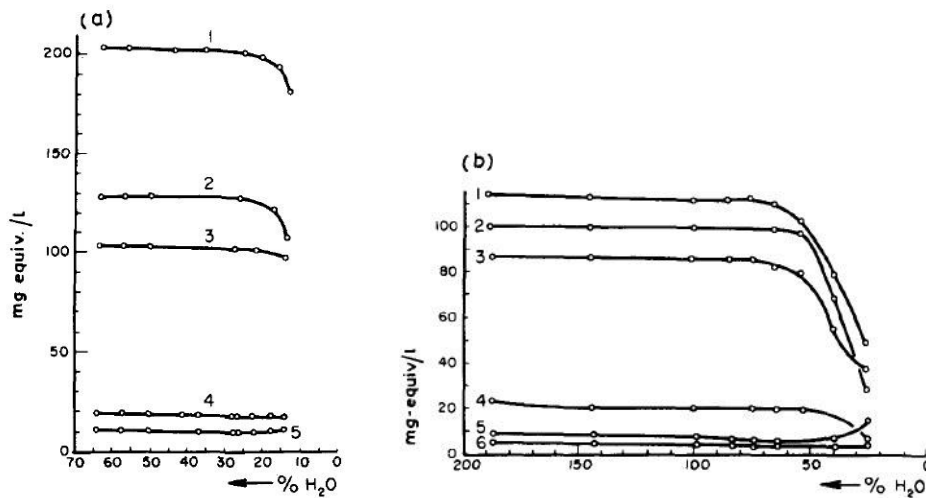


Fig. 2.10 Composition of pressed solutions as a function of the residual water content of compacted clay samples - (a) kaolinitic clay (b) smectitic clay /KRY 63/, /CHI 94/

Higher salinities in porous sediments because of ultrafiltration?

As long as the porous aquifers are not in contact with surface waters that supply fresh-water, salt concentrations can also be found here that exceed seawater. This seems contradictory at first sight, as less salty water was pressed out of the clay formations. If these solutions had been pressed into sandy layers, one would have to find lower salt concentrations here. The opposite is the case, as numerous examples of formation waters from water-bearing layers in German Lower Cretaceous formations show /MÜL 75/, /WOL 11/.

One explanation would be that the solutions pressed out of lower clay layers were ultra-filtered during the vertical, ascending penetration through the sand formation into the next clay layer, so that the ion content was mainly retained in the sand layers /ENG 61/, /HAN 73/. However, it must be remembered that salt solutions that are pressed out of a clay layer can also be pressed back into a similar clay layer under the same pressure conditions. When a solution rises vertically, the only difference between a higher and a lower clay layer is a small difference in lithostatic pressure and an even smaller difference in hydrostatic pressure. Pressing ions into the upper layer would then be somewhat more difficult, and the filter effect would, therefore, be somewhat higher than for the lower

layer. On the other hand, the filter effect decreases with increasing concentration so that the pressure effect should be compensated from a certain concentration on /HAN 73/.

If one follows this logic, the following relationship will result: The pressure difference depends on the thickness of the intermediately stored porous layer. The larger the layer, the greater the pressure difference, the greater the filter effect and the higher the attainable concentration. The observed concentrations in pore waters do not depend on the thickness of the porous formations, but on the depth /MÜL 75/ /CHI 94/. Ultrafiltration may, therefore, play a role in the genesis of the saline solutions found but does not explain the depth-dependent concentration profile.

The observations are more likely to be consistent with the squeezing tests described above. If, after initial salt removal, salt is again concentrated in the compacted clays at higher pressure, the final concentration of the last solutions pressed out should depend on the depth.

On the other hand, the frequently observed changes in the isotope ratios of hydrogen and oxygen in deep waters show that the aquifers must have been in contact with surface waters at least temporarily after their formation /ENG 73/, /NAU 00/.

High salt concentrations due to leaching of salt formations?

The high salt concentrations in formation waters are also conceivable because of subrosion of neighbouring salt formations. Depending on the hydraulic conditions such an explanation seems plausible.

On the other hand, it could be shown that the salt content of formation waters decreased significantly again within a few kilometres of a salt dome /ENG 73/. Also, the composition of the saline solutions stored in the coral lithic rock of the Konrad mine cannot be attributed to the dissolution of evaporites of the Broistedt salt dome a few kilometres away /BRA 93/.

The fact that the clay formations act as an internal filter and retain rather than absorb salt also speaks against this thesis. Elevated salt contents have also been found in areas where no salt deposits are present /ENG 73/.

On the other hand, Naumann /NAU 00/ argues that the salinity of North German deep waters due to the bromide-chloride ratios as well as the boron isotope distribution can be attributed primarily to the leaching of evaporites. For him, the most plausible explanation seems to be the leaching of deposited evaporites by meteoric waters.

There is a whole series of other attempts to explain the occurrence of saline solutions. They are discussed in more detail in /CHI 94/.

Resume

Even from this small literature review, it becomes clear that the question of the composition of saline deep waters, especially in clay formations, can by no means be regarded as clarified. But for time being it seems plausible that clay formations with a high smectite content tend to have rather low salinities whereas formations, where such minerals are lacking quite high salinities, have to be expected:

- a) If the repository is located in Albian or younger formations weakly saline clay pore water with a mineralisation around 10 g/l may be present
- b) If it is located in Aptian or older formations, a more concentrated pore water is possible. The measurements by von Engelhardt /ENG 63/ showed a concentration of up to 5.6 mol/l chloride for clay samples at depths of 1000 to 1100 m. This corresponds to halite saturation and represents an upper concentration limit. The lower limit would be a solution composition near the seawater salinity (0.5 mol/l). Historical contact and dilution with meteoric waters may have caused even lower salt concentrations (depending on depth).

After the closure of the repository, the following three solution scenarios result

1. If the repository is excavated in kaolinitic clay rock, but the backfill is carried out with salt-free smectitic clay, the liners are initially only in contact with the residual moisture of the smectitic clays. Saline solutions penetrating from the formation generates a relatively low swelling pressure in comparison to pure water /HER 02/ so that the sealing effect only sets in late. At high compaction, the smectitic clays only allow diffusion of dilute solutions, while outside the backfill layers a concentration takes place (possibly even with mineral precipitation) (scenario 1a: 10 g/l). However, if the sealing effect starts with a delay, the saline solution can also penetrate to the inner liner and later to the containers (scenario 1b:

0.7 mol/l Cl, 1c: 5 mol/l Cl). The same applies to the hypothetical case of a saline solution inflow from an accompanying sandstone.

2. If the backfill is done with clay from the same formation, saline solutions will penetrate to the liners and later to the containers, irrespective of the swelling behaviour (scenario 2a: 0.7 mol/l, 2b: 5 mol/l Cl).
3. If the repository is located in smectitic clay rock, only weakly saline solutions are expected at the liners, irrespective of the type of clay materials used for backfilling (scenario 3). If there is an inflow of saline solutions (from an undiscovered solution reservoir in the sandstone activated after the closure of the repository), the developments in scenarios 1a) to 1 c) follow

The following questions are still open:

- What is the composition of North German Lower Cretaceous clay pore waters? As far as can be seen, the only data available so far are for Jurassic clay formations (Upper Jurassic/ Malm)
- How does the pore water composition change during excavation and re-compaction? Excavation leads to a partial drying out of the clays. However, it is not clear which effect occurs with salty clays, as they could be hygroscopic due to the CaCl_2 content.
- How is the composition of formation waters related to the composition of the accompanying aquifers with the pore waters? If the clay acts as a filter, the compositions can differ considerably
- Can the saline pore waters of compacted clays in the disturbed zone be mobilized during or after the operating phase? The small pore volumes should not lead to considerable solution inflows, but the interaction of excavation-damaging, drying, hygroscopic effects and later saturation processes could mobilize saline solutions if porous cavities are present in the backfilled drifts.

2.2.6 Assumptions regarding the initial state of porewaters in a repository in Lower Cretaceous clay formations

2.2.7 Analytical data on deep groundwater samples in Northern Germany

As part of the preparation of a new site selection process that started in 1999, several studies were conducted which summarised and interpreted the analysis data available for deep groundwater horizons in Germany /BRA 02/ /BRA 01/. For some regions in Germany, including north-eastern German Lower Cretaceous formations a correlation between depth and salinity could be found. According to Müller /MÜL 75/, who summarized a vast number of analytical data gained on the area of the former German Democratic Republic, most of the waters in the Rhaetian - Lower Cretaceous/ Paleogene were of a Na-Ca-Mg-Cl intermediate type 1. The main components are Na, K, Ca, and Mg with the following relative concentrations:

- Na+K: 47-50 mval %
- Ca: 0-6 mval %
- Mg: 0-3 mval %

The compilation of Stober et al. /STO 14/ suggests that the relative Ca content of waters in Jurassic/ Cretaceous waters could be a little bit higher (Fig. 2.12).

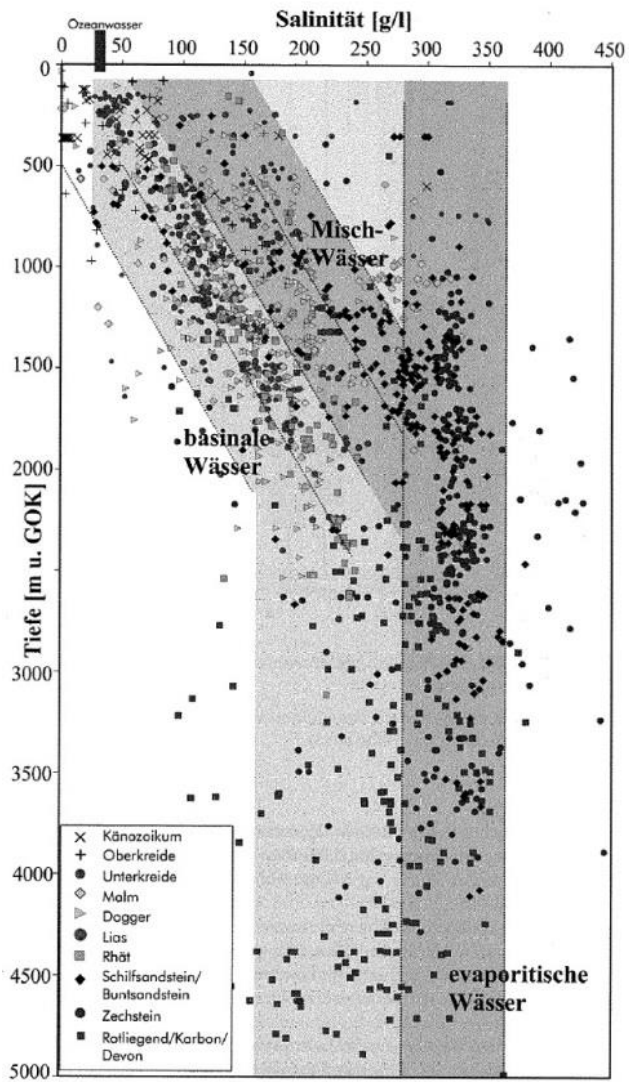


Fig. 2.11 Salinity of deep groundwaters in the Northern German Basin
/WOL 11/

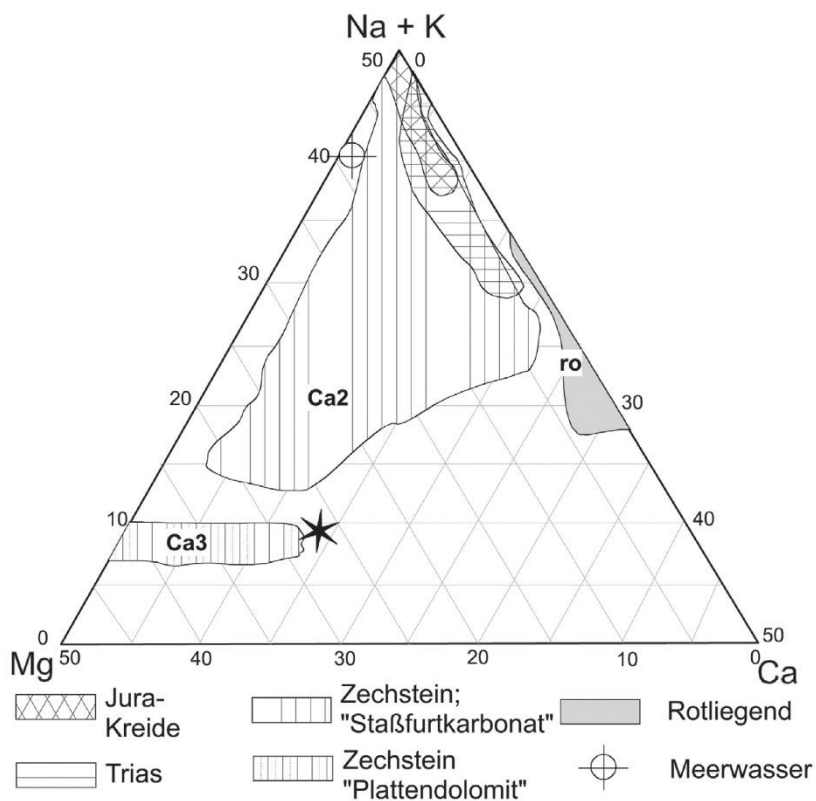


Fig. 2.12 Relative concentrations of Na/K, Ca and Mg in deep groundwaters of the Northern German Basin /STO 14/

Chloride is the main anion. Important minor components are Br^- , I^- , HCO_3^- , SO_4^{2-} , NH_4^+ , Sr and B. The pH in N German deep groundwaters is typically (80 %) between 5 and 7.5, but no information is given about the typical range found in Lower Cretaceous formations /WOL 11/. As a rule, the pH of clay pore waters is near-neutral independent of their origin /GAU 09a/.

Between 250 and 2400 m, the median salt concentration increases from 30 to 250 g/l (Fig. 2.11). For NE Germany the increase equals about 10 g per 100 m, in NW Germany 10-13 g/l is observed, but in the vicinity of salt stocks up to 20-25 g/ 100 m may occur /WOL 11/. However, it must be kept in mind that the majority of data was achieved as a result of oil and gas exploration that intentionally investigated the depressions around salt domes, so that the observed salinity and salinity/depth relation may not be representative for areas with considerable distance to such structures. Overall, the scattering of the depth/salinity relationship is considerable. It was assumed that this deviation is a

consequence of corrupted analytical data caused by a mixture of drilling fluids, dilution and inaccurate sampling /KLI 92/ /BRA 01/.

Brasser and Brewitz /BRA 02/ noted that there are almost no examples where the depth-dependent salinity has been investigated near one site (at least in Germany). The only known exemption they report on is the analytical data collected from drillings and springs in the region around the Konrad mine.

Brewitz /BRE 82/ summarized the analytical results of about 80 water samples collected from drillings and springs of the region Braunschweig-Salzgitter-Peine. Unfortunately, the sources of these data and the origins of the pore water samples are not given in the report. Moreover, instead of individual data sets, ranges are printed for each stratigraphic interval. Tab. 2.5 shows the ranges for the three Lower Cretaceous intervals reported in the study. The maximum Na concentration (117000 mg/l = 5 mol/l) corresponds to a saturated halite solution. Some more details were given for one sampling point at a depth of 469 m (Albian), which is located in a clayey-sandy rock layer. It corresponds to the aquifer occurring elsewhere as Hils sandstone. Initially, large quantities of water (500 l/min) escaped from it, which were strongly pushed back by sealing measures. According to its source, the water is addressed as 'Hils water'. /BRE 82/ reports data on the composition for 20 years (Tab. 2.6). Although there seems to be some variation from sampling to sampling the overall composition remained the same. The total concentration is about 150 g/l mainly consisting of NaCl, CaCl₂ and MgCl₂.

A graphical representation of the Konrad data was presented by Klinge et al. /KLI 92/ (Fig. 2.13). It shows a clear linear trend of salinity in relation to depth across different geological formations. It should be noted, though, that all samples are related to identified water-bearing layers in the formation and do not represent clay pore waters.

/BRA 02/ stress that the gradient may be different at other sites. This is confirmed by /KLI 92/ who compared the gradient with results from other drillings in Northern Germany (Fig. 2.14). The Konrad gradient also differs from the data from von Engelhardt /ENG 60/ (Fig. 2.15).

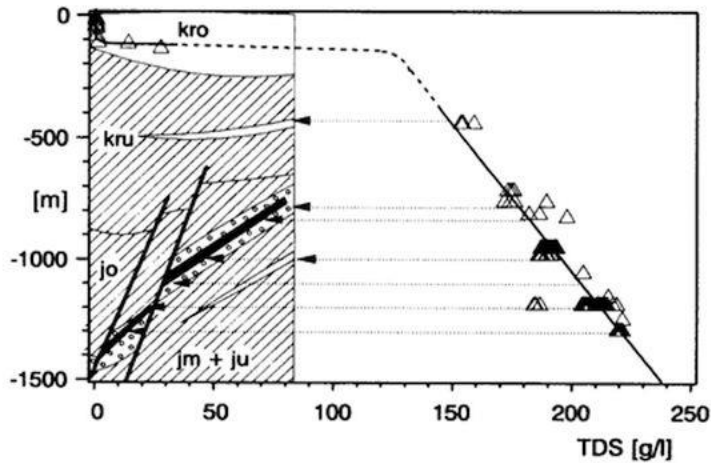


Fig. 2.13 Water analyses from drillings in the Lower Saxonian Basin (/KLI 92/)

Tab. 2.5 Pore water compositions of drillings in the region around the Konrad mine /BRE 82/

Formations	Valanginian (1953)	Valanginian	Berriasian
------------	--------------------	-------------	------------

No of analyses	1	15	16
Concentration	[mg/l]	[mg/l]	[mg/l]
Na	1300	41000-117000	14600-65500
Li		2.3-7.3	12
Ca	784	2350-17500	640-6000
Mg	71	540-3340	1480
K		260-600	100-1500
Sr			60-406
Cl	2059	63000-181000	24350-122000
SO ₄	1787	830	160
Br		565	194
BO ₃		79-107	80
I		10.4	7.8
pH		6-6.7	5.5-7.0

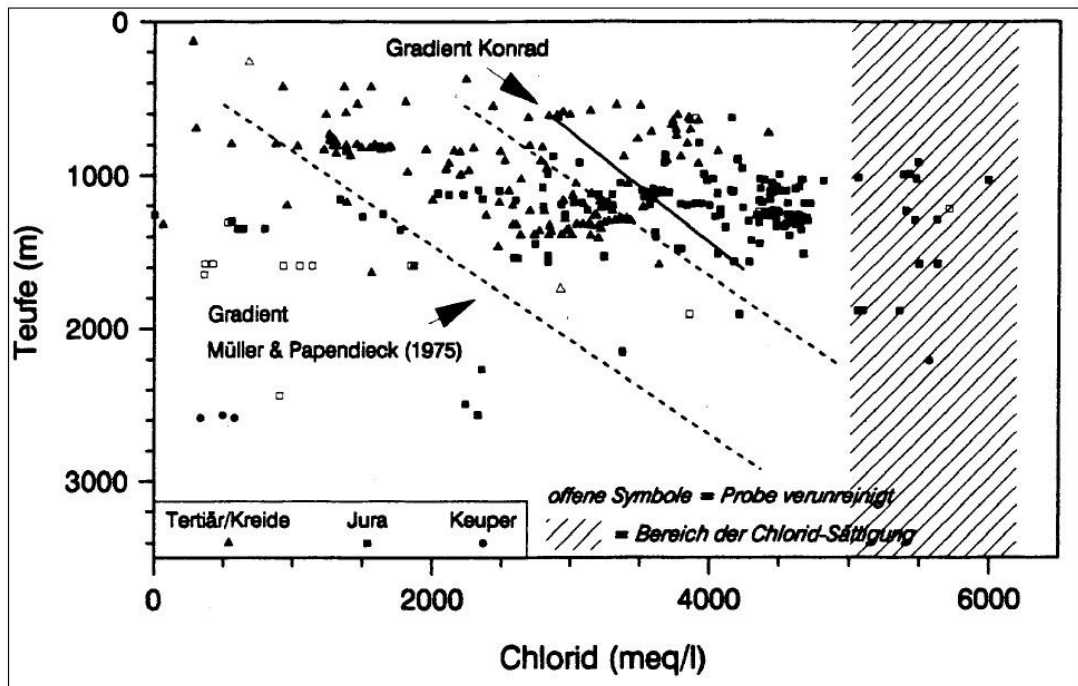


Fig. 2.14 Total salt concentration of water samples in boreholes around the Konrad mine as a function of depth /KLI 92/

Tab. 2.6

Composition of solutions in the Hils sandstone, 480 m /BRE 82/

Formation	Hilssandsteinbank Schacht Konrad 2									
Datum	1961	1964	1965	12.05.75	12.05.75	11.05.76	11.07.78	04.07.79	19.02.80	1981
Probe/Nr./Bohrung		BGR	Treufelrinne	Treufelrinne	Mauer-spalt	Treufelrinne	Treufelrinne	Treufelrinne	Mauer-spalt	Mauer-spalt
Teufe m			480	480	470	480	480	480	470	470
Dichte g/cm ³				1,1130	1,10491	1,0975	1,1001	1,0987		
Temperatur °C						22,1	23,6	25,4		
pH	6,85		6,35			6,7		6,4		
Abdampfückstd. mg/l	168102		173040							173000
Leitfähigkeit mS/cm						141		132		
Eh mV										
Gesamthärte °dH	1005,2		1029							
Na + mg/l		53000	62898	55556	52931	54025	53980	53060	54500	54400
K + "		25		346	319	250	123	112	110	138
Li ++ "				233	227	74		1,41	0,5	0,4
Ca ++ "	4878,4	4850	5077	5230	4609	2360	4730	4987	4470	2830
Mg ++ "	1423,7	1450	1375	194	1568	1048	1394	1133	628	1350
Sr ++ "		390						457	550	364
Fe ++/Fe +++ "		17,8							21	
As +++ "									<2	
Al +++ "										
Si ++++ "										
Cl - "	94075	93000	96915	105167	98484	89833	97770	93100	95000	92800
SO 4 -- "	254,3	306	421	550	751	404	465	497	347	506
CO 3 -- "						155				
HCO 3 - "		39,7						275		
CO 2 "						31		99860		
Br - "		35							191	186
J - "		5							8,44	8
BO 3 --- "									39,7	58

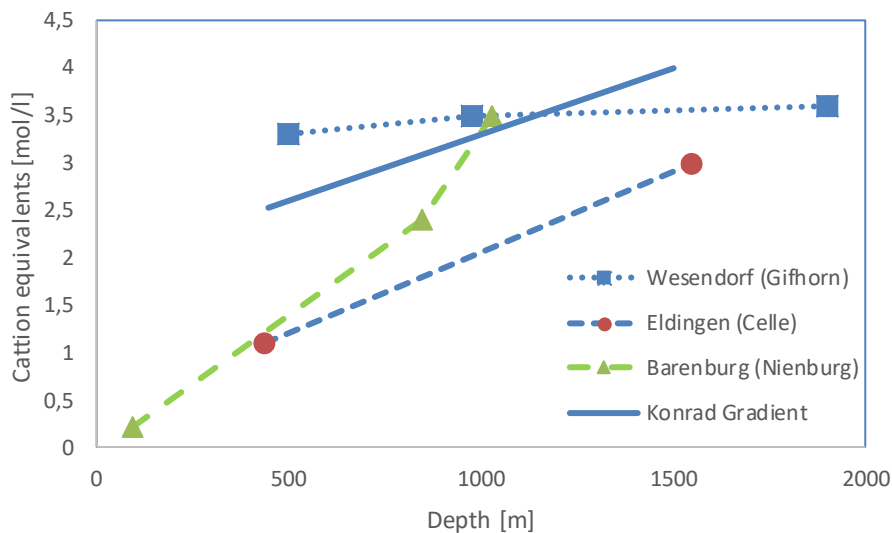


Fig. 2.15

Depth – Salinity relationships at different locations in Northern Germany

No information is available on the redox state (Eh) of pore waters. There are some data on the Eh values of solutions found in the pumping pits of the Konrad mine /BRE 82/, but the origin of the individual samples is uncertain and the scattering severe (80 to 360 mV). Most probably all samples were in contact with air for some time and had altered significantly before being investigated. Because of the organic matter found in Hauterivian clay and the pyrite and siderite content reducing conditions and a low redox potential may be assumed. For the undisturbed argillite claystone in Tournemire, /WIN 14/ estimated a redox potential of -200 mV. The presence of pyrite shows that clay components underwent post sedimentary microbial reduction of sulphate, the extent of which varies with location and depth /HIL 00/. Kosakowski and Berner /KOS 13/ calculated the pore water composition of Opalinus clay from two formations (Effingen and Palfris). Based on the assumption that siderite and pyrite would determine the redox state they derived a p_e of -3.15 (pH 7.31) and -3.44, (pH 7.52) corresponding to Eh values of -186 and -204 mV.

It must be concluded that, for the time being, without site-specific evidence, the salinity cannot be predicted reliably. But there is also strong evidence from other parts of the world that a general dependence on salinity and salinity depth can be expected in the plains, regardless of the type and age of lithology /DIC 69/. It should be noted also that salt diapirs penetrating massive clay formations may have a rather small impact on the composition of the solution around them (see above).

2.2.8 Geology, mineralogy, and geochemistry of the host rock at the model site NORD

Mineralogy of Lower Cretaceous clay

So far, no sites in Germany have been selected for a closer underground investigation to examine their feasibility for an HLW repository. Consequently, the range of possible pore water compositions is unknown. For the sole purpose of developing the concepts for a safety assessment for repositories in northern German Lower Cretaceous clay, a region has been selected that serves as a data source to construct a consistent generic model for further conceptual and theoretical developments. The determination of a site as well as the depth of the emplacement horizon are only exemplary and cannot be generalized for all potential sites in the northern German Lower Cretaceous formation /REI 13/.

In the concept developed in the project AnSichT for the model site NORD the repository is located at 770 m depth in the Lower Hauterivian claystone /REI 13/ /LOM 15/ (Fig. (2.16)). In the region of the model site, the Hauterivian sediments are structured into equally strong Lower and Upper Hauterivian intervals. The Lower Hauterivian is characterized by mixed alternating strata of limestone and lime marl with illite and kaolinite dominated claystone and marl clay layers with spots of pyrite and siderite. On the other hand, the Upper Hauterivian consists of mixed layers of weakly pyritic claystone and weakly bituminous marl clay with occasional lime marl /REI 13/. As an orientation Tab. 2.1 shows the ranges of mineral content in Hauterivian and Barremian clays found at the Konrad mine. Based on these data mean concentrations were calculated (Tab. 2.7).

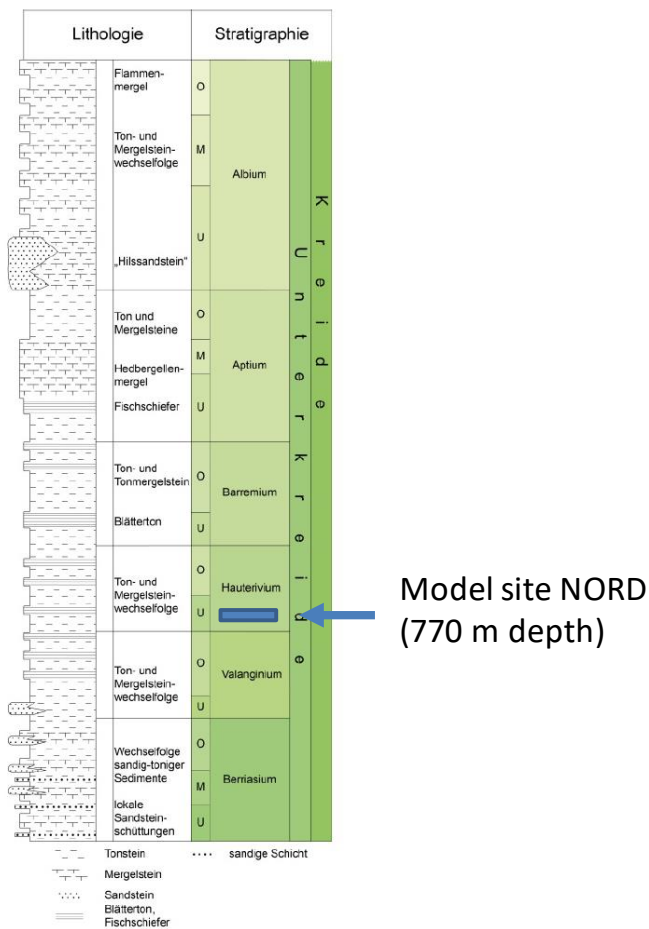


Fig. 2.16 Stratigraphy of Lower Cretaceous clay formation and position of the model site NORD /REI 13/

Pore water chemistry

The generic model site Nord was planned for the lower Hauterivian (REI 13/). According to the analysis above, the composition of pore waters in this formation is expected to be similar to the waters found in the Hils sandstone. However, if a site in the Apt or Alb would have been chosen instead, lower concentrated pore waters could occur. In Apt and Alb kaolinites and smectites occur in similar proportions. Without further investigation, it is not possible to say which of the two mineral groups had a greater impact on the development of pore water salinity. In lack of analytical data, compaction tests on natural Lower Cretaceous clay samples would be of great interest. Before such are available, 10 g/l may be considered as a plausible lower limit of salt concentration.

For the design depth of the repository model NORD a salt content of 150 g/l was assumed based on a salinity/ depth relation of 10–13 g/ 100 m (NOW 13/). If the only component were NaCl its concentration would be about 2.5 mol/l. However, based on the analysis by (BRA 02/ the salinity function in the selected region may be different so that the salt content could be markedly lower or higher.

Based on the mineralogical characterisation of Hauterivian sediments in Konrad 1 borehole (JAH 13/ the pore water is assumed to be in equilibrium with the following minerals

- calcite CaCO_3
- dolomite $\text{CaMg}(\text{CO}_3)_2$
- siderite FeCO_3
- goethite FeOOH
- pyrite FeS_2
- gypsum CaSO_4
- quartz SiO_2
- feldspar
- muscovite/ illite
- kaolinite
- chlorite
- smectite

Undisturbed analytical pH values are not available for deep pore waters, but it may be assumed that the hydrogen concentration is a result of the dissolution of siderite, calcite, and dolomite as well as the buffering impact of clay minerals.

Tab. 2.7 Mineralogical composition of the model clay (Lower Hauterivian) after /JAH 13/

Mineral	Bandwidth [wt.-%]	Mean content [wt.-%]	Content in model clay (standardized to 100 %) [wt.-%]
Quartz	4-29	13	8,9
Feldspar	2-4	3	2,1
Muscovite/Illite	2-27	15	10,3
Kaolinite	2-15	8	5,5
Chlorite	2-8	4	2,7
Smectite	2-6	4	2,7
Mixed Layer	3-5	4	2,7
Gypsum	2	2	1,4
Pyrite	1-8	5	3,4
Calcite	14-79	36	24,7
Dolomite	6-8	7	4,8
Siderite	12	12	8,2
Goethite	20	20	13,7
X ray amorphous	5-22	13	8,9
Organic material		0,4	Not considered

The redox state is probably reducing because siderite, pyrite, and organic residues such as bitumen are present. Which couple of redox-active minerals rules the redox state of porewater cannot be said without in-depth investigation of the undisturbed actual clay and pore water geochemistry.

The following couples are suitable candidates:

- methane/ carbonate and bitumen/ carbonate
- siderite/ goethite
- pyrite/ gypsum
- iron(II) containing silicates/ iron(III) containing silicates

In lack of reliable information, a possible redox state is calculated that should serve as an indicative starting point for modelling and experimental border conditions.

1. The hydrogen concentration is a result of the dissolution of siderite, calcite, and dolomite
2. The redox state is defined by the presence of goethite and siderite
3. Sulphate is not in equilibrium with hydrogen sulphide

2.2.9 Model pore water composition of a Lower Cretaceous clay

There are no analytical data available from Northern Germany on the pore water for the Lower Cretaceous clays. /ENG 63/ provided some values for kaolinitic dominated Jurassic clays. Concentrated salt solutions are present in these clays. This is consistent with the findings from other clay deposits that compacted marine kaolinitic clays tend to have high saline pore waters (see above). Since the mineralogical composition of the lower Hauterivian, the host rock in the North Repository Site Model North is similar to that of the Upper Jurassic, likely, high saline solutions are also present here. The actual composition of the pore waters in the Lower Cretaceous can currently only be speculated. However, since the pore waters in kaolinitic clays differ only slightly from the formation waters in the accompanying water-bearing strata (e. g. sandstone), it is possible to rely on measured data in these formations.

Here, at least for the Konrad shaft and some surrounding boreholes, evaluations are available for the correlation between depth, salinity and solution components (total salt content). /KLI 92/ /KLI 92/ provided a correlation between salinity and depth. From the figures contained in the publication the following relationship could be derived:

$$\text{TDS (total dissolved salts)} = 110 \text{ g/l} + 0,082 \text{ g/ (l m)} \text{ (ca.450 to 1300 m depth)}$$

At 770 m depth, the total dissolved solids (TDS) would be 173.6 g/l. It should be noted that the analytical groundwater data in /MÜL 75/ show a different gradient /BRA 02/. For the complex Rhaetian to Lower Cretaceous the relation between depth and salinity can be expressed as:

$$\text{TDS} = 30 \text{ g/l} + 0,11 \text{ g/(l m)} \text{ (for depths between 250 and 2400 m)}$$

Based on this relationship, the TDS would only be 87 g/l. It should be noted that the Müller database /MÜL 75/ refers primarily to northeast German waters and is not necessarily comparable with the ratio around Schacht Konrad.

From the Konrad data, moreover, correlations for the ion ratios can be derived. According to /KLI 92/, all mine waters of Konrad are of the Na-Ca-Cl type. The ion ratios Na/Cl, Ca/Cl, Mg/Cl and Br/Cl all show a linear correlation with depth, so that it is possible to predict the total composition of groundwater within a certain range of uncertainty if the depth is given. The correlation between the ion ratio and the total dissolved ions (TDI) can be expressed by the functions in Tab. 2.8.

Tab. 2.8 Pore water properties of the mine waters in and around the Konrad mine (according to /KLI 92/)

Ionic ratio	f (TDI)
Na/Cl [meq/l / meq/l]	$1,22 - 6,62 \cdot 10^{-5} \text{ TDI [meq/l]}$
Ca/Cl [meq/l / meq/l]	$-0,194 + 5,26 \cdot 10^{-5} \text{ TDI}$
Mg/Cl [meq/l / meq/l]	$-0,0357 + 1,36 \cdot 10^{-5} \text{ TDI}$
Br/Cl [meq/l / meq/l]	$-0,005 + 1,12 \cdot 10^{-5} \text{ TDI}$

/KLI 92/ did not provide any information on the secondary elements. /BRE 82/ presents a summary overview of sampling in the Lower Cretaceous in the vicinity of the Konrad Pit (Tab. 2.5), but apart from the geological classification of the sampling sites, there is no information on the location and especially on the depth. More information is available on the composition of the formation waters of the coral oolites in the Konrad Pit. However, these belong to a different formation (Jurassic) and interact closely with rocks of completely different chemical composition. The estimation is therefore based on the solution analyses of the inflows from the Hils sandstone Formation documented over almost 20 years (Tab. 2.9)

Tab. 2.9 Hils water composition from the Konrad mine (mean values based on data in /BRE 82/)

Ion	Concentration (mean) [mg/l]	Concentration (mean) [mol/l]
Na	54928	2.38923
K	178	0.00455
Li	89	0.01288
Ca	4349	0.10852
Mg	1127	0.04636
Sr	440	0.00502
Fe	19	0.00035
Cl	95785	2.70176
SO ₄	472	0.00491
HCO ₃	157	0.00258
Br	137	0.00172
I	7	0.00006
BO ₃	49	0.00083
TDS	157738	
pH	6.5	

The concentrations of the minor ions Li, K, Sr, Fe, O, BO₃ and HCO₃ were taken from the mean values of the listed solution analyses. Although the Hils water has a total salt content that is about 10 % lower than at the calculated model site at 770 m, this is in the order of magnitude of the measurement fluctuations for the secondary elements. The composition of the model solution for the model site North was estimated as follows:

1. the total salt content was estimated for 770 m from the salinity/level relationship (173.6 g/l)
2. it was assumed in a first approximation that the salt content can be attributed exclusively to NaCl. In this case, the chloride content would be 2.97 mol/l
3. the equivalent concentrations of the ions Na, Ca, Mg and Br were calculated based on the equivalent ratios (Tab. 2.8)
4. the minor ions were taken from the mean values for Hils water (Tab. 2.9)

5. the charge error (about -0.5 %) was compensated with Na
6. the chloride concentration was increased until the total salt content of the calculated solution was 173.6 g/l
7. the density of the solution was calculated (1.1138 kg/l) using the approach of Krumgalz et al (1996) based on the concentrations of Na, K, Mg, Ca, Cl, Br and SO₄
8. the molar concentrations were converted into molar concentrations using the density

In the next step, the solution obtained was mathematically balanced with minerals from the Lower Cretaceous Formation. The calculations were performed with Geochemist's Workbench. THEREDA Release 1 served as the database, which was supplemented by thermodynamic data for iron from /MOO 04/ and /HAG 14/.

As mineral phases, correspondingly (Tab. 2.7) goethite, pyrite, calcite, dolomite, gypsum and siderite were assumed to be present in the mineral phases in the contents indicated there (last column). All other Fe(III) oxide phases were suppressed to allow the formation of goethite. Clay minerals, as well as all other Al, Si compounds (quartz, feldspar, muscovite/illite, kaolinite, chlorite, smectite), were considered inert in the calculation, mainly because available databases were not considered sufficiently comprehensive and reliable to model clay mineral equilibria in saline environments. The redox balance between sulphate and sulphide was suppressed. As the database used did not contain data for borate, lithium, strontium, bromide and iodide, these trace constituents were not included in the calculation.

The calculation was based on the assumption that the pore space is 7 % (/JAH 13/, p.44). In one cubic metre of clay, 70 l of solution (65.8 kg at a density of 1.1138 kg/l) reacted with 930 l of dry clay (2372 kg at a density of 2.45 kg/l).

The concentrations obtained are listed in Tab. 2.10 (right column). They differ only slightly from the values derived from the salinity gradient of Konrad. An exception is sulphate, which, due to the dissolution of gypsum, reaches a higher concentration than initially calculated.

Tab. 2.10 Lower Cretaceous formation water at a depth of 770 m (calculated based on the relationships in and around Konrad shaft)

Ion	Concentration [mol/l]	Concentration [mol/kg]	Concentration [mol/kg] After saturation with goethite, pyrite, calcite, dolomite, gypsum, and siderite
Li ⁺	0.01288	0.01369	-
Na ⁺	2.48472	2.64095	2.64
K ⁺	0.00455	0.00484	0.00484
Mg ²⁺	0.06751	0.07176	0.0806
Ca ²⁺	0.17841	0.18963	0.194
Fe ²⁺	0.00034738	0.00037	0.000495
Fe ³⁺			4.25·10 ⁻¹¹
Sr ²⁺	0.00502454	0.00534	-
B(OH) ₄ ⁻	0.00083	0.00088	-
HCO ₃ ⁻	0.00257878	0.00274	0.0021
Cl ⁻	2.98642	3.17420	3.16
SO ₄ ²⁻	0.00491	0.00522	0.0191
Br ⁻	0.00503	0.00534	-
I ⁻	0.00006	0.00006	-
HS ⁻			2.28·10 ⁻¹⁰
-log cH			6.41
TDS	173.6		
pH	6.5		

2.3 Time-dependent variables

2.3.1 Temperature

The temperature within and around the borehole is increased from its original site-dependent level by the heat generated by the radioactive decay of nuclear waste. At the model site NORD, the medium surface temperature is estimated to be 8 °C and the temperature gradient 40 K/ km /REI 13/ so that at a depth of 770 m the temperature would

be 39 °C. The temperature profile and evolution around the borehole strongly depends on the loading of the containers as well as the interim storage period of the spent fuel. In the AnSichT concept, the loading of the containers is intentionally set high to save space and at the same time to prevent microbial activity. This results in a maximum temperature of below 160 °C (Fig. 2.17) at the border container/sand⁴, 150 °C in the buffer and 110 at the interface between the outer liner and the host rock⁵. The temperature maximum occurs a few years after emplacing the waste in the boreholes. In the following years, the heat is distributed in the near field leading to an asymptotic temperature decrease. After about 200 years it will fall below 100 °C at the interface between inner liner and buffer. At the same time, the temperature in the clay rock at a distance of 15 m will be at 80 °C.

At least for 1000 years, the temperature around the containers will be above 80 °C and above 50 °C for 5000 years. It may need 20,000 years for the temperature to fall below 40 °C and about 100,000 years to reach the original level (35 °C).

⁴ This section was written before the new Safety requirements for repositories of heat-generating radioactive waste were published /BUN 20b/. They require that the maximum temperature at the surface of containers would be 100 °C. The calculated temperature regime does not affect other parts of this study so that it was decided to leave the section as it is.

⁵ Specifications: one borehole is filled with three containers containing two DWR-BE (fuel element for a pressurised water reactor) that have been intermediately stored for 23 years

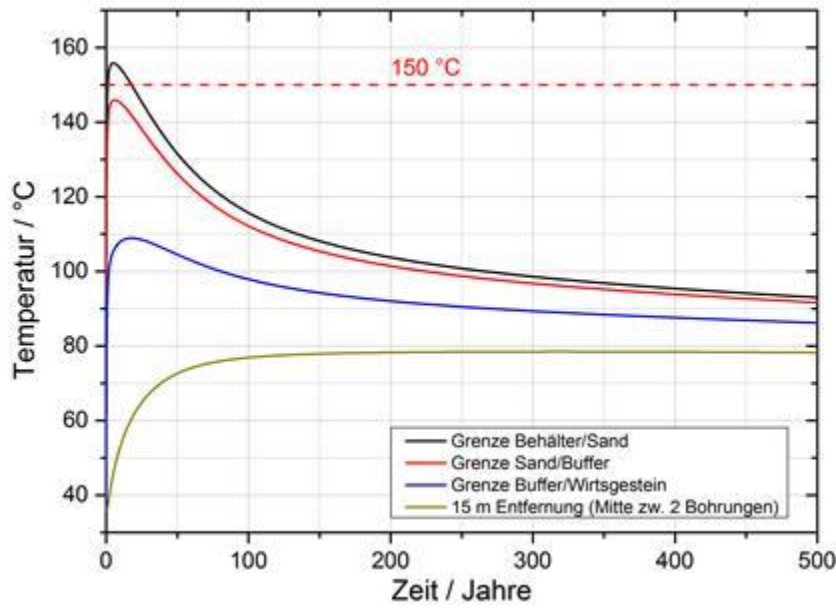


Fig. 2.17 Evolution of temperature around emplaced waste containers in the repository concept for the model site „Nord“ /JOB 15b/

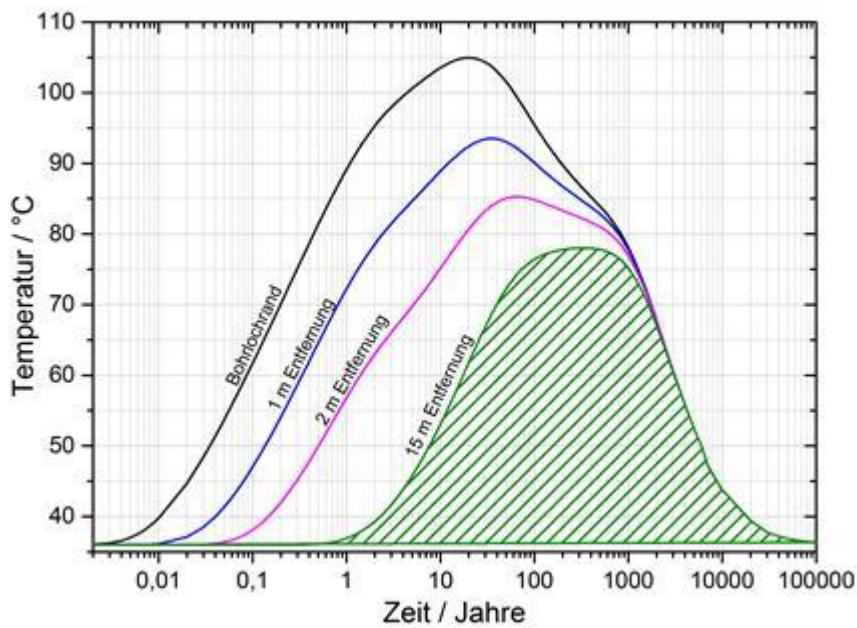


Fig. 2.18 Long-term evolution of temperature around emplaced waste containers in the repository concept for the model site „Nord“ /JOB 15b/

2.3.2 Saturation state of clay

Due to the ventilation of the mine, claystone at the surface of open cavities (drifts, boreholes) as well as material prepared for use as a buffer/ sealing/ backfill will partly become unsaturated. After the emplacement of waste containers and the sealing of the borehole the generated heat (depending on the loading of the containers) will lead to a temperature increase. Pore water still in the buffer or the adjacent host rock will partly evaporate and produce a humid atmosphere. As more heat is produced and the temperature increases even more, part of the clay materials may become completely dry while at a more distant place the partly evaporated water leaves behind solutions of increased salt concentration. Some salts such as halite may even reach saturation and will be precipitated. At the same time, pore water from the undisturbed clay rock will slowly diffuse into the excavation disturbed zone (EDZ) and later into the buffer.

How the entire system buffer/ atmosphere/ adjacent claystone evolves depends on several factors. They include:

- Evolution of temperature
- Gas-filled pore volume
- Solution content of the buffer and the EDZ
- Speed of saturation
- Initial solution composition
- Permeability of undisturbed clay rock with respect to water and dissolved ions

The following water-based processes occur in the borehole system

- **Evaporation:** Water may evaporate until the equilibrium water pressure of the pore water in contact with the gas phase is reached. The equilibrium water pressure is a function of temperature and solution composition. It must be noted that even at temperatures above 100 °C a NaCl solution (the main component of saline groundwaters in the Lower Saxony Basin) does not evaporate completely if the water pressure is sufficiently high. Evaporation could take place at any location that is in contact with an unsaturated gas phase. This could also be the surface of a liner, possibly leading to saturated, most corrosive conditions.
- **Precipitation of salts:** If the evaporation of water is so strong that the saturation concentration of one or more salts is exceeded, these salts start to precipitate.

As NaCl is the main component of deep groundwaters in the Lower Saxony Basin, halite would be expected to precipitate. However, minor components may be saturated first such as gypsum or calcite /LAN 09/.

- **Advection of solution caused by evaporation:** solution flows against the temperature gradient because at the hotter end water is evaporated. This process is only possible when the clay is at least in some parts saturated. It does not take place if the partial water pressure in the gas phase is already in equilibrium with the solution.
- **Diffusion of dissolved salts:** dissolved salts diffuse in the direction of decreasing concentration gradient thereby possibly diluting a higher concentrated salt solution at the solution/ gas interface and increasing the concentration in the near field. This process is only possible when the clay is at least in some parts saturated.
- **Equilibration of distant solutions:** Water transport through the gas phase will likely be fast enough to allow for equilibration between aqueous solutions at distant places of the borehole. Water would be evaporated from less concentrated solutions and condensed on more concentrated solutions until their concentration (more precisely: their equilibrium partial water pressure) is the same.
- **Condensation of water during cooling of the liner/ buffer interface.** When the heat generated by the waste and reaching the inner liner becomes lower than the heat transported into the surrounding host rock the interface between liner and buffer will cool down. It has been assumed that if the temperature would drop below 100 °C water would condensate on the surface of the liner /LAN 09/. In the case of saline groundwaters, such a thing would not happen because all water would only condensate on solutions as they always have a lower equilibrium water pressure than pure water.
- **Dissolution of precipitated salts:** If precipitated salts are present water would condensate on the surface of the salts and dissolve them if the equilibrium water pressure of the resulting saturated solutions is below the actual partial water pressure. This process would only happen if the equilibrium water pressure of pore waters is the same. If the water pressure of pore waters is higher, water would evaporate there and be transported through the gas phase to the precipitated salts. If the water pressure of pore waters is lower, no water would condensate on the precipitated salts but would instead condensate on the pore water.

If freshly formed solutions of precipitated salts are very close to the surface of the liners, local contact of solution/steel may occur. Complete coverage of the liner surfaces with solution will only take place once the EDZ and the buffer are fully saturated.

The re-saturation process of the EDZ and the buffer depends on several factors including the repository concept, the temperature evolution in the borehole, physical characteristics of the claystone and the buffer. Modelling results for other countries and concepts may serve as orientation only. For the Swiss concept, the saturation process is assumed to be complete after about 100 years /LAN 09/. For a UK concept, 150 years were calculated /KIN 10/. In the German concept (AnSichT) the maximum temperature around the borehole is higher and the cooling process takes much longer. Therefore, the re-saturation process is expected to take longer as well⁶.

⁶ Resaturation may be in the same order as in other concepts if a maximum temperature of 100°C is assumed.

3 Previous investigations of iron and steel corrosion in clay systems or in contact with brines

3.1 Overview

Information on the type and conditions of occurrence of iron corrosion phases could in part be taken from previous studies on the corrosion of carbon steel under conditions expected in a deep geological repository for HLW. This includes research done for repository projects in Germany, the USA, Finland, France, Switzerland, Sweden and Belgium. The focus of many earlier studies was on the determination of corrosion rates rather than the identification of the corrosion phases. Improvement of experimental methods and analytical techniques allowed for a more thorough characterisation of the corrosion processes and products that is reflected in studies from the last 10 or more years.

A literature review was conducted that should give an overview of the state of knowledge of the chemical corrosion process and the corrosion products that may occur in a repository under different conditions⁷. It did not intend to give a full picture of all relevant corrosion studied as these amount to a vast number. Moreover, it became clear that after a certain point in the review additional publications did not give entirely new information but often confirmed earlier findings. That does not mean that corrosion science is now completed, but the type and occurrence of corrosion phases and the key chemical processes that lead to their formation are mostly identified. Which of these processes and products occur under which circumstances is still an open field. A general finding is that the course of corrosion and the products strongly depends on the experimental conditions and site-specific features such as clay type, temperature, solution type, container material and so on. That is why we have sorted the studies by country as they mostly refer to specific national conditions.

Results from Belgian studies were not considered because the disposal concept includes a cement buffer around the waste containers /POY 06/. The geochemical conditions are strongly alkaline and not comparable with repository concepts currently discussed in Germany.

⁷ Most of following literature review was conducted in the early phase of this project, so that in part it may reflect that state of knowledge in the years 2015 and earlier. However, some more recent literature was included later.

3.2 Germany

Corrosion in brines

Numerous studies on the corrosion of packaging materials in brines were conducted by the Institut für Nukleare Entsorgungstechnik (INE) in the Forschungszentrum Karlsruhe (now Karlsruhe Institute of Technology). The focus of these studies was on the long-term performance, the corrosion mechanism and the corrosion rate of candidate materials for waste containers /SMA 85/, /SCH 88/, /SMA 95/, /SMA 98/, /SMA 04/, /KUR 04/. In most cases, little or no information is given about the corrosion products. Smailos et al. /SMA 92/ and Smailos /SMA 93/ reported that under initially slightly oxidizing conditions the following oxidation products were found (Tab. 3.1).

Tab. 3.1 Corrosion products found on steel TStE355 in saline brines after one year /SMA 92/, /SMA 93/

Solution	Initial O ₂ concentration [mg/l]	90 °C	150 °C	170 °C
Brine 1 (Q)	2.8	Hematite, magnetite (after 4 years)	Amakinite, akaganeite	amakinite
Brine 2 (conc. MgCl ₂)	1.5	akaganeite	Amakinite, akaganeite	amakinite
Brine 3 (conc. NaCl)	4.9	Magnetite, akaganeite	Magnetite, maghemite	magnetite

It is interesting to see, that pure Fe(II) corrosion phases were only found at 150 and 170 °C. No information was given by the authors if and how effective oxygen exclusion was during the experiment or after the excavation of the metal specimens. The experiments at 170 °C were carried out in a pressure vessel that may have ensured more effective anaerobic conditions. Addition of Na₂S did not change the corrosion products.

/SMA 95/ and /SMA 04/ reported that the aerobic corrosion of unalloyed TStE 355 steel at 150 and 170 °C in NaCl brine leads to the formation of a black layer consisting of magnetite, hematite, goethite and akaganeite. Specimens exposed to MgCl₂-brine and limited oxygen supply developed a coating primarily consisting of amakinite without any traces of magnetite. It was assumed that the high Mg²⁺ concentration inhibited the formation of magnetite

Corrosion in clay

Herbert et al. /HER 11/ investigated the interaction of powdered clay with bentonites (MX80 and Friedland clay). Whereas MX80 contains about 70 % smectite, the Friedland clay used for the experiments had a content of 36 % mixed layer illite-smectite and 20 % montmorillonite. Instead of equilibrium pore water, saturated salt solutions were used to simulate the conditions in a repository in salt rock. They included a saturated sodium chloride solution and an IP21 solution. The latter one is an invariant solution in equilibrium with the halite, carnallite, kainite, sylvite and polyhalite. MX80 was mixed with powdered iron (10:1) and percolated with one of the two salt solutions for up to 2 months at 25 °C (IP21) or 60 and 90 °C (NaCl). Experiments with Friedland clay were conducted analogously but only at 25 °C with NaCl solution. Unfortunately, no information is given about the exclusion of air before, during and after the percolation or during the analytical investigation of the solid products. Therefore, oxidation of product phases cannot be excluded.

In the solid phases resulted from corrosion in MX80 and IP21 solution Akaganeite and Goethite were identified together with berthierite. Experiments with NaCl solution lead to goethite, hematite, wüstite and magnetite. Also, chlorite and cronstedtite were among the product phases. All silicates were identified as mixed layer series between two or three endmembers. The Fe content in chlorite did not change significantly between the start and the end of the experiments so that it cannot be considered an iron corrosion phase.

Experiments with Friedland clay resulted in the formation of lepidocrocite, goethite and magnetite. Increased iron concentrations (in comparison with the starting material) were observed in the following clay phases

- Smectite (Fe^{3+} in octahedra)
- cronstedtite-saponite-trioctahedral vermiculite mixed-layer structures (Fe^{2+} and Fe^{3+} in octahedral and Fe^{2+} in tetrahedra)
- chlorite-saponite-trioctahedral vermiculite mixed-layer structures (Fe^{2+} and Fe^{3+} in octahedra)
- kaolinite-smectite-dioctahedral vermiculite mixed-layer structures (Fe^{3+} in octahedra)

The authors proposed an alteration sequence that would start with dioctahedral Fe-smectites and Fe-oxyhydroxides at low Fe^{2+} concentrations to berthierite-saponite mixed layers and finally to chlorite-saponite-vermiculite mixed layers. If the Fe^{2+} content in relation to H^+ is again decreasing cronstedtite-vermiculite mixed layers would form.

Kaufhold et al. /KAU 15/ investigated the corrosion of iron powder and coupons in slurries made of bentonite and water at 60 °C. All operations were performed in a glovebox. They found berthierite as a corrosion product. Some reddish products were found as well that were interpreted as iron oxyhydroxides formed at the beginning of the experiments when traces of oxygen were still present. In a later experiment iron pellets were mixed with different bentonite samples and deionized water /KAU 20a/, /KAU 20b/. Magnetite was found as the first corrosion product, but the slow dissolution of clay lead to the release of silica which in turn caused iron to precipitate as iron silicates. Experiments indicated that smectites become less stable and release more silica when its structural Fe^{3+} is reduced by corrosion hydrogen.

Microbiologically induced corrosion and sulphate reduction

Venzlaff /VEN 12/ showed that sulphate reducing bacteria in an anoxic seawater medium could effectively accelerate the corrosion of iron surfaces by directly using the electrons from the corroding iron to reduce sulphate to sulphide and iron sulphide. The experiments were conducted in a carbonate-rich solution. Siderite, chukanovite and an unidentified iron sulphide were the main corrosion phases.

3.3 USA: Waste Isolation Pilot Plant (WIPP)

The Waste Isolation Pilot Plant is a repository for long-lived radioactive waste located in a previous mine in bedded salt rock. As part of the certification and re-certification procedures, relevant processes that may affect the long-term safety of the repository are regularly revisited and assessed. This also includes corrosion of container materials used in the plant.

The assumptions regarding the corrosion of iron-based materials under the conditions in the WIPP site were summarized in the Compliance Recertification Application (CRA-2014), Appendix SOTERM-2014 (Actinide Source Term, /U.S 14/). They are mainly

based on the works carried out by Telander et al. /TEL 93/, /TEL 97/ and Rosell et al. /ROS 09/, /ROS 10/, /ROS 11/, /ROS 13/.

A couple of corrosion experiments were undertaken to investigate the influence of varying conditions on the corrosion rate /TEL 93/ /TEL 97/. Four lots of low carbon steel (ASTM A366 and ASTM A570) were used for the experiments. The results are summarized in Tab. 3.3. Coupons that were not immersed in brine but were only in contact with a vapour phase above a brine showed a tan-to-dark-brown corrosion product β - $\text{Fe}_2(\text{OH})_3\text{Cl}$. Coupons immersed in brine A (Tab. 3.2) under 12 atm CO_2 pressure yielded FeCO_3 . Although no CaCO_3 was found by XRD, the reduction of Ca concentration in the brine is consistent with the earlier finding of Murata et al. /MUR 84/ that Fe is also present in mixed $(\text{Ca,Fe})\text{CO}_3$ layers when iron is corroding in CO_2 saturated brines containing Ca. Such a mixed phase (identified by XRD as similar to oligonite $(\text{Fe,Mn,Zn})\text{CO}_3$) was indeed found at 36 atm CO_2 . It contained 92.2 wt.-% Fe and 6.1 wt.-% Ca as well as minor amounts of other divalent metals (Mn, Ni, Zn, Cu).

Tab. 3.2 WIPP brine A used by /TEL 93/, /TEL 97/

Element	Concentration [mg/l]
Na	42000
Mg	30000
K	35000
Ca	600
B	220
Cl	190000
SO_4	3500
HCO_3	700
pH	6.5
Density [kg/l]	1.2
Source	/MOL 83/

If coupons corroded under CO_2 were later exposed to small amounts of H_2S then mackinawite was found as an additional product. If the amount of CO_2 added initially was low ($\leq 0.032 \text{ mol/m}^2 \text{ steel}$), neither siderite nor mackinawite were detected but instead $\text{Fe}_2(\text{OH})_3\text{Cl}$. Moreover, the corrosion phase contained a phase $\text{Fe}_8(\text{OOH})_{16}\text{Cl}_{1.3}$. It was probably the product of oxidation between the extraction of the phase from the container and the placement into the XRD device. The authors stated that there were no special precautions to avoid oxidation.

Some tests were performed with metal coupons packed in moist masses of salt. After the experiments, the coupons showed some corrosion tarnish but no red colour. Such a colour would only appear after the specimens were exposed to air.

Corrosion under N₂ pressure in brine A resulted in blue-green products that rapidly oxidised in air to a red-orange phase within minutes. The blue-green phase could not be identified by XRD, but a chemical analysis revealed that it consists of about 37-38 wt.-% Fe and 6.7 to 7.7 wt.-% Mg, pointing to a mixed Fe(II)/Mg hydroxide phase such as amakinite (Fe^{II},Mg)(OH)₂, although the XRD pattern did not match. Amakinite was identified in earlier experiments with Mg brine /WES 88/, /SMA 95/ (Tab. 3.3).

Tab. 3.3 Corrosion products found after contact with WIPP brine A

Initial solution	Initial conditions	Corrosion product
Brine A	N ₂ (10 atm), 30.5 °C, 6 months	Phase closely related to Amakinite Fe _{2/3} Mg _{1/3} (OH) ₂
vapour phase above brine A	N ₂ (10 atm), 30.5 °C, 3-24 months	β-Fe ₂ (OH) ₃ Cl (tan to dark brown)
Brine A	N ₂ (10 atm), CO ₂ (12 atm)	FeCO ₃ (dark grey), (Fe,Ca)CO ₃ with Fe: 92 wt.-% and Ca: 6 wt.-%
Brine A	H ₂ S (5 atm)	FeS (mackinawite)

Coupons corroded under high H₂ pressure were extracted in a shiny form. No specific product phase was reported but the bluish-green colour of the solution showed that corrosion took place

With regards to a potential repository in clay, one set of experiments deserves special attention: In two sets of experiments (AUT-12 and AUT-13) low carbon steel specimens were surrounded by a 'backfill' of mixed bentonite/crushed salt. The corrosion products were dark brown. No grey, green or blue products were found in the vicinity of the specimens. Such colours were reported for other experiments under anoxic conditions.

Whereas Telander and Westerman always worked with closed systems with a considerable overpressure of either N₂, H₂ or CO₂, Roselle conducted his experiments at unit pressure in open systems with a constant gas stream. They used low carbon steel (ASTM A1008) which was completely or partially immersed in ERDA-6 or a GWB brine (Tab. 3.4). Both brines are in equilibrium with halite and anhydrite as well as with MgO from the engineered barrier. As a result, the brines used by Roselle are slightly alkaline

whereas those of Telander and Westerman were slightly acidic. The corrosion was investigated in a nitrogen atmosphere, which in part of the experiments contained 250 to 3500 ppm CO₂. Four types of corrosion products were found:

1. Iron chloride 1: a green iron magnesium chloride hydroxide (O peak > Cl peak)
2. Iron chloride 2: an iron chloride hydroxide with little or no magnesium and the chlorine peak in EDS larger than the oxygen peak
3. Carbonate 1: containing calcium, carbon, and oxygen
4. Carbonate 2: iron calcium magnesium carbonate
5. Other: containing potassium, sulphur, calcium

Iron chloride 1 was found in almost all experimental settings. Its composition would be compatible with hibbingite (Fe^{II},Mg)(OH)₃Cl. Only in some tests with ERDA-6 brines 'carbonate 2' was the only Fe bearing phase. 'Iron chloride 2' was found sometimes especially in tests with low CO₂ background. The carbonate phase 2 appeared more frequently in ERDA-6 than in GWB brines. No attempt was made to identify the phases with XRD.

It should be noted that the CRA-2014 stated that green rusts were the main corrosion product in low CO₂ settings. However, the cited work /ROS 13/ did not include such a conclusion but only stated that green rusts *may* be a corrosion phase.

/WAN 01/ /WAN 01/ investigated the corrosion of mild steel coupons and iron powder and in GSEEP and ERDA6 brines as well as in a 0.01 M NaCl solution at 25 °C. All solutions were equilibrated with brucite [Mg(OH)₂]. Corrosion of iron in dilute NaCl solution probably lead to the formation of black magnetite (XRD result). On the other side, corrosion in brines delivered a light green product that according to Mossbauer spectra contained Fe(II) and Fe(III) in a ratio of approximately 1.91/1. It was also found that the product was associated with SO₄ and Cl. All these findings show close similarities to sulphate bearing green rust. No Fe(OH)₂ was found.

Tab. 3.4 Composition of GWB and ERDA-6 brines

Element	GWB Concentration [mol/kg]	ERDA-6 Concentration [mol/kg]
Na	4.98	6.05
K	0.559	0.109
Li	$5.5 \cdot 10^{-3}$	-
Ca	$1.24 \cdot 10^{-2}$	$1.28 \cdot 10^{-2}$
Mg	0.635	0.121
Cl	6.3	6
Br	$3.18 \cdot 10^{-2}$	$1.24 \cdot 10^{-2}$
SO ₄	0.209	0.191
B ₄ O ₇ ²⁻	$4.73 \cdot 10^{-2}$	$1.77 \cdot 10^{-2}$
pH	7.595	7.955
Density [kg/l]		

3.4 Switzerland

3.4.1 Disposal concept

In the Swiss concept, it is planned to place cylindrical HLW containers in excavated tunnels in the Jurassic Opalinus Clay formation. The tunnels are stabilized by a low pH shotcrete (ESDRED)/ steel mesh/ bolt structure. Containers shall be placed on blocks of compressed bentonite. The same material is used to backfill the tunnel (Fig. 3.1) /DIO 14/, /BRA 14/.

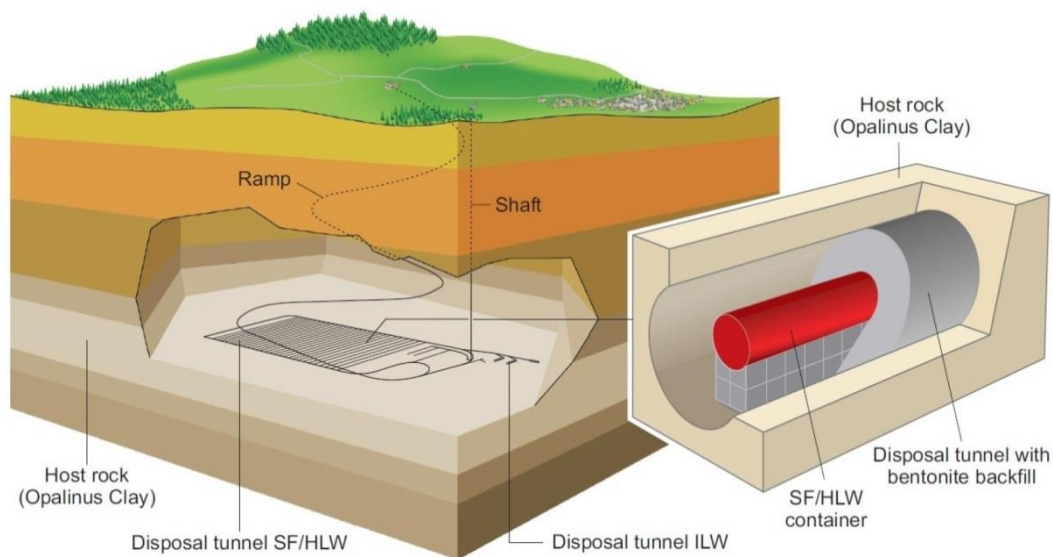


Fig. 3.1 Swiss repository concept (from Diomidis 2014)

Opalinus clay

The average composition of Swiss Opalinus clay formation is given by Berner et al. /BER 13/(Tab. 3.7). It mainly consists of clay minerals illite, kaolinite and montmorillonite as well as calcite and quartz. The pore water is dominated by NaCl (0.16 mol/kg) and minor amounts of Ca, SO₄ and HCO₃ (/KOS 13/, Tab. 3.7).

Tab. 3.5 Average composition of Swiss Opalinus clay

Phase	Average composition (wt.-%)	Opalinus clay model /BER 13/
Illite	25.3	25.2
Kaolinite	18.8	18.7
Illite/ smectite mixed layer	9.4	12.9
Calcite	14.5	14.4
Dolomite	0.5	0.5
Quartz	18.1	18.0
Siderite	3.5	3.5
Pyrite	1.1	1.1
Barite	*	1.24·10 ⁻⁵
Potassium feldspar	1.4	-
Plagioclase	1.1	-
Organic Carbon	0.7	-
Chlorite	8.8	-
Inert	-	8.24

* Not present in this composition but a constituent of some formations 10⁻² to 1.24 10⁻⁴ wt.-%

Tab. 3.6 Initial pore water composition in Opalinus clay /BER 13/, /KOS 13/

Component	Calculated concentration [mol/kg]
Al	1.75·10 ⁻⁸
Ba	1.29·10 ⁻⁷
C ^{IV}	2.17·10 ⁻³
Ca	1.25·10 ⁻²
Cl	1.60·10 ⁻¹
Fe(tot)	5.21·10 ⁻⁵
Fe ^{II}	5.18·10 ⁻⁵
Fe ^{III}	4.07·10 ⁻¹²
K	2.60·10 ⁻³
Mg	9.63·10 ⁻³
Na	1.65·10 ⁻¹
S	2.49·10 ⁻²

Component	Calculated concentration [mol/kg]
S ^{VI}	2.479·10 ⁻²
S ^{II}	1.21·10 ⁻¹¹
Si	1.80·10 ⁻⁴
Sr	2.09·10 ⁻⁴
pH	7.26
pe	-2.85
log p(CO ₂)	-2.32

3.4.2 Experimental results

In the 1980ies several corrosion studies have been performed (see /KIN 08/ for an overview) within the Swiss repository research program. Later on, investigations were mainly based on the review and condensing of literature information from other countries (e. g. /BRA 14/, /DIO 14/, /LAN 09/, /WER 08a/). In the course of international cooperation new corrosion-related projects started at the underground laboratories in Mont Terri and Grimsel.

Aerobic corrosion of steel in contact with bentonite (in-situ)

The FEBEX experiment at the Grimsel test site was not originally intended to observe iron corrosion processes but to test the feasibility of a full scale constructing engineered barrier systems. It involved a carbon steel liner enclosing a heater that was surrounded by a clay barrier and enclosed two heaters. Heating started in 1997 and ended in 2015, after which the experiment was dismantled. Two clay blocks that were close to a corroded liner were removed and the corrosion impact investigated /HAD 19/. The temperature in these blocks was estimated to be around 30 to 60 °C throughout the experiments. The surrounding clay shows large halos of red, orange and blue halos, each associated with specific newly formed minerals

- Blue zone: increased Fe(II), possibly in Fe(OH)₂ or sorbed Fe²⁺, also containing goethite and hematite
- Transition zone between blue and orange: Mainly goethite
- Orange and red zone: goethite
- Crust near the liner: goethite, but iron silicates cannot be ruled out

From the results, it is clear that the experimental conditions were suboxic. The large halos indicate that iron is transported as mobile Fe^{2+} but it is later oxidized to goethite and possible hematite.

Anaerobic corrosion of steel in contact with clay (in-situ)

The corrosion of steel embedded in clay is investigated by an in situ experiment ('Iron Corrosion in Bentonite' (IC-A) experiment) at the Mont Terri Underground Research Laboratory /RED 21a/, /NEC 17a/, /SMA 17/. Similar experiments were conducted in the Grimsel Underground Research Laboratory /RED 21b/.

Steel coupons were embedded in compacted Wyoming MX-80 clay of different density and enclosed in slotted steel containers. The container was then lowered into a borehole in the Opalinus clay, sealed from the atmosphere and then permitted to get into contact with pore water. The first set of containers was removed after 20 months of exposure at 14 °C. The last containers are planned to be removed after 10 years. After 20 months it was not possible to identify the nature of corrosion phases. After 30 months, traces of hematite and erdite ($\text{NaFeS}_2 \cdot 2\text{H}_2\text{O}$) were found, and magnetite was suspected.

Another experiment ('IC') employed annular electrodes made of C-steel (E24 and S235), 1690 Inconel and 315L stainless steel embedded in a clay core. The core was descended in a borehole, maintained at ambient temperature for 20 months and then heated to 85 °C for five years /NEC 19/. The corrosion process was monitored by electrochemical impedance spectroscopy. On carbon steel (E24) the following products were observed:

- Close to the metal an internal corrosion product (ICPa) layer mainly consisting of magnetite and smaller amounts of akaganeite and Fe-hibbingite
- A thin layer of chukanovite (ICPb)
- A layer with mixed patches of goethite, siderite, chukanovite, akaganeite (ICPc)
- A sulphur-rich layer mainly of mackinawite and greigite (ICPd)
- A thick layer of goethite (ICPe)
- The outermost layer at the level of the original steel surface is made of siderite (ICPf), with domains of goethite, lepidocrocite and chukanovite, mackinawite, pyrite and elemental sulphur
- The bulky corrosion layer is enriched in Fe and S. Within the clay matrix particles of ankerite and mackinawite were found.

In comparison to E24, the carbon steel S235 showed fewer corrosion strata:

- The innermost layer (ICPa) mainly consisted of chukanovite and smaller amounts of iron sulphide.
- The second layer (ICPb) consisted of ankerite with a rather low amount of Fe. Some iron sulphide, possibly mackinawite occurred. Also, some crystals of siderite and calcite could be found

The presence of Fe(III) oxides is a hint that at some times of the experiment oxic or suboxic conditions prevailed. At the same time, the decrease of sulphate concentration in solutions was interpreted together with the formation of iron sulphides in many corrosion product layers as an indication of microbial sulphate reduction.

Alkaline plume

Concrete types containing free portlandite, $\text{Ca}(\text{OH})_2$, are characterized by a high pH resulting from its rather high solubility and the presence of dissolved KOH and NaOH. Within the concrete structure, the pH may be as high as 13. If such concrete is used in significant amounts in the emplacement areas of a repository the interaction of portlandite with the clay host rock and its pore water must be considered. Windt et al. /WIN 04/ employed a 1-D reactive transport model to investigate the extend of hydroxyl transport into the surrounding clay rock and the alteration of clay minerals. They found that within 100,000 years clay in some 10 meters distance may be influenced by the presence of portlandite in concrete. Near the concrete/ clay interface, the clay mineralogy is strongly modified. Some less dramatic changes are to be expected at larger distances. Changes in pH are probably limited to some meters due to the buffering capacity of the claystone components. According to more recent modelling by Kosakowski and Berner /KOS 13/ who investigated the impact of concrete on clay at three different sites the zone of altered clay minerals would likely not extend to more than some 10 cm within 100,000 years. The pH of the pore water may increase at a higher distance (6 to 500 m along with the hydrological flow), but outside the mineral alteration zone only from around 7 to 8 or 9.

If instead a low pH concrete (ESDRED) is used the mineral alteration zone is strongly reduced (13 cm in the Opalinus clay and 4 cm in bentonite) the zone of increased pH to less than 10 cm /BER 13/, /BRA 14/. After 100,000 years the pH in the concrete and the clay will be at approximately 8.

These findings mean that corrosion of container materials is probably not or not significantly affected by the presence of concrete in several meter distance.

Impact of radiolysis on the redox potential and the corrosion products in the near field

Radiolysis of water leads to the production of radicals $H\bullet$ and $OH\bullet$ that react with the medium components to hydrogen and oxidizing species such as H_2O_2 , O_2 and oxidized chlorine species (e. g. ClO^-) /SHO 99/.

After several hundred years of storage, alpha radiation may be considered the only relevant cause of radiolysis in the near field. The main source of radiation is the spent fuel in the container. Radionuclides in spent fuel fissures, in solution or sorbed on materials outside the container, have a much lower relevance. Radiolysis of water generates hydrogen and oxidizing species such as hydrogen peroxide. It may produce oxidizing conditions in the nearfield of the reducing components (iron, Fe^{2+} containing corrosions products, components of the bentonite buffer such as siderite and magnetite) release Fe^{2+} slower than oxidizing species are produced by radiolysis. A coupled transport-reaction model showed that even under very conservative assumptions (H_2 completely inert, Fe^{2+} release from corroding iron and magnetite initially less than oxygen produced from radiolysis) the redox front around a canister would be limited to about 10-20 cm. Radionuclides in higher oxidation states would be scavenged by the remaining Fe(II) phases /JOH 00/, /WER 03/.

Oxidation of Fe(II) phases would eventually lead to the formation of Fe(III) phases. It was estimated that it would take about 4000-5000 years after canister failure that the Fe^{2+} release from iron corrosion would exceed the amount of oxidants produced by radiolysis caused by spent fuel (20,000 years in case of MOX). After that point, the redox front would be reduced in thickness and all Fe(III) phases within this front reduced to Fe(II) or mixed Fe(II/III) phases. The calculated duration is considered very pessimistic because reducing agents such as hydrogen and Fe^{2+} are likely to be present within the container so that the effective production of oxidants leaving the container through cracks is much smaller than assumed in the model.

In a review on the influence of radiation on the corrosion rate, Landolt et al. /LAN 09/ summarized earlier investigations and concluded that at dose rate at or below 3.5 Gy/h no significant increase of the corrosion rate has been found independent of the water

type (low concentrate waters to saturated brines) used in the experiments. As the dose rate in the Swiss concept is estimated at 0.35 Gy/h the impact of radiation on corrosion is assumed insignificant.

Based on earlier studies, Bradbury et al. /BRA 14/ concluded that under anoxic conditions molecular oxidants are not produced in detectable amounts and that water hydrolysis is not likely to affect the components outside the containers.

Microbiologically influenced corrosion

Landolt et al. /LAN 09/ discussed the significance of microbiologically influenced corrosion in the Swiss repository concepts. As bacteria are ubiquitous it is expected that some bacteria, as well as algae and fungi, are present in the repository. They may be active during the very short aerobic phase before the temperature at the container-clay interface exceeds 100 °C. During that time, the extent of corrosion caused by microbial activity is highly likely to be minimal. However, a biofilm may have been formed that could influence later corrosion phases. When the temperature has decreased below 100 °C there may be a short period with sufficiently high oxygen supply and moisture that could be used by bacteria that managed to survive the hot and dry period. It is expected that oxygen is depleted soon so that these bacteria must die. Moreover, if the containers are tightly packed with bentonite, there is little room left for the formation of a biofilm. In the following anaerobic phase when the clay becomes saturated again sulphate reducing bacteria (SRB) may become active again if they have survived the preceding aerobic conditions. Whether or not the conditions are favourable for microbial activity is uncertain. The pores of swelled bentonite leave little room for bacteria to develop and the water activity of 0.96 is another reason why the bacteria growth is likely to be limited. It cannot be ruled out that some bacteria survive the rough conditions. It remains unclear whether they can grow and to what extent they can reduce the available sulphate in the buffer. A conservative approach to estimate the maximum effect of microbially induced corrosion is the use of a mass balance. SRB reduce one mole of sulphate so that one mole of iron can be oxidized.

Kosakowski and Berner /KOS 13/ calculated that the pore water of Opalinus clay (two formations) contains between 0.43 and $10.7 \cdot 10^{-3}$ mol/kg sulphate. Sulphate bearing minerals are celestite (SrSO_4) and barite (BaSO_4). At very low redox potentials these phases could be reduced to sulphides.

Influence of hydrogen overpressure

Diomidis /DIO 14/ summarized the findings on the influence of hydrogen overpressure on the corrosion process. The equilibrium hydrogen pressure needed to stop the conversion of Fe into $\text{Fe}(\text{OH})_2$ would be around 39 atm. But experimental studies showed no influence on the corrosion rate up to pressures of 100 atm /SMA 01/.

Influence of the chloride concentration of the corrosion of steel

Cloet et al. /CLO 14/ reviewed the available literature on the impact of chloride concentration on the corrosion of steel in contact with compacted bentonite. According to the studies cited up to a concentration of 1 mol/l NaCl, there is no significant influence on the corrosion rate. The corrosion products formed under high chloride concentrations were not discussed.

Increase of salt concentration at the corrosion front due to the consumption of water

Due to the consumption of water for the formation of iron corrosion products the local concentration of solutes may increase if the gas-based transport of water to the corrosion front is slower than the corrosion rate. According to two-phase-flow modelling by Senger et al. /SEN 08/ and Xu et al. /XU 08/ even at very low gas permeabilities of the Opalinus clay, the water flow to the corrosion front would be sufficient to replace the water needed for the formation of iron corrosion products.

Pressure build-up of hydrogen in the near field

Xu et al. (2008) calculated that in the near field around a container the hydrogen gas pressure would most probably at the same level as the hydrostatic pressure. Only in case of high corrosion rates and very low gas permeabilities pressures of up to 100 bar may occur after about 100 years and then decrease slowly.

3.5 France

3.5.1 Repository concept

In the French reference concept, vitrified waste will be disposed of in primary containers made of stainless steel. These are encased by a carbon steel overpack. The overpack will be placed in horizontal boreholes ('micro tunnels') excavated in the Callovo-Oxfordian clay rock formation (Fig. 3.2). The structure will be stabilized by a liner (or 'sleeve') made of low-carbon steel /CRU 17/, /AGE 16/. The void space between liner and clay rocks is to be filled with a pH buffering substance that shall compensate for the slightly acidic conditions caused by aerobic oxidation of pyrite.

Earlier concepts planned to employ a bentonite buffer between liner and container /AGE 05/ (/AGE 05/). In the current concept, this structural element was removed to allow retrieval of waste packages for at least 100 years after emplacement.

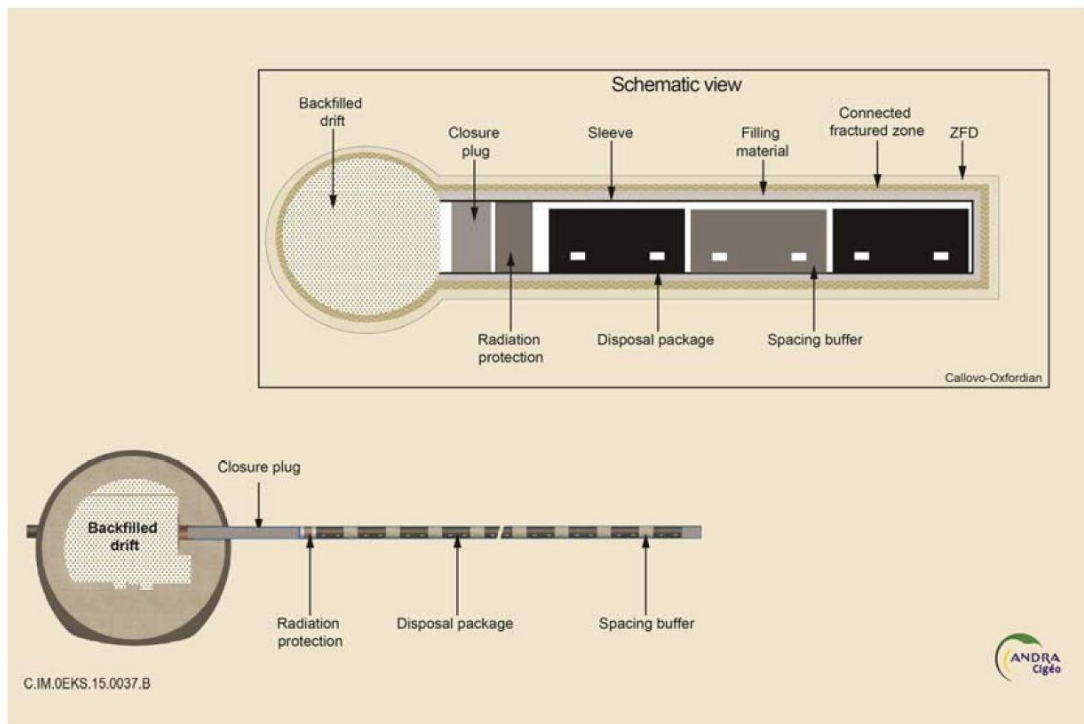


Fig. 3.2 Disposal of HLW waste in micro tunnels according to the French concept /AGE 16/

Host rock (Callovo-Oxfordian)

The claystone at the designated site consists of the following phases /YVE 07/, /WEN 08/, /EL 14/:

- 40–50 % Clay: (50–70 % interstratified illite/smectite, kaolinite, Ca-chlorite, K-muscovite)
- 22–30 % carbonate phase (mostly calcite with a few per cent of dolomite, ankerite)
- 18–32 % quartz
- Few %: Other components such as pyrite, feldspar minerals (albite, microcline), celestine, ferrous oxide, organic matter

The pore water composition at 100 °C was derived by thermodynamic modelling.

Tab. 3.7 Composition of the pore water of Callovo-Oxfordian claystone at 100 °C (modelling)

Element/ Parameter	Measured composition [mol/kg]	Concentration at 100 °C [mol/kg]
K	0.00090	0.00096
Na	0.056	0.039
Ca	0.0076	0.01
Mg	0.0059	0.0025
Si	0.00014	0.00084
Al	-	$8.0 \cdot 10^{-8}$
Fe	$1.5 \cdot 10^{-5}$	$5.0 \cdot 10^{-8}$
Sr	0.00025	0.00017
S	0.019	0.01
Cl	0.041	0.041
TIC	0.0042	
pH	7.2	6.01
Eh (mV)	-199	-300
p _{CO2} (atm)		0.5
Source	/GAU 09/ /GAU 09/	/NGO 14/ /NGO 14/

3.5.2 Experimental and modelling results

In France, several working groups dealt with the investigation of corrosion processes in a nuclear waste repository. The intensity of investigations strongly increased during recent years and gave important insights into corrosion mechanisms and products.

Anaerobic corrosion of iron and steel embedded in clay rock (laboratory experiments)

The corrosion of pure iron (ferrite) in contact with Callovo Oxfordian clay rock was investigated by Martin et al. /MAR 08/ as well as Schlegel et al. /SCH 10/, /SCH 14/ and Leon et al. /LEO 17/. In the Arcorr setup, iron and iron/glass rods were placed in a massive block of Cox claystone for up to two years (one experiment was conducted in compacted MX80 from Wyoming). The corrosion rate was measured voltamperometrically in real-time by adding gold as a pseudo reference electrode. The block was transferred to a cell which was deaerated, heated to 90 °C and then filled with artificial pore water. The progress of the corrosion was monitored by impedance measurements for a total period of four months or two years. A similar setup ('Corrida') but now without additional electrodes was used by Martin et al. /MAR 14/ as well as Schlegel et al. /SCH 19/ to check the corrosion of carbon steel (A37). The experiments lasted from 7 to 76 months at 90 °C. From the perspective of phase formation, the results are quite similar and are discussed together.

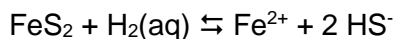
The corrosion front around the iron rod could be characterized by distinct areas:

1. At some places in direct contact to the steel surface, a very thin layer (<400 nm) of iron oxides could be found. If existing it is part of the inner dense product layer (iDPL) that is attributed to a mixture of maghemite, magnetite, Fe(II) carbonates and iron.
2. Following this zone or in direct contact with uncorroded steel a dense product layer (DPL) was identified. It may sometimes be divided into an inner and an outer layer (iDPL and eDPL). Depending on local corrosion behaviour the layer is either a thin coating or occurs in pockets/ depressions that were formerly inhabited by steel. The eDPL consists of Fe-phyllsilicates and relics of the inner DPL. The relics suggest that the eDPL forms at least partly at the expense of the iDPL. Goethite and maghemite were also found in traces in the DPL. Its origin is not quite clear. It may have been formed in the early stages of the experiments when traces of O₂ were still available or after the experiment during sample preparation. After 7 months of reaction, the DPL mainly consisted of (Fe,Si) hydroxide with significant amounts of sodium. In some limited areas, a chloride-rich Fe(III) hydroxide occurred that was identified as akaganeite. After 15 months, akaganeite has disappeared. Iron silicates with varying composition (Fe/Si ratio from 1 to 4) dominate mixed with dispersed chukanovite. Using several techniques the

silicate phase was attributed mainly to the aluminosilicate nontronite /SCH 19/. Other Fe silicates such as berthierite, chamosite, minnesotaite, greenalite and cronstedtite and montmorillonite resemble similar spectroscopic features and were suggested in the earlier publications /SCH 14/. Some sulphur was bound in pyrrhotite, Fe_7S_8 , and possibly gypsum

3. At the top of the DPL sometimes an irregular and thin layer appeared that is designated as the median corrosion layer. It coincides with the original surface of the steel and contains remnants of cementite (iron carbide, Fe_3C in the case of C steel). It also has a relatively high Ca and O content and is identified as ankerite, a mixed Ca, Fe(II) carbonate. Sometimes, ankerite is replaced by iron(II) or copper (I) sulphide.
4. The clay surrounding the original steel surface is partly altered. This is called the transformed matrix layer (TML). In comparison to the original clay, it shows spots of newly formed ankerite and locally chalcopyrite, but otherwise, no Fe rich clay minerals could be detected (in contrast to experiments with iron powder/ clay slurries).

The fate of sulphur and original iron sulphide (pyrite) was investigated because sulphide compounds occurred at places where sulphur originally wasn't present. It was found that some but not all pyrite crystals were strongly corroded. This is an indication that the reaction between corrosion hydrogen (H_2) and pyrite actually takes place at 90 °C:



Although microbial activity was not explicitly investigated, the occurrence of H_2S odour in the first, short-time series of experiments indicated that sulphate-reducing bacteria may have been present. They were thought to exist in the initial space between steel and clay. Empty spaces later closed because of clay swelling and the formation of corrosion products so that microbial activity probably stopped.

The results confirm the outcomes of an earlier experiment, where an iron rod was placed in a claystone block and reacted at 90 °C and 50 bar (gas type not given) for 8 months /SCH 08/. Comparing results after different experimental total durations, it appeared that the reaction reached a steady-state only after 15 months. After that, the type of corrosion layers and corrosion products no longer changed.

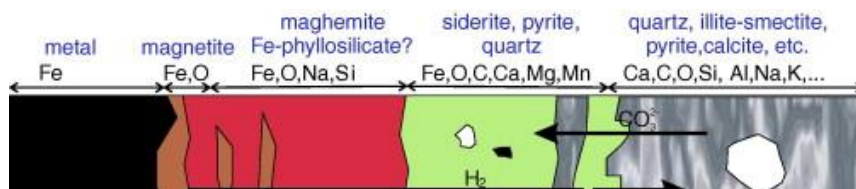
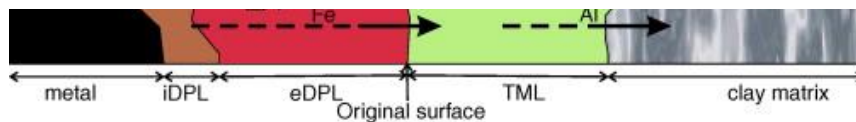


Fig. 3.3 Structure of the corrosion layer between metallic iron and claystone from the Collovo-Oxfordian interval (from /SCH 08/)



Romaine et al. /ROM 13/ let carbon steel rods corrode that were covered by a compacted layer of Cox argillite. The experiments were conducted at 80 °C in a NaHCO₃/ NaCl solution by applying an electrical current. The experiments were conducted for a period of one to 7 days with two different polarizations and carbonate concentrations. The corrosion layer between the electrodes and the argillite generally consisted of two zones. The inner zone always contained magnetite and traces of maghemite, the outer layer consisted of siderite. In some experiments with 0.1 m NaHCO₃ and a lower polarization, maghemite was replaced by carbonate green rust or by mackinawite. In experiments with a lower carbonate concentration (0.01 M NaHCO₃), the magnetite layer contained mackinawite, but in one experiment a mixture of magnetite, maghemite, mackinawite and greigite was found, whereas the outer layer also contained chukanovite.

Anaerobic corrosion of massive steel embedded in clay rock (in-situ experiments)

During an in-situ experiment ('MCO – Gravimetry') conducted under anaerobic conditions, steel rods were lowered in a borehole at the Meuse-Haute Marne underground laboratory /NEC 16/, /NEC 17b/. A part of the samples was exposed to a damp atmosphere, a part was immersed in porewater for up to two years. The procedure was imposed on several samples, including anoxic and transient acidic conditions /NEC 16/, /SCH 16/ and under alkaline and fluctuating temperature /SCH 18/.

Under transient acidic conditions, the innermost corrosion layer (ICP) consisted mainly of β -Fe(OH)₃Cl at some places replaced by GR(SO₄²⁻). The layer contained ribbons of magnetite at places where cementite lamellas were present at the iron/solution interface. The next layers (ICPb and ICPa) consisted of a mixture mainly of chukanovite and siderite with some enrichment in S and Si, pointing to the presence of some iron silicates, possibly iron phyllosilicates. Greenalite was considered a possible phase. This mineral was also found in glass corrosion experiments (50 °C) in the presence of iron /DIL 16/.

In the outer corrosion layer (OCPa) an iron sulphide (possibly mackinawite and pyrrhotite) was identified, accompanied by some Fe(III)oxyhydroxides. The latter may have been formed due to infrequent inflow of oxygen-containing solutions. The next layer (OCPb) was identified as Ca doped siderite (ankerite). Several additional layers could be identified, but they were locally discontinuous. The solids were a mixture of ankerite, FeS and Fe- phyllosilicates. The presence of ankerite and Fe sulphide was interpreted as the product of several periods of microbial activity.

The history of the individual samples played an important role in the corrosion mechanism. Samples that were exposed to low pH do not form a protective layer of carbonate phases and are thus prone to more intense corrosion.

Under alkaline conditions, corrosion was less severe so that the corrosion layers were mostly very thin /SCH 18/. In some less corroded areas, the corrosion products consisted entirely of iron oxides. At least magnetite was identified, but other Fe(III) oxides or carbonates could be present as well. A high concentration of Na suggested the formation of a phyllosilicate. In other areas, the O content was higher pointing to iron (II) oxides and hydroxides. In stronger corroded regions, pockets containing siderite, chukanovite, magnetite and sometimes Fe-hibbingite in direct contact with the metal surface. Iron sulphides were present but not as a full layer. Close to the original metal/clay border, siderite prevailed. The original border presented itself as a sequence of thin layers made of magnetite, Fe-rich silicates (cronstedtite) and enrichments of Cu. The latter was interpreted as the product of an early reduction of aqueous copper ions by metallic iron and subsequent oxidation by aqueous hydrogen sulphide. Specimens that were exposed to 25 °C for a longer time before being heated to 85 °C corroded stronger than those that were heated to 85 °C for most of the time. A similar observation was made in earlier studies /NEC 16/, /SCH 16/ where heavy corrosion occurred in specimens that also went through a prolonged equilibration and heating phase before the final temperature was achieved.

Apparently, the initial period of low-temperature contact with moist clay has a strong impact on the long-term corrosion rate.

Aerobic corrosion of massive steel embedded in clay rock (in-situ experiments)

Gaudin et al. conducted in-situ experiments with carbon steel (A42) disks at the Tournemire underground laboratory /GAU 09/, /GAU 13/. The disks were covered with a mud paste consisting of Toarcian claystone and then placed in vertical boreholes in the wet fractured zone (CR7) and a horizontal borehole (CR5 unfractured zone without free water) for six years. After this period, the disks were recovered by overcoring. Both experiments were assumed to take place under aerobic conditions. In the CR5 and the CR7 experiment lepidocrocite and goethite formed in large amounts. In addition, small amounts of melanterite ($\text{FeSO}_4 \cdot 7\text{H}_2\text{O}$) were found in traces which was accounted for as a secondary product of pyrite oxidation⁸. In any case, pyrite oxidation does take place (very slowly) but contributes only little to the formation of secondary phases. From the results, the authors conclude that considerable amounts of Fe(III)oxyhydroxide may form in the initial aerobic phase of the repository. It is not clear how fast these products will be reduced to Fe(II) compounds like siderite or magnetite once the conditions become reducing.

Dauzères investigated the results of another in-situ corrosion experiment in the Tournemire URL /DAU 13/. Carbon steel disks were placed at the end of the 10 m horizontal borehole (CR6) outside the EDZ and inside the saturated zone for 10 years. The room between the disks and between disks and the main tunnel was filled with crushed and compacted argillite. The discs were recovered by over-coring. The corrosion zone is visible by orange colour and consists of goethite, hematite, and magnetite. Sulphate green rust is suggested to be present in the corrosion zone as well. Moreover, it was found that the corrosion gulf and diffusion halos of iron were closely linked to cracks in the argillite. Although pyrite was present in the claystone it was not oxidised within ten years. If green rust was indeed present, oxygen must have been depleted and the transient period had begun. The absence of significant amounts of Fe(II) minerals, even magnetite showed

⁸ The presence of melanterite is rather surprising as its solubility quite high -1,97 mol/kg (/MOO 04/). The equilibrium concentration of sulphate in the Tournemire porewater is too low ($9.5 \cdot 10^{-3}$ mol/l) to allow the formation of this phase. It is most probably an artefact caused by the preparation of the sample for XRD.

that the oxygen supply must have been sufficient for most of the ten years of experimental time.

Corrosion of massive steel in the transient phase (anaerobic corrosion after extended corrosion under aerobic conditions)

The transient phase when an aerobically oxidised iron item is slowly coming under anaerobic conditions has been investigated by Saheb et al. /SAH 14/. Iron nails were excavated from a 16th-century archaeological site (Castelminier), where they corroded for 400 years in soil under aerobic conditions. The items were transferred to a reactor filled with a calcium hydrogen carbonate solution that was step by step put under anaerobic conditions. The main results of the experiments were that after six months the corrosion layer mostly remained the same. Some cracks occurred suggesting that some of the Fe(III) phases dissolved while Fe(II) carbonates evolved (siderite, chukanovite). It is assumed that the more reactive Fe(III) phases such as ferrihydrite, lepidocrocite and maghemite are dissolved first, while goethite and magnetite are affected.

Haji et al. investigated the sequence of corrosion products formed under conditions that were first aerobic and later anaerobic /EL 13/. The microbiological activity was enhanced by enriching the experimental setup with bacteria cultures. All experiments were conducted at 30 °C with a slurry consisting of COx claystone, artificial porewater and iron coupons. The batches were first operated with limited or unlimited oxygen supply. The coupons were then transferred to new slurries prepared under anoxic conditions and inoculated with sulphate reducing bacteria cultures.

Under limited oxygen supply, lepidocrocite and magnetite were observed. It is assumed that lepidocrocite would transform into goethite. If the corrosion rate is low, lepidocrocite is partially transformed into maghemite. If the oxygen supply was continuous, a mixture of lepidocrocite, maghemite and magnetite was found.

All these iron(III) phases disappear once the conditions become anaerobic. After six months under anoxic conditions, non-stoichiometric pyrrhotite was found (Fe_{1-x}S with $x=0\dots0.125$) with partly hexagonal and monoclinic shape. Under these conditions pyrrhotite is the only oxidation product. It is produced by reduction of the products formed under aerobic conditions (iron oxyhydroxides) as well as through a transformation of mackinawite which is the primary corrosion product under anaerobic conditions.

Anaerobic corrosion of massive steel in contact with a clay slurry

Mendili et al. investigated the corrosion of steel coupons under a 3 %Ar/CO₂ atmosphere in a CO_x slurry at 30 °C for up to six months /EL 14/. After one and three months magnetite was found and traces of mackinawite. After six months the corrosion products consisted of magnetite, siderite, chukanovite, hibbingite and mackinawite. Upon contact with air, hibbingite transformed into akaganeite.

Le Pape et al. investigated the corrosion of an iron foil half immersed in a CO_x suspension and half exposed to an anoxic atmosphere /LE 15/. They found magnetite as the main corrosion product in the atmospheric contact zone while Fe-serpentine was the product in the suspension zone.

Leon et al. examined the corrosion of an iron rod immersed in a slurry of MX80 and CO_x pore water at 90 °C ('Batx' setup). /LEO 17/ In comparison with experiments in contact with clay rock ('Arcorr 2008' setup), the extent of corrosion was significantly larger. A quite thick inner DPL zone was found consisting of magnetite and maghemite. Except for traces of akaganeite in the early stages of the experiment, pure Fe(III) phases were not present if iron was embedded in compact clay rock. This comparison shows that experiments in clay slurries provide only limited insight into the corrosion processes that actually take place under real conditions in a repository.

Experiments at 120 °C with steel (P285NH) and pure iron (Armco) in a slurry with Mx80 were performed by Lotz et al. /LOT 21/. The duration was 30 days. The setup lacked carbonate buffering. Consequently, no carbonate phases were found in the corrosion product layers. They consisted of

- a) a rather compact inner product layer of magnetite that adheres to the metal surface
- b) an external product layer of at least two types of Fe phyllosilicates: smectite (nontronite type) and serpentine

Anaerobic corrosion of iron grains or powder in a mixture with clay powder

Bourdelle et al investigated the interaction of iron powder or grains, CO_x clay and pore water at 90 °C for 90 days under a mixed atmosphere consisting of Argon (~1 bar) and CO₂ (0-0.026 bar) /BOU 14/, /BOU 17/. Different mixing ratios of iron to clay were tested.

The presence of clay buffered the pH at about 7. In the case of the experiment with iron powder, the iron completely disappeared within 90 days. No magnetite was found which was justified by the pH value that was not high enough. The Newly formed clay minerals were enriched in iron but depleted in aluminium and potassium. An iron-containing saponite or poorly crystallized berthierite may be the product, but it could not be confirmed unambiguously. At the same time, quartz and illite-smectite mixed layered minerals dissolve. Parallel experiments without clay and its pH buffering lead to magnetite as the main corrosion phase. Bourdelle et al. /BOU 17/ concluded that two reaction zones have to be distinguished:

1. In direct contact to the corroding iron surface, high pH values occur that allow the formation of magnetite accompanied by Fe-serpentine.
2. Close to unaltered clay the pH and the availability of Fe(II) are lower, leading to the transformation of clay into Fe-poor silicates of kaolinitic type.

Alteration of clay minerals by iron released from the corrosion of steel

Mosser-Ruck et al. investigated the reactions of metallic iron (plates) and magnetite in contact with MX80 (consisting of more than 85 % smectite) for 3 to 12 months /MOS 10/. High temperatures were employed to accelerate reactions. At 80 and 150 °C under alkaline (starting pH 12) and neutral conditions, the clay was partly destroyed by the formation of Fe rich silicates (chamosite, a chlorite or berthierite, a serpentine). At 300 °C vermiculite was predominant, associated with Fe-rich trioctahedral smectites under alkaline conditions and with Fe-rich chlorites under neutral conditions. Silica was removed from the clay phases and crystallized as quartz, feldspars, and zeolites. Another Fe product found in all experiments was magnetite. In interpreting the results, the authors refer to earlier studies regarding the thermal stability of clay minerals. Chlorite is stable between 110 and 420 °C. Fe-rich chlorites have been described for sandstone reservoirs at 100-120 °C. Berthierite has been observed as a low-temperature (15-40 °C) diagenetic phase. The upper stability limit is at 60-130 °C. Above 160 °C, it is transformed into chamosite.

FoCa7 clay is discussed as a material for constructive uses in a repository. It mainly consists of mixed layers kaolinite-smectite (80 wt.-%) and kaolinite (4 %), quartz (6 %), iron oxides (6 %: goethite and hematite), calcite (1.4 %), anatase (TiO₂, not quantified) and gypsum (0.4 %). When brought into contact with Evian mineral water and iron powder for 45 days and 80 °C, both kaolinite and smectite are altered into SiAlFe gels that

mature into Fe-rich di-octahedral phyllosilicates with a composition between odinite and greenalite.

Further results were presented in /MOS 20/. Iron powder, powdered CoX clay and water were mixed in a 1:1:1 weight ratio. Some solid NaHCO_3 was added to provide an initial CO_2 pressure of 20 mbar. The mixture together with two iron plates was heated in a reactor to 90 °C for 107 days. At the end of the experiment, the total pressure made almost entirely of hydrogen reached a level of 50 bar. Water was completely consumed. The reaction led to the dissolution of iron, quartz and clay minerals, especially interstratified illite/smectite and illite. In the bulk clay aluminium and magnesium was depleted while iron was enriched.

- No iron (II) or iron(III) oxides/ hydroxides were found, instead, iron silicates were in direct contact with the iron plate
- Pyrite crystals were often highly corroded. New pyrrhotite crystals were visible (produced through reduction of FeS_2 by hydrogen)
- Illite/smectite and illite partly dissolved to form greenalite, a reaction that also consumes water
- A small amount of iron(II) carbonates was suspected to form but could not be clearly identified

The interaction between metallic iron and kaolinite, a major component of Cox claystone found at the Bure site was studied by Rivard et al. /RIV 13/. Kaolinite was put in contact with powdered iron and simplified pore water (0.0207 M NaCl, 0.0038 M CaCl_2) at 90 °C for 1 to 9 months. The anaerobic reaction resulted in the formation of magnetite and as Fe-rich serpentine phase similar to berthierite with a bulk Fe^{2+} to Fe^{3+} ratio of about 2:1. Upon contact with air, the Fe-silicate dissolved and was transformed into iron oxides and oxyhydroxides. If the corrosion took place under aerobic conditions the phases assemblage was magnetite/ hematite, goethite and maghemite.

The Fe serpentines always crystallize on remaining kaolinite particles so that pure serpentine or kaolinite species are not found /RIV 13b/. For berthierite, a Fe^{2+} to Fe^{3+} ratio of about 4:1 was derived leading, together with other analytical evidence that there must be another Fe silicate present. This Fe-poor phase occurs in minor amounts and was identified to be in the greenalite-cronstedtite group.

The impact of a thermal gradient on clay transformation process was investigated by Jodin-Caumond /JOD 12/. At 300 °C the main corrosion product of a reaction of powdered iron and Callovo Oxfordian claystone was a Fe-chlorite while at 150 °C it was Fe-serpentine. Other products were Fe-saponite and mixed-layered chlorite-smectite and serpentine-smectites. Under the conditions applied Mg was migrating in the direction of higher temperature and formed mixed Fe-Mg clays. Pyrite originally present in the claystone was reduced, possibly to pyrrhotite.

Transformation of iron-rich phyllosilicates produced during iron corrosion during the cooling phase of a repository

Pignatelli et al. studied the mineralogical transformation of iron-rich phyllosilicates during a temperature decrease from 90 to 40 °C to reflect the cooling phase of a repository /PIG 13/. In the first step, iron powder was mixed with Cox clay and a salt solution (0.02 m NaCl/ 0.0038 m CaCl₂) and heated to 90 °C for six months the temperature was reduced in monthly steps of 10 °C to 40 °C. Magnetite was observed to grow on iron particles. Also, iron-containing phyllosilicates were found. One could be identified as cronstedtite, a second one with a higher Si/Fe ratio was suggested to be greenalite. The XRD peaks for cronstedtite became less intense at temperatures ≤ 60 °C, indicating that cronstedtite is no longer stable at lower temperatures as has already been shown by /PIG 13/. However, thermodynamic modelling could not confirm this finding raising questions about the validity of the stability data at low temperatures. The predominance of one or the other phyllosilicate may depend on the local variations of the Si/Fe ratio and pH of the solution. Cronstedtite appears in several polytypes, but only for one thermodynamic data exist. Thermodynamic modelling suggested that cronstedtite would not form above 120 °C and was therefore not found in experiments at this or higher temperatures. Interestingly, cronstedtite is the dominant Fe-phyllosilicate in some meteorites (carbonaceous chondrites, CM type). The corrosion conditions in a repository in the long-term are similar: low temperature, presence of elemental iron, reducing conditions, presence of fluids and neutral to alkaline conditions.

Modelling of iron release from corrosion and its impact on clay mineralogy

Ngo et al. compared the experimental findings of Bourdelle et al. /BOU 14/ with the results of kinetic-thermodynamic modelling /NGO 15/. They calculated that Fe²⁺ released by the corrosion of metallic iron was likely to be incorporated into newly formed Fe-rich phyllosilicates which then convert to odinite-greenalite. Moreover, it was predicted that

chukanovite would form, but would disappear in favour of Fe,Ca-saponite once the iron has been consumed. These predictions strongly depend on the intermediate concentrations of silicic acid and CO₂. High solution concentrations of silicic acid favour the formation of saponite while higher CO₂ pressures stabilize chukanovite. Magnetite was not formed because

- the pH remained in the neutral range due to the buffering by CO₂ and the newly formed phyllosilicates
- the Fe²⁺ concentration in the solution remained low because it was immediately precipitated as phyllosilicates.

The authors noted that in other experiments magnetite was indeed found, probably because the pH was higher because of the iron corrosion and the lack of CO₂ buffer.

Microbially enhanced corrosion of massive steel in a clay slurry under anaerobic conditions

Mackinawite was found as a primary corrosion product when steel coupons were directly placed in an anaerobic claystone/ water slurry that was inoculated with bacteria cultures /EL 13b/. It transformed fast into monoclinic pyrrhotite. Under oxidising conditions, magnetite dominated in the first week but later transformed into maghemite.

In a similar experiment, El Mednili et al. /EL 13/ investigated the corrosion of carbon steel under a 5 % H₂/N₂ atmosphere. Iron coupons were placed in a slurry made of COx argillite. Lactate was added to emulate the growth of sulphate-reducing bacteria. The experiments were conducted at 30 °C for three months and then at 90 °C for another three months. In the first month, magnetite developed. After 3 months the steel coupons turned black and showed the formation of iron sulphide, which was identified as mackinawite. After heating to 90 °C it was transformed to pyrite.

Anaerobic corrosion of massive steel in aqueous solution

Refait et al. investigated the corrosion process that occurred when carbon steel rods immersed in deaerated NaHCO₃ solutions were polarized at room temperature for up to 24h /REF 11/, /REF 12/. Only two compounds were found: magnetite and carbonate green rust. No chukanovite was detected. The authors stated that this mineral would only form at potentials close to the open circuit potential, i. e. in the case of free corrosion. When the solutions also contained sodium sulphate (0.03 M) but only 0.003 M NaHCO₃

sulphate green rust was the main phase, but carbonate green rust was found as well. Experiments with added NaCl (0.5 M) resulted in the same phase assemblage. The results were compared to the observed phases from steel coupons that were placed in the harbour of La Rochelle for 11 years /REF 11/. The inner part of the corrosion layer consisted of magnetite, sulphate green rust and mackinawite, while the outer layer revealed a mixture of magnetite and iron oxyhydroxides such as goethite.

Impact of hydrogen gas on Callovo-Oxfordian clay minerals

Didier et al. /DID 12/ investigated the interaction of hydrogen with Callovo-Oxfordian clay at 90 °C. They could show that hydrogen adsorbs on clay. A limited reduction of Fe(III) was observed in experiments with synthetic montmorillonite samples, but no such reaction was found with untreated Callovo-Oxfordian clay, where Fe(III) is present as a structural element of clay minerals.

Evolution of the aerobic/ anaerobic corrosion regime after the closure of the repository

The duration of the aerobic phase in a repository in clay (France) was estimated by de Windt et al. /WIN 14/. The factors controlling the availability of oxygen in a borehole include:

- The volume of air in and around the borehole: porosity of the unsaturated clay rock and clay buffer, residual voids between buffer and host rock
- Initial water saturation state
- The corrosion rate of metal parts (liners, container)
- The corrosion rate of pyrite
- The operational regime of the handling drift (constantly ventilated or closed)
- Gas diffusion coefficient (transport of oxygen from the drift into the borehole)

In a closed system with no air exchange with the drift, a complete and fast (80 days) consumption of oxygen was expected. If the gas exchange was considered (through the EDZ but not through saturated clay rock), a steady state develops within 6 months. All parts of the borehole are affected by a constant supply of oxygen. Due to the constant reaction of oxygen with iron and pyrite, about 95 % of oxygen are consumed when the gas reaches the end of the borehole. The lining zones (with voids between liners and

host rock) are entirely under oxidizing conditions ($E_h > 800$ mV) while the claystone (beyond the EDZ) remains under reducing conditions ($E_h < -200$ mV). If hydrogen is produced as a corrosion product and considered an active species the redox potential would be around -800 mV. If no voids are present only the first 5 m of the disposal cell are disturbed by air. Thus, distinct zones will develop in a borehole: strongly reducing conditions at the end of the cell and oxidizing conditions at the beginning of the cell.

Reduction of pyrite by corrosion hydrogen

A secondary effect of iron corrosion is the potential reductive action of hydrogen at elevated temperatures. While hydrogen is often considered inert, Truche et al. could show that at temperatures starting at or above 90 °C the reactivity of hydrogen is high enough to reduce the clay rock component pyrite to pyrrhotite /TRU 10/. It forms a crust over the pyrite core. The growth of the crust is controlled by the pyrite reduction process and the diffusion of HS^- through the surface film. On the other hand, the inorganic thermal reduction of sulphate is found to be too slow at temperatures found in the near field and is assumed to be negligible /TRU 09/.

3.6 Sweden

As part of the European NF-PRO project, a couple of corrosion experiments with metallic iron (coupons and wires) in MX-80 bentonite were conducted /MIL 09a/, /MIL 09b/. In experiments at 50 °C and a 1M NaCl solution (90–198 days, starting pH 8.4 or 11), the corrosion products were akageneite, magnetite and Fe-enriched clay minerals that could not be identified. Possible phases include Fe-rich dioctahedral smectite (such as nontronite) or a chlorite (berthierite) or a mixed-layer chlorite-smectite. In the second set of experiments (0.01 M to 1M NaCl, 571 to 614 days) the alteration of bentonite was obvious, but the mineralogical identity of the Fe-rich phases remained unclear. No iron-oxyhydroxides could be detected as well.

Radiation may increase the corrosion rate of iron under anaerobic conditions and in contact with Allard Groundwater (about 0.2 mM NaCl/NaHCO₃), but magnetite was still the major corrosion product /SMA 05/, /SMA 08/. No green rust was found but some indications that iron(III)oxyhydroxides may have formed.

The anaerobic corrosion of cast iron and carbon steel wires and coupons in compacted MX-80 at 30 and 50 °C was followed by Carlson et al. /CAR 07/ for up to 911 days. The main corrosion products were magnetite, hematite, and goethite on coupons. On wires, only magnetite occurred. No $\text{Fe}(\text{OH})_2$ was found. In the surrounding bentonite, the Fe concentration increased, mainly due to additional Fe^{2+} . It was not possible to identify distinct Fe silicate minerals. Iron oxides were not present in the bentonite phase.

For the Swedish KBS-3V facility, it was calculated that anoxic conditions would be re-established within 200 years /GRA 06/.

In the ABM2 experiment, a stack of rings made of different bentonite types and bentonite/sand mixtures was placed around an iron rod and lowered into a borehole in the Äspö hard rock laboratory, where it was flooded with artificial Äspö groundwater /HAD 17/. The system was heated for three years to 130 °C. After that, the heater was turned off and the system was allowed to settle for another year. During the experiment, the system was not sealed from the atmosphere. The results differed slightly among the bentonites used. The following sequence of corrosion product layers was found:

- The innermost layer consisted mainly of goethite with traces of magnetite
- The next layer was made up of a 'mix of iron corrosion products and bentonite' (probably iron silicates)
- Another layer consisted mainly of lepidocrocite

In some samples, siderite could be identified. The presence of maghemite was suspected as well. Although the authors claim that the conditions were anaerobic, the excessive presence of pure Fe(III) phases show that atmospheric oxygen had sufficient access to the borehole. There is no hint that access to air was prevented after the system was removed by overcoring the borehole. In that case, the samples may have been altered before they could be analysed.

3.7 Japan

Corrosion experiments with iron in contact with bentonite under anaerobic conditions in solutions with up to 0.56 M NaCl and 0.1 M NaHCO_3 and an experimental duration of up to four years resulted in the formation of siderite and chukanovite /TAN 04/.

A long-term corrosion experiment was described by Ishidera et al. /ISH 08/. A carbon steel plate was placed in a thick layer of bentonite and saturated with either simulated seawater (approx. 0.5 M NaCl), carbonated seawater (0.1 NaHCO₃ added) or low salinity water (0.005 NaCl/NaHCO₃). No alteration of the clay phases was observed and consequently, no Fe-silicates were identified. By XRD lepidocrocite and chloride green rust were detected. It was assumed that the most important corrosion phase was amorphous Fe(OH)₂ dispersed within the bentonite phase because it was easily extractable by NH₄Cl. This conclusion is surprising since Fe(OH)₂ has never been identified as a corrosion product in clay before. More likely, Fe(II) was present as a phase not included in the XRD database or as part of a reactive Fe-rich silicate that could not be detected in the bentonite matrix.

3.8 Czech Republic

Iron was mixed with seven dioctahedral smectites extracted from different bentonites and heated to 75 °C for 35 days in a nitrogen atmosphere. The main products included magnetite and a berthierite like clay mineral. Traces of lepidocrocite and goethite were found but were accounted for oxidation processes before the beginning of the experiments /OSA 10/.

3.9 Miscellaneous studies on geochemical processes

3.9.1 Corrosion in the presence of H₂S

According to the findings of Wikjord et al. /WIK 80/, the principal products of iron corrosion in presence of H₂S follow the sequence

1. Mackinawite (tetragonal FeS_{1-x})
2. Ferrous sulphide (cubic FeS), later described as the mineral rudashevskyite /BRI 08/
3. Troilite (hexagonal FeS)
4. Pyrrhotite (monoclinic or hexagonal Fe_{1-x}S)
5. Pyrite/ marcasite (cubic FeS₂)

The primary product at 30 °C is mackinawite which is replaced by troilite after a longer reaction time (72h). At 60 °C troilite is the primary product that transforms into pyrrhotite. Even at 160 °C pyrite was not observed. It was found however by Tewari et al. at 120 °C /TEW 79/. Murowchick and Barnes /MUR 86/ reported that the corrosion of iron powder at temperatures up to 92 °C and acidic conditions (pH <6) first led to cubic FeS which within hours converted into mackinawite. At higher temperatures or pH values, no cubic FeS was observed.

Ning et al. /NIN 13/ discussed in detail the potential iron phases and confirmed that mackinawite would be the primary corrosion product at 25 °C, apparently in a nanomolecular form /RIC 06/. Its non-stoichiometric formula may be explained by the presence of other minor elements in the corroded material. Rickard et al. /RIC 06/ just found FeS and assumed that previous findings regarding the formula were incorrect.

Cubic FeS does not form above 92 °C or in the presence of oxygen and chloride /NIN 13/. As chloride is expected to be always present under German repository conditions this phase is of no relevance.

Although pyrite is the most stable iron(II) sulphide under anoxic conditions it does not control the Fe²⁺ concentration in solution because the nucleation and growth under 100 °C are extremely slow. When metastable, more reactive iron sulphide are present, solutions are in equilibrium with them and at the same time oversaturated with respect to pyrite. Pyrite would not form directly from the solution but as an alteration product of the metastable phases /SCH 91/.

It should be noted that under some conditions, greigite, Fe₃S₄, the sulphur analogue of magnetite is formed /ROM 13/. There is currently no experimental evidence that other iron sulphides such as metastable marcasite (orthorhombic FeS₂, a dimorph of pyrite) and smythite (trigonal-hexagonal Fe_{1-x}S) occur during the corrosion of iron in anoxic clay media.

3.9.2 Reduction of Fe(III) oxides by H₂S

At 25 °C H₂S reduces hematite to aqueous Fe²⁺ and eventually FeS. Similar processes were observed for other Fe(III) oxides and oxyhydroxides. Magnetite may be reduced as well /DOS 92/, /POU 04/.

3.9.3 Reduction of pyrite by H₂S

The reduction of pyrite by H₂ is observed at elevated temperatures (>90 °C) and hydrogen pressures (8 bar, /TRU 10/). The reaction cannot be shown to occur at 35 °C or 55 °C even in the presence of bacterial communities /HOL 10/. Pyrite reduction leads to the formation of aqueous or gaseous H₂S that may take part in the corrosion process of metallic iron (see above) or react with aqueous Fe²⁺ or Fe(II) solids to one of the above-mentioned iron sulphides. It may also reduce remaining Fe(III) oxyhydroxides to aqueous Fe(II) /DOS 92/.

3.9.4 Microbial conversion of hydrogen to methane

In the context of the Belgian repository project, it was found that hydrogen in contact with Boom Clay was converted to methane by methanogenic bacteria. This process may take place once sulphate has been reduced /ORT 02/.

3.9.5 Reduction of iron(III) in oxides and clay minerals by H₂

Although thermodynamically favoured, iron(III) oxides are not reduced by hydrogen gas at temperatures below 150 °C /JOZ 07/, such reaction may take place in the presence of certain microorganisms /WEB 06/. Communities of hydrogen oxidising and iron-reducing bacteria are found in anoxic marine sediments. For growing they need a carbon source such as malate, citrate, or fumarate /CAC 94/. Magnetite may be reduced by hydrogen in the presence of iron-reducing and hydrogen oxidizing bacteria. Therefore, initial passivation of the iron surface by dense magnetite layers may be altered or removed by microbial action (/LIB 14/).

Elemental hydrogen could reduce structural Fe(III) in a natural clay/ water suspension at 90 °C and 5 bar H₂ pressure while no reduction could be observed if the clay was in a dry state. However, synthetic clay did react even in the dry state /DID 12/, /DID 14/.

3.9.6 Anaerobic reduction of sulphate by elemental hydrogen

Sulphate may be reduced by hydrogen gas in a homogenous reaction. For 90 °C, the half-life was estimated at 210000 years, while at 25 °C it would amount to 2.7·10⁹ years

/TRU 09/. However, the reaction only takes place when considerable amounts of HSO_4^- are present which requires a pH below 5 – a condition typically not met in underground clay or salt formations.

3.9.7 Green rust formation

A carbonate green rust, $\text{Fe}^{\text{II}}\text{Fe}^{\text{III}}_2(\text{OH})_{12}\text{CO}_3$ has been found when pure iron corroded in a solution containing 10 mM NaCl and 2 mM HCO_3^- /CUI 02/.

/REF 11/ /REF 11/ found that sulphate and carbonate green rusts occur when carbon steel is electrochemically corroded in deaerated seawater.

3.9.8 Corrosion in a humid, anaerobic atmosphere

Newman et al. tested the corrosion behaviour of low carbon steel wires at 30 to 70 °C in an atmosphere with controlled relative humidity between 30 to 85 % /NEW 10/. All wires were pre-corroded in dilute NaCl solution. The salt deposition increased the corrosion rate significantly in comparison with specimens not treated before. Corrosion products almost always include magnetite, sometimes goethite and oxides (maghemite and hematite). Carbonates appeared in a couple of experiments. In single cases, ferrihydrite or akaganeite could be identified.

3.9.9 Corrosion in contact with sand

Pandarathan et al. investigated the corrosion of carbon steel emplaced in silica sand and in contact with a brine consisting of 3 wt.-% NaCl saturated with CO_2 (by addition of 0.01 wt.-% NaHCO_3 .) /PAN 14/. After 24h contact at 80 °C, the main corrosion products were chukanovite and, to a minor extent, siderite. Corrosion experiments without sand lead to siderite only.

3.9.10 Corrosion in unsaturated systems

Morcillo et al. summarized the processes of early corrosion in aerobic, marine systems at different relative humidity /MOR 15/:

1. Contact of chloride-containing water with iron leads to the formation of aqueous FeCl_2 that hydrolysis to FeO and HCl
2. Further action of chloride leads to the formations of Fe-Hibbingite on the steel/water interface
3. This phase is oxidised to green rust one GR1 (Cl^-), whereby electrons and H^+ are released.
4. GR1 (Cl^-) may react with chloride to an “overchlorinated” green rust GR1(Cl^-)* with higher Cl^- content
5. Both GR1 (Cl^-) and GR1(Cl^-)* are precursors for the oxidation to akaganeite. However, akaganeite is only formed if the relative humidity amounts to 80 % at least
6. akaganeite may be reduced by dissolved Fe^{2+} or by electrons from the steel surface to magnetite
7. Lepidocrocite, goethite and maghemite form in parallel to akaganeite

3.10 Natural analogues

3.10.1 Corrosion of archaeological artefacts

So far, the maximum duration of corrosion experiments under near repository like conditions was about 10 years /ISH 08/, /DAU 13/. Processes that need much longer to progress considerably cannot be investigated under controlled conditions due to practical reasons. The investigation of archaeological artefacts may give insight into the long-term corrosion processes of iron materials if the conditions at the site can be reconstructed reliably.

Archaeological objects that were mineralogically investigated include the following types:

- Remnants of World War I artillery shells embedded in clay soil during combat /PON 03/
- Nails and other pieces of metal from artisanal zones and forgeries dating from the 12th to 16th century /RÉG 07a/

The corrosion layer around iron buried in soil is typically composed of four distinct zones /NEF 05/:

- The metallic substrate containing metallic iron as well as inclusion from the forging process (slags, high-temperature corrosion products such as hematite, magnetite)
- A dense product layer (DPL). A zone of well-crystallized and compact phases consisting of iron oxides, iron oxyhydroxides, chlorides and/or carbonates. The DPL may contain slag inclusions (SI) originating from the metallic substrate. Sometimes the DPL may be further divided into an inner (iDPL) and an external zone (eDPL) (e. g. /SCH 10/)
- A transformed medium zone (TM), where corrosion products and components of the soil are mixed. In experiments with clay rock, it could be shown that in the TM the clay minerals are altered as well. The border between the TM and the DPL represents the original border between uncorroded metal and soil
- The soil (S) where only the unaltered soil is present and no corrosion products

The slag inclusions may contain slowly reacting minerals such as fayalite (FeSiO_4), wüstite (FeO) and glassy phases. Under aerobic conditions, the DPL mainly consists of goethite and magnetite. Typically, there is a goethite matrix with embedded magnetite or mixed magnetite/maghemite veins. Other authors report that also ferrihydrite (Saheb et al. 2014), lepidocrocite and ferroxhyte /PON 03/, /NEF 10/ may occur. Cracks parallel to the M/DPL border may contain elements not originally present in the metal. Sometimes carbonates (siderite, calcite) are found here. The DPL may also contain minor elements such as S, Si and P. If chloride is present in the local media special phases such as akaganeite or $\beta\text{-Fe}_2(\text{OH})_3\text{Cl}$ may appear.

Under anaerobic conditions the DPL the most frequent corrosion products are Fe(II)carbonates (siderite, chukanovite or carbonate green rust) /SAH 08/, /SAH 11/, /NEF 10/ together with magnetite and strips of maghemite. Siderite and chukanovite were also found in laboratory corrosion experiments resembling the geochemical milieu at the archaeological sites /SAH 08/. At high chloride concentrations, Fe-Hibbingite may be found /RÉG 07b/, /RÉG 07a/. The DPL on specimens from one site with anaerobic conditions (Glinet) consisted mainly of siderite where 1–4 % of Fe was substituted by Ca. Moreover, at the DPL/TM interface strips of iron sulphides were identified /NEF 05/. Chukanovite is metastable with respect to siderite. It is more often found in direct contact to the metal interface surrounded by siderite, into which it transforms slowly /AZO 12/.

If higher concentrations of chloride are present, akaganeite with 5–8 % Cl or β -/ γ - $\text{Fe}_2(\text{OH})_3\text{Cl}$ may constitute the main phases in the DPL. Akaganeite and types β -/ γ - $\text{Fe}_2(\text{OH})_3\text{Cl}$ may occur as separate layers or in a mixed in one layer /REG 05/, /RÉG 07b/, /RÉG 07a/, /RÉG 15/.

The same phases are also found on artefacts buried for 2000 years in seawater sediments /RÉM 09a/. It was noted that items that were buried under the same conditions do not show Cl-containing phases or only at the interface between metal and DPL. β - $\text{Fe}_2(\text{OH})_3\text{Cl}$ is easily oxidised by oxygen into akaganeite either already in the soil or after the excavation. According to Refait et al. /REF 97/ the concentration ratio $R'=\text{Cl}^-/\text{OH}^-$ must be larger than 8 to precipitate akaganeite rather than goethite, and larger than 6.5 to produce it alongside goethite. The appearance of akaganeite in low chloride media show that at some spots around the iron metal the local Cl concentration must have been high enough. Although there is no analytical evidence of chloride green rust on archaeological artefacts, its occurrence is highly likely. Refait et al. /REF 06/ assume that β - $\text{Fe}_2(\text{OH})_3\text{Cl}$ is oxidised in analogy to solid $\text{Fe}(\text{OH})_2$ which would lead to chloride green rust. This compound may then be further oxidised to akaganeite. The $\text{Fe}^{\text{II}}/\text{Fe}^{\text{III}}$ ratio in chloride green rust may vary from 2.2 to 3 /REF 98/.

Saheb et al. /SAH 14/ investigated how the oxidation products of the aerated/anoxic transient phase influence the corrosion process in the anaerobic phase. They found that neither the type of corrosion products changed nor that the corrosion rate was altered.

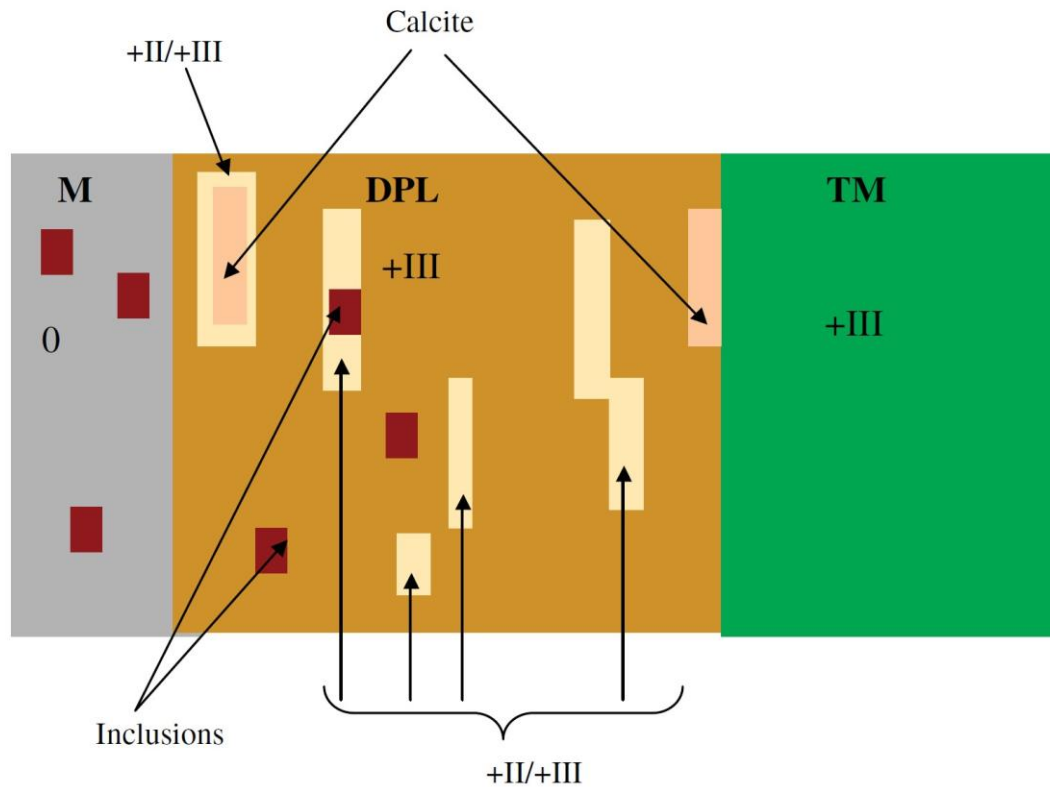


Fig. 3.4 Schematic description of the corrosion zone around iron artefacts /NEF 05/

The TM zone has similar optical properties to clay but may be distinguished by measuring the iron content. The end of the TM zone is located where the iron concentration equals the content of the unaltered soil. The zone may be up to 6 mm thick. If iron phases are detected, then only Fe(III) minerals (goethite). A generalized scheme of the corrosion zones is given in Fig. 3.4.

Of the highest interest is the long-term corrosion of iron in anoxic soils. One example are nails excavated from the ancient iron-making settlement of Glinet (Normandy, France, 16th century) that were investigated by Saheb et al. /SAH 10/. Dissolved oxygen concentrations in the waterlogged soils were below 1 ppm which indicated nearly or fully anaerobic conditions. The corrosion phases evolved are a mixture of siderite, chukanovite, magnetite and calcite.

Thermodynamic modelling supported the findings. It was shown that the corrosion probably took place in three steps /SAH 10b/. In the first step ferrihydrite is formed under oxidising conditions, follows by an intermediary second step when ferrihydrite is in

equilibrium with siderite. In the third anaerobic step, the conditions are more reducing and lead to the formation of magnetite and chukanovite.

The corrosion of historic steel materials in contact with salt rock was investigated by Sawłowicz et al. /SAW 20/. They examined the corrosion process on 30 to 70 years old artefacts (pipes, chains, valves) found in the salt mine of Wieliczka (Poland). The items were in contact with saturated NaCl solution for a long time followed by dry periods. The primary corrosion product appeared to be akaganeite and lepidocrocite. In the outer layer, these were transformed into magnetite in periods of lower redox level. Magnetite later oxidised to goethite.

Another object of interest are shipwrecks, Since the 19th century ships and later submarines have been built with a steel hull. Due to wartime activities and accidents in heavy weather, thousands of shipwrecks are buried on the ground of the sea. Depending on their current depth they are exposed to suboxic or anaerobic conditions. Often, the initial conditions of corrosion were aerobic with at least a limited supply of oxygen. The formation of corrosion layers reduced the access of oxygen to the corrosion front so that the condition became anaerobic /BAE 21/. Nevertheless, the observed primary corrosion product in direct contact with the metal was akaganeite. The exterior surface was composed of calcium and magnesium carbonates and silicates. Low amounts of siderite were found but also magnetite and goethite

3.10.2 Meteorites

Pekov et al. /PEK 07/ investigated buried remnants of an iron meteorite, that fell to earth approx. 5000 years ago. Fragments that were embedded in waterproof clay layers were unaltered, but those situated in sand layers were intensively altered. Although the sand layers were oxidizing by nature and the fragments oxidized to Fe(III) containing minerals on the surface, in some inner cavities pure Fe(II) compounds were found. Obviously, the local conditions within these cavities were anoxic because the water slowly diffusing inside the meteorite body lost its oxygen content. The corrosion process resulted in massive crystals of $\text{Fe}_2(\text{OH})\text{CO}_3$ (up to 20 cm). The compound was identified as a new mineral and named chukanovite.

Wersin et al. /WER 08/ pointed on the occurrence of Fe-rich silicates in meteorites. Some of them are rich in metallic iron (chondritic meteorites) and contain variable amounts of

Ni. These elements are embedded in a silicate matrix. Iron sulphides are the main alteration products. When sulphur is depleted, iron-rich silicates form that include cronstedtite, berthierite, chlorites and Fe-rich smectites.

3.11 Synthesis: Geochemical evolution of the near field and corrosion

The overall redox condition in a sealed emplacement section of the repository may be divided into four phases /LAN 09/:

1. Aerobic corrosion of metal in contact with hot steam and dry clay
2. Aerobic corrosion of metal in contact with solution and unsaturated clay
3. Anaerobic corrosion of metal in contact with solution and unsaturated clay
4. Anaerobic corrosion of metal in contact with solution and saturated clay

The duration of each phase strongly depends on the individual emplacement concept chosen for a specific site. Among the determining factors are the temperature evolution, the availability of oxygen in open pores and cavities, the amount of metal used in the emplacement section, the corrosion rate of liners, containers and metallic components in the support structures of the drift (anchors, steel mesh) as well as the duration until full saturation of the clay rock and buffer. Currently, only some of the necessary information is available for the generic model site 'Nord'. No attempts were made to fill the gaps and then to aggregate the data into a redox evolution model. Such a calculation was undertaken for the Swiss concept of placing containers in drifts in an Opalinus clay formation. The results are given in Fig. 3.5 and they serve as orientation only. For the French repository concept, complete consumption of free oxygen is expected to take place within 80 days after the emplacement borehole is sealed /WIN 14/. If the drift is still ventilated part of the borehole may be supplied by fresh oxygen through fissures in the EDZ.

Despite the differences in the disposal concepts of France, Switzerland, and Germany, it is expected the basic structure of the redox evolution applies to a German site in a clay formation as well.

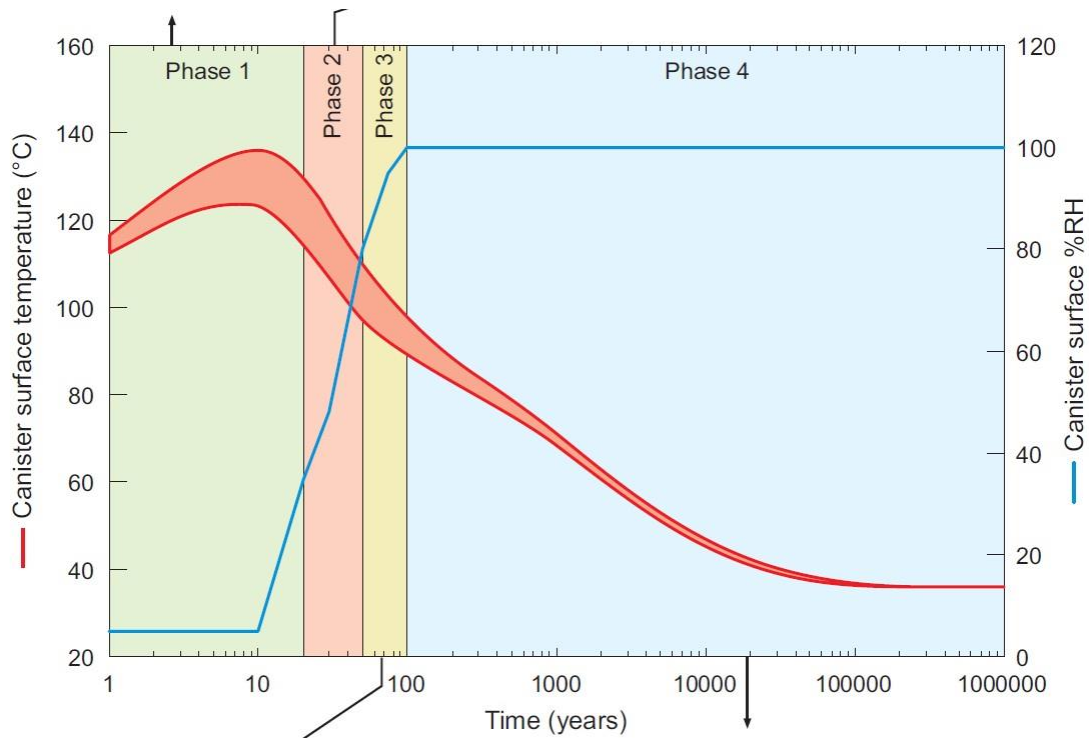


Fig. 3.5 Four phases of the metal corrosion in a repository (Swiss concept, Landolt et al. 2009)

Phase 1: Aerobic corrosion of metal in contact with hot steam and dry clay

After the emplacement of the waste containers and the sealing of the section (drift or borehole) the temperature is rising above 100 °C and drying the clay around the heat-generating waste. Dissolved salts in the remaining pore water precipitate. During this period, the corrosion process is rather slow as the metal is only in contact with gaseous water. It was estimated that even at 300 °C the maximum corrosion thickness on fresh metal would be 150 µm after 100 years. It is expected to be much less on containers that already were exposed to atmosphere before and already possess a layer of corrosion products. The maximum amount of oxygen available in open pores and cracks must be considered as well. Based on the oxidations rates by Terlain et al. /TER 01/, Johnson and King /JOH 08/ predicted a maximum corrosion depth of only 0.2 to 0.3 µm.

Magnetite and hematite are the main corrosion products at temperatures up to 300 °C /TER 01/, /LAN 09/ with magnetite forming first and building up layers that are covered by hematite /DIO 14/.

Phase 2: Aerobic corrosion of metal in contact with solution and unsaturated clay

When the temperature decreases again water may condensate on the metal surface / in the interface between clay and metal. Precipitated salts may dissolve again and influence the corrosion process. The main products at this stage are

- magnetite,
- Fe(III)oxides: hematite, maghemite
- Fe(III)oxyhydroxides: goethite, lepidocrocite, feroxyhyte, ferrihydrite, akaganeite
- Green rust (chloride, sulphate, and carbonate forms)

For the Swiss concept, it was calculated that if all oxygen was consumed by metal corrosion of containers only (144 mol per canister) and not by corrosion of construction steel in the drifts or oxidation of pyrite and organics that the maximum corrosion depth would be about 74 µm in case of uniform corrosion /NAG 02/, /DIO 14/.

Localised corrosion may lead to deeper pits that are considered relevant but small in relation to the wall thickness of the containers (15 cm in the Swiss concept). In the Swiss concept phase, 2 is expected to last 20 to 30 years and the total duration of the aerobic phase would be about 50 years.

Under different settings (higher or longer high temperature period, higher corrosion rate), phase 2 may be entirely skipped.

Phase 3: Anaerobic corrosion of metal in contact with solution and unsaturated clay

When all oxygen has been consumed, the corrosion of the metal leads to a different set of corrosion products with a higher share of Fe(II) in the solid phases and the solution. At the beginning of phase 3, ferric corrosion products may interact with the metal surface or aqueous Fe(II) to form mixed Fe^{II}/Fe^{III} phases such as magnetite, green rust, or Fe-silicates. Ferric phases may also occur as secondary products of aerobic alteration processes that took place during the (long-term) storage of excavated clay at the surface.

If locally no ferric phases are available for reduction or too slow for a reaction, the corrosion of the metal surface leads to the generation of hydrogen gas and the release of aqueous Fe²⁺:



Fe²⁺ may diffuse away from the metal surface and then

- interact with remaining ferric phases to mixed Fe^{II}/Fe^{III} phases (magnetite-Fe₃O₄, green rusts)
- be oxidized to Fe(III) oxo phases such as akaganeite and maghemite (only in disperse form)
- be precipitated as Fe(OH)₂ or amakinite (Fe,Mg)(OH)₂
- and react via the Schikorr mechanism to magnetite

$$3 \text{Fe}(\text{OH})_2 \rightarrow \text{Fe}_3\text{O}_4 + 2 \text{H}_2\text{O} + \text{H}_2$$
- react with silicate released by the dissolution of quartz to form Fe-clays (odinite, cronstedtite, berthierite, greenalite)
- react with other available anions to
 - carbonates (siderite – FeCO₃, ankerite – (Fe,Ca,Mg)CO₃, chukanovite-Fe(OH)₂CO₃)
 - chloride: hibbingite-endmember β-Fe₂(OH)₃Cl, hibbingite - (Fe^{II},Mg)(OH)₃Cl
 - sulphides: mackinawite, FeS_{1-x} that may further react to troilite-FeS, pyrrhotite- Fe_{1-x}S, greigite-Fe₃S₄, pyrite/ marcasite-FeS₂

Hydrogen, although a rather slow reacting reducing agent may at a higher temperature (>90 °C) reduce pyrite to pyrrhotite, thereby releasing hydrogen sulphide (H₂S).

Diomidis et al. /DIO 14/ noted that the production of Fe(OH)₂ and the subsequent Schikorr reaction is often mentioned in the literature but the original work dates to the 1940ies and 1950ies. In more recent investigations and especially in studies dealing with corrosion in bentonite, that were using more advanced analytical methods, Fe(OH)₂ was never found. There is no indication that Fe(II) compounds such as chukanovite, Fe-hibbingite, siderite/ ankerite spontaneously oxidize to Fe(III) oxides even at elevated temperatures.

Phase 3 is expected to last about 50 years. A long-term corrosion rate of about 1 µm/a is considered plausible and consistent with findings from archaeological artefacts /LAN 09/. However, Newman et al. /NEW 10/ found only 0.01 to 0.1 µm/a on pre-corroded steel items and predicted a stable long-term corrosion rate of 1 nm/a after one year.

The resulting hydrogen production rate results in pressure build-up near the container, but migration of hydrogen into the surrounding clay as well as chemical oxidation processes limit the maximum pressure. For example, Sedighi et al. /SED 15/ predicted that the maximum pressure of hydrogen in the bentonite buffer would not exceed 2.45 bar. However, this calculation is concept and site-dependent and must be verified for an individual site. Factors such as salinity may lead to sharply increased corrosion rates thus leading to higher H₂ pressures.

Phase 4: Anaerobic corrosion of metal in contact with solution and saturated clay

In Phase 4 the clay in the host rock and the buffer is completely saturated. All corrosion products formed during the aerobic phase have been consumed. Further corrosion processes generally lead to the generation of hydrogen. The corrosion products are essentially the same as in phase 3.

Influence of concrete structures in the vicinity of the boreholes

According to studies cited above within 100,000 years bentonite buffer and clay rock in contact with alkaline concrete will be altered only within some 10 cm from the interface. In the AnSichT concept, the concrete structure nearest to the liners and the containers in a borehole is the abutment above the borehole sealing. The distance between the abutment and the outer liner is 5 m so that the clay in contact with the outer liner is probably not affected.

Outside the alteration zone, the pH of the pore water increases only slightly (1 to 2 pH units) and no fundamentally different iron corrosion phases are expected than those already described.

The situation is different for reinforcing steel that is used inside or under a shotcrete wall alongside the drifts. But these elements are outside the scope of this study.

Progress of corrosion and redox conditions at the time of first radionuclide release

Which corrosion phases and which geochemical conditions are to be expected when the first radionuclides are released? A release may only start when the container walls are so severely corroded that external solutions may penetrate the containers and get in contact with waste. The expected lifetime of containers placed in clay formations spans

a range of 2,000 to 30,000 years (Tab. 3.8). For a repository in salt rock, it may be as low as 500 years.

Tab. 3.8 Expected container lifetime in different repository concepts /MÜL 08/, /KIN 12/

Country	Host rock	Lifetime [y]	Source
Switzerland	Clay rock	10,000	/NAG 02/
Belgium	Clay rock	2,000	/OND 01/
France	Clay rock	30,000	/AND 05/
Germany	Salt rock	500	/BUH 91/
Canada	Granite/ clay buffer	19,500	/KIN 12/

The container lifetime of carbon steel in contact with saline solutions and clay may be lower than the value found for Belgian, Swiss, or French clay formation. It may be expected that it is still above the 500 years assumed for the aggressive brines in equilibrium with the salt rock formation. However, it must be kept in mind that the concept in AnSichT was based on a triple layer of iron containment: outer liner, inner liner, and container. Although the outer liner is perforated by intention the remaining inner liner and the container wall must be corroded both. If the claystone and the buffer are unsaturated no water may accumulate in the sand buffer between the inner liner and container wall. The corrosion of the container wall that is only in contact with heated moist atmosphere and sand would probably much slower than the corrosion of the two liners. In that case, considerable corrosion would take place only when the clay buffer is fully saturated and surplus pore water fills the pores in the sand buffer. The same applies to the more recent RESUS concept.

Currently, it is not possible to predict the container lifetime and the beginning of radionuclide release but based on the deliberations above it is expected to be well above 500 years. On the other hand, the maximum total duration of the aerobic phase is expected to be in the order of 100–200 years depending on the repository concept /KIN 07/. A radionuclide release would begin only

- after the clay buffer has been fully saturated
- a considerable time after the beginning of the anaerobic phase 4, when all free oxygen and ferric corrosion phases have been fully consumed.

This means that pure Fe(III) phases such as the various modifications of Fe₂O₃ and FeOOH as well as akaganeite will likely be present only in a thin layer near the corrosion front, finely dispersed in the dense product layer or near the original border between metal and clay. A part of these Fe(III) phase may disappear during the further progress of the corrosion. In any case, Fe(III) play only a minor part in the corrosion product layers. Further work on corrosion phases should, therefore, be directed to Fe(II) and mixed Fe(II)/Fe(III) phases.

3.12 Synthesis: corrosion products

3.12.1 Iron (III) oxides and oxyhydroxides

Iron (III) oxides and oxyhydroxides such as hematite, maghemite, goethite, lepidocrocite, akaganeite, amakinite and ferrihydrite mainly form under aerated conditions that will likely be concluded after some tens of years. Some phases such as akaganeite and maghemite may occur in thin layers or in dispersed form in later stages of the corrosion.

Under anaerobic conditions, these phases are partly or fully reduced or react with Fe²⁺ to Fe(II/III) phases such as magnetite or green rusts. No or at least no significant amounts of iron (III) oxides and oxyhydroxides will be present at times (500+ years) when the container hull is broken due to corrosive stress and radionuclides released. An exception is the thin zone in direct contact with corroding steel. Here, the pH is higher and allows the formation of magnetite. When the distance between magnetite grains and the corrosion front increase, the pH will be buffered by the impact of the surrounding clay minerals and becomes unstable.

The neoformation of Fe(III) phases due to the reaction of Fe(II) phases and Fe(II/III) with radiolytically produced oxidants will be limited to an area within some μm distance from spent fuel. Outside the container, only minor amounts of newly formed Fe(III) phases are expected (e. g. magnetite, maghemite, akaganeite).

3.12.2 Iron(II) carbonates, chlorides, and hydroxides

If carbonates are present, the primary solid products formed from an oversaturated solution under anaerobic conditions are probably FeCO₃·nH₂O (at near-neutral pH) and

chukanovite, $\text{Fe}_2(\text{OH})_2\text{CO}_3$ in alkaline solutions. The former product is metastable and transforms into siderite, FeCO_3 and chukanovite within hours /DID 15/. Chukanovite is reported to be metastable with respect to siderite and is expected to transform slowly into the latter phase within some years. The presence of thick layers of chukanovite as corrosion products of archaeological iron artefacts in anoxic soils shows that the transformation process, although thermodynamically driven may be delayed over periods of up to several thousand years.

The presence of other solids in contact with steel also plays a role in determining the predominant corrosion product. Steel rods in presence of sand corrode into chukanovite, while siderite is formed as the only product if the corrosion takes place in free brine. A sufficient supply of calcium and/ or magnesium leads to the formation of ankerite $(\text{Ca},\text{Mg},\text{Fe}^{\text{II}})\text{CO}_3$.

If high chloride concentrations are possible at least locally, then the formation of the hibbingite endmember $\beta\text{-Fe}_2(\text{OH})_3\text{Cl}$ may occur. If magnesium is present it can be incorporated into the structure so that a solid solution $(\text{Fe}^{\text{II}},\text{Mg})_2(\text{OH})_3\text{Cl}$ representing the mineral hibbingite precipitates.

Although often mentioned in the literature, solid $\text{Fe}(\text{OH})_2$ does not form during the corrosion of iron under anoxic conditions. It has not been observed in the corrosion studies summarized above. Consequently, the Schikorr reaction that leads from $\text{Fe}(\text{OH})_2$ to magnetite is probably not relevant. If magnetite is formed then rather through oxidation of other $\text{Fe}(\text{II})$ phases to green rust and later to magnetite.

Only the mixed phase amakinite, $(\text{Fe}^{\text{II}},\text{Mg})(\text{OH})_2$ is observed if iron is corroding at a rather high pH in the presence of aqueous Mg.

3.12.3 Magnetite

Magnetite, Fe_3O_4 , is a corrosion product that forms under aerobic as well as anaerobic conditions. It has often been predicted as the final iron corrosion product under anoxic conditions. However, the experimental investigation showed that although magnetite is present very frequently it is often restricted to the interface between iron metal and solution (the corrosion front) and to thin, probably detached layers that were left over when the corrosion front wandered further into the area that was previously occupied by the

metal. Its extremely slow precipitation and dissolution kinetics make it unlikely that the redox potential in and around the corrosion zone is determined by this mineral. It may, however, be an important place for the oxidation and reduction process of redox-sensitive solutes. The role of “hydrated magnetite” that is frequently reported in laboratory experiments as a precursor phase is unclear.

3.12.4 Green rusts

Four types of green rusts are described in the literature that may be relevant to the near-field of nuclear waste repositories (Tab. 3.9). Besides those listed in the table, several other green rusts with different anions (e. g. oxalate, bromide, sulphite) incorporated in their structures have not been investigated (see /CHR 10/ for a comprehensive overview). Their detection is difficult and most probably they have been overlooked in many studies. In green rusts, Fe^{II} may be partially substituted by Mg /BOU 04/.

They are metastable with respect to magnetite or Fe(II) phases (if reducing agents are present). It has been noted that green rusts act as precursors of magnetite formation /CHR 10/ as well as intermediary products of Fe(III)oxyhydroxide reduction /RUB 10/.

Due to the high affinity of green rusts toward carbonate /REF 97b/, its presence in clay pore waters would not allow the formation of GR1(OH⁻) (fougèrite end member). Most probably the same applies to GR2(SO₄²⁻) and GR1(Cl⁻).

There is some debate on whether GR2(SO₄²⁻) necessarily includes Na⁺. /CHR 10/ /CHR 10/ and /DAV 10/ /DAV 10/ presented some evidence that LDHs such as GR2(SO₄²⁻) are structurally unstable and would probably collapse if no alkali ion is present. However, the existence of Na-free GR2(SO₄²⁻) could not be excluded.

Green rusts are formed from two processes:

- a) Oxidation of primarily produced Fe(II) containing phases. This process may occur only in the early stages of geochemical development (phases 1 and 2) when oxygen is depleted at the corrosion front and fresh oxygen is supplied by diffusion from other areas. It would also require the presence of water. In the early stages (phases 1 to 3) clay is assumed to be unsaturated so that only steam is available to provide the necessary water. If green rusts form under such conditions is not

known. More likely, only Fe(III) oxide, oxyhydroxides and magnetite are produced in the early stages.

- b) Reduction of Fe(III) phases. Diffusion of Fe²⁺ from the corrosion front to previously formed Fe(III) phases would likely lead to the formation of green rusts that are a precursor of magnetite. The amount of Fe(III) phases after the end of the aerobic phase 2 is limited so that the significance of green rusts is probably rather low. Moreover, once the stock of Fe(III) corrosion products is depleted and the green rusts have reacted to magnetite or further to pure Fe(II) phases no more green rust will be present in the near field. A neoformation of green rusts will not take place as there is no source of available Fe(III) and no significant supply of oxidants such as oxygen.

Tab. 3.9 Types of green rust

Name	Ideal Formula
GR1(OH-) (Fougèrite end member)"	[Fe ^{II} _{1-x} Fe ^{III} _x (OH) ₂][x/n OH ⁻ · mH ₂ O] with n = 1/4 - 1/3
GR1(Cl ⁻)	Fe ^{II} ₃ Fe ^{III} (OH) ₈ Cl · nH ₂ O
GR1(CO ₃ ²⁻)	Fe ^{II} ₄ Fe ^{III} ₂ (OH) ₁₂ CO ₃ · 2H ₂ O
GR2(SO ₄ ²⁻)	Fe ^{II} ₄ Fe ^{III} ₂ (OH) ₁₂ SO ₄ · 2H ₂ O NaFe ^{II} ₆ Fe ^{III} ₃ (OH) ₁₈ (SO ₄) ₂ · 12H ₂ O

3.12.5 Iron sulphides

Iron sulphides may be expected to be present in the clay rock of the host formation or the backfill material. The most important naturally occurring iron sulphide in clay formations is pyrite. Under aerobic conditions (phases 1 and 2) pyrite may be oxidized by O₂ or Fe³⁺ to aqueous Fe²⁺ (and subsequently to solid Fe(III) oxyhydroxides) and sulphate. Instead of sulphate, less oxidized sulphur species such as thiosulphate, polythionates and sulphite are sometimes reported. Microbes may accelerate the process. Even in humid air, the oxidation is significant /KIN 13/.

Under anaerobic conditions (phases 3 and 4) and temperatures at or above 90 °C, pyrite could be reduced by hydrogen (H₂) to pyrrhotite /TRU 10/, /KIN 13/. This process would eventually lead to the release of dissolved and gaseous hydrogen sulphide which in turn could form iron sulphides with Fe²⁺ from the pore water, could react with secondary Fe(II)

corrosion phases or directly with iron on the interface metal/ pore water. If other metals are present (e. g. Cr or Ni from stainless steel) analogue sulphides could be formed with these elements as well.

Interaction of hydroxide with material containing ferrous sulphide may lead to the formation of mixed compounds such as $6\text{FeS}\cdot 5\text{Fe}(\text{OH})_2$ (the mineral ferrotuchilinite, /PEK 13/) or $6\text{FeS}\cdot 5\text{Fe}(\text{OH})_2$ (tuchilinite). Iron sulphides may also be formed through microbiological reduction of sulphate in the presence of metallic iron /ENN 14/.

3.12.6 Iron-containing clay minerals

The safety functions of clays used as buffer or backfill material are mainly based on their capacity to swell and thereby to seal a section of the disposal system (drift, tunnel, borehole, shaft). Therefore, clays rich in swelling smectites are chosen for that purpose. Concerns arise if the swelling capacity is diminished or even completely neutralized by chemical alteration of clay. The interest in Fe-rich phyllosilicates that are formed as a product of iron corrosion stems from the fact that most of them have a low swelling capacity and may have an impact on the overall safety performance of the near field system.

Wersin et al. /WER 08/ and Bradbury et al. /BRA 14/ reviewed the existing sources on the formation of iron silicates as corrosion products. Natural clay minerals may contain iron both in its ferrous (Fe^{2+}) and ferric (Fe^{3+}) form. While Fe^{3+} can take a dioctahedral position by replacing Al^{3+} , Fe^{2+} is found in trioctahedral positions where it substitutes Mg^{2+} . Other structural positions (tetrahedral) are less favourable. Like other cations, Fe^{2+} may also be found in the interlayer of smectites. The most important Fe-bearing 1:1 phyllosilicates from the kaolinite/serpentine group include:

- Berthierite – $(\text{Fe}^{\text{II}}, \text{Al}, \text{Fe}^{\text{III}}, \text{Mg})_{2-3}(\text{Si}, \text{Al})_2\text{O}_5(\text{OH})_4$ -
- Odinite - $(\text{Fe}^{\text{III}}, \text{Al}, \text{Mg}, \text{Fe}^{\text{II}})_{2.5}(\text{Si}, \text{Al})_2\text{O}_5(\text{OH})_4$.
- Greenalite - $(\text{Fe}^{\text{II}}, \text{Fe}^{\text{III}})_{2-3}(\text{Si}, \text{Al})_2\text{O}_5(\text{OH})_4$
- Cronstedtite $(\text{Fe}^{\text{II}}_2, \text{Fe}^{\text{III}})(\text{Si}, \text{Fe}^{\text{III}})\text{O}_5(\text{OH})_4$

Among the 2:1 clay minerals, the following members of the smectites group are the most Fe-rich

- Nontronite $(\text{Ca}_{0.5}, \text{Na})_{0.3}\text{Fe}^{\text{III}}_2(\text{Si}, \text{Al})_4\text{O}_{10}(\text{OH})_2\cdot n\text{H}_2\text{O}$

- Saponite $(\text{Ca}_{0.5}, \text{Na})_{0.3}(\text{Mg}, \text{Fe}^{\text{II}})_3(\text{Si}, \text{Al})_4\text{O}_{10}(\text{OH})_2 \cdot n\text{H}_2\text{O}$
- Other minerals included in some modelling studies are Fe(II) beidellite and Fe(II)-montmorillonite

Chlorites also belong to the 2:1 clays. They often belong to a series of solid solutions with Mg and Fe^{II} endmembers. The following trioctahedral chlorite is Fe-rich

- Chamosite - $(\text{Fe}^{\text{II}}, \text{Mg}, \text{Fe}^{\text{III}})_5\text{Al}(\text{Si}_3, \text{Al})\text{O}_{10}(\text{OH})_8$

Another group of the 2:1 clays are micas:

- Glauconite – $(\text{K}, \text{Na})(\text{Fe}^{\text{III}}, \text{Al}, \text{Mg}, \text{Fe}^{\text{III}})_2(\text{Si}, \text{Al})_4\text{O}_{10}(\text{OH})_2$
- Celadonite $\text{K}(\text{Mg}, \text{Fe}^{\text{II}})(\text{Fe}^{\text{III}}, \text{Al})\text{Si}_4\text{O}_{10}(\text{OH})_2$
- Other minerals include in some modelling studies are
 - Biotite -
 - Vermiculite

Among these minerals, only the smectites nontronite and saponite and to a lesser extent glauconite can swell.

Experimental investigations on iron-bentonite interactions were summarized by Mosser-Ruck et al. /MOS 10/:

- At temperatures below 150 °C, near-neutral pH at iron/clay ratio > 0.5 dioctahedral smectite was transformed into a Fe-rich 7Å phase (berthierite, odinite, cronstedtite). At an iron/clay ratio around 0.1 dioctahedral smectite reacted to Fe-rich dioctahedral smectite and Fe-rich trioctahedral smectite
- At temperatures below 150 °C, but alkaline conditions (pH 10–12) dioctahedral smectite reacts to Fe-rich dioctahedral smectite (palygorskite)
- The upper stability limit of berthierite lies within 60–130 °C
- Chlorite is only stable above 110 °C

It should be noted that under some experimental conditions mixed phases between odinite-greenalite and greenalite-cronstedtite were found (/NGO 15/, /MOS 10/).

There are several static and reactive transport modelling studies where authors tried to predict the phase composition in the course of proceeding iron corrosion. Bradbury et al.

/BRA 14/ pointed out that the thermodynamic data for the various potential Fe phyllosilicates are typically not sufficiently reliable. The same applies to kinetic data, especially for precipitation processes. Moreover, each modelling study put together a different set of potential Fe phases so that it is difficult to compare the outcomes and to assess how the thermodynamic and kinetic parameters influenced the model results.

4 Synthesis and characterization of iron corrosion phases

4.1 Selection of solid phases for thermodynamic investigation

Based on the discussions above it becomes clear that in the long-term Fe(II) phases will be the dominating products of steel corrosion processes in the near field. The following corrosion products phases were investigated more closely:

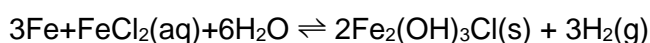
- Fe-Hibbingite, $\text{Fe}_2(\text{OH})_3\text{Cl}$
- Hibbingite, $(\text{Fe,Mg})_2(\text{OH})_3\text{Cl}$
- Chukanovite, $\text{Fe}_2(\text{OH})_2\text{CO}_3$
- Fe,Mg Chukanovite, $(\text{Fe,Mg})_2(\text{OH})_2\text{CO}_3$
- Other Fe(II) containing potential corrosion phases
- Amakinite, $(\text{Fe,Mg})\text{OH}_2$
- Akaganeite, $\text{Fe}(\text{OH})_{3-x}, \text{Cl}_x$

4.2 Fe-Hibbingite, $\text{Fe}_2(\text{OH})_3\text{Cl}$

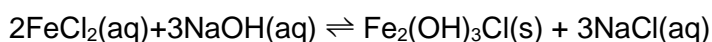
4.2.1 Experimental procedures

In the literature several synthesis routes have been described that lead to the formation of Fe-Hibbingite:

1. Dissolution of iron powder in a boiling concentrated solution of FeCl_2 under strict exclusion of oxygen /HAY 33/, /KEL 48/:



2. Mixing of aqueous FeCl_2 with aqueous NaOH /KEL 48/:



Keller /KEL 48/ reported that the first procedure leads to a granular crystalline and white solid. It was also employed by Rémazeilles and Refait /RÉM 08/ and Nemer et al. /NEM 11/. Multiple attempts to reproduce his findings failed. Although a white solid was observed it always appeared in combination with black-brown precipitates that preferably attached to the inner walls of the heated glass flasks used for the experiment. It became clear that the commercial FeCl_2 products used as starting material were always contaminated with Fe(III) so that pure Fe(II) products could not be received by this method. On

the other hand, usage of Fe(III) free FeCl₂ solution (prepared by dissolving metallic iron in HCl under nitrogen and subsequent filtration) did not solve the problem as the same kind of brown precipitates occurred.

The second route could be realized successfully. In the first step, oxygen- and carbonate-free concentrated NaOH was prepared by adding boiled water (total 171 g) to 150 g solid NaOH in a polyethene bottle. The bottle was closed, and the solution flushed with a steady stream of argon. At the same time, it was shaken and cooled in a water bath to avoid overheating. Carbonate, if present, would have precipitated as Na₂CO₃. After cooling down the bottle was transferred into an oxygen-free glove box. After about a week a sample was taken (6.03 g) and diluted to 50 ml. The dilution was titrated with 1 M HCl with phenolphthalein as an indicator. Four titrations gave a medium value for the concentration of 46.93 wt.-%.

A pure FeCl₂ solution was prepared by adding a slight excess of metallic iron (43.69 g) to dilute HCl (120 ml 37 wt.-% HCl diluted with 600 ml freshly boiled H₂O) under a constant argon flow. When gas generation ceased the solution was filtered in the glove box and set aside in a dark bottle wrapped with aluminium foil. The solution had a density of 1.105919 g/cm³. Using the concentration-density relation of Laliberté and Cooper /LAL 04/ a concentration of 11.68 wt.-% or 1.043 mol/kg was calculated. Similar batches of FeCl₂ solution were later prepared by the same method.

13.6 g of the NaOH solution (0.159 mol) were added to 86.4 g water and mixed with 223 g of the FeCl₂ solution (0.206 mol). An additional 9.5 g of water was used to rinse the funnel. A fluffy and pale green precipitate occurred that settled slowly.

An aliquot of the slurry was transferred to a screw-capped flask in the glovebox and left in the glovebox for four months. The temperature was about 28 to 30 °C. Afterwards, the flask was put inside a steel jacket through which water flowed from the outside via a closed system. In total, the mixture was left standing for five months at room temperature (25 ± 2 °C) and one month at 25.0 ± 0.2 °C. At that time, the pH was measured, and a sample taken. After 37 months the pH was tested again and showed no difference. After 40 months the flask was removed from the steel jacket and placed again in the glove box, which had now a temperature of 27 ± 2 °C. Another sample was taken after 41 months.

A similar experiment was conducted with a higher starting concentration of NaCl

(5 mol/kg). This approach aimed to check, whether there exists a stable Fe(II) hydroxy chloride with higher chloride content than hibbingite.

The above-mentioned methods produced Fe-hibbingite from oversaturation. An alternative approach has been proposed by Hayek /HAY 33/ that has been adapted here. 60 g FeCl₂ solution (2 mol/kg) was given to about 1 g powdered iron (Aldrich p.a.). No heating was applied. Samples were taken after 25 and 32 months when metallic iron could no longer be detected magnetically. The resulting solid is pale green.

The results of the different experiments are summarized in Tab. 4.1. The apparent pH value was converted to a pCH using the functions derived in Hagemann et al. /HAG 14/. As conversion parameters for simple as well as mixed NaCl-FeCl₂ solutions were missing, FeCl₂ was numerically replaced with MgCl₂. This affects all measurements but may be especially significant in the experiments with high FeCl₂ content as they occurred in the undersaturation experiment.

Tab. 4.1 Solubility of Fe-Hibbingite at 25 °C

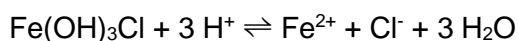
Parameter	From Oversaturation 5 months	From Oversaturation 41 months	From Oversaturation High Cl 31 months	From undersaturation Iron+ FeCl ₂ 25 months	From undersaturation Iron+ FeCl ₂ 32 months	Analytical method
pH (apparent)	6.46	6.45	6.37	5.36	5.36	potentiometric
Δ pH	0.08	0.06	0.902	0.88	0.85	calculated
-log cH	6.54	6.51	7.272	6.24	6.21	calculated
c Na [mol/kg]	0.588	0.565	5.54	-	-	ICP-OES
c Fe [mol/kg]	0.321	0.294	0.0583	2.04	2.01	ICP-OES
c Cl [mol/kg]	1.230	1.153	5.66	4.08	4.02	Amperometry
Temperature [°C]	25 ± 0.2	27 ± 1	27 ± 1	27 ± 1	27 ± 1	
Log K	17.26	17.17	17.96	18.20	18.09	

Based on these findings the activities for all relevant ions were evaluated by using the Pitzer approach. The THEREDA database was taken as a starting point. It did not contain parameters for ion interactions between Fe^{2+} , H^+ and Cl^- . Some vapour pressure investigations of ternary systems exist that would allow the determination of these parameters (e. g. /SUS 63/, /SYR 73/). However, all these investigations were hampered by the fact that in acid solutions always the partial pressure of water and HCl must be measured separately which easily leads to systematic errors. Instead of using these data both $\theta_{\text{H}^+, \text{Fe}^{2+}}$ and $\Psi_{\text{H}^+, \text{Fe}^{2+}, \text{Cl}^-}$ were derived by assuming that the water activity of mixed aqueous solutions of FeCl_2 and HCl obeys the Zdanovskiy rule and remains constant if binary solutions of FeCl_2 and HCl that have the same water activity are mixed. 20 synthetic data points were computed by mixing a 4.0000 m FeCl_2 and a 5.9868 m HCl solution (both with $a_{\text{W}}=0.6746$) in equidistant steps. The calculated Pitzer interactions parameters were

$$\theta_{\text{H}^+, \text{Fe}^{2+}} = 0.04583$$

$$\Psi_{\text{H}^+, \text{Fe}^{2+}, \text{Cl}^-} = -0.00890$$

In the experiment starting from oversaturation, the pH value remained largely constant, whereas the iron concentration decreases slightly. The calculated solubility constant for the reaction



was $\log K=17.26$ after 5 months (at 25 °C) and $\log K=17.17$ after 41 months (27 °C). The latter value corresponds closely with the results by Nemer et al. /NEM 11/ (17.12) and Kim et al. /KIM 17/ (17.08).

In the experiment with a high initial concentration of NaCl the X-ray diffractogram shows only the reflexes of Fe-Hibbingite. This demonstrates that the formation of the compounds $\text{Fe}(\text{OH})\text{Cl}$ and $\text{Fe}_3(\text{OH})_4\text{Cl}_2$ synthesized by Hayek /HAY 33/ and Keller /KEL 48/ is not to be expected to any significant extent. The product of the experiment showed a higher solubility constant ($\log K=17.96$). The reasons for this are not clear since the same solid phase was present as could be demonstrated by XRD.

The solubility constant was also higher in the experiment from undersaturation. It resulted in a $\log K$ of 18.2 after 25 months and of 18.09 after 32 months. In both cases, the

chloride content of the system was much higher (4–5.6 mol/kg) than in the previous experiment (1.2 mol/kg). The reason for the difference could not be identified.

4.2.2 Experiment at 40 °C

Hibbingite from the previous experiment at 25 °C and part of the mother solution were kept in equilibrium for eight months at a temperature of 40 °C. Two weeks after the beginning of the experiment the pH dropped to 6.14 where it remained when the first sample was taken (after one month). After 8 months, though, the pH rose to 6.32. The complete results are presented in Tab. 4.2.

For the calculation of p_cH values from apparent pH data, the functions from Hagemann et al. /HAG 14/ could not be used as they are restricted to 25 °C. Suitable parameters for the temperature range of 25 to 60 °C were developed as part of the project ThermAc3⁹.

After eight months of equilibration, the solubility constant for this temperature is log K=17.16, which is close to the value found for 25 °C in the previous experiment. In that case, the temperature coefficient in the range of 25 to 40 °C would be close to zero. However, the evaluation of the measured data is impaired by the fact that currently, no model for the description of the activity coefficients for Fe(II) in mixed solutions above 25 °C exists. For binary solutions, such a model has been developed /MUÑ 13/, but the temperature functions for ternary interactions are still missing. As an approximation, it can be assumed that the ternary interaction coefficients do not change between 25 and 40 °C and do not play a significantly different role in moderately concentrated solutions as used in this experiment.

⁹ Project supported by the German Federal Ministry of Education and Research. Final report in preparation

Tab. 4.2 Solubility of Fe-Hibbingite at 40 °C

Parameter	From Oversaturation 1 month	From Oversaturation 8 months
pH (apparent)	6.14	6.32
Δ pH	0.16	0.19
-log cH	6.30	6.51
c Na [mol/kg]	0.571	0.582
c Fe [mol/kg]	0.307	0.320
c Cl [mol/kg]	1.184	1.230
Temperature	40 ± 0.5	40 ± 0.5
Log K (preliminary)	16.50	17.16

4.3 Hibbingite - (Fe,Mg)(OH)₃Cl

Natural occurring hibbingite is a mixed compound of iron(II) and magnesium. So far there was no attempt to test whether it is a solid solution and which composition boundaries it has. In our experimental approach, we tried to prepare hibbingite in the same way as before to produce Fe-hibbingite, but 10 to 80 % of the FeCl₂ were replaced by equimolar amounts of MgCl₂. The maximum initial concentration of MgCl₂ was about 0.4 mol/kg. Samples were taken after 11 weeks. In the following table Tab. 4.3 the main results are summarized.

Tab. 4.3 Composition of equilibrium solutions and soil bodies in the preparation of mixed Fe-Mg hibbingite

Nr	Fe	Mg	Na	Cl	pCH	Mg/Fe in solid phase	Assigned phase
1	0.179	0.057	0.508	0.980	6.885	0.00	Fe-Hibbingite
2	0.115	0.111	0.490	0.943	6.904	0.00	Fe-Hibbingite
3	0.0789	0.166	0.490	0.979	6.985	0.00	Fe-Hibbingite
4	0.0213	0.213	0.487	0.956	7.336	0.00	Fe-Hibbingite
5	0.00106	0.269	0.488	1.029	8.171	0.01	Fe-Hibbingite + Amakinite
6	0.000571	0.315	0.489	1.120	8.337	0.07	Amakinite
7	0.000390	0.303	0.481	1.088	8.607	0.41	Amakinite
8	0.000165	0.309	0.493	1.112	8.777	1.15	Amakinite

Fe-Hibbingite was mathematically saturated in all cases. It can be recognized as such in the XRD images in a relatively weak form in batches 1–5. Interestingly, however, the solid phases in these batches did not contain significant amounts of magnesium. In batches 5 to 8, the following phenomena were observed:

- The pCH increased from 8.2 to 8.8 (in previous batches is increased from 6.9 to 7.3)
- The visible volume of the solid phase was considerably higher
- Magnesium was detectable in the solid phases. In batch 8 it even predominated
- According to geochemical calculation, $\text{Fe}(\text{OH})_2$ is also saturated (batches 6 to 8)
- In batches 6 to 8, the XRD no longer showed traces of hibbingite. Instead, signals occurred that indicated a phase similar to brucite, $\text{Mg}(\text{OH})_2$, or amakinite $(\text{Fe,Mg})(\text{OH})_2$. However, according to calculations, brucite was not saturated, nor was magnesium oxychloride.

This means that under the selected boundary conditions up to pCH 8.7 and a concentration of 0.269 mol/kg MgCl_2 magnesium is not incorporated in Fe-Hibbingite. At magnesium concentrations above 0.3 mol/kg, hibbingite is still shown to be mathematically saturated, but it is no longer visible in the soil.

From these observations, it could be concluded that from batch 6 on, magnesium was bound in a common phase with iron(II), possibly amakinite. Up to now the formation of amakinite has only been observed in concentrated MgCl_2 solutions (e. g. /SMA 95/). If the stability already extends to concentrations of 0.3 mol/kg, the region of existence should be characterized more precisely.

Against this background, the question arises where the stability region of existence of the mineralogically proven hibbingite $(\text{Fe,Mg})_2(\text{OH})_3\text{Cl}$ lies. Higher magnesium concentrations, as well as higher pCH values, lead to saturation of brucite or possibly amakinite. Other boundary conditions need to be found where hibbingite is stable.

4.4 Amakinite – $(\text{Fe,Mg})(\text{OH})_2$

The formation of amakinite was examined in more detail in a further series of experiments. Here the test approaches were chosen in such a way that there was always an OH excess and both Fe(II) and Mg could be precipitated completely as hydroxide. In the first series, the final hydroxide concentration was about 0.2 mol/kg. Under these

conditions, the iron and magnesium concentrations were too low to be measured reliably ($< 10^{-5}$ mol/kg). In the second series of experiments, the starting conditions were chosen differently so that only a part of Fe and Mg would be precipitated. After 10 months of equilibration time in the glovebox, the final pCH was in the order of 7 to 9 (Tab. 4.4).

Tab. 4.4 Composition of equilibrium solutions and solid phase in the preparation of amakinite

Nr	Fe [mol/kg]	Mg	Na	Cl	pCH	Mg in solid Mg/(Mg+Fe) [mol-%]	As-signed phase
1	0.0198	0.00000	0.0801	0.120	7.247	0	Fe(OH) ₂
2	0.0128	0.00585	0.0820	0.119	7.377	0	Fe(OH) ₂
3	0.00679	0.0118	0.0828	0.120	7.533	1	Fe(OH) ₂
4	0.00204	0.0177	0.0803	0.120	7.797	1	Fe(OH) ₂
5	0.000191	0.0185	0.0808	0.118	8.550	13	Amakinite
6	0.000491	0.0206	0.0792	0.121	8.676	24	Amakinite
7	0.000145	0.0203	0.0788	0.120	8.790	40	Amakinite
8	0.000138	0.0196	0.0830	0.122	8.907	56	Amakinite
9	0.000321	0.0213	0.0793	0.122	8.911	70	Amakinite
10	0.000497	0.0198	0.0829	0.124	9.009	86	Amakinite
11	0	0.0210	0.0803	0.122	9.126	100	Brucite

The XRD measurements showed a mixture of brucite and amakinite in all cases (Fig. 4.3). The chloride concentration in the final solutions was equal to the initial concentrations showing that no chloride was bound in the solid phases. The concentration of Fe and Mg in the precipitate was calculated based on a mass balance considering the initial and the final solution composition. If the solid were just a mixture of brucite and Fe(OH)₂ their respective activity products would be constant at least in parts of the series. Instead, the products shifted continuously, except in batch 1 to 4 where only Fe(OH)₂ was present. For the remaining batches it was assumed that amakinite was the solubility determining solid phase:



The solubility constant was calculated according to the following formula

$$\log K = 1-x \log a_{\text{Fe}^{++}} + x \log a_{\text{Mg}^{++}} + 2 \log a_{\text{H}_2\text{O}} - 2 \log a_{\text{H}^+}$$

The same evaluation was performed for the hibbingite batches 6, 7, and 8 (see above). It revealed an almost linear relationship between Mg content in the solid phase and the calculated solubility constant. It demonstrates that there is a continuous series of near-ideal solid solutions between 0 to 100 % Mg content. There was no miscibility gap or limited miscibility as described by Delnavaz et al. /DEL 88/.

The solubility constant in our experiments could be expressed by the following formula

$$\text{Log K (amakinite)} = 12.72 + x_{\text{Mg}} 3.72$$

A closer inspection identified two regions that have slightly different properties:

1. Between 0 and 29 % Mg: $\log K (\text{amakinite}) = 12.54 + x_{\text{Mg}} 5.80$
2. Between 29 and 100 %: $\log K (\text{amakinite}) = 13.15 + x_{\text{Mg}} 3.08$

Both can be described by separate linear relationships (Fig. 4.2). In combination, they provide a much better representation of the experimental data than the simple formula mentioned before. However, more experiments would be needed to confirm that these two regions differ significantly from the overall linear trend.

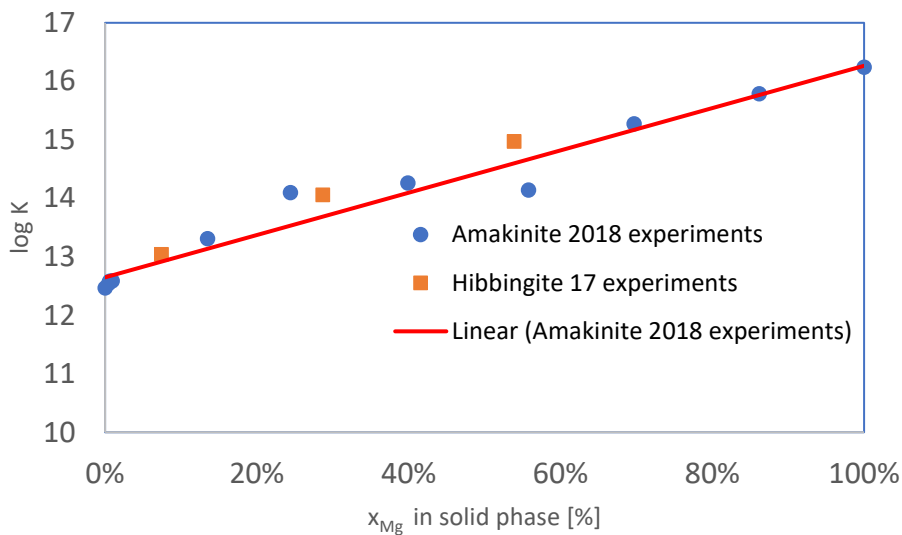


Fig. 4.1 Solubility constant of synthetic amakinite - (Fe,Mg)(OH)₂ depending on the relative Mg content of the solid phase

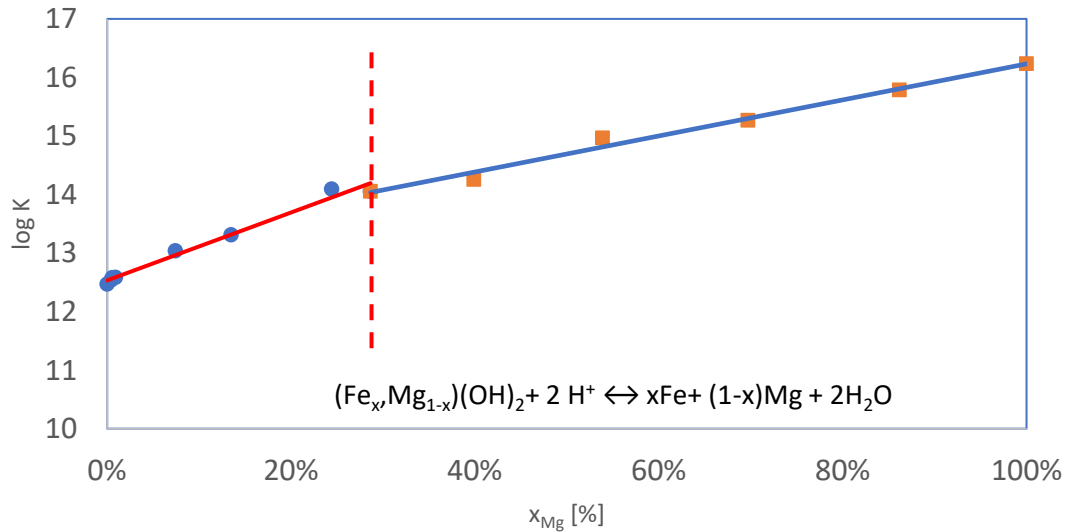


Fig. 4.2 Two regions of solid solutions in the system $\text{Fe}(\text{OH})_2$ - $\text{Mg}(\text{OH})_2$

Amakinite is extremely sensitive to oxidation. When exposed to air, the greenish-white solid turns brown-red within tenths of seconds. In the glovebox, however, it shows no tendency to oxidation, e. g. towards magnetite and brucite, green rust or pyroaurite. Thus, the often postulated Schikorr reaction



under the conditions of the experiment does not take place.

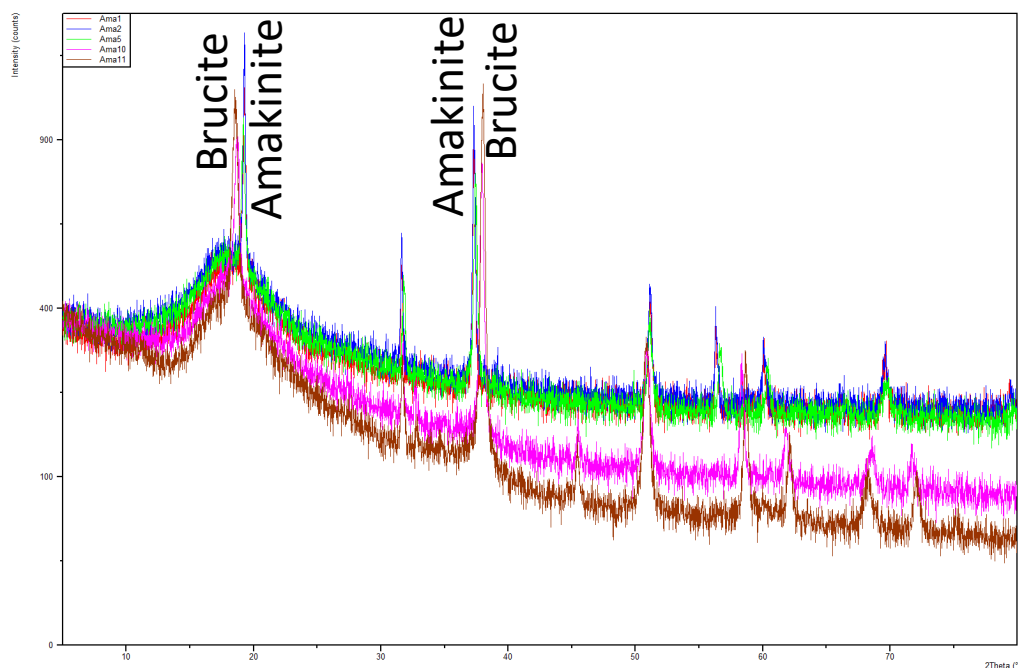
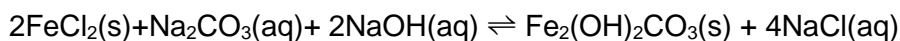


Fig. 4.3 X-ray diffractograms of preparations from the Amakinite measurement series

4.5 Chukanovite

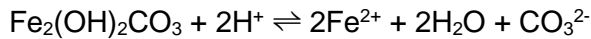
Chukanovite was prepared similarly like Fe-Hibbingite /RÉM 09b/. An oxygen-free solution of Na_2CO_3 was prepared by dissolving 5.7 g (0.054 mol) anhydrous Na_2CO_3 in 94.7 g oxygen-free water in the glove box. To this solution 5.1 g of 46.93 wt.-% NaOH solution (0.0598 mol) and 73.1 g 11.7 wt.% FeCl_2 solution (0.0673 mol) were added and the resulting mixture stirred. A white finely dispersed precipitate formed. The product of this reaction was chukanovite according to the formula



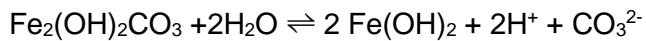
as could be confirmed by XRD.

The procedure for determining the solubility corresponds to the procedure for Fe-hibbingite. After 5 and 48 months, the apparent pH was measured and a liquid sample was taken, filtered, and analysed for iron, chloride, and sodium. During this period, the iron concentration decreased by two orders of magnitude from $3.2 \cdot 10^{-4}$ to $6.6 \cdot 10^{-6}$ while the pH decreased from 9.9 to 9.2. The total carbonate concentration was derived from the ion balance considering the hydrogen carbonate/ carbonate equilibrium at the given pH value and NaCl concentrations. The analytical results are listed in Tab. 4.5.

At a pH value of 9.90, the occurrence of hydroxide and carbonate complexes must be expected. The stability constants for the species were taken from Hagemann et al. /HAG 14/. According to the modelling, the main Fe(II) species of iron in this solution is the carbonate complex $\text{Fe}(\text{CO}_3)_2^{2-}$ (about 70 %). For this complex, no Pitzer ion interaction coefficients are available, so that the calculation of activity coefficients is only approximate. For the reaction



the calculated solubility constant $\log K$ was 2.9 after 5 months which was slightly higher than the value of 1.56 ± 0.5 reported by Lee and Wilkin /LEE 10/ but within the range of 2.5 ± 1 that could be derived by combining the equilibrium constant for



By Azoulay et al. /AZO 12/ with the solubility constant for aged $\text{Fe}(\text{OH})_2$ ($\log K = 13.0 \pm 0.3$) from Hagemann et al. /HAG 14/. It also corresponds to the value of 1.99 that could be derived from the work of Kim et al. /KIM 17/.

The situation changed after 48 months. Then, the solubility constant amounted to only -1.7, which would be an indication of further ageing. At the same time, the calculated activity product for FeCO_3 was -11.40, a value close to the solubility constant of siderite /HAG 14/.

An attempt to produce an even better-crystallized chukanovite by high-temperature synthesis failed. Metallic iron was added to a mixed $\text{NaHCO}_3/\text{NaOH}$ solution under nitrogen in a pressure reactor lined with Teflon and the sealed reactor was kept at 90 °C for two months. The experimental method is analogous to the process described by Feitknecht and Keller /FEI 50/ for the production of Fe-Hibbingite. However, no other solid phase, only non-reacted iron powder was found at the end of the period. Possibly the contact of carbonate-containing waters with iron leads to passivation.

Tab. 4.5 Solubility of chukanovite at 25 °C

Parameter	After 5 months	After 48 months
pH (apparent)	9.96	9.26
Δ pH	-0.06	-0.06
-log cH	9.90	9.2
c Na [mol/kg]	0.592	0.601
c Fe [mol/kg]	0.000322	$6.6 \cdot 10^{-6}$
c Cl [mol/kg]	0.496	0.456
c CO ₃ ²⁻	0.0677	0.021
c HCO ₃ ⁻	0.0404	0.101
Temperature [°C]	25 ± 0.2	27 ± 1
Log K	2.88	-1.70



Fig. 4.4 Chukanovite (left) and Fe-Hibbingite (right)

4.6 Solid solution (Fe,Mg)₂(OH)₂CO₃

Another candidate for solid solutions is chukanovite in combination with a hypothetical Mg analogue. A mineral with the composition Mg₂(OH)₂CO₃ has not been found yet, but a similar compound exists that contains some hydrate water in its structure, the mineral pokrovskite, Mg₂(OH)₂CO₃·0.5H₂O.

The preparation of the mixture was carried out as before for pure chukanovite but increasing amounts of FeCl₂ were replaced by MgCl₂. Altogether, 10 batches with 0 to 100 % relative magnesium content were prepared. The XRD measurements show characteristics of chukanovite in all nine samples that contain Fe²⁺, with two main reflections

near a position (2θ) of 23.5 and 34, slightly shifting to higher values. At 90 % Mg the reflections moved increased by 0.5 units. At 100 % they disappear and are replaced by a different pattern that could be assigned neither to chukanovite nor pokrovskite. That pattern is slightly visible in the solid phase at 90 % Mg as well.

Based on these findings it is assumed that a continuous series of solid solutions is formed between 0 and 90 % Mg content. A thermodynamic evaluation could not be carried out because the equilibrium concentrations of iron and magnesium were too low for measurement in ICP-MS.

All experimental approaches were permanently stable. Even at pH values above 10, no transition into pyroaurite, $Mg_6Fe_2(OH)_{16}CO_3 \cdot nH_2O$ could be observed, which should be more stable according to thermodynamic data from Rozov et al. /ROZ 11/.

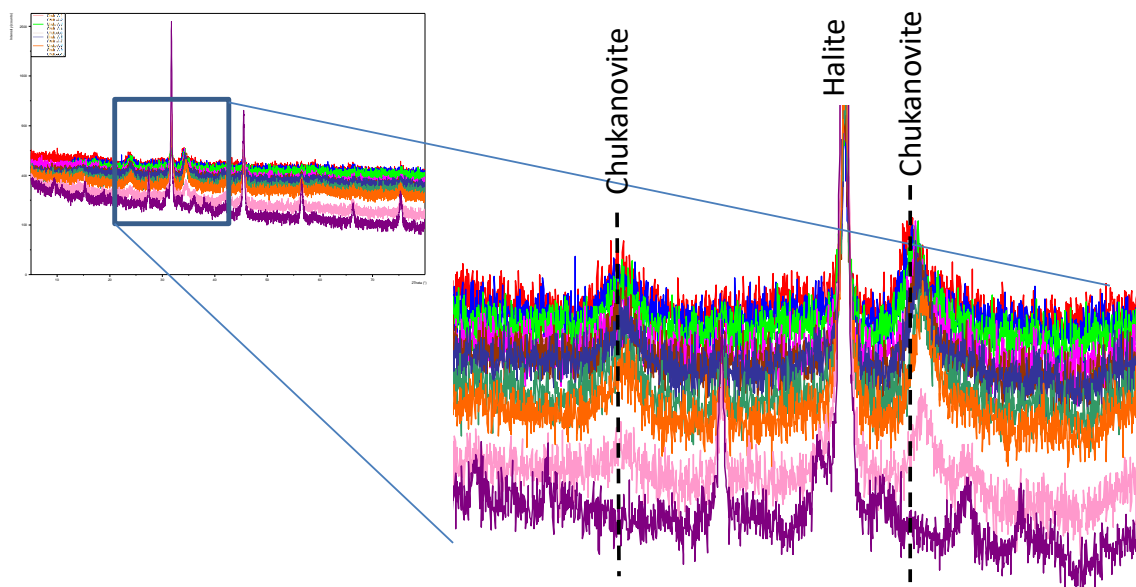


Fig. 4.5 X-ray diffractograms of preparations from the Chukanovite-Pokrovskite mixing series

4.7 Akaganeite

Akaganeite is an iron(III)oxyhydroxide, which has been identified as an important corrosion phase in chloride-containing waters. It is often designated as β -FeOOH and thus thought to be another polymorph of ferric oxide monohydrate /WEI 35/. This is incorrect, since chloride hardly occurs at all in terms of quantity, but is an essential component of the structure /SCH 15/, /DOU 78/. Stahl et al. /STA 03/ stated $FeO_{0.8333}(OH)_{1.167}Cl_{0.167}$ as

the composition. The washing out of chloride leads to the breakdown of the lattice structure and the formation of hematite.

Nothing is known about its thermodynamic stability, nor about the dependence of its composition on the chloride concentration. Therefore, a test series was designed in which akaganeite was formed from FeCl₃-solutions of increasing NaCl-content. The experimental design was based on Schwertmann and Cornell /SCH 00/ For this purpose, a solution of about 0.1 M of FeCl₃ is prepared and left to stand at 40 °C for one week. Akaganeite precipitates from the solution. In a variation of the original instructions, the preparation contained 0 to 3 M NaCl.

At 40 °C, the pH value was first measured, and a solution sample was taken. The precipitate is very fine and can only be separated by vacuum filtration through a filter with 0.1 µm pore width. A part of the slurry was transferred into a vial and stirred at 25 °C for four weeks. Afterwards, another sampling was carried out. The results are summarised in Tab. 4.6.

Tab. 4.6 Composition of the solutions of the akaganeite synthesis experiments

No.1	Fe [mol/kg]	Na [mol/kg]	Cl [mol/kg]	pH	pCh	log K
1	0.0916		0.297	1.55		2.29
2)*	0.0436		0.152	1.62		2.39
3)*	0.0404		0.146	1.62		2.37
4	0.0923		0.317	1.37		1.80
5	0.0902	0.309	0.615	1.41	1.32	1.64)**
6	0.0913	1.080	1.427	1.41	1.33	1.06)**
7	0.0959	3.006	3.538	1.29	1.32	0.11)**

)* prepared by dilution of 1)

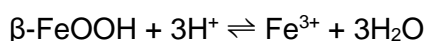
** activity model used for calculating these values not applicable to saline conditions

Akaganeite could be detected in all solid samples with the XRD. The solution compositions show that the iron concentration does not decrease with increasing chloride content. If chloride were also involved in the stability of the compound in the thermodynamic sense, the Fe³⁺ concentration would have to drop sharply. This finding supports the assumption that chloride is a necessary component of akaganeite, but only as a stabilizer of a certain (otherwise chloride-free) crystal structure. For the solutions, iron speciation and activity coefficients were calculated using the combined Lawrence Livermore

database V8 R6 8 (thermo.com.V8.R6+.dat of the calculation code Geochemist's Workbench). From the four measured values in solutions without NaCl addition, a solubility constant of

$$\log K = 2.1 \pm 0.3$$

can be calculated for the reaction



The measurements in solutions with added NaCl cannot be reliably evaluated because no model is available for the specific interactions between Iron(III) hydroxide complexes and chloride. The calculated solubility constants are only preliminary guesses.

The solubility constant for akaganeite is in the same order of magnitude as that observed for other iron(III)oxyhydroxides (Tab. 4.7).

Tab. 4.7 Solubility constants for iron(III) oxyhydroxides /HAG 14/

Compound	Fe	Na
α -FeOOH	Goethite	1,7 \pm 0,5
' β -FeOOH'	Akaganeite	2,1 \pm 0,3)*
γ -FeOOH	Lepidocrocite	0,3 - 4,3
δ -FeOOH	Feroxyhyte	2,2 - 8,2

)* this work

4.8 Other Fe(II) containing solids

Bivalent cations with an ionic radius similar to that of Fe²⁺ form a series of carbonate compounds for which Fe(II)-containing analogues are not yet known /KOS 06/, /HAZ 16/. Some efforts have been undertaken to test whether such compounds could be synthesized.

By systematic comparison with known minerals of cobalt, nickel, and magnesium, it has been checked which relevant hydroxide and carbonate compounds of bivalent iron may still be unknown. Numerous carbonate-containing phases were identified, which suggest an iron-containing analogue could exist (Tab. 4.8).

4.8.1 Fe(II) analogue to kambaldaite, $\text{NaNi}_4(\text{CO}_3)_3(\text{OH})_3 \cdot 3\text{H}_2\text{O}$

The first compound of this type to be studied is kambaldaite. This is a basic sodium nickel carbonate with the formula $\text{NaNi}_4(\text{CO}_3)_3(\text{OH})_3 \cdot 3\text{H}_2\text{O}$ (/NIC 85/). It is formed naturally as a product of the decomposition of nickel sulphides. It has already been possible to produce analogues with cobalt instead of nickel /OHN 09/, but not the nickel compound itself. The synthesis method is based on the mixture of a nickel or cobalt nitrate solution with sodium hydrogen carbonate solution at 40 °C.

Tab. 4.8 Mineral phases, for which an iron(II) containing analogue is conceivable

Mineral	Fe-Analogue
Otwayite $\text{Ni}(\text{CO}_3)(\text{OH})_2 \cdot \text{H}_2\text{O}$	$\text{Fe}_2(\text{CO}_3)(\text{OH})_2 \cdot \text{H}_2\text{O}$
Artinite $\text{Mg}_2(\text{CO}_3)(\text{OH})_2 \cdot 3\text{H}_2\text{O}$	$\text{Fe}_2(\text{CO}_3)(\text{OH})_2 \cdot 3\text{H}_2\text{O}$
Claraite $\text{Cu}^{2+}_3(\text{CO}_3)(\text{OH})_4 \cdot 4\text{H}_2\text{O}$	$\text{Fe}_3(\text{CO}_3)(\text{OH})_4 \cdot 4\text{H}_2\text{O}$
Hydromagnesite $[\text{Mg}_5(\text{CO}_3)_4(\text{OH})_2 \cdot 4\text{H}_2\text{O}]$	$\text{Fe}_5(\text{CO}_3)_4(\text{OH})_2 \cdot 4\text{H}_2\text{O}$
Dypingite, Giorgiosite $[\text{Mg}_5(\text{CO}_3)_4(\text{OH})_2 \cdot 5\text{H}_2\text{O}]$	$\text{Fe}_5(\text{CO}_3)_4(\text{OH})_2 \cdot 5\text{H}_2\text{O}$
Callaghanite $[\text{Cu}_2\text{Mg}_2(\text{CO}_3)(\text{OH})_6 \cdot 2\text{H}_2\text{O}]$	$\text{Fe}_2\text{Mg}_2(\text{CO}_3)(\text{OH})_6 \cdot 2\text{H}_2\text{O}$
Kambaldaite $\text{NaNi}_4(\text{CO}_3)_3(\text{OH})_3 \cdot 3\text{H}_2\text{O}$	$\text{NaFe}_4(\text{CO}_3)_3(\text{OH})_3 \cdot 3\text{H}_2\text{O}$
Synthetically prepared $\text{Na}_2\text{Co}(\text{CO}_3)_2 \cdot 4\text{H}_2\text{O}$	$\text{Na}_2\text{Fe}(\text{CO}_3)_2 \cdot 4\text{H}_2\text{O}$
Synthetically prepared $\text{K}_2\text{Co}(\text{CO}_3)_2 \cdot 4\text{H}_2\text{O}$	$\text{K}_2\text{Fe}(\text{CO}_3)_2 \cdot 4\text{H}_2\text{O}$
Synthetically prepared $\text{Na}_3\text{Co}(\text{CO}_3)_2\text{Cl}$	$\text{Na}_3\text{Fe}(\text{CO}_3)_2\text{Cl}$
Shortite $\text{Na}_2\text{Ca}_2(\text{CO}_3)_3$	$\text{Na}_2\text{Fe}_2(\text{CO}_3)_3$
Shortite $\text{Na}_2\text{Ca}_2(\text{CO}_3)_3$	$\text{K}_2\text{Fe}_2(\text{CO}_3)_3$
Huntite- $\text{CaMg}_3(\text{CO}_3)_4$	$\text{CaFe}_3(\text{CO}_3)_3$
Chalconatronite $\text{Na}_2\text{Cu}^{2+}(\text{CO}_3)_2 \cdot 3\text{H}_2\text{O}$	$\text{Na}_2\text{Fe}(\text{CO}_3)_2 \cdot 3\text{H}_2\text{O}$
Baylissite $\text{K}_2\text{Mg}(\text{CO}_3)_2 \cdot 4\text{H}_2\text{O}$	$\text{K}_2\text{Fe}(\text{CO}_3)_2 \cdot 4\text{H}_2\text{O}$
Gaylussite $\text{Na}_2\text{Ca}(\text{CO}_3)_2 \cdot 5\text{H}_2\text{O}$	$\text{Na}_2\text{Fe}(\text{CO}_3)_2 \cdot 5\text{H}_2\text{O}$ -
Gaylussite $\text{Na}_2\text{Ca}(\text{CO}_3)_2 \cdot 5\text{H}_2\text{O}$	$\text{K}_2\text{Fe}(\text{CO}_3)_2 \cdot 5\text{H}_2\text{O}$ -
Rapidcreekite $[\text{Ca}_2(\text{SO}_4)(\text{CO}_3) \cdot 4\text{H}_2\text{O}]$	$\text{Fe}_2(\text{SO}_4)(\text{CO}_3) \cdot 4\text{H}_2\text{O}$
Tychite $[\text{Na}_6\text{Mg}_2(\text{CO}_3)_4(\text{SO}_4)]$	Ferritychite $\text{Na}_6\text{Fe}_2(\text{CO}_3)_4(\text{SO}_4)]$
Chlorartinite $\text{Mg}_2(\text{CO}_3)\text{Cl}(\text{OH}) \cdot 3(\text{H}_2\text{O})$	$\text{Fe}_2(\text{CO}_3)\text{Cl}(\text{OH}) \cdot 3(\text{H}_2\text{O})$

With a similar method, it was tried to produce $\text{NaFe}_4(\text{CO}_3)_3(\text{OH})_3 \cdot 3\text{H}_2\text{O}$ from a FeCl_2 -solution and NaHCO_3 . The XRD analysis showed that siderite, FeCO_3 , had formed instead. Possibly the temperature used (by 50 °C) was too low for Fe(II). Ohnishi et al. /OHN 06/ reported that at 35 °C CoCO_3 was formed instead of Co-kambaldaite. It could also be that presence of nitrate is essential.

4.8.2 Other Fe(II) hydroxo chlorides and Fe(II) analogue of nepskoite

The experiments leading to Fe-hibbingite showed that no stable Fe(II) hydroxy chloride with a higher chloride/ hydroxide ratio than $\text{Fe}_2(\text{OH})_3\text{Cl}$ could be prepared at 25 °C. On the other hand, other compounds of the type $x\text{M}(\text{OH})_2 \cdot y\text{MCl}_2$ with a lower chloride content are known from other chemical literature. Among them is $\text{Mg}_4\text{Cl}(\text{OH})_7 \cdot 6\text{H}_2\text{O}$ with $\text{OH}/\text{Cl}=7$, the rare mineral nepskoite. A test series was started in which 2 m FeCl_2 solutions were mixed with NaOH in an OH/Cl ratio of 3 to 7. According to the XRD investigation, the forming solids were similar to $\text{Fe}(\text{OH})_2$ and showed no sign of a different structure.

4.8.3 Fe(II) analogue to Northupite, $\text{Na}_3\text{Mg}(\text{CO})_2\text{Cl}$

Northupite is a sodium magnesium carbonate chloride with the formula $\text{Na}_3\text{Mg}(\text{CO})_2\text{Cl}$. It was first observed by Winkler /WIN 93/ as an accidental product in chemical production and shortly afterwards found as a mineral phase /FOO 95/. The preparation of an iron(II) analogue was attempted in the style of de Schulten /SCH 96/ by boiling a mixed solution of NaCl, Na_2CO_3 and FeCl_2 . However, the XRD image only showed the reflexes of chukanovite as a result.

5 Prediction of long-term redox conditions in the nearfield

5.1 Preliminary remarks

In the near field of a repository, the redox conditions are dominated in the long term by the corrosion of the ferrous materials (casks, liners, possibly reinforcing steel or rails). According to previous findings and modelling, the oxidising substances present at the beginning of emplacement (atmospheric oxygen, partially oxidised clay, Fe(III)-containing corrosion products on steels) have such a small molar quantity relative to metallic iron that their influence will have almost completely disappeared after a few decades to centuries.

The prediction of the redox conditions in the near-field of a repository requires a profound understanding of the corrosion processes both in their temporal sequence and in their spatial characteristics. In-situ experiments have shown that combined diffusion and reaction processes lead to a pH and redox profile between the corrosion front (surface of the corroding metal and the unaltered clay). Uniform conditions cannot be assumed in the near field of corroding metal parts (containers, liners). Corrosion kinetics determined under simple boundary conditions (coupon in a salt solution) cannot be transferred to the real conditions in direct contact of steel with compacted clay or even sand. For many chemical processes that take place in the vicinity of a corrosion front, the speed of reaction is unknown. Sometimes the question even arises whether they take place at all under the expected conditions (e. g. reactivity of dissolved or gaseous hydrogen, microbial sulphate reduction). Also, the data on important redox-sensitive phases, especially of ferrous clay minerals, is rather weak.

Against this background, it becomes clear that a comprehensive prediction of the redox conditions in the near field is not trivial and cannot be provided within the scope of this work. But by varying certain conditions of the corrosion process it is possible to learn about the range of redox states and p_cH values to be expected in the vicinity of the corroding container.

5.2 Calculation of the redox level in the near field assuming different chemical boundary conditions

5.2.1 Purpose and border conditions of the calculations

The calculations aimed to get a feeling for the corrosion processes and the redox level when the inner liner has corroded to an extent that clay pore water may enter the sand quartz sand filling between the (inner) liner and the waste containers. This event is not expected to happen before the end of the potential retrieval phase (500 years).

The following assumptions were made:

- The (inner) liner surrounding the sand filling loses its barrier function when 50 % of the material is corroded.
- The pore room in the sand filling is flooded instantaneously. The outer surface of the containers and the inner surface of the remaining liner will start to corrode at the same time.
- The inflow of the solution is faster than the corrosion process at the outside of the liner. Initial pathways through the liner will widen because inflowing unsaturated pore water will dissolve the corrosion products along the pathway. The inflowing solution has not been altered significantly. The composition is unchanged, but the corrosion hydrogen will already impose strongly reducing conditions
- Once the pore room is filled there is no further exchange of solution or gases between the solution inside and outside the liner (this is not correct, but at the moment, data are not available to model gas flow and diffusion of aqueous species.). In some calculations, though, it is assumed that the pressure build-up of hydrogen is limited because of diffusion and sometimes subsequent reaction.
- In accordance with the RESUS concept three BSK containers containing spent fuel are placed in one borehole (the number of containers per borehole does not affect the course of corrosion)

5.2.2 Dimensions of the borehole, the liner and the container /reaction masses

The emplacement concepts in AnSichT and RESUS both plan to use a sand-filled liner the contains BSK containers for spent fuel or vitrified waste. Tab. 5.1 summarizes relevant geometrical and physical data that were used to calculate the initial chemical conditions at the start of the corrosion process. In combination with the chemical composition of the liner and container materials (Tab. 2.1) the masses of the reaction in Tab. 5.2 were calculated. The database for manganese was insufficient. As the chemistry of Mn under anaerobic conditions is similar to that of Fe, the mass of Mn was added to the mass of iron.

Tab. 5.1 Dimensions and masses of containers, sand filling, solution and liner in a vertical borehole

Property	Value	Source
BSK container: length	5 m	1
BSK container: diameter	520 mm	1
BSK container: wall thickness	40 mm	1
BSK container: total volume	1.06 m ³	Calc.
BSK container: volume of the outer hull	0.319 m ³	
BSK container: Number per borehole (spent fuel)	3	1
BSK container: mass (hull) (3 containers)	7.50 t	Calc.
Liner: length	32.4 m	1
Liner: wall thickness	5 cm	1
Liner: distance between BSK and the inner wall	12 cm	2
Liner: diameter	840 mm	Calc.
Liner: inner volume	14.7 m ³	Calc.
Liner: volume filled with sand	11.51 m ³	Calc.
Liner: density of metal (GGG40)	7100 kg/m ³	
Quartz sand filling: bulk density	1700 kg/m ³	1
Quartz sand: grain density	2650 kg/m ³	5
Quartz sand filling: porosity	35.8 %	Calc.
Quartz sand filling: pore volume	4.13 m ³	Calc.
Solution in pore space volume	4.13 m ³	Calc.
Solution in pore space: density	1.1138	Calc.
Solution in pore space: mass	4.60 t	Calc.
Solution in pore space: mass of H ₂ O	3.88 t	Calc.
Liner: corroded portion at the time of failure	50 %	Assumption
Liner: Mass of not corroded metal	11.8 t	Calc.

1: /ALF 20/ /ALF 20/, 2: /LOM 15/ /LOM 15/, 3: /MEU 21/ /MEU 21/, 4: /RIC XX/ /RIC XX/, 5: /RUM 20/ /RUM 20/

Tab. 5.2 Reaction masses at the beginning of the corrosion process

Reactant	Mass [kg]
Clay pore water	4600 water content: 3888
C	438
Si	19
Mn (added to Fe)	(151)
S	0.88
Ni	51
Al	2.8
Fe	(18596) 18747 (incl. Mn)
Quartz	19571

5.2.3 Geochemical modelling of the corrosion process inside the liner

The calculation of corrosion processes was performed with Geochemist's Workbench (version 11). The database was composed of the following sources:

- Ions of the seawater system (H, Na, K, Mg, Ca, Cl, SO₄, CO₃, OH): THEREDA Release 1
- Iron species, solids and Pitzer interaction coefficients: /HAG 14/ /HAG 14/
- Nickel species, solids and Pitzer interaction coefficients: /HAG 15/ /HAG 15/ including additions from /HAG 21/ /HAG 21/
- Si and Al species: Pitzer interaction coefficients: THEREDA Release 6
- Si and Al species: equilibrium reactions: Thermochimie database 10a
- Si and Al-containing solids including clay minerals: Thermochimie database 10a

In accordance with previous analytical findings hematite, lepidocrocite and troilite were suppressed in the calculations. Instead of these phases, maghemite and pyrrhotite were allowed to precipitate. Six model calculations were performed that tested the impact of geochemical factors on the corrosion process, the corrosion products formed and the occurring pH levels:

- Diffusion of hydrogen gas or aqueous H₂(aq) from the sand filling into the host rock. The H₂ pressure in the disposal cell was either unlimited or fixed at a/ limited level (100 bar)

- Availability of sulphate-reducing bacteria, so that under the strongly reducing conditions near the redox front sulphate in the inflowing pore water is reduced to sulphide.
- Partial pressure of CO₂. Calcite is abundant in the clay rock so that any consumption of aqueous carbonate caused by corrosion processes may be balanced by CO₂(g)/HCO₃(aq) provided by carbonate minerals in the host rock. Whether this process will be active across the corrosion product layer of the (inner) liner has not been investigated yet. The CO₂ pressure was either free or fixed at the level found in calculations for the equilibrium CO₂ pressure in Lower Cretaceous clay rock
- Supply of silicate from quartz. Quartz has a strong buffering influence on the system pH. Experimental results showed that near the corrosion front the pH may be higher despite the availability of quartz and other silicate minerals. To simulate this behaviour the amount of quartz available to take part in the corrosion process was reduced to 10 % of its original value
- Formation of aged or fresh siderite. Siderite like other MII carbonates often does not form directly from solution but only as a follow-up product of initially forming minerals such as fresh siderite or chukanovite

There are of course other geochemical processes for which it is unknown to what extent they will take place. These include for example:

- Type of iron-containing clay minerals that precipitate inside the sand filling
- Temperature at the beginning of the corrosion
- Displacement of the solution inside the liner by hydrogen gas
- Diffusion of other ions from the corrosion product layer at the outside of the liner and from the host rock into the sand filling and to the corrosion front

A part of these questions could be answered with more detailed experimental investigations (clay minerals, diffusion of H₂). Others represent arbitrary properties and pathways that cannot be predicted (point of entry of the solutions, speed of inflowing solution).

The following calculations cover several combinations of these factors. They allow a first view in the multidimensional room of plausible developments:

- a) Reduction of sulphate (inorganic or microbiological) suppressed, Carbonate not buffered
- b) Reduction of sulphate suppressed, Carbonate not buffered, H₂ pressure fixed at 100 bar
- c) Reduction of sulphate suppressed, carbonate buffered by fixed CO₂ partial pressure (0.02574 bar, the resulting pressure from the equilibrium calculations for the Lower Cretaceous pore water) H₂ fixed at 100 bar
- d) Reduction of sulphate suppressed, carbonate buffered by fixed CO₂ partial pressure (0.02574 bar, the resulting pressure from the equilibrium calculations for the Lower Cretaceous pore water), H₂ pressure fixed at 100 bar
- e) Reduction of sulphate allowed, carbonate buffered by fixed CO₂ partial pressure (0.02574 bar, the resulting pressure from the equilibrium calculations for the Lower Cretaceous pore water), H₂ pressure fixed at 100 bar
- f) Simulation of the processes at the corrosion front: like b, but available quartz reduced to 10 % and siderite(aged) suppressed
- g) Like f but H₂ pressure fixed to 1 bar
- h) Consumption of H₂ by reduction of pyrite faster than corrosion process: like f, but H₂ pressure not fixed and unlimited supply of pyrite

In these calculations, the reaction progress is measured in terms of reacted iron (kg Fe).

5.2.4 Corrosion reaction a – Reduction of sulphate suppressed, carbonate not buffered

The solution composition remained unchanged up to about to corrosion of about 100 kg Fe. At this time the consumption of water by the corrosion process became so large that the amount of free solution started to drop. All concentrations rose to the point where halite was saturated which occurred at 3500 kg Fe. Sulphate was precipitated because the calcium concentration increased.

At about 5500 kg the system stabilized as iron became stable under a hydrogen pressure of 10000 bar. This value cannot be reached in a real system as hydrogen would start to diffuse into the surrounding host rock, displace pore water or, in an extreme case build up pressure beyond the rock pressure and produce fissures that could be filled with gas. The pH remains quite stable around 6.7 to 7.5.

Iron corrosion phases were produced in the following sequence: siderite, greenalite, saponite, berthierite and minnesotaite (only when Fe became stable). Pyrite was continuously formed from the sulphur content in GGG40. Graphite that is part of GGG40 remained unaltered and would be surrounded by iron corrosion phases.

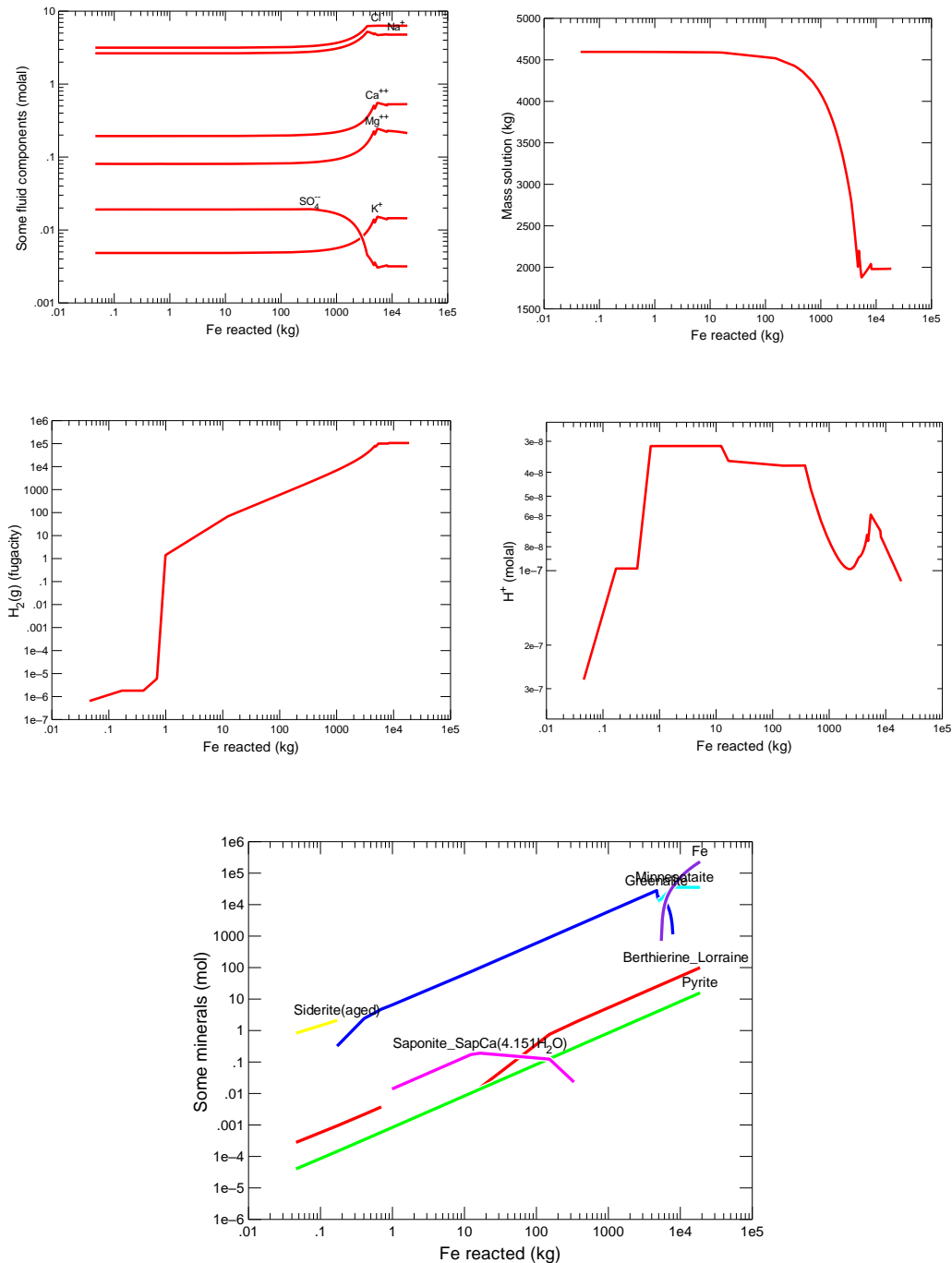


Fig. 5.1 Modelling results (case a) for corrosion of steel in Lower Cretaceous pore water in contact with quartz sand

5.2.5 Corrosion reaction b – reduction of sulphate suppressed, carbonate not buffered, hydrogen pressure fixed at 100 bar

In this run, solid carbon had to be suppressed to allow the code to calculate the corrosion process. The reaction ended after the water in the solution was fully consumed (approximately at 6800 kg Fe). The solution concentrations increased similar to case a. The pH varied between 6.5 and 7.0. Four iron corrosion products occurred throughout the reaction: berthierite, greenalite, siderite and pyrite.

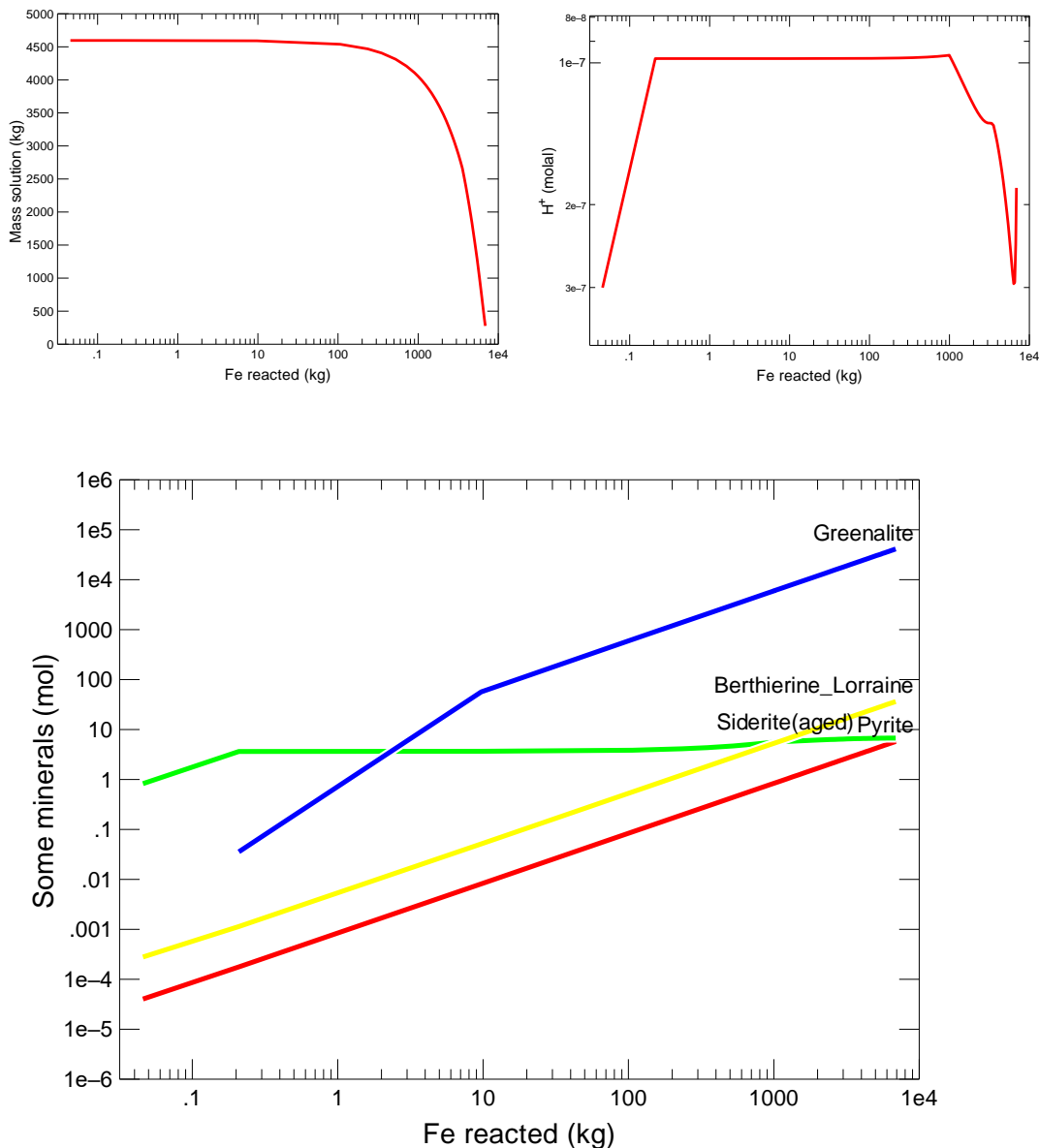


Fig. 5.2 Modelling results (case b) for corrosion of steel in Lower Cretaceous pore water in contact with quartz sand

5.2.6 Corrosion reaction c: Reduction of sulphate suppressed, carbonate buffered by fixed CO₂ partial pressure

Elemental carbon had to be suppressed in this calculation because otherwise, corrosion hydrogen would react with CO₂(g) to carbon. Even then, the reaction could not proceed beyond 9400 kg Fe. At that point, the code stopped because it did not converge. Until then the solution mass had dropped to 1426 kg and the hydrogen pressure increased to 200000 bar. Almost all iron reacted to siderite and only to a much lesser extent to berthierite and pyrite. The pH started at 6.5, decreased slowly to 6.3 and only at high corroded Fe masses increased to a maximum of 7.2

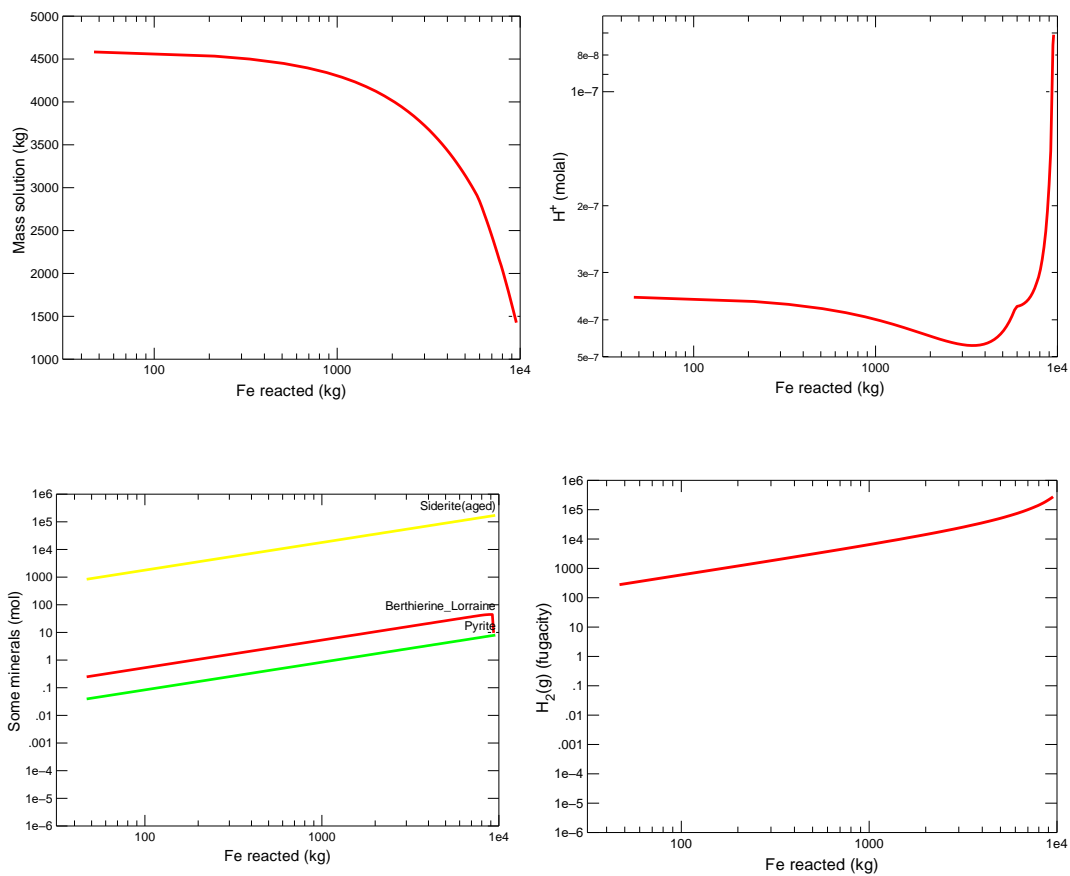


Fig. 5.3 Modelling results (case c) for corrosion of steel in Lower Cretaceous pore water in contact with quartz sand

5.2.7 Corrosion reaction d: Reduction of sulphate suppressed, CO₂ partial pressure fixed at 0.02574 bar, H₂ pressure fixed at 100 bar

Fixing the hydrogen pressure at 100 bar caused a water consumption at 9000 kg Fe. The pcH went through a minimum at 5.9 and at extreme corrosion, progress turned back to 6.4. Because of the consumption of water, the concentration of all major cations increased. Halite became saturated so that any further increase of CaCl₂ and MgCl₂ lead to the precipitation of more halite and a steep decrease of Na concentration. Siderite (aged) was the most important Fe mineral, followed by pyrite and berthierite. Suppression of aged siderite lead to the formation of fresh siderite, not to chukanovite

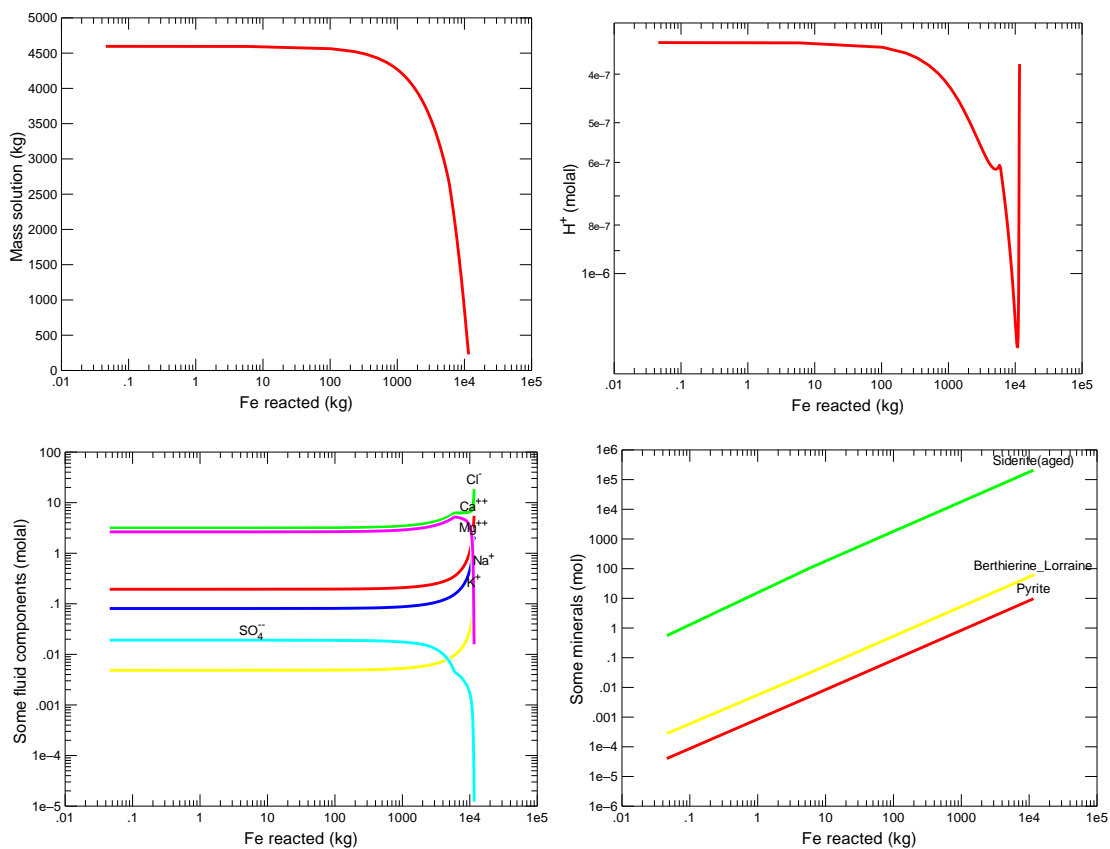


Fig. 5.4 Modelling results (case d) for corrosion of steel in Lower Cretaceous pore water in contact with quartz sand

5.2.8 Corrosion reaction e: Reduction of sulphate allowed, CO₂ partial pressure fixed at 0.02574 bar, H₂ partial pressure fixed at 100 bar

In this case, all sulphate was reduced to sulphide, which then reacts with Fe²⁺ to pyrite and later into pyrrhotite instead of pyrite. The most important corrosion phase was

siderite. Beidellite and berthierite occurred in small amounts. The consumption of water took place when 11000 kg Fe have reacted. The pH was stable at 6.4 most of the time. Shortly before water was fully consumed it dropped to 6 but mostly recovered to the original value at the end of the reaction. A higher amount of sulphide minerals would be expected if there is a resupply of sulphate from the host rock (not calculated here).

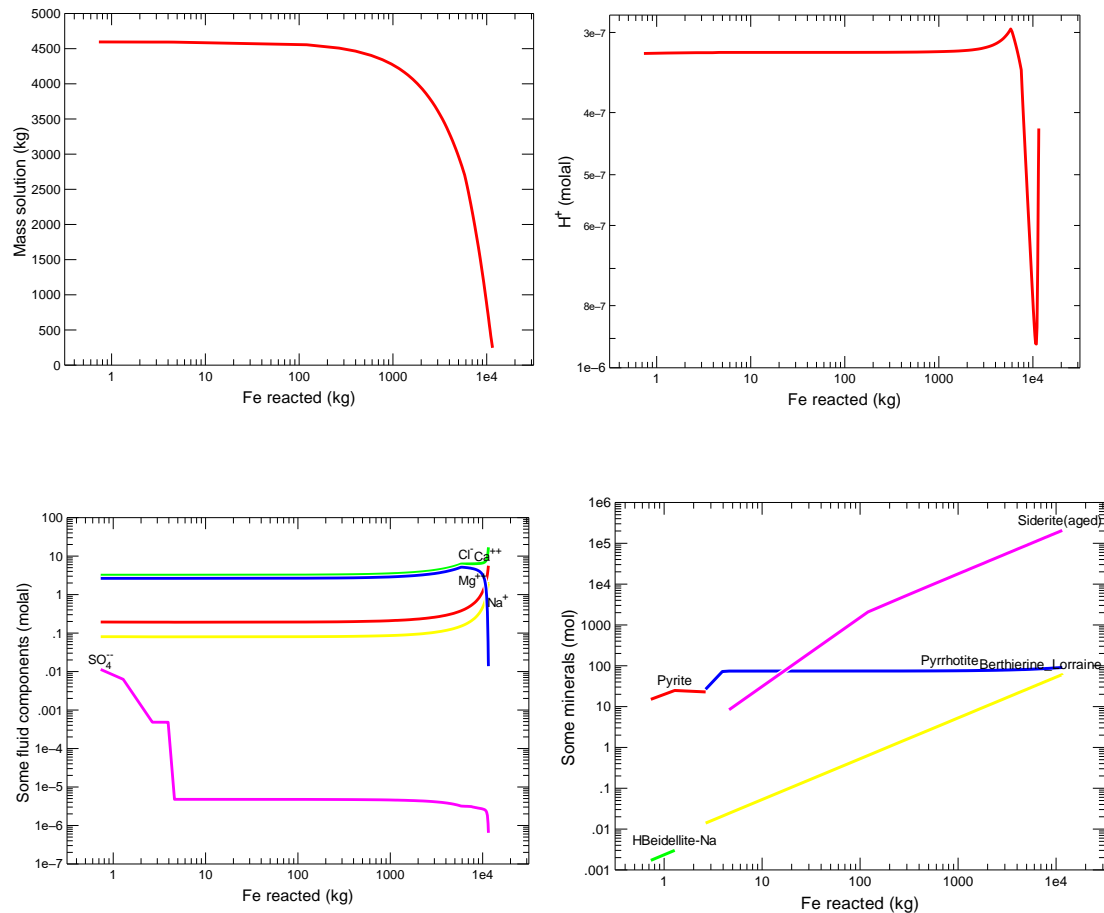


Fig. 5.5 Modelling results (case e) for corrosion of steel in Lower Cretaceous pore water in contact with quartz sand

5.2.9 Corrosion reaction f: reduction of sulphate suppressed, carbonate not buffered, hydrogen pressure fixed at 100 bar, quartz limited to 10 %, siderite (aged) suppressed

This calculation aimed to simulate the situation close to the corrosion front. Experimental results clearly showed that there is a distinct pH profile across the corrosion layers between the metal surface and the surrounding matrix. Close to the metal, the redox level is very low and the pH obviously higher than close to the matrix (e. g. clay) that acts as

an effective buffer. This buffering performance was lowered by reducing the amount of available quartz to 10 % of its original value. Moreover, aged siderite was suppressed as it typically does not form directly from solution but through ageing of fresh siderite or chukanovite. The partial pressure of H_2 was fixed at 100 bar. As before, solid carbon was suppressed as a phase and a constituent of GGG40:

- Water was already consumed at 6100 kg Fe because more water was bound in the corrosion phases
- The pCH rises to 9.5 at 3 kg, stays there up to 1000 kg Fe and finally rises to 11.5 at the end of the reaction
- The sequence of iron phases is berthierite, pyrite, chukanovite (for a short time), Fe-Hibbingite, $Fe(OH)_2$, greenalite. The occurrence of the three iron(II) hydroxide phases is caused by the rise of pCH. If aged siderite is allowed, chukanovite forms instead
- After 3.2 kg Fe, Mg progressively precipitated in dolomite and then in antigorite, a Mg silicate after the pCH surpassed 9.1
- The concentrations of Na, K, Ca, Cl and SO_4 go up slowly. At the highest corrosion progress, the increase of $CaCl_2$ concentration causes halite to precipitate

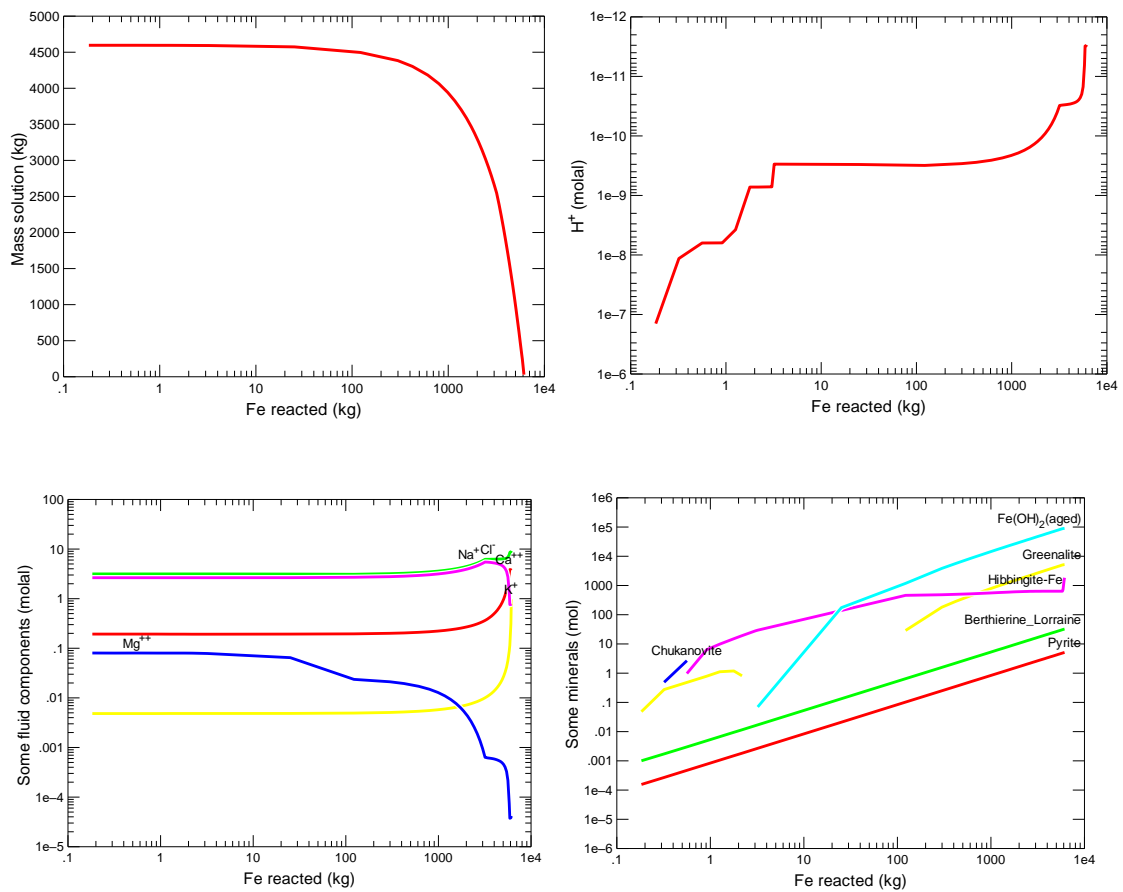


Fig. 5.6 Modelling results (case f) for corrosion of steel in Lower Cretaceous pore water in contact with quartz sand

5.2.10 Corrosion reaction g: reduction of sulphate suppressed, carbonate not buffered, hydrogen pressure fixed at 10 bar, quartz limited to 10 %, siderite (aged) suppressed

The results of this reaction were similar to case f.

- The reaction ended at 7700 kg when water was fully consumed.
- The pH quickly rose to 9.1 and above 1000 kg Fe increased to 11.5
- The sequence of minerals was pyrite, berthierite (little), chukanovite and greenalite (only a short time), Fe-hibbingite, cronstedtite, magnetite

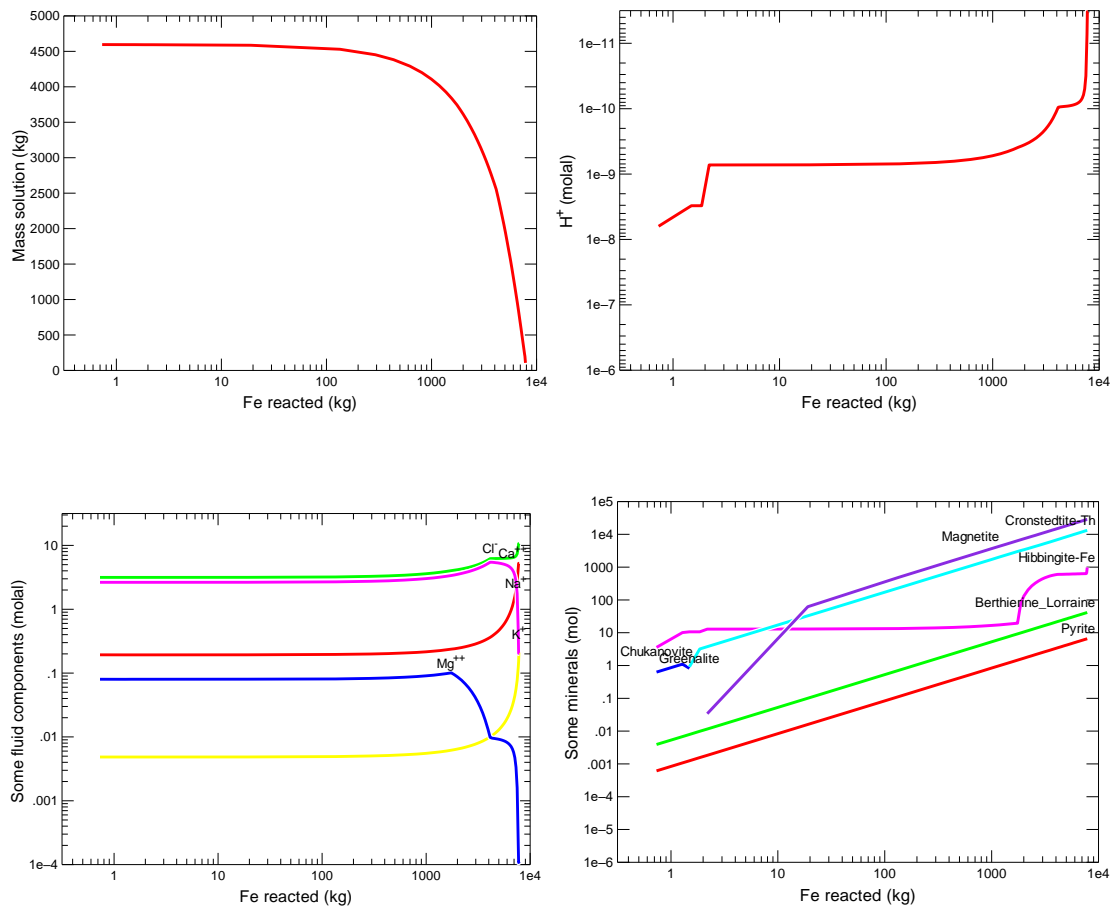
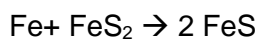


Fig. 5.7 Modelling results (case g) for corrosion of steel in Lower Cretaceous pore water in contact with quartz sand

5.2.11 Corrosion reaction h: reduction of sulphate allowed, carbonate not buffered, quartz limited to 10 %, siderite (aged) suppressed, unlimited supply of pyrite

The addition of pyrite to the system had quite interesting effects. First, the amount of solution remained constant throughout the reaction. Water was not consumed, because the net reaction only included iron, pyrite and pyrrhotite



Consequently, the ion concentrations remained constant too. In contrast to all other simulations, iron was completely dissolved. The partial hydrogen pressure rose only slowly to 0.002 bar at 100 kg Fe and to 0.09 bar at 1700 kg Fe. Only later it slowly increased to

600 bar. The p_H increases to 9.5 fast, but at 27 kg decreased again to 7.5 at 100 where it remained until 1700 kg.

The sequence of iron minerals was berthierite (little), maghemite, cronstedtite and magnetite (only at the beginning), pyrrhotite (from 12 kg Fe), and greenalite that was later replaced by saponite. Pyrrhotite would be by far the most important corrosion phase, at least in the long run. Experimental results show that this is not the case, even in situations where the ratio Fe/clay was very high. Hydrogen likely dissipates into the surrounding clay rock where it may be converted hydrogen sulphide. But such H₂S would not completely return to the corrosion front to convert primary corrosion phases such as silicates and carbonates into pyrrhotite. The low level of hydrogen pressure in the early phases of reaction (0.002 bar) is taken as a lower limit for the redox level.

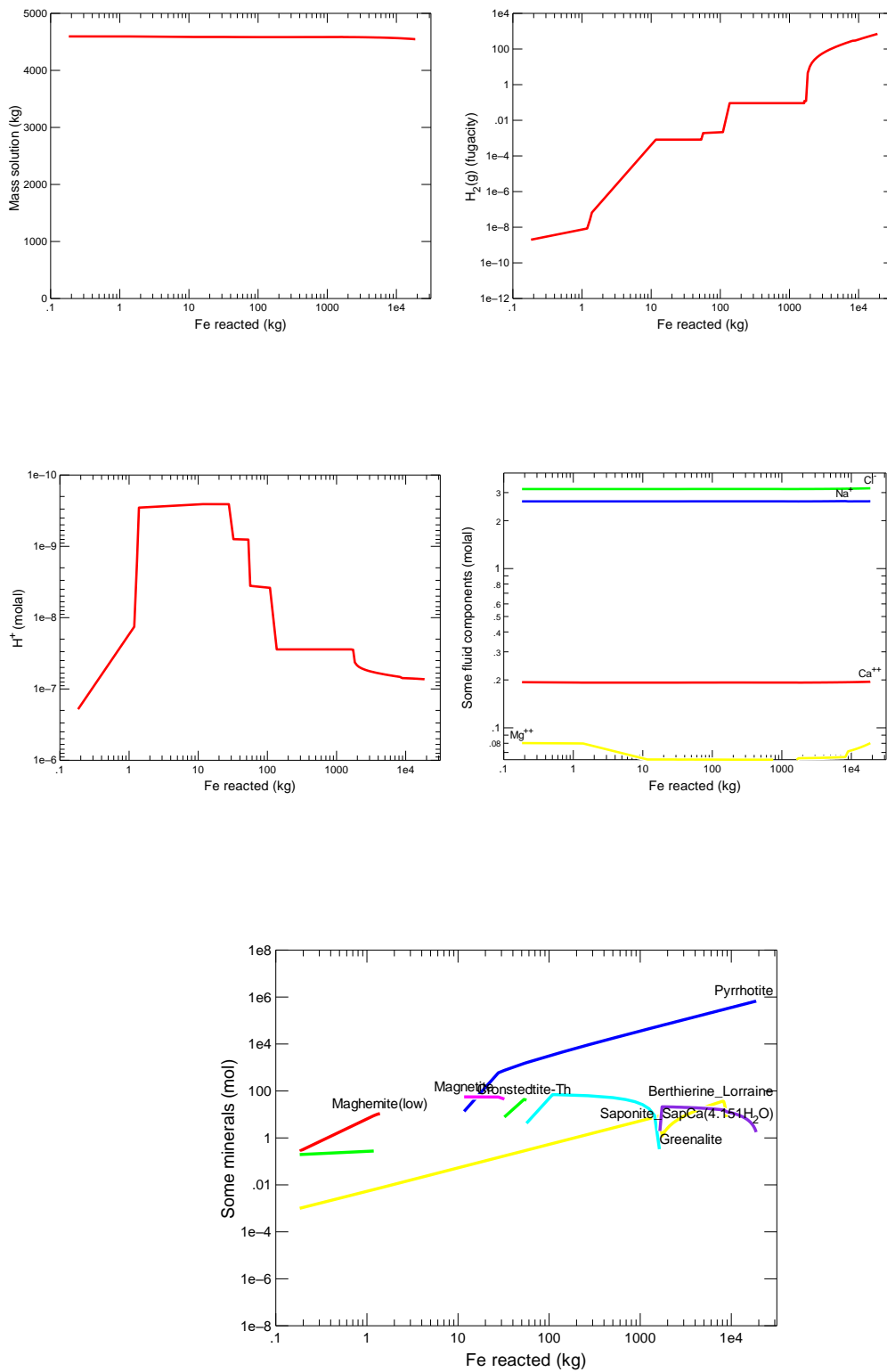


Fig. 5.8 Modelling results (case h) for corrosion of steel in Lower Cretaceous pore water in contact with quartz sand

5.2.12 Summary

Depending on the type of corrosion phases formed the reaction either ended by consumption of water by reaching a (very high) H_2 equilibrium pressure. Both end-points will not occur in a repository as hydrogen can leave the nearfield by diffusion and (two-phase) gas flow and water may be replenished from the unlimited supply in the host rock. But the calculation shows the inherent drive of the corrosion reaction towards these limits. Thus, the extreme hydrogen pressures that occurred at the end of some calculations do not need to be further considered as they are unrealistic. The upper end probably of H_2 pressures cannot be estimated from static geochemical models. As part of the FORGE project, benchmark transport model calculations addressing the production and fate of hydrogen in repository cells indicated that the maximum pressure of hydrogen may be in the order of 50–55 bar. Such conditions are predicted after about 20,000 to 40,000 years after the closure of the repository /YU 13/. A comparison of all eight model calculations shows that the p_H level may range from 6.4 to 9.6 (in extreme conditions up to 11.5).

According to the modelling, the following iron phase may occur:

- Sulphides: pyrite, pyrrhotite
- Carbonates and chlorides: siderite, chukanovite, Fe-hibbingite,
- Hydroxides, oxyhydroxides and oxides: $Fe(OH)_2$, magnetite, maghemite
- Silicates: saponite, beidellite, berthierite, greenalite, minnesotaite, cronstedtite.

Unlike the other minerals in this list, minnesotaite has not been found in the corrosion studies discussed above, but it is often associated with greenalite /WER 08b/ and has been found in corrosion studies at higher temperatures /BAS 18/.

At least in the first six cases, magnetite did not occur. In the five first cases, the p_H is buffered to rather low values (around 7) that do not allow a formation of this phase. In reaction f, the redox level is too low so that only pure Fe(II) phases occur. In case g magnetite could be forced to precipitate only if the hydrogen pressure is fixed at a lower level (e. g. at 1 bar) and only if the amount of available quartz is reduced (otherwise all iron would end up in siderite or silicates). In case h magnetite becomes stable for a short period because the H_2 level is sufficiently low and the p_H high enough, at least for a certain period of time.

The variability of minerals in the eight cases show that probably local, sometimes arbitrary conditions such as silicate availability and the fate of hydrogen determine the type of occurring corrosion phases. This explains why in different experimental studies some phase are found side by side that normally would not be in equilibrium with each other or with the whole system.

Tab. 5.3 Calculations that represent the four corners of the p_H/ p_{H₂} area

Case	1	2	3	4
p _{H₂}	0.09	0.0008	100	100
p _H	7.6	9.6	9.5	6.4
Represented by test case	h	h	f	e
Corrosion progress [kg Fe]	1000	27	1000	1000
Solid/liquid ratio [kg Fe corroded/ kg solution]	0.22	0.0059	0.22	0.22
Solid phase present	Berthierite, antigorite, calcite, pyrrhotite, pyrite, quartz, greenalite, NiSiO ₃	Berthierite, antigorite, calcite, magnetite, pyrrhotite, pyrite	Berthierite, antigorite, calcite, pyrite, greenalite, gypsum, Fe(OH) ₂ (aged), Fe-hibbingite, nickel	Berthierite, calcite, pyrrhotite, NiSiO ₃ , quartz, dolomite, siderite

The calculations in the previous sections allowed a first narrowing down of the p_H and redox conditions in the near field of a repository in the Lower Cretaceous Claystone. Based on the results, the following ranges could be defined:

- Hydrogen pressure: minimum 0.0008 bar, maximum 100 bar
- p_H: minimum: 6.4, maximum 9.6

These conditions form a four-sided area whose corners are represented by certain points in some of the corrosion calculations (Tab. 5.3).

The bandwidths above are valid only for the solution composition derived for the generic site Nord. However, it is assumed that the influence of salinity on these limits is rather small, as most of the anticipated corrosion phases do not incorporate the main ions of the pore waters (Na,Ca,Cl). The situation would be somewhat different in weakly mineralised waters. However, according to current knowledge, such waters do not occur in the North German Lower Cretaceous.

5.3 Predominant speciation and solubility of selected radionuclides

The geochemical conditions in the vicinity of the corroding waste container determine the solubility and thus mobility of radionuclides released from the waste matrix. Four radionuclides (Tc, Se, U, Pu) were selected for which the impact of the pCH and p_{H2} bandwidth on the solubility should be tested. The following databases/ datasets were used to achieve this:

- Se: /HAG 21/
- Tc, U: THEREDA
- Pu: THEREDA, supplemented with data for Pu(III) species /KIT 17/.

For comparison, technetium and uranium stability fields were also calculated with the JAEA database for GWB (Version 2019/03, Status 19.3.2019¹⁰). It is largely based on the NEA database and contains more solid phases than THEREDA.

5.3.1 Selenium

Under strongly reducing conditions (p_{H2}>0.1 bar) the speciation of selenium is dominated by HSe⁻ and H₂Se(aq) (Fig. 5.9 left). At lower H₂ pressures polyselenide species such as Se³⁻, Se⁴⁻ or HSe₄⁻ may occur. Stable selenium phases were calculated under the assumption that pyrite is present. In the relevant pCH/pH₂ region either β-Fe_{1.04}Se or γ-Fe₃Se₄ or FeSe₂ would be the solubility limiting phase. The formation of mixed iron sulphides/ selenides is plausible in cases where there is a supply of hydrogen sulphide, e. g. from the reduction of pyrite by hydrogen.

¹⁰ See https://migrationdb.jaea.go.jp/tdb_e2/tdb_pre_e.html

There is experimental evidence that the reduction of selenite and selenate by metallic iron may lead to the zero-valent state instead of the more stable iron selenides /SCH 03/, /BÖR 18/. In that case, the primary product would be amorphous red selenium. If the formation of selenide and polyselenide species is suppressed, aqueous selenium, 'Se(aq)' (in reality probably $\text{Se}_8(\text{aq})$), would dominate the selenium speciation in the relevant pCH/pH₂ field (Fig. 5.10 left). This species was included in the database because of the analogy to aqueous cyclo-octasulphur, $\text{S}_8(\text{aq})$ that has a low, but significant water solubility (see /HAG 21/ for further information). Omitting this species would lead to extremely low selenium solubilities around 10^{-48} mol/kg if all selenide species are suppressed. In the calculations, other selenium allotropes are suppressed.

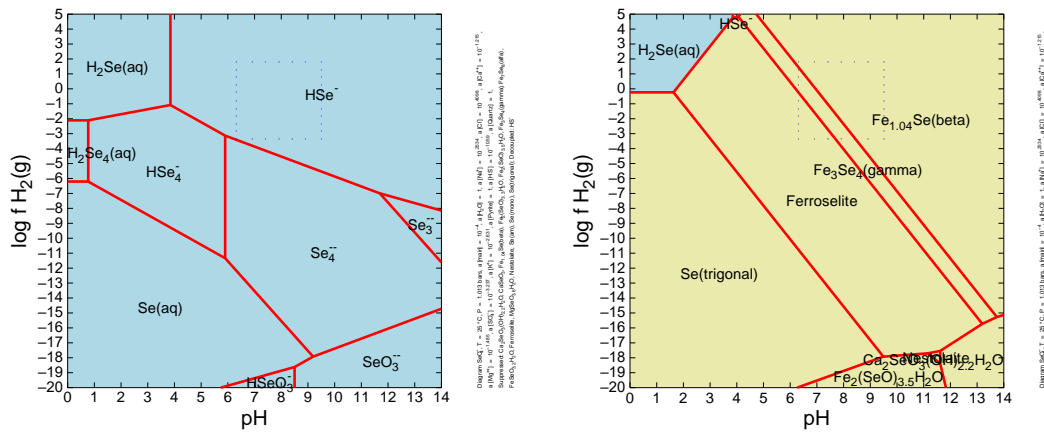


Fig. 5.9 Stability fields of selenium species (left) and solids (right) in Lower Cretaceous clay model pore water ($a_{\text{SeO}_4} = 10^{-4}$ mol/kg)

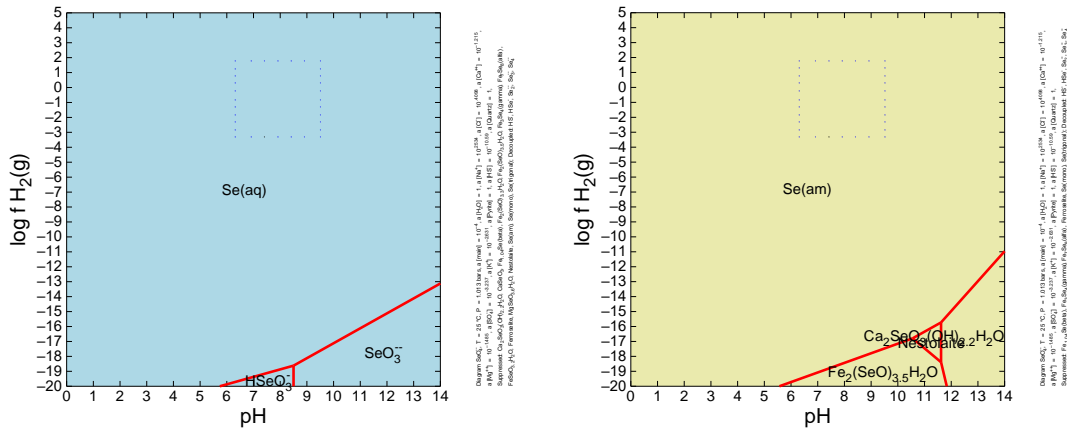


Fig. 5.10 Stability fields of selenium species (left) and solids (right) in Lower Cretaceous clay model pore water ($a_{\text{SeO}_4} = 10^{-4}$ mol/kg) with all selenide and polyselenide species as well as crystalline selenium allotropes suppressed

5.3.2 Uranium

Equilibria for uranium were calculated with release 9 of the THEREDA database. According to this database, $\text{U}(\text{OH})_4(\text{amorphous})$ dominates in the relevant pH/redox range. The neutral species $\text{U}(\text{OH})_4(\text{aq})$ would dominate in the aqueous phases (Fig. 5.11). If the JAEA database is used instead, a calcium uranate (VI) with low water content is present in part of the relevant pH/ H_2 range. However, this only forms at higher temperatures. The latter phase is not included in the THEREDA database that has an entry for the more water-rich and better soluble becquerelite (it is missing in the JAEA database). The THEREDA database should be given preference because it has been designed for use in saline systems.

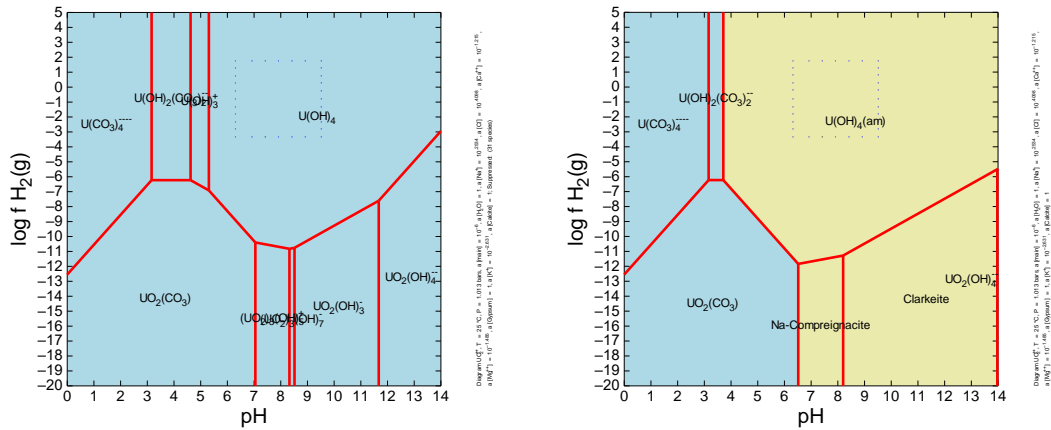


Fig. 5.11 Stability fields of uranium in Lower Cretaceous clay model pore water (THEREDA) ($a_{UO_2^{2+}} = 10^{-6}$)

For comparison, modelling with the JAEA database was carried out (Fig. 5.12)

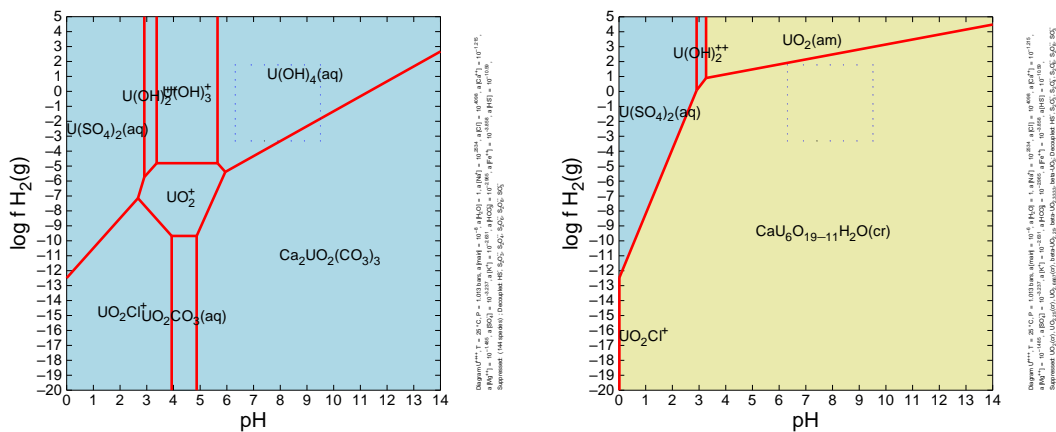


Fig. 5.12 Stability fields of uranium in Lower Cretaceous clay model pore water (JAEA) ($a_{U^{4+}} = 10^{-6}$)

The following table shows the expected solubilities. In Lower Cretaceous clay model pore water, a U-concentration of about $3 \cdot 10^{-9}$ mol/kg can be expected. The result is the same for all four considered cases.

5.3.3 Plutonium

If the JAEA database is taken as a basis, Pu(III) species, especially carbonate species $Pu(CO)_n^{3-2n}$ ($n=1-3$), predominate in direct contact with metallic iron under very strongly reducing conditions. A basic Pu(III) carbonate or plutonium(III) hydroxide would occur as

the equilibrium solid phase, assuming that crystalline $\text{PuO}_2(\text{cr})$ is not formed (Fig. 5.13). At lower H_2 pressures or at a distance from iron, Pu(IV) species are more likely to be present, again with the involvement of carbonate. As solid phase $\text{PuO}_2(\text{am})$ would be most stable.

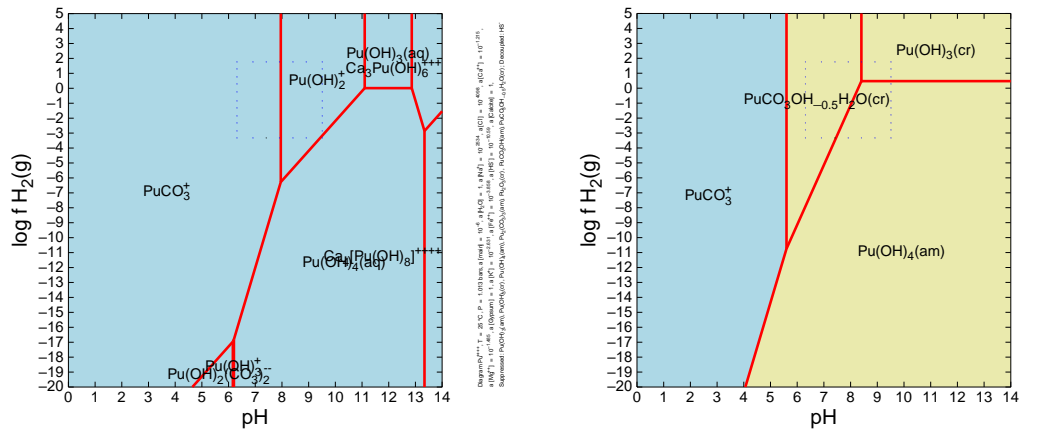


Fig. 5.13 Stability fields of plutonium in Lower Cretaceous clay model pore water

5.3.4 Technetium

In aqueous solutions under reducing conditions Tc(IV) species, especially oxyhydroxide complexes, always predominate (Fig. 5.15). At the hydrogen pressures considered, technetium is reduced to the elementary state. In this case, the solubility would be extremely low. Whether this process takes place in this way is currently unclear. In long-term safety considerations, it is currently assumed that Tc(IV) is the lowest relevant oxidation state.

It should be noted that the JAEA database does not contain any entry for TcS_2 , which according to other representations would cover the entire stability field of metallic Tc. However, the nature and stability of technetium sulphides is still a subject of intensive research /PEA 18/.

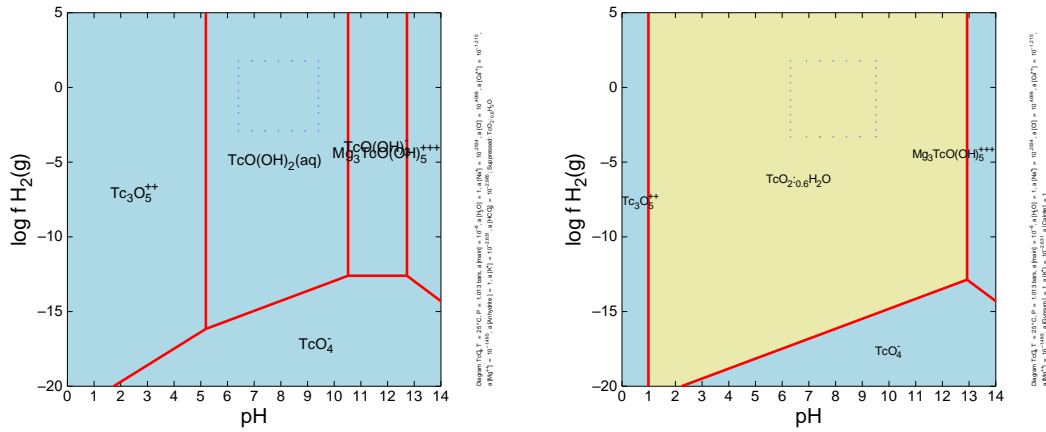


Fig. 5.14 Stability fields of technetium in the Lower Cretaceous clay model pore water (THEREDA)

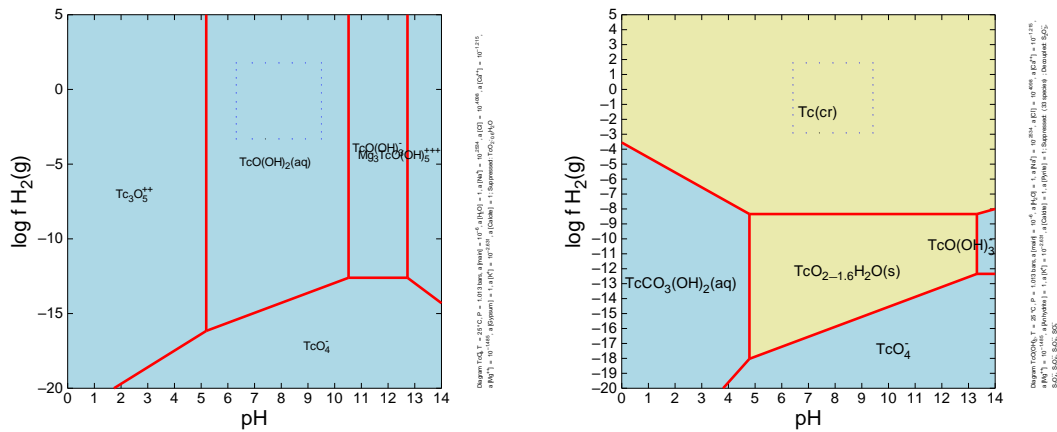


Fig. 5.15 Stability fields of technetium in the Lower Cretaceous clay model pore water (JAEA)

5.3.5 Solubility of Se, U, Pu and Tc in model pore water at pCh 6.4 to 9.6 and pH₂ 0.008 to 100 bar

For each radionuclide, the solubility was calculated by adding the equilibrium phase identified for these conditions and fixing the pCh and pH₂ values to one of the combinations in Tab. 5.3. The results of these modelling calculations are shown in Tab. 5.4.

In the chosen bandwidths, pCh and pH₂ have little impact on the solubility of uranium and technetium (log c -8.5 / -8.8). They mainly occur as neutral species U(OH)₄(aq) and TcO(OH)₂(aq) that are in equilibrium with the hydroxides U(OH)₄(am) and TcO₂·0.6H₂O. The equilibrium reaction neither involves H⁺ or a reduction/oxidation process. The

situation is different for plutonium, where two different oxidation states, Pu(III) and Pu(IV) and three solid phases, $\text{Pu}(\text{OH})_4(\text{am})$, $\text{Pu}(\text{OH})_3(\text{cr})$ and $\text{PuCO}_3(\text{OH}) \cdot 0.5\text{H}_2\text{O}$ are predominant. The solubility ranges from $\log c$ -5.6 to -9.7.

The main selenium species would be HSe^- . Depending on the pH/pH_2 condition either $\text{Fe}_{1.04}\text{Se}$ or Fe_3Se_4 would occur. The solubility ($\log c$) would be in the order of -7.8 to -6.6. If the formation of selenides is suppressed the total concentration of selenium would be caused by $\text{Se}(\text{aq})$ in equilibrium with $\text{Se}(\text{am})$ ($\log c = 5.9$).

Tab. 5.4 Solubility of Se, Tc, U and Pu in Lower Cretaceous Pore water and solid equilibrium phases

No.	pH	pH_2 [bar]	$\text{Se}^{\text{II-}} / \text{Se}^0$ log [mol/kg]	Tc log [mol/kg]	U log [mol/kg]	Pu log [mol/kg]
1	7.6	0.09	-6.7 / -5.9 $\text{Fe}_3\text{Se}_4 /$ $\text{Se}(\text{am})$	-8.8 $\text{TcO}_2 \cdot 0.6\text{H}_2\text{O}$	-8.5 $\text{U}(\text{OH})_4(\text{am})$	-6.6 $\text{PuCO}_3(\text{OH}) \cdot 0.5\text{H}_2\text{O}$
2	9.6	0.0008	-6.7 / -5.9 $\text{Fe}_{1.04}\text{Se} /$ $\text{Se}(\text{am})$	-8.8 $\text{TcO}_2 \cdot 0.6\text{H}_2\text{O}$	-8.5 $\text{U}(\text{OH})_4(\text{am})$	-9.7 $\text{Pu}(\text{OH})_4(\text{am})$
3	9.5	100	-7.8 / -5.9 $\text{Fe}_{1.04}\text{Se} /$ $\text{Se}(\text{am})$	-8.8 $\text{TcO}_2 \cdot 0.6\text{H}_2\text{O}$	-8.5 $\text{U}(\text{OH})_4(\text{am})$	-7.9 $\text{Pu}(\text{OH})_3(\text{cr})$
4	6.4	100	-6.5 / -5.9 $\text{Fe}_{1.04}\text{Se} /$ $\text{Se}(\text{am})$	-8.8 $\text{TcO}_2 \cdot 0.6\text{H}_2\text{O}$	-8.4 $\text{U}(\text{OH})_4(\text{am})$	-5.6 $\text{PuCO}_3(\text{OH}) \cdot 0.5\text{H}_2\text{O}$

6 Summary and conclusions

For repository concepts in clay rock, access of pore waters to the stored waste containers must be expected for all developments of the repository system to be considered within the framework of a long-term safety demonstration. In the case of North German clay formations that are considered for the construction of a repository for heat-generating radioactive waste, saline pore waters must also be assumed. The inflowing solutions lead to progressive corrosion of the containers, which after a certain time, especially with sufficient solution quantities, can lead to failure of the waste containers and mobilisation of radionuclides into the near-field system. The radionuclides released from the waste matrix encounter a geochemical environment that is strongly determined by the corrosion of the metallic components in the near-field (containers, liners, internals). Although it is based on the geochemical conditions in the host rock formation, it is decisively influenced locally by the solid, dissolved and gaseous corrosion products. The mobility of radionuclides in the immediate environment of the waste is then influenced by the following processes

- reduction/oxidation processes, as well as the formation of complexes and solid phases under the boundary conditions of the geochemical environment (redox level, hydrogen ion concentration, solution composition), and
- the sorption of radionuclides on the corrosion phases formed.

For an evaluation and quantification of these processes, it is necessary on the one hand to be able to describe the corrosion itself, i. e. its kinetics and the type of products, and on the other hand to develop a sufficient understanding of the properties of the corrosion products with regard to their thermodynamic stability and their sorption properties towards radionuclides.

While the parallel KORSO¹¹ project focused on the electrochemical investigation of corrosion processes taking place under anaerobic conditions and on corrosion kinetics, the KORPHA project was dedicated to the thermodynamic aspects of corrosion. On this basis, estimates were made for the geochemical environment and the solubility of radionuclides.

¹¹ „Korrosions- und Sorptionsprozesse an Stahloberflächen bei hohen Temperaturen und Drücken im anaeroben salinaren Milieu“ BMWI-Fkz 02 E 11496A

Previous studies have shown that widely differing solubilities are reported in the literature for the iron (II/III) and iron (III) compounds formed during the corrosion of iron. These apparently depend on both the formation conditions of the solid phases and the analytical method used to determine the solubilities. As long as the boundary conditions of corrosion cannot be predicted unambiguously, solubilities of possible corrosion phases cannot be predicted with certainty either. Statements about the geochemical near-field environment must therefore always be based on a range of possible thermodynamic characteristics. Other processes relevant to the development of the redox level must also be taken into account, such as the formation and fate of corrosion hydrogen and the occurrence of kinetically inhibited processes. These include the inorganic or microbially catalysed reduction of sulphate and the formation of magnetite at only moderately elevated temperatures.

Composition of pore waters of North German Lower Cretaceous clays

Due to a lack of analytical data, it is currently only possible to speculate about the chemistry of pore waters in North German Lower Cretaceous clays. However, based on comparisons with information from other deposits and studies on the compaction behaviour of saline clays, two types of clays and solutions can be distinguished:

- Pore waters in clay formations where kaolinite and illite predominate can have a strongly saline character. This would be the case in northern Germany in the Apt or older formation. Historical measurements showed a concentration of up to 5.6 mol/l chloride for clay samples at depths of 1000 to 1100 metres. This corresponds to halite saturation. This would represent an upper concentration limit. The lower limit would be a solution composition close to the salinity of seawater (0.5 mol/l), but historical contact with meteoric waters may have caused dilution of salinity.
- The smectite-dominated clays are more likely to have weakly mineralised waters because ions are preferentially squeezed out during the reaction. Thus, if the repository is in the Alb or younger formation, weakly saline clay pore waters with mineralisation around 10 g/l may be present

On the other hand, the occurrence of saline solutions in accompanying sandstone layers (e. g. in the Hils sandstone) alone is no proof for the presence of saline clay pore waters.

Based on these considerations and the salinity gradients determined by the boreholes in the vicinity of the Konrad shaft, a pore water composition was derived for the model site NORD (project AnSichT). It is a NaCl/CaCl₂ dominated water saturated in the minerals of the formation (goethite, pyrite, calcite, dolomite, gypsum and siderite). Its chloride concentration is about 3 mol/l.

Predominant solid phases in the corrosion of iron

The corrosion of ferrous container materials and liners leads to strongly reducing conditions. After the end of the aerobic phases in the repository (some 10 to 100 years), practically only iron(II) phases occur as corrosion phases in contact with the container. Depending on the geochemical environment, these include hibbingite (a basic chloride), chukanovite (a basic carbonate), siderite/artinite (carbonates, partly mixed with Mg), possibly also amakinite (a hydroxide mixed with Mg), and, depending on the availability of sulphide, also pyrite and other sulphides. Initially present in small quantities, pure iron(III) phases are reduced to iron(II/III) phases in the course of anaerobic corrosion. Magnetite is found only to a minor extent in anaerobic corrosion experiments in contact with clay. Its formation is therefore obviously kinetically inhibited or the local chemical conditions do not allow its formation. Occasionally, small amounts of maghemite ($\gamma\text{-Fe}_2\text{O}_3$) and chloride-containing akaganeite ($\beta\text{-Fe}^{3+}\text{O}(\text{OH}, \text{Cl})$) are found, but the latter only temporarily. The new formation of iron-containing silicates in both the inner and outer corrosion layers is significant. These include 1:1 phyllosilicates from the kaolinite/serpentine group (greenalite, berthierite, odinite, cronstedtite) and 2:1 clay minerals from the smectite group (nontronite, saponite, beidellite, Fe-montmorillonite). They are formed by diffusion of silicate from the surrounding clay material towards the corrosion front or by diffusion of iron ions into the surrounding clay.

It should be noted, however, that corrosion studies in contact with saline clays have not yet taken place. Experience to date shows that iron corrosion in free solution exhibits both different kinetics and different corrosion products, so that previous research on corrosion in salt solutions cannot be transferred to real installation conditions in the clay.

Stability of corrosion phases

In the course of the project, important corrosion phases were synthesised and thermodynamically characterised. These include pure Fe-hibbingite and chukanovite. The focus was also on mixed phases, as can be expected in the presence of magnesium. These

include hibbingite, $(\text{Fe,Mg})_2(\text{OH})_3\text{Cl}$, Fe/Mg chukanovite, $(\text{Fe,Mg})_2(\text{OH})_2\text{CO}_3$ and amakinite $(\text{Fe,Mg})(\text{OH})_2$. For amakinite, it could be shown that it is an ideal solid solution with a variable Mg/Fe ratio. This allows an improved prediction of the geochemical environment in the near field. However, the investigations were designed for temperatures at or near 25 °C. Data on the stability of the phases at higher temperatures (up to 80 °C), as relevant in the first centuries after closure, still have to be obtained. There are still only few experimental data available on the stability of Fe(II)-containing clay minerals.

Redox level in the near field of a repository in the course of container corrosion

Based on the new findings on the stability of iron corrosion phases and the composition of clay pore waters, the reaction process during the corrosion of a cast-iron container was calculated. Current investigated repository concepts for sites in clay served as a basis. Here, the emplacement of repository containers in a quartz sand filling is planned, which are enclosed by a steel liner. Various variables were taken into account to be able to estimate the range of possible system developments:

- Allowing or suppressing sulphate reduction by hydrogen
- Buffering of the CO_2 partial pressure at the initial value or waiving of buffering
- Free development of the H_2 partial pressure or determination of a constant maximum pressure
- Mass of the quartz sand involved in the corrosion process
- Availability of pyrite as a sink for hydrogen corrosion and source of hydrogen sulphide

The calculations allowed an insight into the possible characteristics of corrosion processes under saline conditions and in contact with silicate materials. Depending on the boundary conditions, the sequence of the occurring corrosion phases and thus also the resulting hydrogen ion concentrations (pH values) and hydrogen partial pressures change. However, it became clear that buffering by silicate causes a limitation of the range of pH values to a range of 6.4 to 9.6. The range of hydrogen partial pressures is more difficult to grasp because diffusion processes and gas transport via two-phase flow could not be taken into account in the static calculations. If hydrogen is consumed rather quickly by reaction with pyrite in the host rock, low partial pressures in the order of 10^{-3} bar would be expected. If the diffusion of hydrogen into the surrounding host rock is slower than the gas production at the corrosion front, much higher pressures can be reached. As a preliminary upper limit, 100 bar is assumed. This is in agreement with

benchmark calculations for pressure build-up in a repository in clay, which arrived at maximum pressures of 50 bar after about 20,000 to 40,000 years.

Impact on radionuclide mobility

For the range of H_2 pressures and p_cH values obtained in this way, predominant aqueous species and solids were calculated for selected radionuclides (Se, Tc, U, Pu). For this purpose, the THEREDA database was used with some additions.

It became clear that generally, low oxidation states are to be expected (Se^0 or Se^{-II} , Tc^{IV} , U^{IV} , Pu^{III} or Pu^{IV}). These are usually, but not always, associated with low solubilities. For uranium and technetium, the solubility was the same in the whole p_cH/p_{H2} field considered. However, a reduction to elemental technetium was not considered, which would be expected according to another database (JAEA). For selenium, a bandwidth of two orders of magnitude resulted, which is mainly caused by the unclear nature of the actually occurring oxidation state (0 or -II). For plutonium, there was a bandwidth of three orders of magnitude. Here, both oxidation state and stable solid phases change, so that larger differences between the individual calculations resulted.

For some elements, it should be examined more intensively in future which oxidation states actually occur in contact with corroding steel materials, because thermodynamically stable phases often form only with a delay due to kinetic inhibitions. In future, research efforts should concentrate on the reduced phases/species. For these, often only a few usable data are available. This is especially true for saline conditions.

The project showed that major questions are still open on anaerobic iron corrosion in clay, especially under saline conditions. Predictions about future geochemical developments in the near-field of a repository must be considered speculative as long as basic data on the geochemical properties of Lower Cretaceous clays are not available and important corrosion processes and secondary reactions of reaction products have not been studied under realistic conditions. Knowledge gaps include:

- Analytical data on clay pore waters in North German Lower Cretaceous formations
- Swelling behaviour of bentonite from open pits (as potential buffers) in contact with saline pore waters from kaolinitic clays

- Corrosion of steel in saline clays of the Lower Cretaceous (so far, corrosion studies have concentrated on clays with weakly mineralised pore waters)
- Reaction of corrosion hydrogen with minerals present in clay or primary corrosion products, diffusion of H₂ in saturated Lower Cretaceous clays
- Influence of oxidised bentonite from opencast mining on Fe corrosion
- Relevance of microbial sulphate reduction and methane production under saline conditions.

Such questions should be considered in more detail by future research activities to enable a fundamental understanding of the geochemical evolution of the near field and subsequently the migration behaviour of radionuclides.

7 References

- /AGE 05/ Agence nationale pour la gestion des déchets radioactifs (ANDRA) (Ed.): Dossier 2005 Argile. Tome Architecture and management of a geological repository. 2005.
- /AGE 16/ Agence nationale pour la gestion des déchets radioactifs (ANDRA): Safety Options Report - Post-Closure Part (DOS-AF). CG-TE-D-NTE-AMOA-SR2-0000- r 5-0062, 466 p., 2016.
- /ALF 20a/ Alfarra, A., Bertrams, N., Bollingerfehr, W., Eickemeier, R., Flügge, J., Frenzel, B., Maßmann, J., Mayer, K.-M., Mönig, J., Mrugalla, S., Müller-Hoeppe, N., Reinhold, K., Rübel, A., Schubarth-Engelschall, N., et al.: RESUS. Grundlagen zur Bewertung eines Endlagersystems in einer Tongesteinsformation größerer Mächtigkeit. GRS-Bericht, No. 571, 186 p., 2020.
- /ALF 20b/ Alfarra, A., Bertrams, N., Bollingerfehr, W., Eickemeier, R., Flügge, J., Frenzel, B., Liu, W., Maßmann, J., Mayer, K.-M., Mönig, J., Mrugalla, S., Müller-Hoeppe, N., Reinhold, K., Rübel, A., et al.: RESUS. Grundlagen zur Bewertung eines Endlagersystems in einer Tongesteinsformation geringerer Mächtigkeit. GRS-Bericht, No. 572, 186 p., 2020.
- /AME 04/ Amelung, P., Kutowski, J.: Gegenüberstellung von Endlagerkonzepten in Salz und Tongestein. Vergleich der Wirtsgesteine Ton-/ Tonstein und Steinsalz in den Ablagerungsräumen der Norddeutschen Senke und des Süddeutschen Molassebeckens. DBE TECHNOLOGY GmbH, 101 p.: Peine, 2004.
- /AME 07/ Amelung, P., Jobmann, M., Uhlig, L.: Untersuchungen zur sicherheitstechnischen Auslegung eines generischen Endlagers im Tonstein in Deutschland - GENESIS - Anlagenband Geologie der Referenzregionen im Tonstein. Deutsche Gesellschaft zum Bau und Betrieb von Endlagern für Abfallstoffe mbH, 2007.
- /AND 05/ ANDRA: Dossier 2005 Argile. Tome Safety evaluation of a geological repository. Paris, 2005.

- /AZO 12/ Azoulay, I., Rémazeilles, C., Refait, P.: Determination of standard Gibbs free energy of formation of chukanovite and Pourbaix diagrams of iron in carbonated media. *Corrosion Science*, Bd. 58, pp. 229–236, 2012.
- /BAE 21/ Baere, K. de, van Haelst, S., Chaves, I., Luyckx, D., van den Bergh, K., Verbeken, K., Meyer, E. de, Verhasselt, K., Meskens, R., Potters, G., Melchers, R.: The influence of concretion on the long-term corrosion rate of steel shipwrecks in the Belgian North Sea. *Corrosion Engineering, Science and Technology*, Bd. 56, Nr. 1, pp. 71–80, DOI 10.1080/1478422X.2020.1807163, 2021.
- /BAS 18/ Bassez, M.-P.: Water near its Supercritical Point and at Alkaline pH for the Production of Ferric Oxides and Silicates in Anoxic Conditions. A New Hypothesis for the Synthesis of Minerals Observed in Banded Iron Formations and for the Related Geobiotropic Chemistry inside Fluid Inclusions. *Origins of life and evolution of the biosphere : the journal of the International Society for the Study of the Origin of Life*, Bd. 48, Nr. 3, pp. 289–320, DOI 10.1007/s11084-018-9560-y, 2018.
- /BEN 98/ Benesch, M.: *Mineralogische Untersuchungen von Unterkreide-Sedimenten aus dem Niedersächsischen Becken*, Zugl.: Göttingen, Univ., Diss., 1998. 1. ed., 68 p., ISBN 389712128X, Cuvillier: Göttingen, 1998.
- /BER 13/ Berner, U., Kulik, A., Kosakowski, G.: Geochemical impact of a low-pH cement liner on the near field of a repository for spent fuel and high-level radioactive waste. *Physics and Chemistry of the Earth*, Bd. 64, pp. 46–56, 2013.
- /BÖR 18/ Börsig, N., Scheinost, A. C., Shaw, S., Schild, D., Neumann, T.: Retention and multiphase transformation of selenium oxyanions during the formation of magnetite via iron(ii) hydroxide and green rust. *Dalton transactions (Cambridge, England : 2003)*, Bd. 47, Nr. 32, pp. 11002–11015, DOI 10.1039/C8DT01799A, 2018.
- /BOU 04/ Bourrié, G., Trolard, F., Refait, P.: A solid-solution model for Fe(II)-Fe(III)-Mg(II) green rusts and fougérite and estimation of their Gibbs free energies of formation. *Clays Clay Min.*, Bd. 52, Nr. 3, pp. 382–395, 2004.

- /BOU 14/ Bourdelle, F., Truche, L., Pignatelli, I.: Iron-clay interactions under hydrothermal conditions: impact of specific surface area of metallic iron on reaction pathway. *Chemical Geology*, Bd. 381, pp. 194–205, 2014.
- /BOU 17/ Bourdelle, F., Mosser-Ruck, R., Truche, L., Lorgeoux, C., Pignatelli, I., Michau, N.: A new view on iron-claystone interactions under hydrothermal conditions (90 °C) by monitoring in situ pH evolution and H₂ generation. *Chemical Geology*, Bd. 466, pp. 600–607, DOI 10.1016/j.chemgeo.2017.07.009, 2017.
- /BRA 93/ Brammer, K. -J., Knipping, B. J.: The origin of formation waters in the abandoned Konrad iron ore mine (Salzgitter, Germany). *European Journal of Mineralogy*, Bd. 5, pp. 787–797, 1993.
- /BRA 01/ Brassler, T., Fischer-Appelt, K., Larue, J.: Hydrochemischer Charakter von Tiefenwässern in ausgewählten Regionen Deutschlands. Fachliche Unterstützung des BMU-Arbeitskreises zur Auswahl von Endlagerstandorten. GRS-Bericht, A 2956, Anlage, 2001.
- /BRA 02/ Brassler, T., Brewitz, W.: Anwendbarkeit der Indikatoren "teufenabhängige Mineralisation / Salzgehalt" für die Erfüllung der allgemeinen Anforderung keine oder langsame Grundwasserbewegung. Bericht an den AKEnd. GRS-Bericht, A, Nr. 2956, 2002.
- /BRA 14/ Bradbury, M. H., Berner, U., Curti, E.: The long term geochemical evolution of the nearfield of the HLW repository. Nagra, Technical Report, Bd. 12, Nr. 01, 2014.
- /BRE 82/ Brewitz, W.: Eignungsprüfung der Schachtanlage Konrad für die Endlagerung radioaktiver Abfälle (2 Bände). GSF-Bericht, T 136, 1982.
- /BRI 08/ Britvin, S. N., Bogdanova, A. N., Boldyreva, M. M., Aksenova, G. Y.: Rudashevskyite, the Fe-dominant analogue of sphalerite, a new mineral: Description and crystal structure. *The American Mineralogist*, Bd. 93, No. 5-6, pp. 902–909, DOI 10.2138/am.2008.2582, 2008.

- /BRO 76/ Brockamp, O.: Nachweis von Vulkanismus in Sedimenten der Unter- und Oberkreide in Norddeutschland. *Geologische Rundschau*, Bd. 65, pp. 162–173, 1976.
- /BUH 91/ Buhmann, D., Nies, A., Storck, R.: Analyse der Langzeitsicherheit von Endlagerkonzepten für wärmeerzeugende radioaktive Abfälle. GSF (Gesellschaft für Umwelt und Gesundheit mbH), GSF-Bericht 27/91: Braunschweig, 1991.
- /BUN 20a/ Bundesgesellschaft für Endlagerung (BGE) (Ed.): Sub-areas interim report pursuant to Section 13 StandAG. SG01101/16-1/2-2021#1 – Object ID: 850052 – Revision: 00, 2034 p., 2020.
- /BUN 20b/ Verordnung über Sicherheitsanforderungen an die Endlagerung hochradioaktiver Abfälle (Endlagersicherheitsanforderungsverordnung) (EndlSiAnfV) as amended on 6 October 2020, last changed 2020 (*Bundesgesetzblatt* 2020, No. 45, pp. 2094–2106).
- /CAC 94/ Caccavo, F., Lonergan, D. J., Lovley, D. R., Davis, M., Stolz, J. F., McInerney, M. J.: *Geobacter sulfurreducens* sp. nov., a hydrogen- and acetate-oxidizing dissimilatory metal-reducing microorganism. *Applied and Environmental Microbiology*, Bd. 60, Nr. 10, pp. 3752–3759, DOI 10.1128/AEM.60.10.3752-3759.1994, 1994.
- /CAR 07/ Carlson, L., Karnland, O., Oversby, V. M.: Experimental studies of the interactions between anaerobically corroding iron and bentonite. *Physics and Chemistry of the Earth*, Bd. 32, pp. 334–345, 2007.
- /CHI 73/ Chilingarian, G. V., Sawabini, C. T., Rieke, H. H.: Effect of compaction on chemistry of solutions expelled from the montmorillonite clay saturated in seawater. *Sedimentol.*, Bd. 20, pp. 391–398, 1973.
- /CHI 76/ Chilingar, G. V., Rieke, H. H.: Chemistry of interstitial solutions in under-compacted (overpressured) versus well-compacted shales. In: Bailey, S. W. (Ed.): *Proceedings of the International Clay Conference 1975*, Mexico City, Mexico, July 16-23, 1975. International Clay Conference, Mexico City, Mexico, 16 - 23 July 1975, pp. 673–678, Applied Publishing: Wilmette, Illinois 1976.

- /CHI 94/ Chilingarian, G. V., Rieke, H. H., Kazi, A.: Chemistry of Pore Water. In: Fertil, W. H., Chapman, R. E., Hotz, R. F. (Eds.): Studies in abnormal pres-sures. Developments in Petroleum Science, Vol. 38, No. 38, pp. 107–153, ISBN 9780444899996, DOI 10.1016/S0376-7361(09)70229-8, Elsevier: Amsterdam, New York, 1994.
- /CHR 10/ Christiansen, B. C., Balic-Zunic, T., Petit, P. -O.: Composition and structure of an iron-bearing, layered double hydroxide (LDH) - Green rust sodium sulphate. *Geochimica et Cosmochimica Acta*, Bd. 73, pp. 3579–3592, 2010.
- /CLO 14/ Cloet, V., Schwyn, B., Baeyens, B.: Einfluss der Salinität des Porenwassers der Wirtgesteine auf die Langzeitsicherheit der Tiefenlager. NAGRA Arbeitsbericht, Bd. 14, Nr. 09, 2014.
- /CRU 17/ Crusset, D., Deydier, V., Necib, S., Gras, J.-M., Combrade, P., Féron, D., Burger, E.: Corrosion of carbon steel components in the French high-level waste programme: evolution of disposal concept and selection of materials. *Corrosion Engineering, Science and Technology*, Bd. 52, sup1, pp. 17–24, DOI 10.1080/1478422X.2017.1344416, 2017.
- /CUI 02/ Cui, D., Spahiu, K.: The reduction of U(VI) on corroded iron under anoxic conditions. *Radiochimica Acta*, Bd. 90, pp. 623–628, 2002.
- /DAU 13/ Dauzères, A., Maillet, A., Gaudin, A.: The years of Toarcian argillite - carbon steel in situ interaction. *Proc. Earth and Planetary Science*, Bd. 7, pp. 195–198, 2013.
- /DAV 10/ Davesne, E., Dideriksen, K., Christiansen, B. C.: Free energy of formation for green rust sodium sulphate ($\text{NaFe}^{\text{II}}_6\text{Fe}^{\text{III}}_3(\text{OH})_{18}(\text{SO}_4)_2(\text{s})$). *Geochimica et Cosmochimica Acta*, Bd. 74, pp. 6451–6467, 2010.

- /DEL 88/ Delnavaz, H., Allmann, R.: Synthesen von Fe-Brucit, Coalingit und Pyroaurit im System MgO-Fe-O₂-H₂O-(CO₂). Z. Krist., Bd. 183, No. 1-4, DOI 10.1524/zkri.1988.183.14.175, 1988.
- /DIC 69/ Dickey, P. A.: Increasing concentration of subsurface brines with depth. Chemical Geology, Bd. 4, No. 1-2, pp. 361–370, DOI 10.1016/0009-2541(69)90055-2, 1969.
- /DID 12/ Didier, M., Leone, L., Greneche, J., Giffaut, E., Charlet, L.: Adsorption of hydrogen gas and redox processes in clays. Env. Sci. Techn., Bd. 46, pp. 3574–3579, 2012.
- /DID 14/ Didier, M., Géhin, A., Grenèche, J.-M., Charlet, L., Giffaut, E.: Method development for evaluating the redox state of Callovo-Oxfordian clayrock and synthetic montmorillonite for nuclear waste management. Applied Geochemistry, Bd. 49, pp. 184–191, DOI 10.1016/j.apgeochem.2014.06.015, 2014.
- /DID 15/ Dideriksen, K., Frandsen, C., Bovet, N., Wallace, A. F., Sel, O., Arbour, T., Navrotsky, A., Yoreo, J. J. de, Banfield, J. F.: Formation and transformation of a short range ordered iron carbonate precursor. Geochim. Cosmochim. Acta, Bd. 164, pp. 94–109, 2015.
- /DIL 16/ Dillmann, P., Gin, S., Neff, D., Gentaz, L., Rebiscoul, D.: Effect of natural and synthetic iron corrosion products on silicate glass alteration processes. Geochimica et Cosmochimica Acta, Bd. 172, pp. 287–305, DOI 10.1016/j.gca.2015.09.033, 2016.
- /DIO 14/ Diomidis, N.: Scientific basis for the production of gas due to corrosion in a deep geological repository. NAGRA Arbeitsbericht, Bd. 14, Nr. 21, 2014.
- /DOS 92/ dos Santos Afonso, M., Stumm, W.: Reductive dissolution of iron(III) (hydr)oxides by hydrogen sulfide. Langmuir, Bd. 8, pp. 1671–1675, 1992.
- /DOU 78/ Dousma, J., van den Hoven, T. J., Bruyn, P. L. d.: The influence of chloride ions on the formation of iron(III) oxyhydroxide. Journal of inorganic and nuclear chemistry, Bd. 40, Nr. 6, pp. 1089–1093, DOI 10.1016/0022-1902(78)80515-6, 1978.

- /ECK 91/ Eckhardt, F.-J.: Geotechnische Probleme der marinen Unterkreide Niedersachsens. In: Schwaighofer, B., Müller, H. W. (Eds.): Tonmineralogie und Geotechnik, Vorträge im Rahmen der Tagung der Deutschen Ton- und Tonmineralgruppe am 31.5. und 1.6. 1990 in Wien. Mitt. Inst. Bodenforsch. Baugeol. Univ. Bodenkultur Wien, Vol. 1, pp. 123–158: Wien, 1991.
- /EL 13a/ El Hajj, H., Abdelouas, A., El Mendili, Y.: Corrosion of carbon steel under sequential aerobic-anaerobic environmental conditions. *Corrosion Science*, Bd. 76, pp. 432–440, 2013.
- /EL 13b/ El Mendili, Y., Abdelouas, A., Bardeau, J. -F.: Corrosion of P235GH carbon steel in simulated Bure soil solution. *J. Mater. Environ. Sci.*, Bd. 4, pp. 786–791, 2013.
- /EL 13c/ El Mendili, Y., Abdelouas, A., Bardeau, J. -F.: Insight into the mechanism of carbon steel corrosion under aerobic and anaerobic conditions. *Physical Chemistry Chemical Physics*, Bd. 15, pp. 9197, 2013.
- /EL 14/ El Mendili, Y., Abdelouas, A., Chaou, A. A.: Carbon steel corrosion in clay-rich environments. *Corrosion Science*, Bd. 88, pp. 56–65, 2014.
- /ENG 60/ Engelhardt, W. v.: Der Porenraum der Sedimente. Mineralogie und Petrographie in Einzeldarstellungen, Vol. 2, 201 p., Springer-Verlag: Berlin, 1960.
- /ENG 61/ Engelhardt, W. v.: Zum Chemismus der Porenlösung der Sedimente. *Bull. Geol. Inst. Univ. Uppsala*, Bd. 40, pp. 189–204, 1961.
- /ENG 63/ Engelhardt, W. V., Gaida, K. H.: Concentration changes of pore solutions during compaction of clay sediments. *Journal of Sedimentary Research*, Bd. 33, Nr. 4, pp. 919–930, DOI 10.1306/74D70F74-2B21-11D7-8648000102C1865D, 1963.

- /ENG 73/ Engelhardt, W. v.: Die Bildung von Sedimenten und Sedimentgesteinen. Sediment-Petrologie, Teil III, 378 p., Schweizerbart'sche Verlagsbuchhandlung: Stuttgart, 1973.
- /ENN 14/ Enning, D., Garrelfs, J.: Corrosion of iron by sulfate-reducing bacteria. New views of an old problem. Applied and Environmental Microbiology, Bd. 80, Nr. 4, pp. 1226–1236, DOI 10.1128/AEM.02848-13, 2014.
- /FEI 50/ Feitknecht, W., Keller, G.: Über die dunkelgrünen Hydroxyverbindungen des Eisens. Zeitschrift für Anorganische Chemie, Bd. 262, pp. 61–68, 1950.
- /FOO 95/ Foote, W. M.: Preliminary note on a new alkali mineral. American Journal of Science, Bd. 50, pp. 480–481, 1895.
- /GAI 81/ Gaida, K. H., Gedenk, R., Kemper, E.: Lithologische, mineralogische und organisch-geochemische Untersuchungen an Tonsteinen und Tonmergelsteinen der Unterkreide Nordwestdeutschlands. Geologisches Jahrbuch, A58, pp. 15–47, 1981.
- /GAU 09a/ Gaucher, E. C., Tournassat, C., Pearson, F. J.: A robust model for pore-water chemistry of clayrock. Geochimica et Cosmochimica Acta, Bd. 73, Nr. 21, pp. 6470–6487, 2009.
- /GAU 09b/ Gaudin, A., Gaboreau, S., Tinseau, E.: Mineralogical reactions in the Tournemire argillite after in-situ interaction with steels. Applied Clay Science, Bd. 43, pp. 196–207, 2009.
- /GAU 13/ Gaudin, A., Bartier, D., Truche, L.: First corrosion stages in Tournemire claystone/steel interaction: in situ experiment and modelling approach. Applied Clay Science, Bd. 457, Nr. 468, pp. 83–84, 2013.
- /GER 86/ Gerardi, J.: Bohrung Konrad 101, Teil I: Geologischer Bericht; Teil II: Schichtenverzeichnis (BGR Archiv-Nr.: 99599);. Ed.: Bundesanstalt für Geowissenschaften und Rohstoffe (BGR), BGR Tech. Ber., 200 p., 1986.

- /GRA 06/ Grandia, F., Doménech, C., Arcos, D.: Assessment of the oxygen consumption in the backfill. Geochemical modelling in a saturated backfill. SKB Technical Report, R, No. 06-106, 2006.
- /GRA 12/ Gradstein, F. M., Ogg, J. C., Schmitz, M. D.: The geologic time scale 2012. 1176 p., Elsevier B.V., Amsterdam, 2012.
- /HAD 17/ Hadi, J., Wersin, P., Jenni, A., Greneche, J. M.: Redox evolution and Fe-bentonite interaction in the ABM2 experiment, Äspö Hard Rock Laboratory. Nagra Technical Report, 17-10, 330 p., 2017.
- /HAD 19/ Hadi, J., Wersin, P., Serneels, V., Greneche, J.-M.: Eighteen years of steel–bentonite interaction in the FEBEX in situ test at the Grimsel Test Site in Switzerland. *Clays and Clay Minerals*, Bd. 67, Nr. 2, pp. 111–131, DOI 10.1007/s42860-019-00012-5, 2019.
- /HAG 14/ Hagemann, S., Bischofer, B., Scharge, T.: Entwicklung von Methoden und Modellen zur Bestimmung des Redoxpotentials salinärer Lösungen. GRS-Bericht, Bd. 260, 2014.
- /HAG 15/ Hagemann, S., Scharge, T., Willms, T.: Entwicklung einer thermodynamischen Datenbasis für ausgewählte Schwermetalle. GRS-Bericht, Bd. 244, 2015.
- /HAG 21/ Hagemann, S., Meyer, T., Mönig, H., Bischofer, B., Jantschik, K.: Solubility limits of fission and activation products in saline near field solutions (In Vorbereitung). GRS-Bericht, 2021.
- /HAN 73/ Hanshaw, B. B., Coplen, T. B.: Ultrafiltration by a compacted clay membrane. II - Sodium ion exclusion at various ionic strengths. *Geochimica et Cosmochimica Acta*, Bd. 37, pp. 2311–2327, 1973.
- /HAY 33/ Hayek, E.: Zur Kenntnis der basischen Salze 2. Einfache basische Chloride zweiwertiger Schwermetalle. *Zeitschrift für anorganische und allgemeine Chemie*, Bd. 210, 1933.

- /HAZ 16/ Hazen, R. M., Hummer, D. R., Hystad, G., Downs, R. T., Golden, J. J.: Carbon mineral ecology: Predicting the undiscovered minerals of carbon. *Am. Min.*, Bd. 101, Nr. 4, pp. 889–906, DOI 10.2138/am-2016-5546, 2016.
- /HER 02/ Herbert, H.-J., Kasbohm, J., Venz, C., Kull, H., Moog, H., Sprenger, U.: Langzeitstabilität von Tondichtungen in Salzformationen. *GRS-Bericht*, No. 185, 272 p., 2002.
- /HER 11/ Herbert, H.-J., Kasbohm, J., Lan, N. T.: Fe-Bentonite. Experiments and modelling of the interactions of bentonites with iron. *GRS-Bericht*, Bd. 295, 2011.
- /HIL 00/ Hild, E.: Haupt- und Spurenelementchemismus von Unterkreidesedimenten (Apt / Alb) aus dem Niedersächsischen Becken. Dissertation, Universität Oldenburg: Oldenburg, 2000.
- /HOL 10/ Hol, A., van der Weijden, R. D., van Weert, G.: Bio-reduction of pyrite investigated in a gas lift loop reactor. *International Journal of Mineral Processing*, Bd. 94, pp. 140–146, 2010.
- /HOT 07/ Hoth, P., Wirth, H., Reinhold, K., Bräuer, V., Krull, P., Feldrappe, H.: Endlagerung radioaktiver Abfälle in tiefen geologischen Formationen Deutschlands - Untersuchung und Bewertung von Tongesteinsformationen. Ed.: Bundesanstalt für Geowissenschaften und Rohstoffe (BGR), 124 p., 2007.
- /ISH 08/ Ishidera, T., Ueno, K., Kurosawa, S.: Investigation of montmorillonite alteration and form of iron corrosion products in compacted bentonite in contact with carbon steel for ten years. *Physics and Chemistry of the Earth*, Bd. 33, pp. S269-S275, 2008.
- /JAH 13/ Jahn, S., Sönke, J.: Endlagerstandortmodell Nord (AnSichT) - Teil II: Zusammenstellung von Gesteinseigenschaften für den Langzeitsicherheitsnachweis. Zwischenbericht. Bundesanstalt für Geowissenschaften und Rohstoffe, 2013.
- /JOB 97/ Jobe, D. J., Lemire, R. J., Taylor, P.: Iron oxide redox chemistry and nuclear fuel disposal. AECL Canada, AECL, Nr. 11667, 1997.

- /JOB 07/ Jobmann, M., Uhlig, L., Amelung, P.: Untersuchungen zur sicherheitstechnischen Auslegung eines generischen Endlagers im Tonstein in Deutschland - GENESIS - Abschlussbericht. Deutsche Gesellschaft zum Bau und Betrieb von Endlagern für Abfallstoffe mbH, 2007.
- /JOB 15a/ Jobmann, M., Lommerzheim, A.: Projekt ANSICHT. Endlagerkonzept sowie Verfüll- und Verschlusskonzept für das Endlagerstandortmodell SUEDE. Technischer Bericht. DBETec Techn. Ber., TEC-26-2015-TB, 2015.
- /JOB 15b/ Jobmann, M., Maßmann, J., Meleshyn, A., Polster, M.: Projekt ANSICHT. Quantifizierung von Kriterien für Integritätsnachweise im Tonstein. Ed.: DBETec, DBETec Tech. Bericht, TEC-08-2013_AP, 44 p., 2015.
- /JOD 12/ Jodin-Caumon, M. -C., Mosser-Ruck, R., Randi, A.: Mineralogical evolution of claystone after reaction with iron under thermal gradient. Clays and Clay Minerals, Bd. 60, pp. 443–455, 2012.
- /JOH 00/ Johnson, L. H., Smith, P. A.: The interaction of radiolysis products and canister corrosion products and the implications for spent fuel dissolution and radionuclide transport in a repository for spent fuel. Nagra Technical Report, Vol. 00, NAGRA-NTB-00-04, 2000.
- /JOH 08/ Johnson, L., King, F.: The effect of the evolution of environmental conditions on the corrosion evolutionary path in a repository for spent fuel and high-level waste in Opalinus Clay. Journal of Nuclear Materials, Bd. 379, pp. 9–15, 2008.
- /JOZ 07/ Jozwiak, W. K., Kaczmarek, E., Maniecki, T. P., Ignaczak, W., Maniukiewicz, W.: Reduction behavior of iron oxides in hydrogen and carbon monoxide atmospheres. Applied Catalysis A: General, Bd. 326, Nr. 1, pp. 17–27, DOI 10.1016/j.apcata.2007.03.021, 2007.
- /KAU 15/ Kaufhold, S., Hassel, A. W., Saners, D.: Corrosion of high-level radioactive waste iron-canisters in contact with bentonite. Journal of Hazardous Material, Bd. 285, pp. 464–473, 2015.

- /KAU 20a/ Kaufhold, S., Schippers, A., Marx, A., Dohrmann, R.: SEM study of the early stages of Fe-bentonite corrosion—The role of naturally present reactive silica. *Corrosion Science*, Bd. 171, pp. 108716, DOI 10.1016/j.corsci.2020.108716, 2020.
- /KAU 20b/ Kaufhold, S., Klimke, S., Schloemer, S., Alpermann, T., Renz, F., Dohrmann, R.: About the Corrosion Mechanism of Metal Iron in Contact with Bentonite. *ACS Earth and Space Chemistry*, Bd. 4, Nr. 5, pp. 711–721, DOI 10.1021/acsearthspacechem.0c00005, 2020.
- /KEL 48/ Keller, G.: Über Hydroxide und basische Salze des zwertigen Eisens und deren dunkelgrünen Oxydationsprodukte. Diss., Universität Bern, 1948.
- /KEM 73/ Kemper, E.: The Valanginian and Hauterivean stages in northwest Germany. In: Casey, R., Rawson, P. F. (Eds.): *The boreal Lower Cretaceous, Proceedings of an international symposium organized by Queen Mary College (University of London) and the Institute of Geological Science 17 - 30 September 1972*. *Geological Journal Special Issue*, Vol. 5, pp. 327–344, 1973.
- /KEM 78/ Kemper, E., Zimmerle, W.: Die anoxischen Sedimente der präoberaptischen Unterkreide NW-Deutschlands und ihr paläogeographischer Rahmen. *Geologisches Jahrbuch*, A 45, pp. 3–41, 1978.
- /KIM 17/ Kim, S., Marrs, C., Nemer, M., Je-Hun Jang, J.: Solubility model for ferrous iron hydroxide, hibbingite, siderite, and chukanovite in high saline solutions of sodium chloride, sodium sulfate, and sodium carbonate. *ACS Earth and Space Chemistry*, Bd. 1, Nr. 10, pp. 647–663, DOI 10.1021/acsearthspacechem.7b00065, 2017.
- /KIN 07/ King, F.: Overview of a carbon steel container corrosion model for a deep geological repository in sedimentary rock. *NWMO Report, TR, No. 2007-0*, 2007.
- /KIN 08/ King, F.: Corrosion of carbon steel under anaerobic conditions in a repository for SF and HLW in opalinus clay. *Nagra, Technical Report, Bd. 08, Nr. 12*, 2008.

- /KIN 10/ King, F., Watson, S.: Review of the corrosion performance of selected metals as canister materials for UK spent fuel and/or HLW. Quintessa Report, QRS, 1384J-, 2010.
- /KIN 12/ King, F., Kolar, M.: Simulation of the anaerobic corrosion of carbon steel used fuel containers using the steel corrosion model version 1.0 (SCM V1.0). NWMO Report, TR, No. 2012-0, 2012.
- /KIN 13/ King, F.: A review of the properties of pyrite and the implications for corrosion of the copper canister. SKB Technical Report, TR, No. 13-19, 2013.
- /KIT 17/ KIT-INE: Experimentelle Arbeiten zur Absicherung von Modellrechnungen und Maximalkonzentrationen für Plutonium und Americium. Ed.: Bundesamt für Strahlenschutz (BfS), 2017.
- /KLI 92/ Klinge, H., Vogel, P., Schelkes, K.: Chemical composition and origin of saline formation waters from the Konrad mine, Germany. In: Kharaka, Y. K. (Ed.): Moderate and high temperature environments. 7th International Symposium on Water-Rock Interaction, Park City, Utah, USA,, 13 - 18 July 1992, Water-rock interaction, Vol. 2, ISBN 905410077X, Balkema: Rotterdam, 1992.
- /KOS 06/ Kostov, I., Kostov, R. I.: Systematics and crystal genesis of carbonate minerals. Godishnik na Minno-Geolozhkiya Universitet Sv. Ivan Rilski, Bd. 49, pp. 111–117, 2006.
- /KOS 13/ Kosakowski, G., Berner, U.: The evolution of clay rock/cement interfaces in a cementitious repository for low- and intermediate level radioactive waste. Physics and Chemistry of the Earth, Bd. 64, pp. 65–86, 2013.
- /KRY 63/ Kryukov, P. A., Zhuchkova, A. A.: Fiziko-khimicheskie yavleniya, svyazaniye s vydeleniem rastvorov iz gornykh porod. In: Laboratorija Hidrogeologičeskikh Problem im. F. P. Savarenskogo. Akademija Nauk SSSR: Sovremennoe Predstavlenie o svjazannoj vode v porodach. pp. 95–105, Izdanie Akademii Nauk SSSR: Moskau, 1963.

- /KUR 04/ Kursten, B., Smailos, E., Azkarate, I.: COBECOMA. State-of-the-art document on the corrosion behaviour of container materials. Final report. European commission: nuclear science and technology, 2004.
- /LAL 04/ Laliberté, M., Cooper, W. E.: Model for calculating the density of aqueous electrolyte solutions. *Journal of Chemical and Engineering Data*, Bd. 49, Nr. 5, pp. 1141–1151, 2004.
- /LAN 09/ Landolt, D., Davenport, A., Payer, J., Shoesmith, D.: A review of materials and corrosion issues regarding canisters for disposal of spent fuel and high-level waste in Opalinus clay. *NAGRA Tech. Rep.*, Vol. 09, NAGRA-NTB-09-02, 2009.
- /LE 15/ Le Pape, P., Rivard, C., Pelletier, M., Bihannic, I., Gley, R., Mathieu, S., Salsi, L., Migot, S., Barres, O., Villiéras, F., Michau, N.: Action of a clay suspension on an Fe(0) surface under anoxic conditions: Characterization of neoformed minerals at the Fe(0)/solution and Fe(0)/atmosphere interfaces. *Applied Geochemistry*, Bd. 61, pp. 62–71, DOI 10.1016/j.apgeochem.2015.05.008, 2015.
- /LEE 10/ Lee, T. R., Wilkin, R. L.: Iron hydroxy carbonate formation in zerovalent iron permeable reactive barriers: characterization and evaluation of phase stability. *Journal of Contaminant Hydrology*, Bd. 116, pp. 47–57, 2010.
- /LEO 17/ Leon, Y., Dillmann, P., Neff, D., Schlegel, M. L., Foy, E., Dynes, J. J.: Interfacial layers at a nanometre scale on iron corroded in carbonated anoxic environments. *RSC Advances*, Bd. 7, Nr. 33, pp. 20101–20115, DOI 10.1039/c7ra01600j, 2017.
- /LER 11/ Lerouge, C., Grangeon, S., Gaucher, E. C.: Mineralogical and isotopic record of biotic and abiotic diagenesis of the Callovian-Oxfordian clayey formation of Bure (France). *Geochimica et Cosmochimica Acta*, Bd. 75, pp. 2633–2663, 2011.
- /LIB 14/ Libert, M., Schütz, M. K., Esnault, L.: Impact of microbial activity on the radioactive waste disposal: long term prediction of biocorrosion process. *Bio-electrochemistry*, Bd. 97, pp. 162–168, 2014.

- /LIP 55/ Lippmann, F.: Ton, Geoden und Minerale des Barrême von Hoheneggelsen. *Geologische Rundschau*, Bd. 43, Nr. 2, pp. 475–503, DOI 10.1007/BF01764034, 1955.
- /LOM 15/ Lommerzheim, A., Jobmann, M.: Projekt ANSICHT. Endlagerkonzept sowie Verfüll- und Verschlusskonzept für das Endlagerstandortmodell NORD. Technischer Bericht. DBETec Techn. Ber., TEC-14-2015-TB, 2015.
- /LOT 21/ Lotz, H., Carrière, C., Bataillon, C., Gardes, E., Monnet, I., Foy, E., Schlegel, M. L., Dynes, J. J., Neff, D., Mercier-Bion, F., Dillmann, P.: Investigation of steel corrosion in MX80 bentonite at 120°C. *Materials and Corrosion*, Bd. 72, No. 1-2, pp. 120–130, DOI 10.1002/maco.202011777, 2021.
- /MAR 08/ Martin, F. A., Bataillon, C., Schlegel, M. L.: Corrosion of iron and low alloyed steel within a water saturated brick of clay under anaerobic deep geological disposal conditions: An integrated experiment. *Journal of Nuclear Materials*, Bd. 379, pp. 80–90, 2008.
- /MAR 14/ Martin, F., Perrin, S., Fenart, M., Schlegel, M., Bataillon, C.: On corrosion of carbon steels in Callovo-Oxfordian clay: complementary EIS, gravimetric and structural study providing insights on long term behaviour in French geological disposal conditions. *Corrosion Engineering, Science and Technology*, Bd. 49, Nr. 6, pp. 460–466, DOI 10.1179/1743278214Y.0000000181, 2014.
- /MAT 91/ Mattiat, B., Kreimeyer, R.: Mineralogisch-Petrographische Untersuchungen an Gesteinsproben aus dem Bereich der Untersuchungsstrecke 541 m Sohle (Barreme) der Schachanlage Konrad. Schacht 2. BGR Tech. Ber, BGR-Archiv-Nr 0108659, 141 p., 1991.
- /MCC 08/ McCann, T.: *The geology of Central Europe. Volume 2: mesozoic and cenozoic.* The Geological Society, London, 2008.
- /MEU 21/ Meuselwitz Guss (Ed.): *Werkstoffkenndaten - Sphäroguss. Gusseisen mit Kugelgraphit.* Available from https://www.meuselwitz-guss.de/fileadmin/daten/Dateien/pdf/werkstoffe/Werkstoffkenndaten_Kugelgraphit_getrennt_gegossen.pdf, retrieved on 9 February 2021.

- /MIL 09a/ Milodowski, A. E., Cave, M. R., Kemp, S. J.: Mineralogical investigations of the interaction between iron corrosion products and bentonite from the NF-PRO experiments (phase 1). SKB Technical Report, TR, No. 09-02, 2009.
- /MIL 09b/ Milodowski, A. E., Cave, M. R., Kemp, S. J.: Mineralogical investigations of the interaction between iron corrosion products and bentonite from the NF-PRO experiments (phase 2). SKB Technical Report, TR, No. 09-03, 2009.
- /MOL 83/ Molecke, M. A.: A Comparison of Brines Relevant to Nuclear Waste Experimentation. Sandia National Laboratories, Report, 1983.
- /MOO 04/ Moog, H. C., Hagemann, S.: Thermodynamische Modellierung hochsaliner Lösungen. GRS-Bericht, Bd. 195, 2004.
- /MOR 15/ Morcillo, M., González-Calbet, J. M., Jiménez, J. A., Díaz, I., Alcántara, J., Chico, B., Mazarío-Fernández, A., Gómez-Herrero, A., Llorente, I., La Fuente, D. de: Environmental conditions for akaganeite formation in marine atmosphere mild steel corrosion products and its characterization. Corrosion, Bd. 71, Nr. 7, pp. 872–886, DOI 10.5006/1672, 2015.
- /MOS 10/ Mosser-Ruck, R., Cathelineau, M., Guillaume, D.: Effects of temperature, pH, and iron/clay and liquid/clay ratios on experimental conversion of dioctahedral smectite to berthierine, chlorite, vermiculite, or saponite. Clays and Clay Minerals, Bd. 58, pp. 280–291, 2010.
- /MOS 20/ Mosser-Ruck, R., Sterpenich, J., Michau, N., Jodin-Caumon, M.-C., Randi, A., Abdelmoula, M., Barres, O., Cathelineau, M.: Serpentinization and H₂ production during an iron-clay interaction experiment at 90°C under low CO₂ pressure. Applied Clay Science, Bd. 191, pp. 105609, DOI 10.1016/j.clay.2020.105609, 2020.
- /MÜL 75/ Müller, E. P., Papendieck, G.: Zur Verteilung, Genese und Dynamik von Tiefenwässern unter besonderer Berücksichtigung des Zechsteins. Zeitschrift der Deutschen Gesellschaft für Geowissenschaften, Bd. 3, Nr. 2, pp. 167–196, 1975.

- /MÜL 95/ Müller, E.: Geochemische und sedimentologische Untersuchung der grenzsschichten Barreme-Apt unter Berücksichtigung der Laminite. Geologisches Jahrbuch, A141, pp. 533–549, 1995.
- /MÜL 08/ Müller-Lyda, I., Rübél, A.: Endlagerung wärmeentwickelnder radioaktiver Abfälle in Deutschland. Anhang Behälterstandzeiten. Langzeitstabilität von Behältermaterialien und Abfallmatrix. GRS-Bericht, Bd. 247, 2008.
- /MUÑ 13/ Muñoz, A. G., Scharge, T., Moor, H. C.: Thermodynamic data for iron(II) in high-saline solutions up to 90°C. GRS-Bericht, No. 326, 97 p., 2013.
- /MUR 84/ Murata, T., Sato, E., Matsunami, R.: Factors controlling corrosion of steels in CO₂-saturated environments. 1984.
- /MUR 86/ Murowchick, J. B., Barnes, H. L.: Formation of cubic FeS. The American Mineralogist, Bd. 71, pp. 1243–1246, 1986.
- /NAG 02/ NAGRA: Project Opalinus Clay. Safety Report. Demonstration of disposal feasibility for spent fuel, vitrified high-level waste and long-lived intermediate-level waste (Entsorgungsnachweis). Nagra Technical Report, Vol. 02, 02-05, 2002.
- /NAU 00/ Naumann, D.: Salinare Tiefenwässer in Norddeutschland. GeoForschungszentr. Potsdam Sci. Tech. Rep., Vol. 00, STR00/21, 2000.
- /NEC 16/ Necib, S., Linard, Y., Crusset, D., Michau, N., Daumas, S., Burger, E., Romaine, A., Schlegel, M. L.: Corrosion at the carbon steel-clay borehole water and gas interfaces at 85 °C under anoxic and transient acidic conditions. Corrosion Science, Bd. 111, pp. 242–258, DOI 10.1016/j.corsci.2016.04.039, 2016.
- /NEC 17a/ Necib, S., Diomidis, N., Keech, P., Nakayama, M.: Corrosion of carbon steel in clay environments relevant to radioactive waste geological disposals, Mont Terri rock laboratory (Switzerland). In: Bossart, P., Milnes, A. G. (Eds.): Mont Terri Rock Laboratory, 20 Years Two Decades of Research and Experimentation on Claystones for Geological Disposal of Radioactive Waste. Swiss Journal of Geosciences Supplement Ser, Vol. 5, No. 5, pp.

329–342, ISBN 978-3-319-70457-9, DOI 10.1007/978-3-319-70458-6_17, Birkhauser Verlag GmbH: Cham, 2017.

- /NEC 17b/ Necib, S., Linard, Y., Crusset, D., Schlegel, M., Daumas, S., Michau, N.: Corrosion processes of C-steel in long-term repository conditions. *Corrosion Engineering, Science and Technology*, Bd. 52, sup1, pp. 127–130, DOI 10.1080/1478422X.2017.1320155, 2017.
- /NEC 19/ Necib, S., Schlegel, M. L., Bataillon, C., Daumas, S., Diomidis, N., Keech, P., Crusset, D.: Long-term corrosion behaviour of carbon steel and stainless steel in Opalinus clay: influence of stepwise temperature increase. *Corrosion Engineering, Science and Technology*, Bd. 54, Nr. 6, pp. 516–528, DOI 10.1080/1478422X.2019.1621456, 2019.
- /NEF 05/ Neff, D., Dillmann, P., Bellot-Gurlet, L.: Corrosion of iron archaeological artefacts in soil: characterisation of the corrosion system. *Corrosion Science*, Bd. 47, pp. 515–535, 2005.
- /NEF 10/ Neff, D., Saheb, M., Monnier, J.: A review of the archaeological analogue approaches to predict the long-term corrosion behaviour of carbon steel overpack and reinforced concrete structures in the French disposal systems. *Journal of Nuclear Materials*, pp. 196–205, 2010.
- /NEM 11/ Nemer, M. B., Xiong, Y., Ismail, A. E.: Solubility of $\text{Fe}_2(\text{OH})_3\text{Cl}$ (pure-iron end-member of hibbingite) in NaCl and Na_2SO_4 brines. *Chemical Geology*, Bd. 280, pp. 26–32, 2011.
- /NEW 10/ Newman, R. C., Wang, S., Kwong, G.: Anaerobic corrosion studies of carbon steel used fuel containers. NWMO Report, TR, No. 2010-0, 2010.
- /NGO 14/ Ngo, V. V., Delelande, M., Clément, A.: Coupled transport-reaction modeling of the long-term interaction between iron, bentonite and Callovo-Oxfordian claystone in radioactive waste confinement systems. *Applied Clay Science*, Bd. 101, pp. 430–443, 2014.

- /NGO 15/ Ngo, V. V., Clément, A., Michau, N.: Kinetic modeling of interactions between iron, clay, water: comparison with data from batch experiments. *Applied Geochemistry*, Bd. 53, pp. 13–26, 2015.
- /NIC 85/ Nickel, E. H., Robinson, B. W.: Kambaldaite - a new hydrated Ni-Na carbonate mineral from Kambalda, Western Australia. *Am. Min.*, Bd. 70, pp. 419–422, 1985.
- /NIN 13/ Ning, J., Theng, Y., Young, D.: A thermodynamic study of hydrogen sulfide corrosion of mild steel. Paper 2462-, 2013.
- /NOW 13/ Nowak, T., Maßmann, J.: Endlagerstandortmodell Nord (AnSichT) - Teil III: Auswahl von Gesteins- und Fluideigenschaften für numerische Modellberechnungen im Rahmen des Langzeitsicherheitsnachweises. Zwischenbericht. Bundesanstalt für Geowissenschaften und Rohstoffe, 2013.
- /OHN 06/ Ohnishi, C., Asano, K., Iwamoto, S., Chikama, K., Inoue, M.: Preparation of Co₃O₄ Catalysts for Direct Decomposition of Nitrous Oxide under Industrial Conditions. In: *Scientific Bases for the Preparation of Heterogeneous Catalysts. Studies in Surface Science and Catalysis*, No. 162, pp. 737–744, ISBN 9780444528278, DOI 10.1016/S0167-2991(06)80975-4, Elsevier, 2006.
- /OHN 09/ Ohnishi, C. H., Asano, K., Jeon, H.-J., Hosokawa, S., Iwamoto, S., Inoue, M.: Synthesis of alkali-metal cobalt kambaldaite by precipitation method. *Polyhedron*, Bd. 28, Nr. 7, pp. 1295–1300, DOI 10.1016/j.poly.2009.02.026, 2009.
- /OND 01/ ONDRAF/ NIRAF (Ed.): Technical overview of the SAFIR 2 report. Safety Assessment and Feasibility Interim Report 2. Vol. 2001, 05E, 2001.
- /ORT 02/ Ortiz, L., Volckaert, G., Mallants, D.: Gas generation and migration in Boom Clay, a potential host rock formation for nuclear waste storage. *Engineering Geology*, Bd. 64, pp. 287–296, 2002.

- /OSA 10/ Osacký, M., Sucha, V., Czímerová, A.: Reaction of smectites with iron in a nitrogen atmosphere at 75°C. *Applied Clay Science*, Bd. 50, pp. 237–244, 2010.
- /PAN 14/ Pandarinathan, V., Lepková, K., van Bronswijk, W.: Chukanovite ($\text{Fe}_2(\text{OH})_2\text{CO}_3$) identified as a corrosion product at sand-deposited carbon steel in CO_2 -saturated brine. *Corrosion Science*, Bd. 85, pp. 26–32, DOI 10.1016/j.corsci.2014.03.032, 2014.
- /PEA 18/ Pearce, C. I., Icenhower, J. P., Asmussen, R. M., Tratnyek, P. G., Rosso, K. M., Lukens, W. W., Qafoku, N. P.: Technetium stabilization in low-solubility sulfide phases: a review. *ACS Earth and Space Chemistry*, Bd. 2, Nr. 6, pp. 532–547, DOI 10.1021/acsearthspacechem.8b00015, 2018.
- /PEK 07/ Pekov, I. V., Perchiazzi, N., Merlino, S., Kalachev, V. N., Merlini, M., Zadov, A. E.: Chukanovite, $\text{Fe}_2(\text{CO}_3)(\text{OH})_2$, a new mineral from the weathered iron meteorite Dronino. *European Journal of Mineralogy*, Bd. 19, Nr. 6, pp. 891–898, DOI 10.1127/0935-1221/2007/0019-1767, 2007.
- /PEK 13/ Pekov, I. V., Sereda, E. V., Polekhovskiy, Y. S., Britvin, S. N., Chukanov, N. V., Yapaskurt, V. O., Bryzgalov, I. A.: Ferrotchilinite, $6\text{FeS}\cdot 5\text{Fe}(\text{OH})_2$, a new mineral from the Oktyabr'sky deposit, Noril'sk district, Siberia, Russia. *Geology of Ore Deposits*, Bd. 55, Nr. 7, pp. 567–574, DOI 10.1134/S1075701513070106, 2013.
- /PFE 11/ Pfeiffer, F., McStocker, B., Gründler, D., Ewig, F., Thomauske, B., Havenith, A., Kettler, J.: Abfallspezifikation und Mengengerüst. Basis Ausstieg aus der Kernenergienutzung (Juli 2011). Bericht zum Arbeitspaket 3. Vorläufige Sicherheitsanalyse für den Standort Gorleben. GRS-Bericht, No. 278, 2011.
- /PIG 13/ Pignatelli, I., Mugnaioli, E., Hybler, J.: A multi-technique characterization of cronstedtite synthesized by iron-clay interaction in a step-by-step coling procedure. *Clays and Clay Minerals*, Bd. 61, pp. 277–289, 2013.
- /PON 03/ Pons, E., Uran, L., Joiret, S.: Long term behaviour of iron in clay soils: a study of archaeological analogues. In: European Federation of Corrosion workshop-Predictions of long term corrosion behaviour in nuclear waste systems. pp. 334–345, 2003.

- /POU 04/ Poulton, S. W., Krom, M. D., Raiswell, R.: A revised scheme for the reactivity of iron (oxyhydr)oxide minerals towards dissolved sulfide. *Geochimica et Cosmochimica Acta*, Bd. 68, Nr. 18, pp. 3703–3715, DOI 10.1016/j.gca.2004.03.012, 2004.
- /POY 06/ Poyet, S.: The Belgian supercontainer concept: Study of the concrete buffer behaviour in service life. *Journal de Physique IV (Proceedings)*, Bd. 136, pp. 167–175, DOI 10.1051/jp4:2006136018, 2006.
- /RED 21a/ Reddy, B., Padovani, C., Smart, N. R., Rance, A. P., Cook, A., Milodowski, A., Field, L., Kemp, S., Diomidis, N.: Further results on the in situ anaerobic corrosion of carbon steel and copper in compacted bentonite exposed to natural Opalinus Clay porewater containing native microbial populations. *Materials and Corrosion*, Bd. 72, No. 1-2, pp. 268–281, DOI 10.1002/maco.202011785, 2021.
- /RED 21b/ Reddy, B., Padovani, C., Rance, A. P., Smart, N. R., Cook, A., Haynes, H. M., Milodowski, A. E., Field, L. P., Kemp, S. J., Martin, A., Diomidis, N.: The anaerobic corrosion of candidate disposal canister materials in compacted bentonite exposed to natural granitic porewater containing native microbial populations. *Materials and Corrosion*, Bd. 72, No. 1-2, pp. 361–382, DOI 10.1002/maco.202011798, 2021.
- /REF 97a/ Refait, P., Génin, J. -M. R.: The mechanismus of oxidation of ferrous hydroxychloride $b\text{-Fe}_2(\text{OH})_3\text{Cl}$ in aqueous solution: The formation of akaganite vs goethite. *Corrosion Science*, Bd. 39, Nr. 3, pp. 539–553, 1997.
- /REF 97b/ Refait, P., Drissi, S. H., Pytkiewicz, J.: The anionic species competition in iron aqueous corrosion: Role of various green rust compounds. *Corrosion Science*, Bd. 39, Nr. 9, pp. 1699–1710, 1997.
- /REF 98/ Refait, P., Abdelmoula, M., Génin, J. -M. R.: Mechanisms of formation and structure of green rust one in aqueous corrosion of iron in the presence of chloride ions. *Corrosion Science*, Bd. 40, pp. 1547–1560, 1998.

- /REF 06/ Refait, P., Abdelmoula, M., Génin, J. -M. R.: Green rusts in electrochemical and microbially influenced corrosion of steel. *Comptes rendus geoscience / Académie des Sciences Paris*, Bd. 338, pp. 476–487, 2006.
- /REF 11/ Refait, P., Nguyen, D. D., Jeannin, M.: Electrochemical formation of green rusts in deaerated seawater-like solutions. *Electrochimica Acta*, Bd. 56, pp. 6481–6488, 2011.
- /REF 12/ Refait, P., Bourdoiseau, J. A., Jeannin, M.: Electrochemical formation of carbonated corrosion products on carbon steel in eaerated solutions. *Electrochimica Acta*, Bd. 79, pp. 210–217, 2012.
- /REG 05/ Reguer, S., Dillmann, P., Mirambet, F.: Local and structural characterisation of chlorinated phases formed on ferrous archaeological artefacts by μ XANES. *Nuclear Instruments and Methods in Physics Research*, B240, pp. 500–504, 2005.
- /RÉG 07a/ Réguer, S., Neff, D., Bellot-Gurlet, L., Dillmann, P.: Deterioration of iron archaeological artefacts, Micro-Raman investigation on Cl-containing corrosion products. *Journal of Raman Spectroscopy*, Bd. 38, Nr. 4, pp. 389–397, DOI 10.1002/jrs.1659, 2007.
- /RÉG 07b/ Réguer, S., Dillmann, P., Miramber, F.: Buried iron archaeological artefacts: corrosion mechanisms related to the presence of Cl-containing phases. *Corrosion Science*, Bd. 49, pp. 2726–2744, 2007.
- /RÉG 15/ Réguer, S., Mirambet, F., Rémazeilles, C., Vantelon, D., Kergourlay, F., Neff, D., Dillmann, P.: Iron corrosion in archaeological context, Structural refinement of the ferrous hydroxychloride β -Fe₂(OH)₃Cl. *Corrosion Science*, Bd. 100, pp. 589–598, DOI 10.1016/j.corsci.2015.08.035, 2015.
- /REI 13/ Reinhold, K., Jahn, S., Kühnlenz, T.: Endlagerstandortmodell Nord (An-SichT) - Teil I: Beschreibung des geologischen Endlagerstandortmodells. Bundesanstalt für Geowissenschaften und Rohstoffe, 2013.

- /RÉM 08/ Rémazeilles, C., Refait, P.: Formation, fast oxidation and thermodynamic data of Fe(II) hydroxychlorides. *Corrosion Science*, Bd. 50, pp. 856–864, 2008.
- /RÉM 09a/ Rémazeilles, C., Neff, D., Kergourlay, F.: Mechanisms of long-term anaerobic corrosion of iron archaeological artefacts in seawater. *Corrosion Science*, Bd. 51, pp. 2932–2941, 2009.
- /RÉM 09b/ Rémazeilles, C., Refait, P.: Fe(II) hydroxycarbonate $\text{Fe}_2(\text{OH})_2\text{CO}_3$ (chukanovite) as iron corrosion product: Synthesis and study by Fourier Transform Infrared Spectroscopy. *Polyhedron*, Bd. 28, pp. 749–756, 2009.
- /RIC 06/ Rickard, D., Griffith, A., Oldroyd, A.: The composition of nanoparticulate mackinawite, tetragonal iron(II) monosulfide. *Chemical Geology*, Bd. 235, pp. 286–298, 2006.
- /RIC XX/ Richter, F.: Die physikalischen Eigenschaften der Stähle „Das 100 - Stähle - Programm“ Teil I: Tafeln und Bilder. no year.
- /RIV 13a/ Rivard, C., Montargès-Pelletier, E., Vantelon, D.: Combination of multi-scale and multi-edge X-ray spectroscopy for investigating the products obtained from the interaction between kaolinite and metallic iron in anoxic conditions at 90°C. *Phys. Chem. Miner.*, Bd. 40, pp. 115–132, 2013.
- /RIV 13b/ Rivard, C., Pelletier, M., Michau, N.: Berthierine-like mineral formation and stability during the interaction of kaolinite with metallic iron at 90°C under anoxic and oxic conditions. *The American Mineralogist*, Bd. 98, pp. 163–180, 2013.
- /ROM 13/ Romaine, A., Sabot, R., Jeannin, M.: Electrochemical synthesis and characterization of corrosion products on carbon steel under argillite layers in carbonated media at 80°C. *Electrochimica Acta*, Bd. 114, pp. 152–158, 2013.
- /ROS 76/ Rosenbaum, M.: Effect of compaction on the pore fluid chemistry of montmorillonite. *Clays and Clay Minerals*, Bd. 24, pp. 118–121, 1976.

- /ROS 09/ Roselle, T. G.: Iron and lead corrosion in WIPP-relevant conditions, 6 month results. Sandia Report, ERMS, Nr. 546084, 2009.
- /ROS 10/ Roselle, G. T.: Iron and lead corrosion in WIPP-relevant conditions, 12 month results. Sandia Report, ERMS, Nr. 55483, 2010.
- /ROS 11/ Roselle, G. T.: Iron and lead corrosion in WIPP-relevant conditions, 18 month results. Sandia Report, ERMS, Nr. 554715, 2011.
- /ROS 13/ Roselle, G. T.: Determination of corrosion rates from iron/lead corrosion experiments to be used for gas generation calculations. Sandia Report, ERMS, Nr. 559077, 2013.
- /ROZ 11/ Rozov, K. B., Berner, U., Kulik, D. A.: Solubility and thermodynamic properties of carbonate-bearing hydrotalcite-pyroaurite solid solutions with a 3:1 Mg/(Al+Fe) mole ratio. *Clays and Clay Minerals*, Bd. 59, pp. 215–232, 2011.
- /RUB 10/ Ruby, C., Abdelmoula, M., Naile, S.: Oxidation modes and thermodynamics of FeII-III oxyhydroxycarbonate green rust: dissolution-precipitation versus in situ deprotonation. *Geochimica et Cosmochimica Acta*, Bd. 74, pp. 953–966, 2010.
- /RUM 20/ Rumble, J. R., Bruno, T. J., Doa, M. J. (Eds.): CRC handbook of chemistry and physics, A ready-reference book of chemical and physical data. 101. ed., 1 Band (verschiedene Seitenzählungen), ISBN 9780367417246, CRC Press, Taylor & Francis Group: Boca Raton, London, New York, 2020.
- /U.S 14/ U.S. Department of Energy (USDOE) (Ed.): Title 40 CFR Part 191. Subparts B and C. Compliance Recertification application 2014 for the Waste Isolation Pilot Plant. Appendix SOTERM-2014. Actinide chemistry source term. DOE/WIPP-14-3503. 2014.
- /SAH 08/ Saheb, M., Neff, D., Dillmann, P.: Long-term corrosion behaviour of low-carbon steel in anoxic environment: characterisation of archaeological artefacts. *Journal of Nuclear Materials*, Bd. 379, pp. 118–123, 2008.

- /SAH 10a/ Saheb, M., Neff, D., Demory, J.: Characterisation of corrosion layers formed on ferrous archaeological artefacts buried in anoxic media. *Corr. Eng. Sci. Technol.*, Bd. 45, pp. 381–387, 2010.
- /SAH 10b/ Saheb, M., Descostes, M., Neff, D.: Iron corrosion in an anoxic soil: Comparison between thermodynamic modelling and ferrous archaeological artefacts characterised along with the local in situ geochemical conditions. *Applied Geochemistry*, Bd. 25, pp. 1937–1948, 2010.
- /SAH 11/ Saheb, M., Neff, D., Bellot-Gurlet, L.: Raman study of a deuterated iron hydroxycarbonate to assess long-term corrosion mechanisms in anoxic soils. *Journal of Raman Spectroscopy*, Bd. 42, pp. 1100–1108, 2011.
- /SAH 14/ Saheb, M., Gallien, J. -P., Descostes, M.: Influence of an aerated/anoxic transient phase on the long-term corrosion of iron. *Corrosion Science*, Bd. 86, pp. 71–80, 2014.
- /SAW 20/ Sawłowicz, Z., Malinowski, Ł., Giże, A., Stanek, J., Przybyło, J.: Mineralogical-geochemical study of corroded iron-based metals from a salt mine environment. *Corrosion*, Bd. 76, Nr. 7, pp. 666–677, DOI 10.5006/3493, 2020.
- /SCH 96/ Schulten, M. A. d.: Production artificielle d'un chlorocarbonate de sodium et de magnesium. *Bull. Soc. Fr. Min.*, Bd. 19, pp. 164–169, 1896.
- /SCH 73/ Schmidt, G. W.: Interstitial water composition and geochemistry of deep Gulf coast shales and sandstones. *American Association of Petroleum Geologists Bulletin*, pp. 321–337, 1973.
- /SCH 88/ Schwarzkopf, W., Smailos, E., Köster, R.: In-situ corrosion studies on selected high-level waste packaging materials under simulated disposal conditions in rock salt formations. *Kernforschungszentrum Karlsruhe*, Vol. 4324, KfK 4324, 1988.
- /SCH 91/ Schoonen, M. A. A., Barnes, H. L.: Reactions forming pyrite and marcasite from solution: I. Nucleation of FeS₂ below 100°C. *Geochimica et Cosmochimica Acta*, Bd. 55, pp. 1495–1504, 1991.

- /SCH 00/ Schwertmann, U., Cornell, R. M.: Iron oxides in the laboratory, 2nd ed. Wiley-VCH: Weinheim, 2000.
- /SCH 03/ Scheidegger, A. M., Grolimund, D., Cui, D., Devoy, J., Spahiu, K., Wersin, P., Bonhoure, I., Janousch, M.: Reduction of selenite on iron surfaces: A micro-spectroscopic study. *Journal de Physique IV (Proceedings)*, Bd. 104, pp. 417–420, DOI 10.1051/jp4:20030112, 2003.
- /SCH 08/ Schlegel, M. L., Bataillon, C., Benhamida, K.: Metal corrosion and argillite transformation at the water-saturated, high-temperature iron\clay interface: A microscopic-scale study. *Applied Geochemistry*, Bd. 23, pp. 2619–2633, 2008.
- /SCH 10/ Schlegel, M., Bataillon, C., Blanc, C.: Anodic activation of iron corrosion in clay media under water-saturated conditions at 90 °C: characterization of the corrosion interface. *Environmental Science & Technology*, Bd. 44, pp. 1503–1508, 2010.
- /SCH 14/ Schlegel, M. L., Bataillon, C., Brucker, F.: Corrosion of metal iron in contact with anoxic clay at 90°C: characterization of the corrosion products after two years of interaction. *Applied Geochemistry*, Bd. 51, pp. 1–14, 2014.
- /SCH 15/ Scheck, J., Lemke, T., Gebauer, D.: The role of chloride ions during the formation of akaganéite revisited. *Minerals*, Bd. 5, Nr. 4, pp. 778–787, DOI 10.3390/min5040524, 2015.
- /SCH 16/ Schlegel, M. L., Necib, S., Daumas, S., Blanc, C., Foy, E., Trcera, N., Romaine, A.: Microstructural characterization of carbon steel corrosion in clay borehole water under anoxic and transient acidic conditions. *Corrosion Science*, Bd. 109, pp. 126–144, DOI 10.1016/j.corsci.2016.03.022, 2016.
- /SCH 18/ Schlegel, M. L., Necib, S., Daumas, S., Labat, M., Blanc, C., Foy, E., Linnard, Y.: Corrosion at the carbon steel-clay borehole water interface under anoxic alkaline and fluctuating temperature conditions. *Corrosion Science*, Bd. 136, pp. 70–90, DOI 10.1016/J.CORSCI.2018.02.052, 2018.

- /SCH 19/ Schlegel, M. L., Martin, F., Fenart, M., Blanc, C., Varlet, J., Foy, E., Prêt, D., Trcera, N.: Corrosion at the carbon steel-clay compact interface at 90°C: Insight into short- and long-term corrosion aspects. *Corrosion Science*, Bd. 152, pp. 31–44, DOI 10.1016/j.corsci.2019.01.027, 2019.
- /SED 15/ Sedighi, M., Thomas, H. R., Al Masum, S., Vardon, P. J., Nicholson, D., Chen, Q.: Geochemical modelling of hydrogen gas migration in an unsaturated bentonite buffer. In: Shaw, R. P. (Ed.): *Gas Generation and Migration in Deep Geological Radioactive Waste Repositories*. Geological Society, London, Special Publications, Vol. 415, pp. 189–201, DOI 10.1144/SP415.12, 2015.
- /SEN 08/ Senger, R., Marschall, P., Finsterle, S.: Investigation of two-phase flow phenomena associated with corrosion in an SF/HLW repository in Opalinus Clay, Switzerland. *Physics and Chemistry of the Earth*, Bd. 33, pp. S317–S326, 2008.
- /SHO 99/ Shoesmith, D. W., King, F.: The effects of gamma radiation on the corrosion of candidate materials for the fabrication of nuclear waste packages. AECL Canada, AECL, Nr. 11999, 1999.
- /SMA 85/ Smailos, E.: Korrosionsuntersuchungen an ausgewählten metallischen Werkstoffen als Behältermaterialien für die Endlagerung von hochradioaktiven Abfallprodukten in Steinsalzformationen. Kernforschungszentrum Karlsruhe, Vol. 3953, KfK 3953, 1985.
- /SMA 92/ Smailos, E., Schwarzkopf, W., Kienzler, B.: Corrosion of carbon-steel containers for heat-generating nuclear waste in brine environments relevant for a rock-salt repository. *Materials Research Society, Symposium Proceedings*, Bd. 257, pp. 399–406, 1992.
- /SMA 93/ Smailos, E.: Corrosion of high-level waste packaging materials in disposal relevant brines. *Nuclear Technology*, Bd. 104, pp. 343–350, 1993.
- /SMA 95/ Smailos, E., Gago, J. A., Azkarate, I., Fieh, B.: Corrosion studies on selected packaging materials for disposal of heat-generating radioactive

wastes in rock-salt formations. Forschungszentrum Karlsruhe Wissenschaftliche Berichte, Bd. 5587, 1995.

- /SMA 98/ Smailos, E., Gago, J. A., Kursten, B.: Corrosion Evaluation of Metallic Materials for Long-Lived HLW/Spent Fuel Disposal Containers. Forschungszentrum Karlsruhe Wissenschaftliche Berichte, Vol. 5889, No. 5889, 1998.
- /SMA 01/ Smart, N. R., Blackwood, D. J., Werme, L.: The anaerobic corrosion of carbon steel and cast iron in artificial groundwaters. SKB Technical Report, TR, No. 01-22, 2001.
- /SMA 04/ Smailos, E., Cunado, M. A., Kursten, B.: Long-term performance of candidate materials for HLW/spent fuel disposal containers. Final report. Forschungszentrum Karlsruhe Tech. Rep., FZKA-6809, 2004.
- /SMA 05/ Smart, N. R., Rance, A. P.: Effect of radiation on aerobic corrosion of iron. SKB Technical Report, TR, No. 05-05, 2005.
- /SMA 08/ Smart, N. R., Rance, A. P., Werme, L. O.: The effect of radiation on the anaerobic corrosion of steel. Journal of Nuclear Materials, Bd. 379, pp. 97–104, 2008.
- /SMA 17/ Smart, N. R., Reddy, B., Rance, A. P., Nixon, D. J., Fruttschi, M., Bernier-Latmani, R., Diomidis, N.: The anaerobic corrosion of carbon steel in compacted bentonite exposed to natural Opalinus Clay porewater containing native microbial populations. Corrosion Engineering, Science and Technology, Bd. 52, sup1, pp. 101–112, DOI 10.1080/1478422X.2017.1315233, 2017.
- /STA 03/ Stahl, K., Nielsen, K., Jaiang, J.: On the akaganéite crystal structure, phase transformations and possible role in post-excavational corrosion of iron artifacts. Corrosion Science, Bd. 43, pp. 2563–2575, 2003.
- /STO 14/ Stober, I., Wolfgramm, M., Birner, J.: Hydrochemie der Tiefenwässer in Deutschland. Z. Geol. Wiss., Vol. 41/42, pp. 339–380, 2014.

- /SUS 63/ Susarev, M. P., Prokof'eva, P. V.: Ravnovesie zidkost' - par v sisteme voda - chloristyj vodorod - chlornoe zelezo pri 25°. Zurnal Fiziceskoj Chimiii, Bd. 37, pp. 2408–2412, 1963.
- /SYR 73/ Syrkina, I. G., Krasheninnikova, A. A., Zaliopo, V. M.: Liquid-vapour equilibrium in the hydrogen chloride-water-ferrous chloride system. Russian Journal of Physical Chemistry, Bd. 47, Nr. 11, pp. 1646–1647, 1973.
- /TAN 04/ Taniguchi, N., Kawasaki, M., Kawakami, S.: Corrosion behaviour of carbon steel in buffer material under anaerobic condition. Japan Nuclear Cycle Development Institute, TN8400, Nr. 040, 2004.
- /TEL 93/ Telander, M. R., Westerman, R. E.: Hydrogen generation by metal corrosion in simulated waste isolation pilot plant environments: Progress report for the period November 1989 through December 1992. Sandia National Laboratories, SAND92, SAND92-7347, 1993.
- /TEL 97/ Telander, M. R., Westerman, R. E.: Hydrogen generation by metal corrosion in simulated waste isolation pilot plant environments. Sandia National Laboratories, SAND96, SAND96-2538, 1997.
- /TER 01/ Terlain, A., Desgranges, C., Gauvain, D.: Oxidation of materials for nuclear waste containers under long term disposal. In: National Association of Corrosion Engineers (Ed.): Corrosion 2001. Houston, Texas, pp. NACE-01119, 2001.
- /TEW 79/ Tewari, P. H., Bailey, M. G., Campbell, A. B.: The erosion-corrosion of carbon steel in aqueous H₂S solutions up to 120°C and 1.6 MPa pressure. Corrosion Science, Bd. 19, pp. 573–585, 1979.
- /TRU 09/ Truche, L., Berger, G., Destrigneville, C.: Experimental reduction of aqueous sulphate by hydrogen under hydrothermal conditions: Implication for the nuclear waste storage. Geochimica et Cosmochimica Acta, Bd. 73, pp. 4824–4835, DOI 10.1016/j.gca.2009.05.043, 2009.
- /TRU 10/ Truche, L., Berger, G., Destrigneville, C.: Kinetics of pyrite to pyrrhotite reduction by hydrogen in calcite buffered solutions between 90°C:

Implications for nuclear waste disposal. *Geochimica et Cosmochimica Acta*, Bd. 74, pp. 2894–2914, 2010.

- /VEN 12/ Venzlaff, H.: Die elektrisch mikrobiell beeinflusste Korrosion von Eisen durch sulfatreduzierende Bakterien. Diss. Ruhr-Univ. Bochum, 2012.
- /WAL 07/ Walter, R., Dorn, P.: *Geologie von Mitteleuropa*. 7. ed., 511 p., ISBN 9783510652297, Schweizerbart: Stuttgart, 2007.
- /WAN 01/ Wang, Z., Moore, R. C., Felmy, A. R.: A study of the corrosion products of mild steel in high ionic strength brines. *Waste management*, Bd. 21, pp. 335–341, 2001.
- /WEB 06/ Weber, K. A., Achenbach, L. A., Coates, J. D.: Microorganisms pumping iron: anaerobic microbial iron oxidation and reduction. *Nature Reviews Microbiology*, Bd. 4, Nr. 10, pp. 752–764, 2006.
- /WEI 35/ Weiser, H. B., Milligan, W. O.: x-Ray Studies on the Hydrated Oxides. V. Beta Ferric Oxide Monohydrate. *Journal of the American Chemical Society*, Bd. 57, Nr. 2, pp. 238–241, DOI 10.1021/ja01305a003, 1935.
- /WEN 08/ Wenk, H. -R., Vololini, M., Mazurek, M.: Preferred orientations and anisotropy in shales: Callovo-Oxfordian shale (France) and Opalinus clay (Switzerland). *Clays and Clay Minerals*, Bd. 56, pp. 285–306, 2008.
- /WER 03/ Wersin, P., Johnson, L. H., Schwyn, B.: Redox conditions in the near field of a repository for SF/HLW and ILW in opalinus clay. *NAGRA Tech. Rep.*, Vol. 02, 02-13, 2003.
- /WER 08a/ Wersin, P., Birgersson, M., Olsson, S.: Impact of corrosion-derived iron on the bentonite buffer within the KBS-3H disposal concept- the Olkiluoto site as case study. *SKB Rapport*, Vol. 11, R-08-34, 58 p., 2008.
- /WER 08b/ Wersin, P., Birgersson, M., Olsson, S.: Impact of corrosion-derived iron on the bentonite buffer within the KBS-3H disposal concept. The Olkiluoto site as case study. *SKB Technical Report*, R, No. 08-34, 2008.

- /WES 88/ Westerman, R. E., Haberman, J. V., Pitman, S. G., Pool, K. H., Rhoads, K. C., Telander, M. R.: Corrosion behavior of A216 Grade WCA mild steel and Ti grade 12 alloy in hydrothermal brines. Salt repository project. Annual report. FY 1986. Pacific Northwest National Laboratory Report, PNL/SRT 6221, 1988.
- /WIK 80/ Wikjord, A. G., Rummery, T. E., Doern, F. E.: Corrosion and deposition during the exposure of carbon steel to hydrogen sulphide-water solutions. Corrosion Science, Bd. 20, pp. 651–671, 1980.
- /WIN 93/ Winkler, C.: Über künstliche Mineralien, entstanden beim chemischen Grossbetriebe. Zeitschrift für Angewandte Chemie, Bd. 6, Nr. 15, pp. 445–447, DOI 10.1002/ange.18930061503, 1893.
- /WIN 04/ Windt, L. D., Pelligrini, D., van der Lee, J.: Coupled modeling of cement/claystone interactions and radionuclide migration. Journal of Contaminant Hydrology, Bd. 68, pp. 165–182, 2004.
- /WIN 14/ Windt, L. D., Marsal, F., Corvisier, J.: Modeling of oxygen gas diffusion and consumption during the oxic transient in a disposal cell of radioactive waste. Applied Geochemistry, Bd. 41, pp. 115–127, 2014.
- /WOL 11/ Wolfgramm, M., Thorwart, K., Rauppach, K.: Zusammensetzung, Herkunft und Genese geothermaler Tiefengrundwässer im Norddeutschen Becken (NDB) und deren Relevanz für die geothermische Nutzung. Zeitschrift der Deutschen Gesellschaft für Geowissenschaften, Bd. 339, pp. 173–193, 2011.
- /XU 08/ Xu, T., Senger, R., Finsterle, S.: Corrosion-induced gas generation in a nuclear waste repository: Reactive geochemistry and multiphase flow effects. Applied Geochemistry, Bd. 23, pp. 3123–3433, 2008.
- /YU 13/ Yu, L., Treille, E., Wendling, J., Dymitrowska, M., Pellegrini, D., Ahusborde, E., Jurak, M., Amaziane, B., Caro, F., Genty, A., Poskas, P., Justinavicius, D., Senrtis, M., Norris, S., et al.: FORGE Deliverable D1.6-R. Final report on benchmark studies on repository-scale numerical simulations of gas migration Part 1: cell scale benchmark. 168 p., 2013.

/YVE 07/ Yven, B., Sammartino, S., Geraud, Y.: Mineralogy, texture and porosity of Callovo-Oxfordian argillites of the Meuse/Haute-Marne region (eastern Paris Basin). *Memoires de la Societe Geologique de France*, Bd. 178, pp. 73–90, 2007.

List of figures

Fig. 2.1	Schematic description of a borehole for the emplacement of waste containers in clay rock. Left: concept in the project AnSichT (Lommerzheim and Jobmann 2015), right: concept in the project RESUS (Alfarra et al. 2020b).....	12
Fig. 2.2	Storage of waste containers in a drift (Jobmann and Lommerzheim 2015)	13
Fig. 2.3	Geology of Central Europa and location of the Lower Saxony Basin (Niedersächsisches Becken, from Walter 2007).....	16
Fig. 2.4	Western, central and eastern part of the Lower Saxony Lower Cretaceous Basin (Kemper 1973).....	17
Fig. 2.5	Western part of the Lower Saxony Basin (from Walter 2007).....	18
Fig. 2.6	Regions worthy of further investigation during the site selection process. Left: Hoth et al. (2007), right: BGE (2020)	19
Fig. 2.7	Composition of clay minerals of Malm (Upper Jura) to Santon (Upper Cretaceous) in near-surface Lower Cretaceous clay samples (Amelung and Kutowski 2004 based on Brockamp 1976).....	24
Fig. 2.8	Content of smectites (thick black line) and clay minerals (thin black line) in Hauterivian to Albian sediments at shafts 1 and 2 of the Konrad mine (Brewitz 1982).....	25
Fig. 2.9	Composition of clay pore waters and solutions in the accompanying sandstones in the Louisiana Basin (in Chilingarian et al. 1994).....	29
Fig. 2.10	Composition of pressed solutions as a function of the residual water content of compacted clay samples - (a) kaolinitic clay (b) smectitic clay. According to Kryukov and Zhuchkova (1963) and Chilingarian et al.	32

Fig. 2.11	Salinity of deep groundwaters in the Northern German Basin (Wolfgramm et al. 2011)	37
Fig. 2.12	Relative concentrations of Na/K, Ca and Mg in deep groundwaters of the Northern German Basin (Stober et al. 2014)	38
Fig. 2.13	Water analyses from drillings in the Lower Saxonian Basin (Klinge et al. 1992)	40
Fig. 2.14	Total salt concentration of water samples in boreholes around the Konrad mine as a function of depth (from Klinge et al. 1992b)	41
Fig. 2.15	Depth – Salinity relationships at different locations in Northern Germany	42
Fig. 2.16	Stratigraphy of Lower Cretaceous clay formation and position of the model site NORD (Reinhold et al. 2013)	44
Fig. 2.17	Evolution of temperature around emplaced waste containers in the repository concept for the model site „Nord“ (Jobmann et al. 2015)	53
Fig. 2.18	Long-term evolution of temperature around emplaced waste containers in the repository concept for the model site „Nord“ (Jobmann et al. 2015)	53
Fig. 3.1	Swiss repository concept (from Diomidis 2014)	64
Fig. 3.2	Disposal of HLW waste in micro tunnels according to the French concept (ANDRA 2016)	72
Fig. 3.3	Structure of the corrosion layer between metallic iron and claystone from the Collovo-Oxfordian interval (from Schlegel et al. 2008)	76
Fig. 3.4	Schematic description of the corrosion zone around iron artefacts (Neff et al. 2005)	95
Fig. 3.5	Four phases of the metal corrosion in a repository (Swiss concept, Landolt et al. 2009)	98

Fig. 4.1	Solubility constant of synthetic amakinite - $(\text{Fe,Mg})(\text{OH})_2$ depending on the relative Mg content of the solid phase	119
Fig. 4.2	Two regions of solid solutions in the system $\text{Fe}(\text{OH})_2$ - $\text{Mg}(\text{OH})_2$	120
Fig. 4.3	X-ray diffractograms of preparations from the Amakinite measurement series.....	121
Fig. 4.4	Chukanovite and Fe-Hibbingite.....	123
Fig. 4.5	X-ray diffractograms of preparations from the Chukanovite-Pokrovskite mixing series	124
Fig. 5.1	Modelling results (case a) for corrosion of steel in Lower Cretaceous pore water in contact with quartz sand.....	135
Fig. 5.2	Modelling results (case b) for corrosion of steel in Lower Cretaceous pore water in contact with quartz sand.....	136
Fig. 5.3	Modelling results (case c) for corrosion of steel in Lower Cretaceous pore water in contact with quartz sand.....	137
Fig. 5.4	Modelling results (case d) for corrosion of steel in Lower Cretaceous pore water in contact with quartz sand.....	138
Fig. 5.5	Modelling results (case e) for corrosion of steel in Lower Cretaceous pore water in contact with quartz sand.....	139
Fig. 5.6	Modelling results (case f) for corrosion of steel in Lower Cretaceous pore water in contact with quartz sand.....	141
Fig. 5.7	Modelling results (case g) for corrosion of steel in Lower Cretaceous pore water in contact with quartz sand.....	142
Fig. 5.8	Modelling results (case h) for corrosion of steel in Lower Cretaceous pore water in contact with quartz sand.....	144

Fig. 5.9	Stability fields of selenium species (left) and solids (right) in Lower Cretaceous clay model pore water ($a_{\text{SeO}_4}=10^{-4}$ mol/kg)	148
Fig. 5.10	Stability fields of selenium species (left) and solids (right) in Lower Cretaceous clay model pore water ($a_{\text{SeO}_4}=10^{-4}$ mol/kg) with all selenide and polyselenide species as well as crystalline selenium allotropes suppressed.....	149
Fig. 5.11	Stability fields of uranium in Lower Cretaceous clay model pore water (THEREDA) ($a_{\text{UO}_2^{++}} = 10^{-6}$).....	150
Fig. 5.12	Stability fields of uranium in Lower Cretaceous clay model pore water (JAEA) ($a_{\text{U}^{4+}}=10^{-6}$).....	150
Fig. 5.13	Stability fields of plutonium in Lower Cretaceous clay model pore water	151
Fig. 5.14	Stability fields of technetium in the Lower Cretaceous clay model pore water (THEREDA)	152
Fig. 5.15	Stability fields of technetium in the Lower Cretaceous clay model pore water (JAEA)	152

List of tables

Tab. 2.1	Composition of spheroidal grey cast iron GGG40 (EN-GJS-400-15) and fine-grained steel (type 1.6210, 15MnNi6.3) /PFE 11/.....	14
Tab. 2.2	Ranges of the composition of clay rock in Hauterivian and Barremian in the sediments encountered in the Konrad 1 well /JAH 13/	21
Tab. 2.3	Ranges of the composition of clay rock in from the Upper Barremian from the Wichendorf 1/86, Hoheneggelsen KB9 and Ahlum wells /JAH 13/.....	22
Tab. 2.4	Analyses of clay pore waters and accompanying waters from the North German area /ENG 63/	30
Tab. 2.5	Pore water compositions of drillings in the region around the Konrad mine /BRE 82/	40
Tab. 2.6	Composition of solutions in the Hils sandstone, 480 m /BRE 82/	42
Tab. 2.7	Mineralogical composition of the model clay (Lower Hauterivian) after /JAH 13/.....	46
Tab. 2.8	Pore water properties of the mine waters in and around the Konrad mine (according to /KLI 92/)	48
Tab. 2.9	Hils water composition from the Konrad mine (mean values based on data in /BRE 82/)	49
Tab. 2.10	Lower Cretaceous formation water at a depth of 770 m (calculated based on the relationships in and around Konrad shaft.....	51
Tab. 3.1	Corrosion products found on steel TStE355 in saline brines after one year /SMA 92/, /SMA 93/	58
Tab. 3.2	WIPP brine A used by /TEL 93/, /TEL 97/	61
Tab. 3.3	Corrosion products found after contact with WIPP brine A.....	62

Tab. 3.4	Composition of GWB and ERDA-6 brines.....	63
Tab. 3.5	Average composition of Swiss Opalinus clay	65
Tab. 3.6	Initial pore water composition in Opalinus clay /BER 13/, /KOS 13/	65
Tab. 3.7	Composition of the pore water of Callovo-Oxfordian claystone at 100 °C (modelling)	73
Tab. 3.8	Expected container lifetime in different repository concepts /MÜL 08/, /KIN 12/	102
Tab. 3.9	Types of green rust.....	106
Tab. 4.1	Solubility of Fe-Hibbingite at 25 °C	113
Tab. 4.2	Solubility of Fe-Hibbingite at 40 °C	116
Tab. 4.3	Composition of equilibrium solutions and soil bodies in the preparation of mixed Fe-Mg hibbingite.....	116
Tab. 4.4	Composition of equilibrium solutions and solid phase in the preparation of amakinite	118
Tab. 4.5	Solubility of chukanovite at 25 °C.....	123
Tab. 4.6	Composition of the solutions of the akaganeite synthesis experiments	125
Tab. 4.7	Solubility constants for iron(III) oxyhydroxides /HAG 14/.....	126
Tab. 4.8	Mineral phases, for which an iron(II) containing analogue is conceivable.....	127
Tab. 5.1	Dimensions and masses of containers, sand filling, solution and liner in a vertical borehole.....	131
Tab. 5.2	Reaction masses at the beginning of the corrosion process	132

Tab. 5.3	Calculations that represent the four corners of the pCH/ pH ₂ area.....	146
Tab. 5.4	Solubility of Se, Tc, U and Pu in Lower Cretaceous Pore water and solid equilibrium phases.....	153

**Gesellschaft für Anlagen-
und Reaktorsicherheit
(GRS) gGmbH**

Schwertnergasse 1
50667 Köln
Telefon +49 221 2068-0
Telefax +49 221 2068-888

Forschungszentrum
Boltzmannstraße 14
85748 Garching b. München
Telefon +49 89 32004-0
Telefax +49 89 32004-300

Kurfürstendamm 200
10719 Berlin
Telefon +49 30 88589-0
Telefax +49 30 88589-111

Theodor-Heuss-Straße 4
38122 Braunschweig
Telefon +49 531 8012-0
Telefax +49 531 8012-200

www.grs.de